Title

Simulation of Cumulative Annual Impact of Pavement Structural Response on Vehicle Fuel Economy for California Test Sections

Authors

Harvey, John
Lea, Jeremy
Kim, Changmo
et al.

Publication Date

2016-05-01

May 2016
Research Report: UCPRC-RR-2015-05

Simulation of Cumulative Annual Impact of Pavement Structural Response on Vehicle Fuel Economy for California Test Sections

Authors:
John Harvey, Jeremy Lea, Changmo Kim, Erdem Coleri, Imen Zaabar, Arghavan Louhghalam, Karim Chatti, Jeffrey Buscheck, and Ali Butt

Partnered Pavement Research Program (PPRC) Contract Strategic Plan Elements 4.49, Verification of Pavement Structure and Deflection Effects on Vehicle Fuel Economy and GHG Emissions, and 4.53, Validation of Vehicle Fuel Consumption and Greenhouse Gas Emissions from Pavement Deflection

PREPARED FOR:

California Department of Transportation
Division of Research, Innovation and System Information

PREPARED BY:

University of California
Pavement Research Center
UC Davis, UC Berkeley

DOCUMENT RETRIEVAL PAGE	UCPRC Research Report No.: UCPRC-RR-2015-05

Title: Simulation of Cumulative Annual Impact of Pavement Structural Response on Vehicle Fuel Economy for California Test Sections

Authors: J. Harvey, J.D. Lea, C. Kim, E. Coleri, I. Zaabar, A. Louhghalam, K. Chatti, J. Buscheck, and A. Butt

Caltrans Technical Lead: Deepak Maskey

Prepared for:	FHWA No.:	Work Submitted:	Month Work Completed:	Final Publication Date:
California Department of Transportation Division of Research, Innovation and System Information Office of Roadway Material Testing, Materials and Engineering Services	CA162639A	Jan. 15, 2016	August 2015	May 2016

Strategic Plan Element Nos.:	DRISI Task No.:	Status:	Version No.:
4.49 and 4.53	2639	Stage 6, final	1

Abstract:
This report presents the preliminary results of a study of the effects of pavement structural response on excess fuel consumption (EFC_S), which is defined as the additional fuel required to propel a vehicle on an "imperfect" pavement compared to the amount required on an "ideal" pavement. The study compared EFC_S for a set of asphalt-surfaced test sections with a pavement with no structural response as well as with the effects of roughness and macrotexture on EFC. EFC_S was calculated using three different models for a factorial that included seventeen asphalt-surfaced pavement field sections on the California state highway network with different structure types that were characterized by their viscoelastic properties. The results of the modeling were used to simulate annual EFC_S for a factorial of vehicles, traffic flows, speed distributions, and climate regions typical of California. The sensitivity of EFC_S to the variables in the factorial was analyzed, and the effects of structural response on EFC were compared with those of roughness and macrotexture to determine whether structural response is sufficiently important to warrant a second phase of the project to validate and calibrate the models using field test sections and instrumented vehicles.

It is recommended to complete models for concrete pavements in addition to asphalt-surfaced pavements, to consider multiple layers in the asphalt, particularly near the surface to better evaluate the effects of rubberized asphalt surface materials, and to check the effects of full dynamic pavement modeling (inertial effects in the pavement) on more than the one section analyzed. It is also recommended to begin field validation and calibration of the models and rerun the simulations with the improved and calibrated models for all pavement surface types.

Keywords: Excess fuel consumption, pavement structural response, rolling resistance, macrotexture, pavement deflection, pavement vehicle interaction

Proposals for implementation:
No recommendations for implementation

Related documents:

- Coleri, E., J. Harvey, I. Zaabar, A. Louhghalam, and K. Chatti. 2016. *Model Development, Field Section Characterization, and Model Comparison for Excess Vehicle Fuel Use Due to Pavement Structural Response.* UCPRC-RR-2015-04 (not yet published).

Signatures:

J. Harvey **1st Author**	J. Harvey D. Reger **Technical Review**	D. Spinner **Editor**	J. Harvey **Principal Investigator**	Deepak Maskey **Caltrans Technical Lead**	T.J. Holland **Caltrans Contract Manager**

DISCLAIMER

This document is disseminated in the interest of information exchange. The contents of this report reflect the views of the authors who are responsible for the facts and accuracy of the data presented herein. The contents do not necessarily reflect the official views or policies of the State of California or the Federal Highway Administration. This publication does not constitute a standard, specification or regulation. This report does not constitute an endorsement by the Department of any product described herein.

For individuals with sensory disabilities, this document is available in alternate formats. For information, call (916) 654-8899, TTY 711, or write to California Department of Transportation, Division of Research, Innovation and System Information, MS-83, P.O. Box 942873, Sacramento, CA 94273-0001.

ACKNOWLEDGMENTS

The authors would like to thanks Shmuel Weissman of Symplectic Engineering Corporation for his review and comments on the information included in this report. The assistance of the District 3 METS deflection testing staff, Districts 3, 4, and 10 Maintenance closure staff, and NCE deflection testing staff is greatly appreciated. The authors would also like to thank Deepak Maskey, Caltrans technical reviewer, T. Joe Holland, Caltrans project contract manager, and Nick Burmas, Caltrans program manager for their contributions to this study.

PROJECT OBJECTIVES

The purpose of this project is to develop calibrated and validated models for vehicle energy consumption due to pavement deflection for use in pavement management and design. The goals of this project are, first, to compare different pavement structural response energy dissipation models and the results they provide for estimated fuel consumption for a range of California pavements, vehicles, and climates using well-characterized and well-documented field test sections, and, second, to verify the same models using the results of the field measurements on the same sections with instrumented vehicles following the general approach used by Michigan State University for NCHRP Project 1-45. This work is part of Caltrans/UCPRC participation in the MIRIAM (Models for rolling resistance In Road Infrastructure Asset Management systems) project which is being performed by a consortium of European national highway research laboratories and the Federal Highway Administration (FHWA) as well as Caltrans and UCPRC.

Each goal will be accomplished through a separately funded phase with the following tasks:

Phase I (Partnered Pavement Research Center Strategic Plan Element [PPRC SPE] 4.49)

1. Identify modelers interested in participating in the project, and critically review the existing models.
2. Identify pavement test sections that span the range of pavement structures, traffic, and climate conditions across the state, then have modelers estimate vehicle fuel consumption differences due to pavement structural response (called excess fuel consumption) for the range of California vehicles and conditions for each test section.
3. Summarize and compare modeling results received from each group in a report. Prepare a summary report of results.
4. Use the model results to simulate the annual vehicle excess fuel consumption caused by pavement structural response on each of the asphalt-surfaced test sections for typical traffic and climate in California and to compare those results with the excess fuel consumption caused by roughness and surface macrotexture, and then prepare a report summarizing the results. Based on those results regarding the importance of fuel consumption attributed to structural response, include in the report a recommendation regarding the need for Phase II experimental work.
5. Develop and submit an experimental plan for fuel economy evaluation in Phase II.
6. Hold a webinar and a question session to communicate results of Phase I.

Phase II (PPRC SPE 4.53)

1. Update characterizations of the pavement test sections included in Phase I.
2. Provide updated characterization data to modelers to update modeling results for the sections. Obtain results of the updated modeling of test sections.
3. Measure vehicle fuel consumption of a range of vehicles on the pavement test sections modeled as part of Phase I, including consideration of all factors potentially affecting the results.
4. Analyze measurements and use the results to calibrate the updated modeling results from each of the modeling teams.
5. Prepare a report summarizing the test sections, characterization testing results, analysis of the fuel consumption measurements, and calibration of the models with those results conducted in Phase II of the study, and include recommendations for implementation of the results in pavement design and management.

This report presents the results of Phase I Task 4 for the asphalt-surfaced sections in the Phase I factorial. The structural response modeling for the concrete-surfaced sections is currently being completed and will be reported in a separate technical memorandum. The results of Phase I Tasks 1 through 3 are presented in a separate companion report titled “Model Development, Field Section Characterization and Model Comparison for Excess Vehicle Fuel Use Due to Pavement Structural Response” (UCPRC-RR-2015-04) that has been summarized in this report.

EXECUTIVE SUMMARY

Pavements can influence the fuel efficiency of vehicles, and therefore of their associated GHG and air pollution emissions as well, through three mechanisms that together are called *pavement-related rolling resistance* (also referred to as *pavement-vehicle interaction*, PVI). Vehicle fuel consumption and combustion-associated emissions are also influenced by a large number of other factors—among them vehicle and cargo mass, engine size and type, fuel type, tire type and inflation, driving behavior, vehicle maintenance, grades and curves, traffic congestion, traffic control, wind, as well as several other factors, and the number of miles traveled—and many of these are actually known to have a greater influence on fuel economy than pavement characteristics. However, not all these factors are present at all times, many must be controlled vehicle by vehicle or driver by driver, and some, such as grades and curves, either cannot be changed or are extremely expensive to change. Although the effects of pavements on vehicle fuel economy are not necessarily the largest ones, they are sufficiently large to warrant attention because they affect every vehicle traveling on the pavement and can be managed on a fairly widespread basis through pavement management and design.

A general summary of the effects of pavement characteristics on vehicle fuel economy is presented below, along with the resulting environmental impacts of fuel economy changes,

- For the typical ranges of pavement roughness—measured in terms of International Roughness Index (IRI)—found on U.S. highway networks, roughness generally has a greater effect on fuel economy than either structural responsiveness or macrotexture. According to recently calibrated models, the effect is essentially linear, with the sensitivity of the relationship between fuel economy and roughness dependent on the vehicle type.
- According to recently calibrated models, for the typical ranges of IRI found on well-maintained U.S. highway pavements, macrotexture generally exerts a much smaller influence than IRI, to the point that it is statistically insignificant for all types of traffic except heavy trucks moving at low speeds.
- Regarding structural responsiveness and its effect on vehicle fuel economy: several models have been developed for measuring vehicle fuel economy on different pavement structures under different conditions, and there have been a number of field studies where measurements of this type have been performed. These studies indicate that under certain conditions the structural responsiveness of different pavements to vehicle loading can have a measureable effect which, like that of roughness and macrotexture, is variable, again depending on vehicle type and operating conditions. Unlike roughness and macrotexture, the effect of structural responsiveness is highly variable, and depends on temperature, which fluctuates daily and seasonally, and the underlying support conditions, which fluctuate seasonally. In general, the measured effects from different pavement structures range from

approximately no difference under some conditions of vehicle type/operation and climate conditions to effects on the same order of magnitude as high levels of highway roughness under the most extreme temperature and loading conditions at certain times of the year. The effects also depend on the viscoelastic properties of the pavement materials, primarily the type and age of the asphalt materials located near the surface.

In general, structural response modeling and measurements to date indicate that lighter and faster vehicles, as well as colder conditions, result in smaller differences in rolling resistance between different pavements whereas heavier and slower vehicles under hotter conditions result in larger differences. The frequencies at which these conditions occur in combination with traffic patterns control the net effect on fuel economy of structural responsiveness for a given structure.

- The influence of structural responsiveness on vehicle fuel economy has not yet been comprehensively validated with any experiment that has characterized pavement structures in terms of their responsiveness under different conditions. As a result, the available models have not been calibrated with the type of data that allows the general application of the models to evaluate in-service pavements under the range of traffic and climatic conditions that occur daily, seasonally, and from location to location. Research is needed that uses field measurements of fuel economy for a range of vehicles, climates, and pavement structural responses, while controlling for roughness and macrotexture, to complete the calibration and validation of models that can be used to make design and management decisions.
- The relative impacts of decisions affecting the different pavement vehicle interaction mechanisms discussed in this section are highly context sensitive, with the benefits from changing existing practices dependent on the baseline conditions in terms of existing roughness, macrotexture conditions, and pavement structural responsiveness.

This study addresses two problems: (a) the structural response energy dissipation models have not been compared with each other for the range of pavement types, vehicles, and climates in California, and (b) the models have also not been validated with comprehensive field data. This is summed up by a statement from a recent review of pavement rolling resistance prepared by the Swedish Road and Transport Research Institute (VTI) and other MIRIAM partners:

> The overall conclusion is that pavement stiffness cannot be excluded as an important factor influencing rolling resistance, and should be included in studies in the MIRIAM project. The still open question is as to what extent and under which conditions (temperature, type of pavement and light versus heavy vehicles) stiffness is a major factor to consider.

The purpose of this project is to develop calibrated and validated models for vehicle energy consumption due to pavement deflection for use in pavement management and design. The goals of this project are, first, to compare different pavement structural response energy dissipation models and the results they provide for estimated fuel consumption for a range of California pavements, vehicles, and climates using well-characterized and well-documented field test sections, and, second, to verify the same models using the results of field measurements on the same sections with instrumented vehicles following the general approach used by Michigan State University for NCHRP Project 1-45. This work is part of Caltrans/UCPRC participation in the MIRIAM (Models for rolling resistance In Road Infrastructure Asset Management systems) project which is being performed by a consortium of European national highway research laboratories and the Federal Highway Administration (FHWA) as well as Caltrans and UCPRC.

Each goal will be accomplished through a separately funded phase with the following tasks:

Phase I (Partnered Pavement Research Center Strategic Plan Element [PPRC SPE] 4.49)

1. Identify modelers interested in participating in the project, and critically review the existing models.
2. Identify pavement test sections that span the range of pavement structures, traffic, and climate conditions across the state, then have modelers estimate vehicle fuel consumption differences due to pavement structural response (called excess fuel consumption) for the range of California vehicles and conditions for each test section.
3. Summarize and compare modeling results received from each group in a report. Prepare a summary report of results.
4. Use the model results to simulate the annual vehicle excess fuel consumption caused by pavement structural response on each of the asphalt-surfaced test sections for typical traffic and climate in California and to compare those results with the excess fuel consumption caused by roughness and surface macrotexture, and then prepare a report summarizing the results. Based on those results regarding the importance of fuel consumption attributed to structural response, include in the report a recommendation regarding the need for Phase II experimental work.
5. Develop and submit an experimental plan for fuel economy evaluation in Phase II.
6. Hold a webinar and a question session to communicate results of Phase I.

Phase II (PPRC SPE 4.53)

1. Update characterizations of the pavement test sections included in Phase I.
2. Provide updated characterization data to modelers to update modeling results for the sections. Obtain results of the updated modeling of test sections.
3. Measure vehicle fuel consumption of a range of vehicles on the pavement test sections modeled as part of Phase I, including consideration of all factors potentially affecting the results.
4. Analyze measurements and use the results to calibrate the updated modeling results from each of the modeling teams.
5. Prepare a report summarizing the test sections, characterization testing results, analysis of the fuel consumption measurements, and calibration of the models with those results conducted in Phase II of the study, and include recommendations for implementation of the results in pavement design and management.

This report presents the results of Phase I Task 4 for the asphalt-surfaced sections in the Phase I factorial. The structural response modeling for the concrete-surfaced sections is currently being completed and will be reported in a separate technical memorandum. The results of Phase I Tasks 1 through 3 are presented in a separate companion report titled "Model Development, Field Section Characterization and Model Comparison for Excess Vehicle Fuel Use Due to Pavement Structural Response" (UCPRC-RR-2015-04) that has been summarized in this report.

All of the tasks for this project are summarized in the figure below. The tasks included in the report on field section characterization and modeling and those included in this report on the simulations are indicated in the figure.

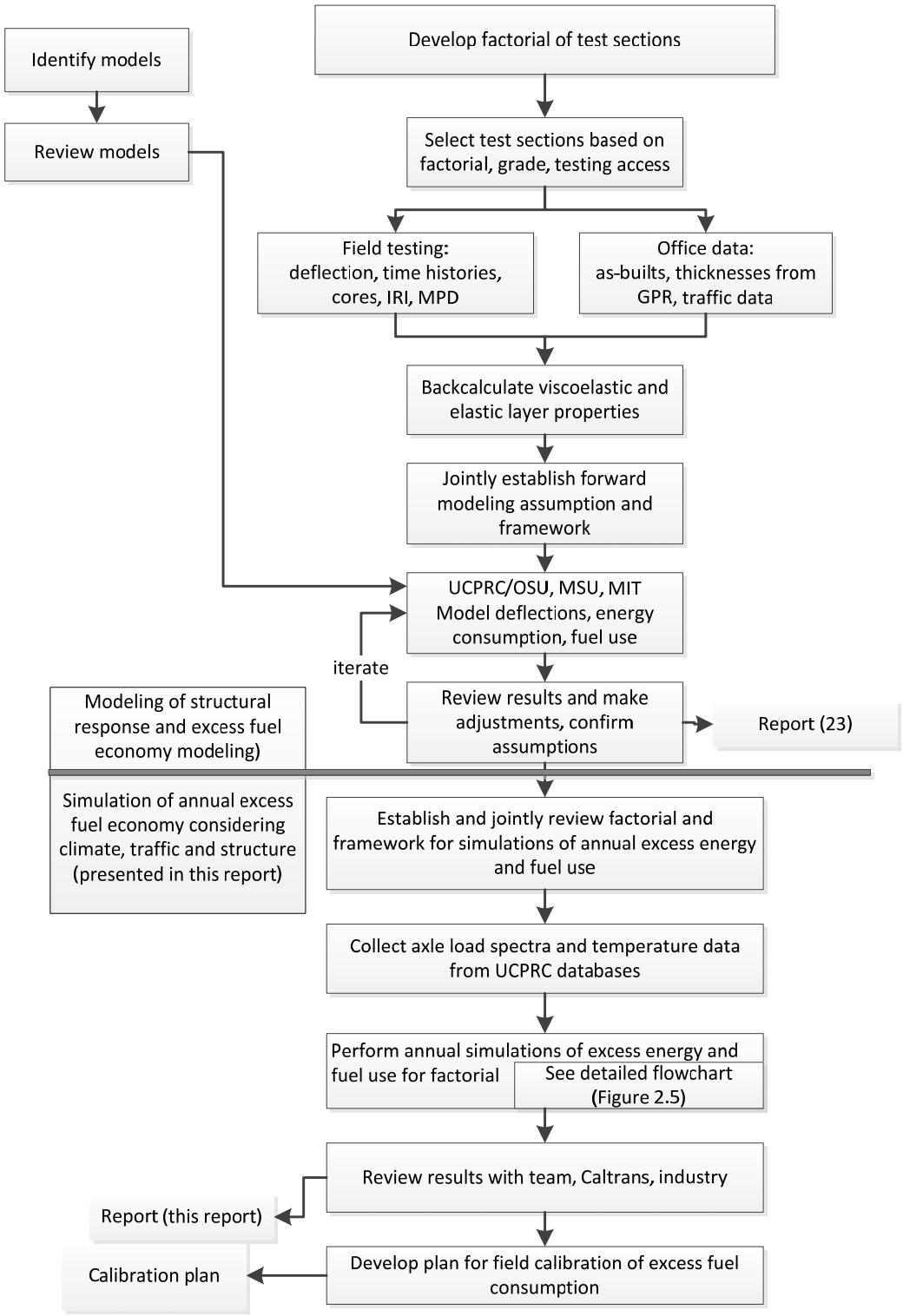

Overall process of modeling and simulation.

The next figure shows a more detailed flow chart of the process of simulating excess fuel consumption due to structural response (EFC_S) used in this step. First, the results of the modeling factorial (three axle loads, two speeds, two temperatures) for energy consumed by structural response (whether by the pavement or by the vehicle without consideration of inefficiency, depending on the approach in each model) were used to develop continuous functions of energy consumed by structural response for the model approaches used by each participating modeling group: Oregon State University (OSU), Michigan State University (MSU), and the Massachusetts Institute of Technology (MIT). The continuous function was used for interpolation between the few values in the modeling factorial to all conditions of temperature and traffic across the year for each section. Extrapolation was needed for a few extremely heavy truck axle loads. The simulation of EFC_S used the continuous energy function for each section to calculate the hourly energy consumed across all weekdays and weekends with the joint distribution of traffic flow and composition (cars, SUVs, trucks), axle load spectra for the trucks, traffic speed for cars and trucks, and asphalt temperature across the year. Traffic flow, axle load distributions, and traffic speeds for weekdays and weekends were assumed to be constant across the year.

The final step in the simulations was to sum the EFC for each mechanism (structural response, IRI, and macrotexture as measured by mean profile depth [MPD]) across the year. The results were then reviewed by all of the modeling teams and their comments were incorporated into this report, which has been prepared for submission to Caltrans and then industry.

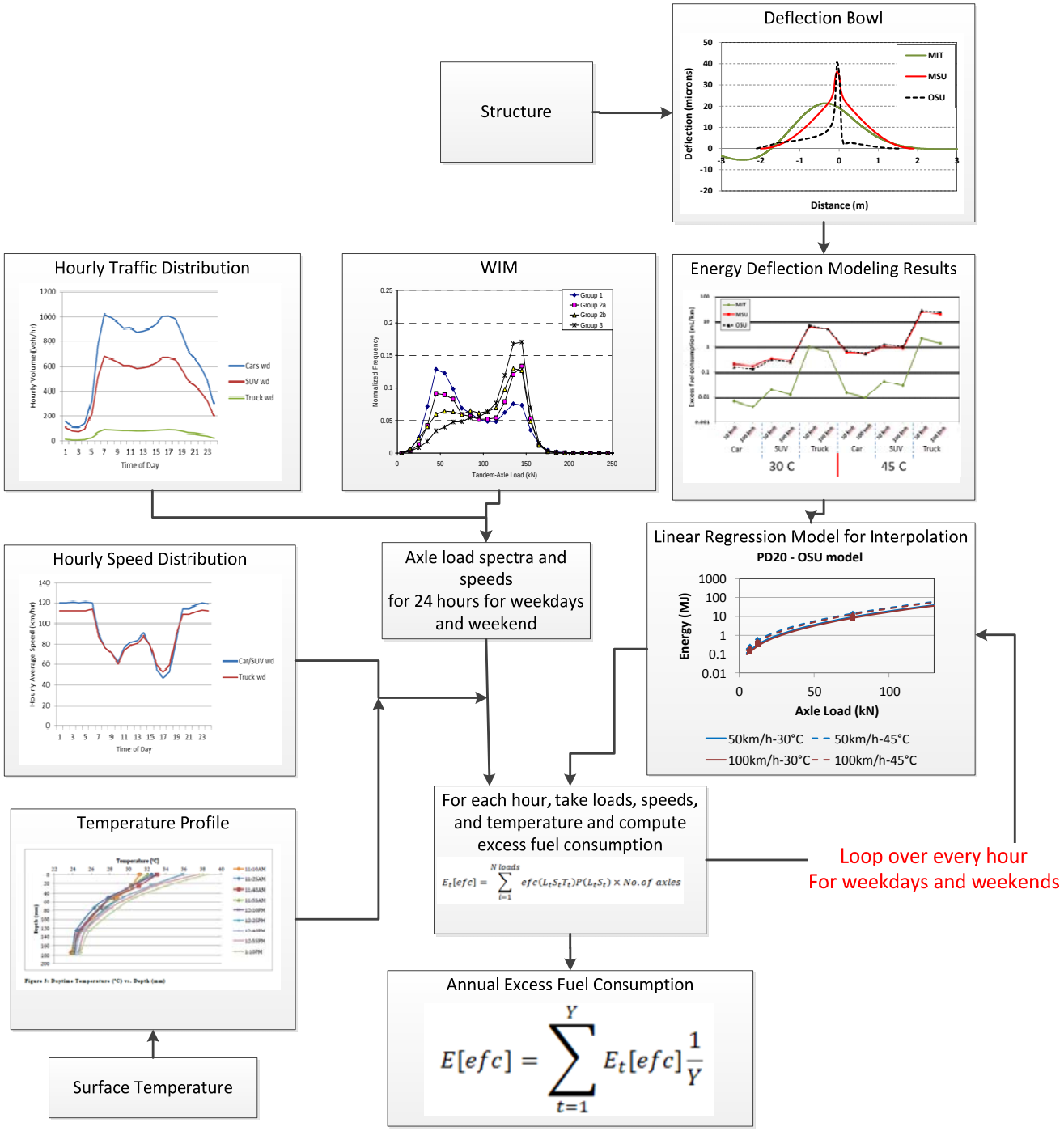

Flowchart of approach for simulation of annual excess fuel consumption due to structural response.

The following conclusions have been drawn from the results of this study:

- General modeling conclusions:
  - The three modeling approaches produced different results, although with similar orders of magnitude. Overall, the MIT approach produced the smallest estimates of excess fuel consumption due to structural response (EFC_S), as expected from the modeling approach, while the MSU approach produced the largest, and the OSU approach generally produced EFC_S results in between the others. However, there were a number of exceptions to these average results for individual sections.
  - Without field validation to determine how well each approach models the broad range of pavement structures in the field experiment factorial, the best modeling approach is not apparent.
  - Field validation, and if necessary field calibration, is needed to produce models that can be used in practice because of there are limitations in any modeling approach.
- Results for seventeen asphalt-surfaced sections analyzed for excess fuel consumption due to structural response and averages across the factorial of climate and traffic conditions show the following:
  - Compared to an ideal pavement with no structural response, EFC_S ranged from 0.02 to 0.61 mL/km/veh for the MIT model, 0.03 to 0.48 mL/km/veh for the OSU model, and 0.04 to 0.92 mL/km/veh for the MSU model, using section-specific traffic and climate data. The sections had an average of 7.5 percent trucks. Across all sections, the MIT, MSU, and OSU models predicted average EFC_S of 0.12, 0.18, and 0.28 mL/km/veh, which translates to average fuel economy percentage changes of 0.09, 0.13, and 0.20 percent in fuel economy per vehicle across all vehicles.
  - Compared to an ideal pavement with no structural response, EFC_S ranged from 0.03 to 0.70 mL/km/veh for the MIT model, 0.04 to 0.79 mL/km/veh for the OSU model, and 0.06 to 1.41 mL/km/veh for the MSU model, across the test sections from simulation of the factorial of traffic and climate data. The factorial had an average of 10 percent trucks. Across all sections, the MIT, MSU, and OSU models predicted average EFC_S of 0.18, 0.30, and 0.43 mL/km/veh, which translates to average fuel economy changes of 0.12, 0.21, and 0.29 percent per vehicle across all vehicles.
  - These results show that the EFC_S increases as the percentage of trucks increases, with trucks having between 6 and 15 times greater increase per vehicle than cars and SUVs, depending on the model.
  - EFC_S is approximately 1.4 times greater in the Desert and Inland Valley climate regions compared with the average of the cooler Central and South Coast climate regions, based on results of the factorial simulation.

- EFC_S increases at a rate of approximately 0.014 to 0.025 mL/km/veh (depending on the model) with each one percent increase in the percentage of trucks.
- From the section-specific simulations, excess fuel consumption due to roughness (IRI) and macrotexture (MPD) ranged from 0.14 to 3.20 mL/km/veh compared with an ideal pavement, with an IRI of 38 inches/mile (0.6 m/km) and macrotexture of 0.5 mm, with the effects of roughness approximately ten times greater than those of macrotexture.
- The combined effects of roughness and macrotexture on EFC far exceeded the EFC values calculated based on the effect of structural response using the MIT, OSU, and MSU models. The combined effect of roughness and macrotexture was roughly seven times greater than the structural response result from the MIT model, five times greater than the OSU model's result, and three times greater than the result from the MSU model. It should be noted that these are average values across section-specific simulations with an average truck percentage of 7.5 percent, and that the sections analyzed for structural response were nearly all fairly smooth (IRI less than 100 inches/mile [1.6 m/km]). Compared with the one rough section (Pavement Deflection [PD] Section 14, IRI of 226 inches/mile [3.57 m/km]), these ratios become 27, 18, and 11 times greater for roughness plus macrotexture effects versus structural response effects for the MIT, OSU, and MSU models respectively.
- It should be noted that none of the models includes predictions of damage caused by traffic and the environment which would change stiffness; damage must be predicted separately using mechanistic-empirical or other models. Similarly, change in IRI over time must be predicted separately from the models used in this study.

- Within the factorial of climate regions and traffic across the seventeen asphalt-surfaced sections analyzed for structural response:
  - Results are generally more sensitive to pavement temperature (climate region) compared with urban versus rural traffic speed and volume patterns typical for California.
  - Axle loads are very important, as was reflected in the high sensitivity of EFC_S to axle load spectra and the percentage of trucks.
  - The MIT model ranked the pavement types (composite, flexible, semi-rigid) differently from the OSU and MSU models for EFCS. MIT ranked them 1, 2, and 3 in terms of best to worst, while OSU and MSU ranked them 3, 2, and 1, for the small sample of each type in the factorial analyzed.
- General conclusions
  - Although it appears to be generally less important than the effects of roughness for the sections analyzed, the results for EFC_S appear to be sufficiently large, and the differences between the

models large enough, to warrant field validation and calibration of the models. Field testing is necessary to enable consideration of structural response in project-level and network-level analysis to support decision-making.

- Calibration should focus on the most sensitive variables:
  - Pavement structure in terms of asphalt thickness and stiffness/phase angle master curve (analysis of the concrete sections in the field section factorial needs to be completed as well)
  - Wheel load
  - Pavement temperature, which is important for asphalt pavements
  - Speed, which is important for asphalt pavements and may be important for concrete pavements
- Validation and calibration should consider any possible interaction of roughness and structural response and include a check on the EFC model for roughness used in this study by including several rough sections in the field section factorial.

The following recommendations are based on the conclusions of the study:

- Complete and improve modeling
  - Model the concrete pavements using different approaches.
  - Consider multiple layers in the asphalt, particularly near the surface to better evaluate the effects of rubberized asphalt surface materials.
  - Check the effects of full dynamic pavement modeling (inertial effects in the pavement) on more than the one section analyzed which showed an approximate 6 percent increase in EFC_S compared with the results for the OSU model (results presented in companion modeling report), if it is decided that the cost of addition modeling is warranted by the potential additional accuracy.
- Begin field validation and calibration of the models and rerun the simulations with the improved and calibrated models for all pavement surface types.

CONVERSION FACTORS

SI* (MODERN METRIC) CONVERSION FACTORS

APPROXIMATE CONVERSIONS TO SI UNITS

Symbol	When You Know	Multiply By	To Find	Symbol
		LENGTH		
in	inches	25.4	Millimeters	mm
ft	feet	0.305	Meters	m
yd	yards	0.914	Meters	m
mi	miles	1.61	Kilometers	Km
		AREA		
in^2	square inches	645.2	Square millimeters	mm^2
ft^2	square feet	0.093	Square meters	m^2
yd^2	square yard	0.836	Square meters	m^2
ac	acres	0.405	Hectares	ha
mi^2	square miles	2.59	Square kilometers	km^2
		VOLUME		
fl oz	fluid ounces	29.57	Milliliters	mL
gal	gallons	3.785	Liters	L
ft^3	cubic feet	0.028	cubic meters	m^3
yd^3	cubic yards	0.765	cubic meters	m^3
		NOTE: volumes greater than 1000 L shall be shown in m^3		
		MASS		
oz	ounces	28.35	Grams	g
lb	pounds	0.454	Kilograms	kg
T	short tons (2000 lb)	0.907	megagrams (or "metric ton")	Mg (or "t")
		TEMPERATURE (exact degrees)		
°F	Fahrenheit	5 (F-32)/9 or (F-32)/1.8	Celsius	°C
		ILLUMINATION		
fc	foot-candles	10.76	Lux	lx
fl	foot-Lamberts	3.426	$candela/m^2$	cd/m^2
		FORCE and PRESSURE or STRESS		
lbf	poundforce	4.45	Newtons	N
lbf/in^2	poundforce per square inch	6.89	Kilopascals	kPa

APPROXIMATE CONVERSIONS FROM SI UNITS

Symbol	When You Know	Multiply By	To Find	Symbol
		LENGTH		
mm	millimeters	0.039	Inches	in
m	meters	3.28	Feet	ft
m	meters	1.09	Yards	yd
km	kilometers	0.621	Miles	mi
		AREA		
mm^2	square millimeters	0.0016	square inches	in^2
m^2	square meters	10.764	square feet	ft^2
m^2	square meters	1.195	square yards	yd^2
ha	Hectares	2.47	Acres	ac
km^2	square kilometers	0.386	square miles	mi^2
		VOLUME		
mL	Milliliters	0.034	fluid ounces	fl oz
L	liters	0.264	Gallons	gal
m^3	cubic meters	35.314	cubic feet	ft^3
m^3	cubic meters	1.307	cubic yards	yd^3
		MASS		
g	grams	0.035	Ounces	oz
kg	kilograms	2.202	Pounds	lb
Mg (or "t")	megagrams (or "metric ton")	1.103	short tons (2000 lb)	T
		TEMPERATURE (exact degrees)		
°C	Celsius	1.8C+32	Fahrenheit	°F
		ILLUMINATION		
lx	lux	0.0929	foot-candles	fc
cd/m^2	$candela/m^2$	0.2919	foot-Lamberts	fl
		FORCE and PRESSURE or STRESS		
N	newtons	0.225	Poundforce	lbf
kPa	kilopascals	0.145	poundforce per square inch	lbf/in^2

*SI is the symbol for the International System of Units. Appropriate rounding should be made to comply with Section 4 of ASTM E380 (Revised March 2003)

TABLE OF CONTENTS

PROJECT OBJECTIVES ..... **iii**
EXECUTIVE SUMMARY ..... **v**
CONVERSION FACTORS ..... **xv**
LIST OF FIGURES ..... **xviii**
LIST OF TABLES ..... **xix**
LIST OF ABBREVIATIONS ..... **xx**
1. INTRODUCTION **1**
1.1 Project Background 1
1.1.1 Roughness and Macrotexture Effects 5
1.1.2 Pavement Structural Responsiveness to Loading Effects 5
1.2 Project Goal and Objectives 9
1.3 Scope of Report 10
2. EXPERIMENT DESIGN, TESTING, MODELING, AND SIMULATION APPROACHES **11**
2.1 Overall Approach 11
2.2 Approach and Experiment Design for Field Characterization and Modeling of Energy Due to Structural Response 12
2.2.1 Modeling Approach 12
2.2.2 Field Test Sections 13
2.3 Summary of Field Section Characterization and Modeling Results 17
2.3.1 Field Test Section Characterization 17
2.3.2 Overview of Structural Response Models 19
2.3.3 Dissipated Energy due to Structural Response Modeling Results 23
2.4 Annual Impact Simulation Approach and Experiment Design 24
2.4.1 Simulation Approach 24
2.4.2 Simulation Experiment Design Factorial 27
2.5 Interpolation and Extrapolation of Structural Response Modeling Results 43
3. ANNUAL FUEL USE SIMULATION RESULTS FOR TEST SECTIONS **47**
4. ANALYSIS AND INTERPRETATION **53**
4.1 Analysis of Results for Different Vehicle Types 53
4.2 Analysis of Results for Different Structures and Surfaces for Structural Response 53
4.2.1 Pavement Structure Type 53
4.2.2 Pavement Surface Type (Conventional or Rubberized) 54
4.3 Analysis of Results for Traffic and Climate for Structural Response 54
4.3.1 Rural and Urban Traffic Regimes 54
4.3.2 Climate Region 57
4.3.3 Axle Load Spectra 58
4.4 Analysis of Results for Different Surfaces for Roughness and Macrotexture 59
4.5 Summary of Results and Interpretation 60
5. CONCLUSIONS AND RECOMMENDATIONS **65**
5.1 Conclusions 65
5.2 Recommendations 67
REFERENCES **69**
APPENDIX A: TEMPERATURE DISTRIBUTION DATA **73**
APPENDIX B: AXLE LOAD SPECTRUM DATA **82**
APPENDIX C: TRAFFIC DISTRIBUTION DATA **108**
General Description on Traffic Information for PD Sections 108
Traffic Information (Urban Highway) 109
Traffic Information (Rural Highway) 110
APPENDIX D: DETAILED SIMULATION RESULTS FOR EACH STRUCTURAL MODELING APPROACH **111**

LIST OF FIGURES

Figure 2.1: Overall process of modeling and simulation. 11
Figure 2.2: Locations of final test sections. 17
Figure 2.3: Meshed OSU model structure in Abaqus. 20
Figure 2.4: Location of the wheel in the deflection basin and tire/pavement contact area where gradient is considered for energy needed to move up the side of basin in the MSU approach. 21
Figure 2.5: Flowchart of approach for simulation of annual excess fuel consumption due to structural response. 26
Figure 2.6: Nine California pavement design climate regions. 29
Figure 2.7: Example cumulative distributions of pavement temperature at one-third of asphalt depth from *CalME* 1-d approximation and interpolation based on database of EICM runs for nine California climate regions (PD 7 example shown). 30
Figure 2.8: Comparison of average monthly air temperatures for 1961, used for simulations, and other years... 30
Figure 2.9: Flowchart for grouping highways based on axle load spectra. 33
Figure 2.10: Four most common axle load spectra groups on California state highways. 34
Figure 2.11: Example axle load frequencies for different weekday periods for rural section with Group 2a axle load spectrum and 10 percent trucks. 36
Figure 2.12: Urban volume distributions. 39
Figure 2.13: Urban speed distributions. 40
Figure 2.14: Rural volume distributions. 41
Figure 2.15: Rural speed distributions. 42
Figure 2.16: Best fit continuous relationships for energy consumption versus axle load, temperature,and speed for PD 20. 45
Figure 3.1: Average structural response simulation results in terms of Excess Fuel Consumption due to structural response (EFC_S) by asphalt section relative to no structural response effect (avg mL/km/veh EFC) simulated with section-specific traffic and climate. 50
Figure 3.2: Average structural response simulation results in terms of Excess Fuel Consumption due to structural response (EFC_S) by asphalt section relative to no structural response effect (avg mL/km/veh EFC) across traffic and climate factorial. 51
Figure 3.3: Average roughness, macrotexture, and combined roughness and macrotexture simulation results in terms of Excess Fuel Consumption due to roughness and macrotexture (EFC_{IRI}, EFC_{MPD}) and combined roughness and macrotexture ($EFC_{IRI+MPD}$) relative to 38 inches/mile IRI and 0.5 mm MPD by section (avg mL/km/veh EFC) simulated with section-specific traffic and climate. 52
Figure 4.1: Structural response simulation results: factorial by percent of trucks and vehicle speed regime (urban/rural) from factorial simulation. 56
Figure 4.2: Average structural response simulation results across factorial with change in percent trucks. 56
Figure 4.3: Average structural response simulation results by climate region across factorial. 58
Figure 4.4: Average structural response simulation results by axle load spectrum group across factorial. 59
Figure 4.5: Average combined EFC for roughness and macrotexture across factorial. 60

LIST OF TABLES

Table 2.1: Summary of Final Test Sections 15
Table 2.2: Coefficients pij (with 95% Confidence Bounds) 23
Table 2.3: Vehicles Used for Structural Response Modeling 24
Table 2.4: WIM Site Groupings Based on All Axle Load Spectra 32
Table 3.1: Summary of Excess Fuel Consumption due to Structural Response, Roughness, and Macrotexture for Each Test Section Simulated with Section-Specific Traffic and Climate 48
Table 3.2: Summary of Excess Fuel Consumption due to Structural Response, Roughness, and Macrotexture for Each Test Section Simulated Across Factorial 49
Table 4.1: Average EFC_S for Each Vehicle Type and Model Approach across the Simulation Factorial and All Sections (mL/km/veh) 53
Table 4.2: Average EFC Due to Structural Response by Asphalt-Surfaced Pavement Type and Model from Factorial Simulation 53
Table 4.3: Average EFC Due to Structural Response by Rubberized and Conventional Asphalt-Surfaced Type and Model from Factorial Simulation 54
Table 4.4: Average EFC_S (mL/km/veh) for Rural and Urban Speed and Flow Regimes and Different Percentages of Trucks from Factorial Simulation 55
Table 4.5: Average EFC_S (mL/km/veh) for Nine Pavement Design Climate Regions from Factorial Simulation 57
Table 4.6: Average EFC_S (mL/km/veh) for Four Axle Load Spectra from Factorial Simulation 58
Table 4.7: Descriptive Statistics for EFC Results for Site-Specific Traffic and Climate of Asphalt-Surfaced Test Sections 61
Table 4.8: Approximate Percent Change in Fuel Economy across Asphalt-Surfaced Sections and Site-Specific Simulations if EFC_S Reduced to Zero 63
Table 4.9: Approximate Percent Change in Fuel Economy across Asphalt-Surfaced Factorial and All Sections if EFC_S Reduced to Zero for Hot Inland Valley Climate and Desert Regions and Cool Coastal Regions 63
Table 4.10: Approximate Percent Change in Fuel Economy across All Asphalt-Surfaced Sections Analyzed and for a High Roughness Section Only (PD 14) if IRI Reduced to 0.6 m/km (38 inches/mile) Using Section-Specific Simulations 63
Table D.1: Excess Fuel Consumption for Structural Response (mL/km/veh) by Vehicle Type for Section-Specific Actual Traffic and Climate 111

LIST OF ABBREVIATIONS

AADTT	Annual average daily truck traffic
AC	Asphalt concrete
APCS	Automated Pavement Condition Survey
CRCP	Continually reinforced concrete pavement
DGAC	Dense-graded asphalt concrete
EFC	Excess fuel consumption
EFC_{IRI}	EFC for roughness
EFC_{MPD}	EFC for macrotexture
EFC_{S}	EFC for structural response
EICM	Enhanced Integrated Climate Model
FE	Finite element
FHWA	Federal Highway Administration
FSCH	Frequency sweep at constant height
FWD	Falling Weight Deflectometer
GHG	Greenhouse gas
GPR	Ground penetrating radar
IRI	International Roughness Index
JPCP	Jointed plain concrete pavement
LTS	Laser Texture Scanner
MIRIAM	*Models for rolling resistance In Road Infrastructure Asset Management systems* project
MIT	Massachusetts Institute of Technology
MPD	Mean profile depth
MSU	Michigan State University
MTD	Mean texture depth
NCHRP	National Cooperative Highway Research Program
OSU	Oregon State University
PD	Deflection project test section
PeMS	Performance Measurement System
PG	Performance Graded
PPRC	Partnered Pavement Research Center
PVI	Pavement-vehicle interaction
RHMA	Rubberized hot mix asphalt
SUV	Sport utility vehicle
UCPRC	University of California Pavement Research Center
VMT	Vehicle miles-traveled
VTI	Swedish Road and Transport Research Institute
WIM	Weigh-in-motion
WLF	Williams-Landel-Ferry

1. INTRODUCTION

1.1 Project Background

Pavements can influence the fuel efficiency of vehicles, and therefore of their associated GHG and air pollution emissions as well, through three mechanisms that together are called *pavement-related rolling resistance* (also referred to as *pavement-vehicle interaction*, PVI). Vehicle fuel consumption and combustion-associated emissions are also influenced by a large number of other factors—among them vehicle and cargo mass, engine size and type, fuel type, tire type and inflation, driving behavior, vehicle maintenance, grades and curves, traffic congestion, traffic control, wind, as well as several other factors, and the number of miles traveled—and many of these are actually known to have a greater influence on fuel economy than pavement characteristics. However, not all these factors are present at all times, many must be controlled vehicle by vehicle or driver by driver, and some, such as grades and curves, either cannot be changed or are extremely expensive to change. Although the effects of pavements on vehicle fuel economy are not necessarily the largest ones, they are sufficiently large to warrant attention because they affect every vehicle traveling on the pavement and can be managed on a fairly widespread basis through pavement management and design.

The Federal Highway Administration's recently published *Towards Sustainable Pavement Systems: A Reference Document (1)* includes a summary of the information available as of 2014 regarding pavement-related rolling resistance. That information, prepared by the UCPRC and reviewed by an FHWA task group, is presented in condensed form in a companion report to this one on the modeling of pavement structural response on vehicle fuel economy modeling. That companion report is briefly summarized here to provide background for the results presented in this current report.

Analysis of the effects of pavement rolling resistance on vehicle fuel economy and emissions needs to consider the total system of the pavement, road geometry, vehicles and their operation, and climate. The pavement characteristics influencing vehicle fuel economy are summarized as follows (more details are presented in Sandberg *[2]* and Jackson et al. *[3]*):

1. *Roughness:* the consumption of vehicle energy through the working of shock absorbers and drive train components, and deformation of tire sidewalls as the wheels pass over deviations from a flat surface in the wheelpath with wavelengths greater than 1.6 ft (0.5 m) and less than 164 ft (50 m). The working of these vehicle components converts mechanical energy into heat that is then dissipated into the air, requiring greater work by the engine than would be necessary to propel the vehicle along a perfectly smooth surface. Roughness is built into the pavement during construction and generally increases over time as the pavement ages and distresses develop, and is further influenced by subsequent maintenance

and rehabilitation timing and treatment type. Roughness on some pavement types can undergo relatively small changes with daily temperature fluctuations. For a given roughness condition, this rolling resistance mechanism affects all vehicles all the time. The relationship between IRI and fuel consumption has some sensitivity to speed.

2. *Macrotexture:* the consumption of vehicle energy through the viscoelastic working of the deformable tire tread rubber in the tire-pavement contact patch as it passes over positive surface macrotexture and converts it into heat dissipated into the rest of the tire and into the air. Positive macrotexture is produced by stones or other texture protruding above the average plane of the pavement surface with wavelengths of 0.02 to 2 inches (0.5 to 50 mm). It is the primary pavement characteristic controlling surface friction at high speeds under wet conditions and the potential for hydroplaning *(4, 5)*. Pavements serving high-speed vehicles must have a minimum amount of surface macrotexture and/or sufficient permeability to remove water films from the pavement surface so that frictional resistance is maintained for steering and braking. Macrotexture is provided by the characteristics of the surfacing materials (primarily relevant to asphalt surfaces) and texturing (primarily relevant to concrete surfaces), as well as by subsequent maintenance and rehabilitation timing and treatment type. Macrotexture does not change due to daily or seasonal temperature and moisture conditions, although it can increase or decrease with age depending on the pavement surface materials, texture type, traffic, climate, and use of chains or studded tires. For a given macrotexture, this rolling resistance mechanism affects all vehicles all the time. The relationship between macrotexture and fuel consumption has some sensitivity to speed.
3. *Structural responsiveness:* the consumption of vehicle energy caused by the structural response of the pavement through deformation of pavement materials under passing vehicles, including delayed deformation of viscoelastic materials and other damping effects that consume energy in the pavement and subgrade. This mechanism has also been characterized in terms of the delayed deformation of the pavement under the wheel such that the moving wheel is moving against a slope *(6, 7)*. Pavement structural responsiveness to loading is determined by layer thicknesses, stiffnesses and material types that determine viscoelastic and elastic pavement response under different conditions of wheel loading and vehicle speed, and temperature and moisture conditions. For a given pavement structure, the effect of this mechanism on viscoelastic materials such as asphalt can be highly dependent on daily and seasonal changes in pavement temperatures (particularly near the surface), and is more sensitive to vehicle speeds and loading than are roughness and macrotexture. Structural responsiveness can change with time.

As noted above, roughness, macrotexture, and structural responsiveness can change over the life of the pavement surface. In addition, structural responsiveness can change under daily and seasonal temperature and

moisture conditions independent of pavement deterioration depending on pavement type and other conditions, while macrotexture and roughness generally remain constant due to seasonal variations in temperature and water (except in some cases for undoweled jointed plain concrete pavement which can experience some changes in roughness due to curling from temperature gradient changes). The effects of these mechanisms over the life cycle are controlled by decisions regarding design, construction, and maintenance and rehabilitation applications.

The pavement structural responsiveness at the time of construction under different conditions of temperatures, traffic speeds, and wheel loadings is determined by the pavement type, the materials used, and the design of the structural section. The overall deformation of the pavement structure is controlled by the stiffness and thickness of the layers, and the extent of viscoelastic (delayed elastic) stiffness behavior that the layer materials exhibit under different temperatures and at specific times of loading. Together, these factors determine the energy dissipated by the pavement structural response and the effect on vehicle fuel economy. Thicker and stiffer layers reduce the deformation response of the pavement, with a given percent change of thickness generally having a greater effect than a same percent change in stiffness because in simplified terms, the deflection of the pavement is related to the Eh^3 of the pavement layers, where E is the stiffness and h is the thickness. In addition, materials with a greater delay in their response (more viscoelastic as opposed to elastic) will consume more energy due to the interaction of the wheel and the pavement.

Most concrete and cement-stabilized materials demonstrate elastic response and do not change stiffness under the range of temperature and traffic-loading conditions typically experienced by in-service pavements. For asphalt layers and asphalt-stabilized layers, the stiffness and extent of delayed elastic response is dependent on the type of asphalt binder, temperature, and traffic speed. Stiffness decreases under hotter temperatures and slower-moving wheel loads, but increases under colder temperatures and faster-moving wheel loads.

The interaction of variations in pavement temperature profiles through the asphalt layers and variations in traffic loading and speeds with the materials properties determines the structural responsiveness of the asphalt layers throughout the year. Because temperatures change more at the surface, these effects are most important near the surface. Asphalt materials tend to “age” over time, increasing in stiffness by having less viscoelastic and more elastic response, which reduces deflections but is also associated with increased risk of top-down cracking. Aging occurs most rapidly over the first five years after placement, and is also greater near the surface due to increased exposure to heat, UV light from the sun, and atmospheric oxygen. Research indicates that the stiffness of asphalt mixes can increase by a factor of approximately 2.3 to 4.3 over periods of up to eighteen years,

dependent primarily on the asphalt binder and the climate *(8).* The stiffness of asphalt layers in the wheelpaths can be reduced towards the end of their structural life as a result of fatigue damage caused by repeated loading.

The stiffness of unbound granular layers depends on the applied stress (both magnitude and duration) and the saturation of the material. Subgrade materials can also be a source of damping. High moisture contents in the subgrade and granular pavement layers, due to unsealed surface cracking or poor drainage, can cause significant reductions in their stiffness.

The additional fuel use of on-road vehicles caused by different levels of roughness, macrotexture, and structural responsiveness can have an environmental impact. From a life-cycle perspective, these impacts must be balanced with consideration of the environmental impacts of building, maintaining, and rehabilitating pavements in order to sustain a smooth condition, to minimize excessive positive macrotexture, and to elicit lower levels of structural responsiveness. The on-road transportation sector is a leading source of greenhouse gas (GHG) emissions in California (33.6 percent of total, 154.06 million metric tons CO2-e per year *[9]),* but it must be remembered that the production and transportation of pavement materials such as asphalt, cement, steel, lime and aggregate, as well as the consumption of fuel by construction equipment, also produce emissions. Optimization in pavement design and management of the longevity of the pavement design and of the maintenance/rehabilitation treatment type and frequency must take into consideration all of the life-cycle phases (Materials Production, Construction, Use and End-of-Life), but is also highly dependent on the level of traffic using the pavement.

The relative impact of pavement-related rolling resistance on fuel economy and vehicle emissions depends primarily on the level of roughness, surface macrotexture, and structural responsiveness. Vehicle types, traffic volumes and speeds, and climatic conditions also play an important role. Similarly, the relative impact of changing an agency's practices regarding different elements of pavement-related rolling resistance depends on the starting points in the network for roughness, macrotexture, and structural responsiveness on all of the individual pavement sections in the network and their traffic and climate. For example, if the network is already particularly smooth, then those practices should be continued, and additional changes in practice to further improve smoothness will likely have a small effect. On the other hand, if the network has high roughness, particularly on high volume routes, then improvements in smoothness may result in high returns in reduced environmental impacts. Similar analyses can be applied to the other factors influencing pavement-related rolling resistance.

1.1.1 Roughness and Macrotexture Effects

Pavement roughness is defined as the components of pavement profile with wavelengths of 1.6 to 164 feet (0.5 to 50 m), while macrotexture is defined as the components with wavelengths of 0.02 to 2 inches (0.5 to 51 mm). The most common measure of roughness is the International Roughness Index (IRI), which is calculated using the longitudinal profile measured with an inertial profiler in the wheelpaths of the pavement. Although IRI was not primarily developed to capture the effects of pavement roughness on fuel consumption, and there are likely better parameters for that purpose, IRI does correlate with vehicle fuel use for all vehicle types, and is used by most highway agencies.

Macrotexture can be measured on asphalt-surfaced pavements and concrete pavements that do not have directional textures (tining, grooving, grinding) using high-speed lasers on the profilers used for IRI, and can be measured for directionally textured concrete pavements using other measurement techniques. The relationships between different types of concrete directional textures and vehicle fuel economy are not as clear as it is for the macrotexture of asphalt-surfaced pavements. Macrotexture as measured by mean profile depth (MPD) on asphalt and mean texture depth (MTD) on concrete (MPD and MTD are generally considered interchangeable in terms of values for fuel economy models) have an approximately linear effect on vehicle fuel economy.

A recent evaluation/calibration of the World Bank's HDM-4 model *(10)* for vehicle operating costs was made using measurements made with a fleet of representative North American vehicles. The models developed in that study that pertain to fuel consumption due to roughness and macrotexture have been used in this study.

The effects of vehicle speed have some interaction with roughness. Speed does not change the overall sensitivity of the fuel economy of cars to roughness, while roughness has approximately double the effect on heavy truck fuel economy at slow speeds compared with high speeds *(11).* The relationship between fuel consumption and macrotexture is also affected by speed, with the sensitivity varying depending on the vehicle type (*11*). Modeling results also indicate that the effects of pavement roughness on fuel economy under stop-and-start congested traffic are similar to those under steady-state traffic, even including stop-and-start traffic in congested areas *(12).*

1.1.2 Pavement Structural Responsiveness to Loading Effects

Pavement structural response to loading, the third mechanism of effective rolling resistance that can affect fuel consumption, has been modeled as two phenomena:

1. Dissipation of energy in the pavement due to the pavement's structural response under traffic loading
2. Pavement surface structural responsiveness modeled as a change in geometry between the tire and the surface

For both phenomena, larger deflections and greater delayed elasticity (more viscous damping as opposed to elastic behavior) increase the pavement rolling resistance. The first pavement structural responsiveness phenomenon, dissipation of energy in the pavement structure due to the viscoelastic nature of asphalt materials, has been the subject of recent model development by the LUNAM University/IFSTTAR *(6)*, the University of Lyon, France *(13)*, and by the University of Nottingham *(14)*. There have also been a number of previous studies employing various approaches to model structural responsiveness (e.g., *15, 16, 17, 18, 19)* that consider viscoelastic properties for some or all layers.

The second phenomenon is the subject of recent and ongoing model development at the Massachusetts Institute of Technology (MIT *[20]*, since updated). Flugge *(7)*, Chupin, Piau, and Chabot *(6)*, and Louhghalam, Akbarian, and Ulm *(21, 22)* and Zaabar and Chatti *(unpublished)* have derived or reviewed relationships between the energy needed to move vehicles forward based on the position of the wheel in the deflection basin as it is affected by the delayed elasticity of viscoelastic deflections (the second structural responsiveness phenomenon described above) and the energy dissipated in the pavement (the first phenomenon). The approach developed by Louhghalam et al. *(22)* has been used to develop a scaled relationship between the vehicle energy used to overcome pavement rolling resistance as a function of the square of the vehicle weight and the inverse of the viscous relaxation time, in addition to distinct power relations of top-layer stiffness, thickness, and subgrade modulus. This relationship was calibrated against the modeling results presented by Pouget et al. in 2012 *(21)*.

The following modeling approaches for calculating vehicle fuel consumption from pavement rolling resistance are used in this study:

- Pouget et al. as implemented with updates by Coleri and Harvey *(23)*
- Chatti and Zaabar *(11)*
- Louhghalam et al. *(22)*

An additional approach is currently being developed by the University of Illinois *(unpublished)*.

A number of field studies conducted under different temperature conditions and with different vehicles have also been performed to measure the effects of pavement type on vehicle fuel economy; these studies are summarized and cited in the companion modeling report *(23)*. Some of these field studies have shown measurable differences between pavement types, although without characterizing the structural response characteristics of the pavements, while others have not. Modeling results for structural responsiveness and its effects on vehicle fuel consumption have only been considered in one study, by Hultqvist *(24)*. This study compared the results of test section measurements against results obtained using VETO *(25)*, a mechanistic model of pavement energy consumption from vehicles that yielded results similar to the measurements. Many of the models in VETO are similar to those in HDM-4.

From the review of the various studies it can be said with reasonable certainty that the influence of structural responsiveness on fuel economy and associated environmental impacts has not been comprehensively validated with an experiment that has accounted for the broad range of environmental conditions or the various types of pavement structures used in the nation's highway network (e.g., composite pavements, semirigid pavements, rubberized and polymer-modified mixtures, doweled and nondoweled JPCP, and CRCP). The field studies conducted to date to measure the effects of dissipated energy on vehicle fuel efficiency suffer from a serious lack of characterization of the pavement structures in terms of their structural responsiveness to loading as a function of the stiffness and thickness of the pavement layers or the viscoelastic nature of the materials under different conditions of temperature and traffic speed. The structural responsiveness to vehicle loading of pavements depends on subgrade, subbase, and base support conditions, and, particularly for asphalt pavements the temperature and time of loading. Further, these responses change as the pavement materials age and deteriorate. Therefore, consideration of pavement structural responsiveness effects must be analyzed separately for each project and consider the intersection of structural responsiveness, traffic levels, traffic speeds, and pavement temperatures, and the moisture conditions in the underlying unbound layers, which vary widely with daily and seasonal climatic fluctuations.

It must also be recognized that none of the effects on vehicle fuel consumption and pavement characteristics matter much if only a few vehicles are using the pavement, and that these effects should only be considered for higher traffic volume locations from the standpoint of environmental impact on the network.

Summary

A general summary of the effects of pavement characteristics on vehicle fuel economy is presented below with the resulting environmental impacts:

- For the typical ranges of pavement roughness—measured in terms of International Roughness Index (IRI)—found on U.S. highway networks, roughness generally has a greater effect on fuel economy than either structural responsiveness or macrotexture. According to recently calibrated models, the effect is essentially linear, with the sensitivity of the relationship between fuel economy and roughness dependent on the vehicle type *(11)*.
- According to recently calibrated models *(11)*, for the typical ranges of IRI found on well-maintained U.S. highway pavements, macrotexture generally exerts a much smaller influence than IRI, to the point that it is statistically insignificant for all types of traffic except heavy trucks moving at low speeds.
- Regarding structural responsiveness and its effect on vehicle fuel economy: several models have been developed for measuring vehicle fuel economy on different pavement structures under different conditions, and there have been a number of field studies where measurements of this type have been

performed. These studies indicate that under certain conditions the structural responsiveness of different pavements to vehicle loading can have a measureable effect which, like that of roughness and macrotexture, is variable, again depending on vehicle type and operating conditions. Unlike roughness and macrotexture, the effect of structural responsiveness is highly variable, and depends on temperature, which fluctuates daily and seasonally, and the underlying support conditions which fluctuate seasonally. In general, the measured effects from different pavement structures range from approximately no difference under some conditions of vehicle type/operation and climate conditions to effects on the same order of magnitude as high levels of highway roughness under the most extreme temperature and loading conditions at certain times of the year. The effects also depend on the viscoelastic properties of the pavement materials, primarily the type and age of the asphalt materials located near the surface.

In general, structural response modeling and measurements to date indicate that lighter and faster vehicles, as well as colder conditions, result in the smaller differences in rolling resistance between different pavements whereas heavier and slower vehicles under hotter conditions result in larger differences. The frequencies at which these conditions occur in combination with traffic patterns control the net effect on fuel economy of structural responsiveness for a given structure.

- The influence of structural responsiveness on vehicle fuel economy has not yet been comprehensively validated with any experiment that has characterized pavement structures in terms of their responsiveness under different conditions. As a result, the available models have not been calibrated with the type of data that allows the general application of the models to evaluate in-service pavements under the range of traffic and climatic conditions that occur daily, seasonally, and from location to location. Research is needed that uses field measurements of fuel economy for a range of vehicles, climates, and pavement structural responses, while controlling for roughness and macrotexture, to complete the calibration and validation of models that can be used to make design and management decisions.
- The relative impacts of decisions affecting the different pavement vehicle interaction mechanisms discussed in this section are highly context sensitive, with the benefits from changing existing practices dependent on the baseline conditions in terms of existing roughness, macrotexture conditions, and pavement structural responsiveness.

This study addresses two problems: (a) the structural response energy dissipation models have not been compared with each other for the range of pavement types, vehicles, and climates in California, and (b) the models have also not been validated with comprehensive field data. This is summed up by a statement from a recent review of pavement rolling resistance prepared by the Swedish Road and Transport Research Institute (VTI) and other MIRIAM partners *(2)*:

The overall conclusion is that pavement stiffness cannot be excluded as an important factor influencing rolling resistance, and should be included in studies in the MIRIAM project. The still open question is as to what extent and under which conditions (temperature, type of pavement and light versus heavy vehicles) stiffness is a major factor to consider.

1.2 Project Goal and Objectives

The purpose of this project is to develop calibrated and validated models for vehicle energy consumption due to pavement deflection for use in pavement management and design. The goals of this project are, first, to compare different pavement structural response energy dissipation models and the results they provide for estimated fuel consumption for a range of California pavements, vehicles, and climates using well-characterized and well-documented field test sections, and, second, to verify the same models using the results of field measurements on the same sections with instrumented vehicles following the general approach used by Michigan State University for NCHRP Project 1-45. This work is part of Caltrans/UCPRC participation in the MIRIAM (Models for rolling resistance In Road Infrastructure Asset Management systems) project which is being performed by a consortium of European national highway research laboratories and the Federal Highway Administration (FHWA) as well as Caltrans and UCPRC.

Each goal will be accomplished through a separately funded phase with the following tasks:

Phase I (Partnered Pavement Research Center Strategic Plan Element [PPRC SPE] 4.49)

1. Identify modelers interested in participating in the project, and critically review the existing models.
2. Identify pavement test sections that span the range of pavement structures, traffic, and climate conditions across the state, then have modelers estimate vehicle fuel consumption differences due to pavement structural response (called excess fuel consumption) for the range of California vehicles and conditions for each test section.
3. Summarize and compare modeling results received from each group in a report. Prepare a summary report of results.
4. Use the model results to simulate the annual vehicle excess fuel consumption caused by pavement structural response on each of the asphalt-surfaced test sections for typical traffic and climate in California and to compare those results with the excess fuel consumption caused by roughness and surface macrotexture, and then prepare a report summarizing the results. Based on those results regarding the importance of fuel consumption attributed to structural response, include in the report a recommendation regarding the need for Phase II experimental work.
5. Develop and submit an experimental plan for fuel economy evaluation in Phase II.
6. Hold a webinar and a question session to communicate results of Phase I.

Phase II (PPRC SPE 4.53)

1. Update characterizations of the pavement test sections included in Phase I.
2. Provide updated characterization data to modelers to update modeling results for the sections. Obtain results of the updated modeling of test sections.
3. Measure vehicle fuel consumption of a range of vehicles on the pavement test sections modeled as part of Phase I, including consideration of all factors potentially affecting the results.
4. Analyze measurements and use the results to calibrate the updated modeling results from each of the modeling teams.
5. Prepare a report summarizing the test sections, characterization testing results, analysis of the fuel consumption measurements, and calibration of the models with those results conducted in Phase II of the study, and include recommendations for implementation of the results in pavement design and management.

This report presents the results of Phase I Task 4 for the asphalt-surfaced sections in the Phase I factorial. The structural response modeling for the concrete-surfaced sections is currently being completed and will be reported in a separate technical memorandum. The results of Phase I Tasks 1 through 3 are presented in a separate companion report titled "Model Development, Field Section Characterization and Model Comparison for Excess Vehicle Fuel Use Due to Pavement Structural Response" (UCPRC-RR-2015-04) that has been summarized in this report.

1.3 Scope of Report

Chapter 2 includes a summary of the approaches, methods, and experiment designs for the modeling part of this study, and the details of the approach, methods, and experiment design for the simulation of excess fuel consumption using the structural response and vehicle fuel economy models. The summary of the results of the modeling and the detailed results of the simulations are presented in Chapter 3. Analysis and interpretation of the simulation results is presented in Chapter 4, and conclusions and recommendations are presented in Chapter 5. Appendices present detailed plots of the input data and results for the simulations.

2. EXPERIMENT DESIGN, TESTING, MODELING, AND SIMULATION APPROACHES

2.1 Overall Approach

All of the tasks for this project are summarized in Figure 2.1. The tasks included in the report on field section characterization and modeling *(23)* and those included in this report on the simulations are indicated in the figure.

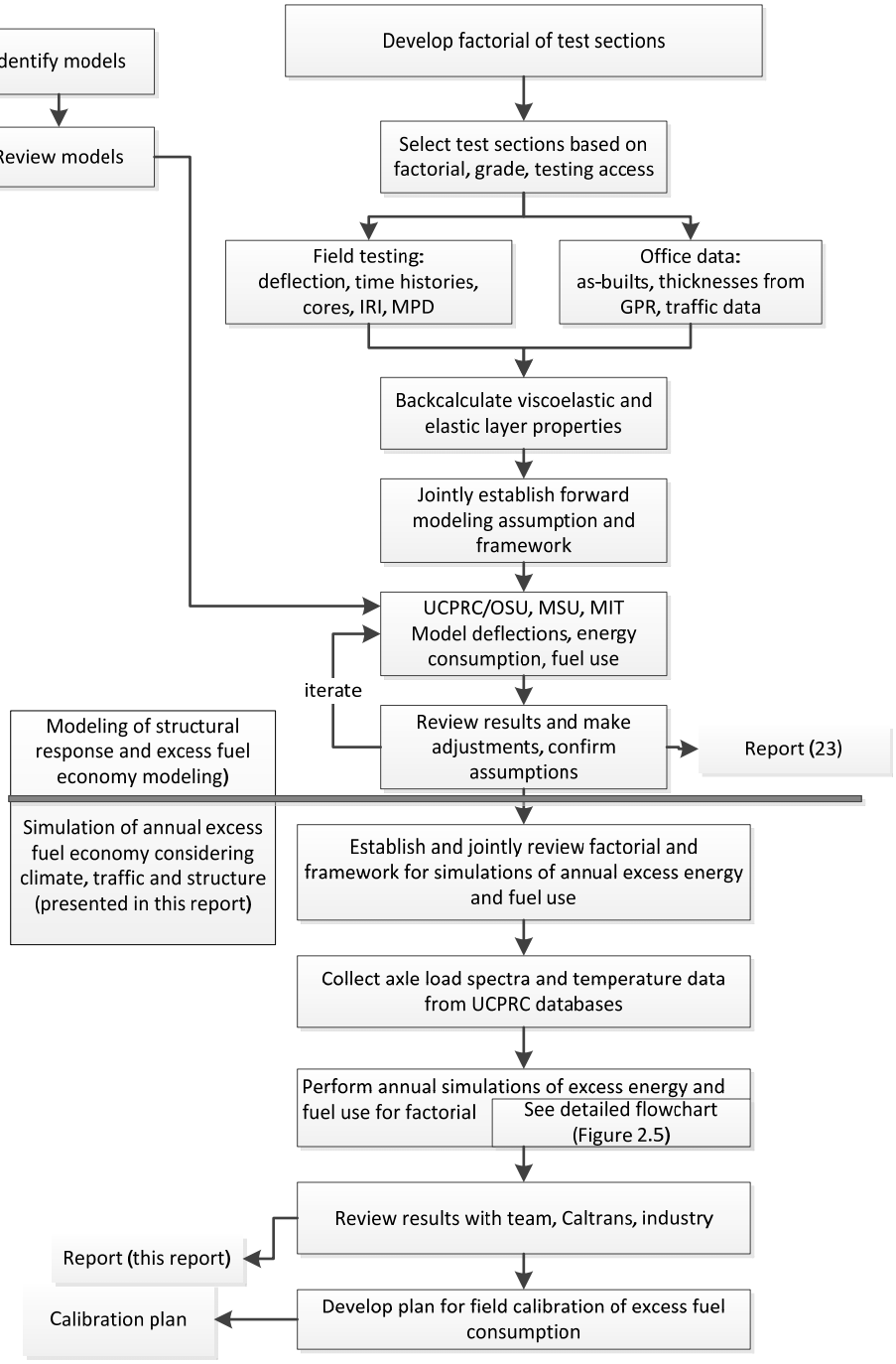

Figure 2.1: Overall process of modeling and simulation.

2.2 Approach and Experiment Design for Field Characterization and Modeling of Energy Due to Structural Response

2.2.1 Modeling Approach

The details of the materials characterization and modeling approach for energy dissipation due to structural response and excess vehicle fuel consumption as a function of pavement characteristics are presented in the companion modeling report *(23)*. The following is a brief overview of the process followed, with some further summarized information regarding each step presented later in this chapter.

As can be seen in Figure 2.1, the first step in the process was to have the modeling team identify models and for the team to review how they evaluate energy consumption due to structural response under vehicle loading. The literature survey summarized in Chapter 1 resulted in the identification of the models to be considered and the modeling teams that were available to participate in the study. The other starting point for the study was to develop a factorial of pavement test sections in California to be characterized and modeled, and for potential later use for field calibration of the fuel use models. Once the test sections were selected, the pavement structural sections were determined using as-builts and were cross-checked and evaluated for variability at 10 m (33 ft) or 100 m (328 ft) intervals, depending on location, using structural information from ground-penetrating radar (GPR) data. Traffic data were collected from Caltrans PeMS and CalTruck databases.

Field testing consisted of measurement of deflections using a heavy weight deflectometer, measurement of profile in both wheelpaths using an inertial profilometer from which IRI and MPD were calculated, and measurement of MPD in the wheelpaths using a laser texture scanner (LTS). A number of concrete sections were tested for profile twice, during the day and night, to see if there was any effect of temperature on the calculated IRI values. There was very little difference between the day and night IRI values calculated.

Time histories of load and deflections were collected during deflection testing and were used for backcalculation of viscoelastic master curves for relaxation time and to find the stiffness and phase angle of pavements with asphalt surfaces. Deflections were collected twice on almost all sections, during the day and night, to obtain a wide range of temperatures and pooled for the backcalculations. Temperatures measured in the pavement at one-third depths were used for each deflection testing station so that actual temperatures could be used in the backcalculation for each station. Elastic stiffnesses were backcalculated for layers other than the asphalt layers in pavements with asphalt surfaces. For pavements with concrete surfaces, the subgrade was backcalculated to consider damping of the k-value, while all of the other pavement layers were characterized in terms of elastic stiffness. The deflection data was also used to divide some sections into two subsections.

All backcalculations were performed by Michigan State University and reviewed by all modelers. The same materials information and pavement cross sections were used by all modelers without any changes, although some models used the relaxation master curves and others used the stiffness and phase angle master curves.

While the backcalculation was being completed, the modelers produced results for a small set of sections. The results of the analysis of these sections were used to develop the common assumptions for the forward modeling. After several iterations and discussion, agreement was reached on the forward modeling assumptions and they were documented.

2.2.2 Field Test Sections

Safety was the first consideration for section selection, and the network was reviewed for locations that appeared to be generally safe for traffic closures for pavement characterization testing and for later fuel economy testing. All sections were selected to have no horizontal curves and to have average slopes of less than 0.5 percent, with only PD 21 not meeting this criterion. All sections were selected to have lengths of at least 0.6 miles (1 km). (The section lengths may need to be increased later if it is found that they are too short to produce sufficiently reproducible results. Some sections may also need to be changed later if it is found that the current sections have insufficient geometries or traffic levels to allow steady speed testing.)

The development of the factorial of field test sections considered the following variables:

- Pavement types commonly used on the California state highway network
  - Jointed plain concrete
  - Continuously reinforced concrete
  - Flexible pavement (asphalt layers on unbound bases), with and without rubberized surfaces and open-graded surfaces and a range of thicknesses and stiffnesses
  - Composite pavement (asphalt overlays on cracked-and-seated jointed plain concrete, typically without dowels)
  - Semi-rigid pavement (asphalt layers on cement-treated base)
- Roughness
  - Most sections were selected to be no more than moderately rough, with IRI values less than 100 inches/mile (1.6 m/km).
  - A few sections were selected to have high roughness to test the independence of the effects of structural response, roughness, and macrotexture on fuel economy.

- Macrotexture
  - Most sections were selected to have macrotexture values typical of concrete and dense-graded asphalt materials.
  - A few sections were selected to have open-graded asphalt materials with higher macrotexture to test the independence of the effects of structural response, roughness, and texture on fuel economy.
- Subgrade type
  - Clay, considered to potentially have more damping effect
  - Sand, considered to potentially have less damping effect

The sections were selected to be as homogenous as possible with respect to pavement structure, roughness, and macrotexture. Caltrans databases for as-builts and the database of pavement structures determined from GPR were used to help identify sections with homogenous structures. Roughness and macrotexture measurements from the 2011 and 2012 Caltrans Automated Pavement Condition Survey (APCS) were also used for initial screening of sections.

The final factorial of field test sections is shown in Table 2.1 and their locations are shown in Figure 2.2.

Table 2.1: Summary of Final Test Sections

Section Number	Experiment Design Factorial				Section Data						
	Structure and Surface Type[1]	Htop (mm)	Sub-grade	IRI (m/km)	Section	Length (mi)	Avg. Slope (%)	Avg. IRI (inches/mile)[2]	Avg. IRI (m/km)[2]	Avg. MPD (mm)[2, 3]	Elev. (ft)
PD 01	Concrete (JPCP)	200 – 225	Clay	<1.3	MER152E2-PM24/25.5	1.51	-0.04	70	1.10	0.29	30
PD 02	Concrete (JPCP)	200 – 225	Sand	<1.3	SAC50E4-PM13.2/14.2	1.01	0.1	62	0.98	0.34	39
PD 03	Concrete (JPCP)	200 – 225	Sand	<1.3	SAC50W4-PM14.0/13.2	1.21	-0.04	78	1.23	0.35	38
PD 04	Concrete (JPCP)	200 – 225	Any	>2.7	SJ132W1-PM2.56/1.56	1.01	0.17	197	3.10	0.32	63
PD 05	Concrete (CRCP)	200 – 225	Any	<1.3	SJ5N3-PM31.5/32.7	1.21	0.06	74	1.17	0.44	7
PD 06	Composite-DGAC surface	105	Sand	<1.3	SOL80W1-PM13.0/13.9	1.92	-0.09	94	1.49	1.23	7
PD 07	Composite-DGAC surface	>105	Sand	<1.3	SOL80W1-PM29.2/30.5	1.30	0.09	51	0.81	1.06	28
PD 08	Composite-DGAC surface	105	Clay	<1.3	SCL237W3-PMR5.08/R4.48	0.61	-0.1	88	1.39	1.00	3
PD 09	Composite-DGAC surface	105	Clay	>2.7	No sections found	—	—	—	—	—	—
PD 10	Composite-DGAC+ RHMA-G	105 mm DGAC + 60 mm RHMA-G	Sand	<1.3	SOL505S1-PMR6.2/R7.5	1.30	-0.06	62	0.99	1.11	36
PD 11	Old DGAC/Flex	>250	Clay	<1.3	SM101S1-PM17.5/18.5	1.01	0.05	85	1.35	1.23	3
PD 12	New DGAC/Flex	<250	Clay	<1.3	SM101S1-PM12.9/13.9	1.01	-0.02	83	1.30	1.11	3
PD 13	New DGAC/Flex	>250	Clay	<1.3	SUT113N1-PM13.0/14.0	1.01	0.13	95	1.50	0.68	3
PD 14	Old DGAC/Flex	>250	Clay	>2.7	SOL113N1-PM3.0/4.0	1.01	-0.49	226	3.57	0.80	10
PD 15	RHMA-O on DGAC/Flex	>250	Sand	<1.3	SAC50E1-PM14.2/16.0	1.82	0.08	63	1.00	1.31	41

Section Number	Experiment Design Factorial				Section Data						
	Structure and Surface Type[1]	Htop (mm)	Sub-grade	IRI (m/km)	Section	Length (mi)	Avg. Slope (%)	Avg. IRI (inches/mile)[2]	Avg. IRI (m/km)[2]	Avg. MPD (mm)[2, 3]	Elev. (ft)
PD 16	Old DGAC/Flex	>250	Sand	<1.3	SJ120E1-PM11.5/12.5	1.01	0.12	65	1.03	0.78	32
PD 17	New DGAC/Flex	>250	Sand	<1.3	SAC50W1-PMR7.9/R6.9	1.01	-0.08	86	1.35	0.80	19
PD 18	RHMA-G on old DGAC/Flex	<60	Any	<1.3	YUB20W-PMR5.0/R4.3	0.71	-0.01	40	0.63	0.97	25
PD 19	RHMA-G on new DGAC/ Flex	<60	Any	<1.3	SM101S1-PM24.5/25.7	1.21	0.01	71	1.11	0.89	5
PD 20	RHMA-O on DGAC/ Semi-rigid	>125	Clay	<1.3	SJ99N1-PM25.7-26.5	0.80	-0.02	94	1.49	1.33	13
PD 21	RHMA-O on DGAC/ Semi-rigid	<125	Clay	<1.3	AMA16E-PMR0.3/R0.9	0.61	1.01	94	1.49	1.33	92
PD 22	RHMA-G on DGAC/ Semi-rigid and on granular/ Flex	>125	Clay	<1.3	SCL101N2-PM3.1/4.0	0.90	0.25	77	1.21	0.74	54
PD 23	DGAC/ Semi-rigid	>125	Sand	<1.3	STA132W1-PM24/25	1.01	-0.11	63	0.99	0.92	52
PD 24	Semi-rigid (RHMA-G or DGAC)	>125	Sand	>2.7	No sections found	—	—	—	—	—	—

Notes:
[1] DGAC is dense-graded asphalt concrete; RHMA-G is gap-graded rubberized hot mix asphalt; RHMA-O is open-graded rubberized hot mix asphalt.
[2] Measured in 2014 by UCPRC using inertial profiler.
[3] Measured in 2014 by UCPRC using high-speed inertial profiler and laser texture scanner.

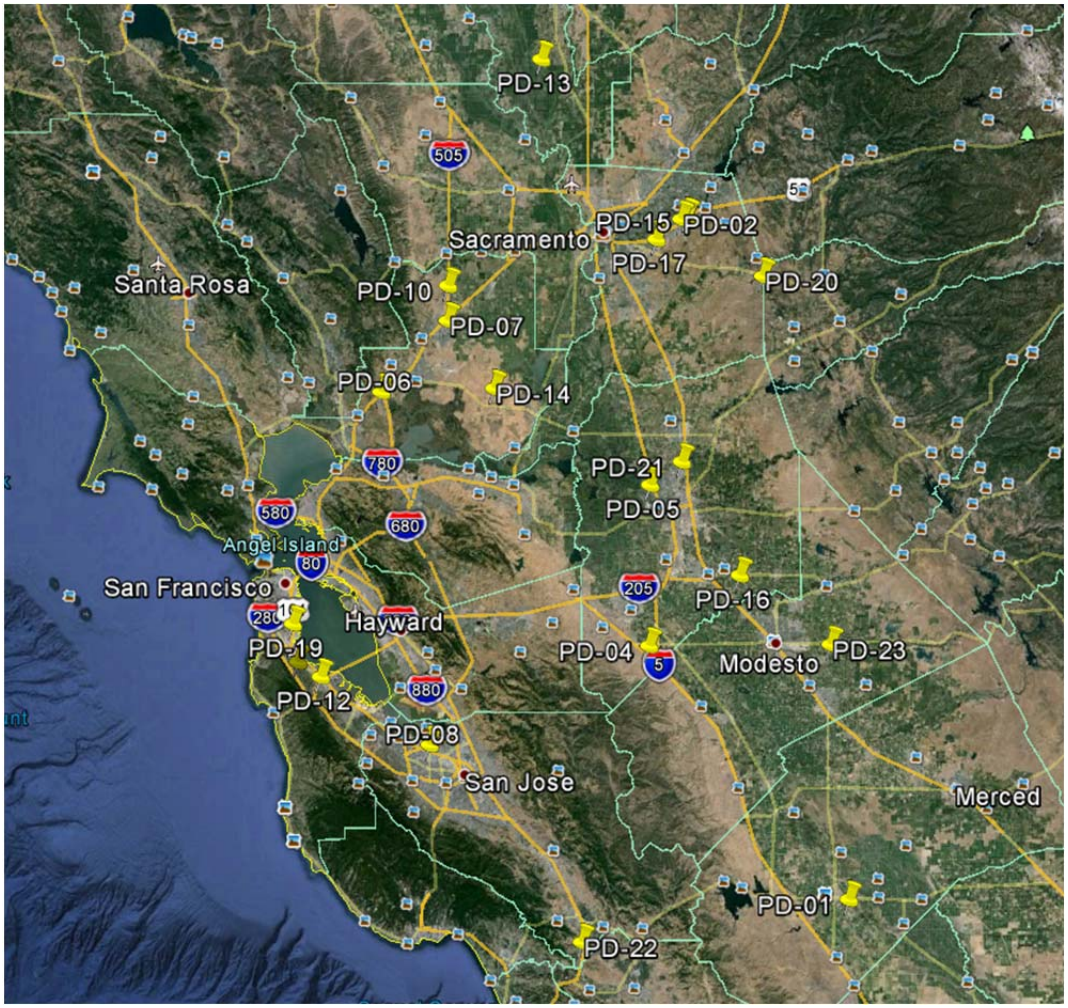

Figure 2.2: Locations of final test sections.
(Image from Google Earth™)

2.3 Summary of Field Section Characterization and Modeling Results

2.3.1 Field Test Section Characterization

Details of the field test section characterization are presented in the companion modeling report *(23)*. After the selection of the test sections, section characteristics were determined by field testing. The three major tests conducted on every section were deflection testing using the falling weight deflectometer for use in backcalculation of stiffness, measurement of macrotexture using the laser texture scanner for the concrete sections, and measurement of profiles with the inertial profiler which were used to calculate macrotexture on the asphalt surfaced sections and IRI on all sections. Cores were also collected to conduct shear frequency sweep at constant height (FSCH) tests that were used to develop asphalt stiffness master curves (stiffness as a function of time of loading and temperature) for later comparison with backcalculated viscoelastic properties of the asphalt layers.

Falling Weight Deflectometer Tests

Deflection testing responsibility was divided between Caltrans district forces, NCE Consultants and the UCPRC, using JILS (Caltrans) and Dynatest (NCE and UCPRC) equipment. Three loads (5,000, 8,000, and 12,000 lbs [22, 36 and 53 kN]) and two repetitions for each load were applied at each station in each section. In order to estimate the viscoelastic properties of the nonelastic layers, the full time history of the deflection was collected. Each asphalt-surfaced test section had 100 test points evenly spaced along the section. Each JPCP section had fifty slabs tested, evenly spaced along the section. Tests on JPCP were conducted at midslab and over the joint (200 and 300 mm sensors). All testing was performed in the outside wheelpath.

For each section, two tests were conducted, one early in the morning (3 a.m. to 7 a.m.) and the other in the afternoon (12 p.m. to 3 p.m.) in order to capture the effects of temperature. Temperature data were collected every fifteen minutes at one location at the end of the test section concurrent with the FWD testing. When the temperature profile data were not collected during the experiments due to mandatory moving road closures, temperature gradients were estimated by inputting measured surface temperatures into the *Enhanced Integrated Climate Model* (EICM) software or using BELLS temperature formulas.

Laser Texture Scanner Tests

The laser texture scanner (LTS) calculates pavement surface macrotexture from the surface profile of an area 3 inches wide by 4 inches long (75 mm by 100 mm). Manufactured by Ames Engineering, the LTS has laser dot size of approximately 0.050 mm, a vertical sample resolution of 0.015 mm, and a horizontal sample spacing of 0.015 mm. In this study, the LTS was used to measure the MPD of the surface of each pavement section. Macrotexture measurement was performed at five points along the section.

Inertial Profiler

Road profile was measured using the UCPRC profiler vehicle equipped with a Dynatest® inertial profiler, Mk-III. The Mk-III profiler has laser instruments that measure the pavement profile in the left and right wheelpaths. The profiler utilizes a RoLine® laser on the right wheelpath to measure pavement profile on concrete pavements. The profiler car is also equipped with a high-resolution dot laser with sampling capability of up to 64 kHz that is used to collect profile data from which macrotexture (mean profile depth, MPD) is calculated in the right wheelpath. For analysis, data from the RoLine sensor only were used for the concrete sections, and data from the normal-speed dot laser in the left wheelpath and the high-speed dot laser in the right wheelpath were used for asphalt-surfaced sections.

Laboratory Frequency Sweep at Constant Height Tests

Laboratory frequency sweep at constant height (AASHTO 2003) tests were conducted with the top part of the cores collected from the field sections. Experiments were conducted at four temperatures, 20°C, 30°C, 40°C, and 50°C, and ten loading frequencies, 0.01 Hz, 0.0 2Hz, 0.05 Hz, 0.1 Hz, 0.2 Hz, 0.5 Hz, 1 Hz, 2 Hz, 5 Hz, and 10 Hz. Master curves for a reference temperature of 19°C were developed using the test results. Although the test results were not used for viscoelastic model development, they were used for comparison with the shape of the master curves from FWD backcalculation as a check on reasonableness.

2.3.2 Overview of Structural Response Models

More detailed documentation of the structural response models is presented in the companion modeling report (22).

Backcalculation by Michigan State University (MSU)

The dynamic viscoelastic backcalculation program (DYNABACK-VE *[26, 27, 28]*), developed as part of the FHWA DTFH61-11-C-00026 project, was used to backcalculate the relaxation time master curve E(t) for the AC layer of the test sections using the time histories of FWD sensor deflections at different temperatures. The method uses ViscoWave-II *(29, 30)* as a forward routine and a hybrid routine (DYNABACK-VE) that uses a genetic algorithm and modified Levenberg-Marquardt method for backcalculation analysis. The approach is used to generate a master curve using the time-temperature superposition principle *(31)*. The advantage of this solution is that it can analyze the response of pavement systems in the time domain and can therefore accommodate time-dependent layer properties and incorporate wave propagation. Also, since the backcalculation is performed in the time domain, the algorithm is not sensitive to deflection truncation. The algorithm is capable of backcalculating the modulus for each layer and the depth-to-stiff layer reliably. This enables backcalculating the master curve of the asphalt concrete layer at every reduced time and the depth-to-stiff layer if it exists. The results using simulated deflection time histories and field FWD data showed excellent stability and accuracy.

Oregon State University (OSU)

The OSU approach uses a viscoelastic finite element (FE) model to calculate the dissipated energy under different conditions. Energy dissipation due to subgrade damping is not simulated in the model. In the developed viscoelastic FE model, only the linear behavior is considered (small strain domain). No nonlinearities (fatigue, permanent deformations, and cracks) are taken into account.

The temperature dependency of the asphalt mix was defined by using the Williams-Landel-Ferry (WLF, *31)* equation.

The generalized Maxwell-type viscoelastic model was used in this study to simulate the time dependency. The model consists of two basic units, a linear elastic spring and a linear viscous dashpot. Various combinations of these spring and dashpot units define the type of viscoelastic behavior. The implementation procedure developed by Pouget et al. *(13)* was used to simulate the effects of truck loads, vehicle speed, and temperature on dissipated energy.

Abaqus™ software was used for model development. The pavement structure is represented by a 6 meter long, 2.5 meter wide (19.7 feet by 8.2 feet) slab (Figure 2.3). The finite-element mesh consists of Lagrange brick elements with a second-order interpolation function. The mesh is refined under the wheelpath.

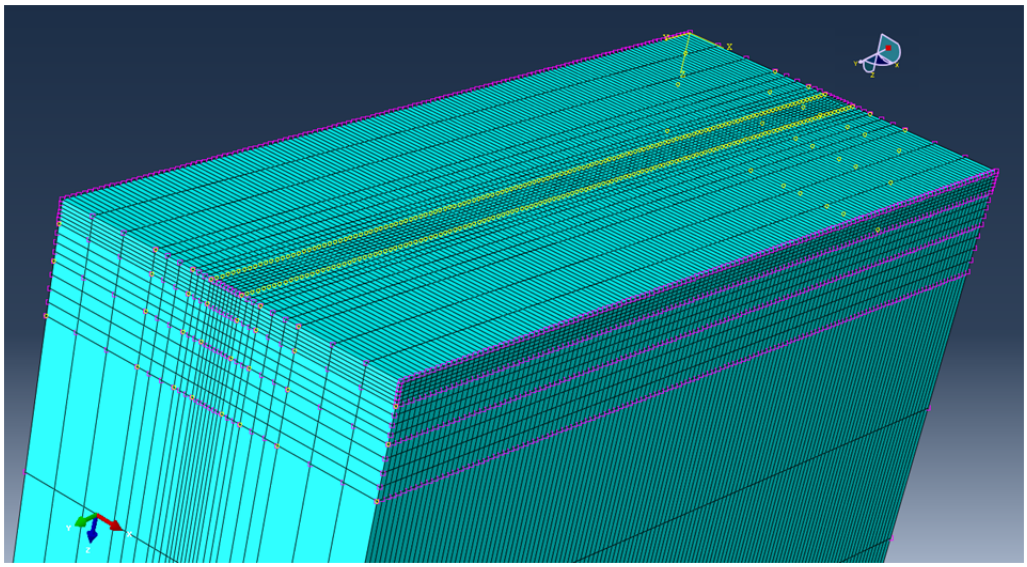

Figure 2.3: Meshed OSU model structure in Abaqus.

The bottom side of the model is clamped. The symmetry condition in the transverse direction imposes a boundary condition on one side. To ensure the continuity of this slab with the rest of pavement, only vertical displacement is allowed for other lateral sides *(13)*. Perfect bonding is assumed between the different pavement layers.

In order to simulate moving wheel loading in the viscoelastic FE model, the trapezoidal impulsive loading method (quasi-static) was used *(32)*. The tire is assumed to have a square contact area and the distribution of load on the tire is assumed to be constant. The dissipated energy per time w(t) is integrated on a Δd long slice of the asphalt layer, located in the center of the 6 meter long structure. The dissipated energy for a truck (Wtruck) with Z dual wheels, covering a distance of X can be calculated using the following equation *(13)*:

$$W_{truck} = \left(\int w(t).dt \right).\frac{X}{\Delta d}.Z$$

where w(t) is calculated using the following equation in which ϕ_E is the phase angle, σ_{0z} is the stress and ε_{0z} is the strain for a unit volume *dV*.

Michigan State University

The MSU approach uses an axisymmetric time domain spectral element finite element implementation, with an infinite layer in the horizontal direction (semi-analytical solution) and a semi-infinite half-space element for the subgrade, although it can accommodate a stiff layer at finite depth. ViscoWave-II is a time domain dynamic viscoelastic solution that requires E(t) and the pavement temperature profile at different depths as inputs to compute the pavement response under a moving load *(29, 30)*.

Energy consumption in the vehicle is due to the wheel rolling uphill calculated with the average gradient of the wheel against the deflection basin assuming a wheel location at the bottom of the basin as shown in Figure 2.4. The total dissipated energy per unit distance is calculated as:

$$\delta E = P \times G$$

where P is the vehicle mass and G is the average slope across the tire-pavement contact area.

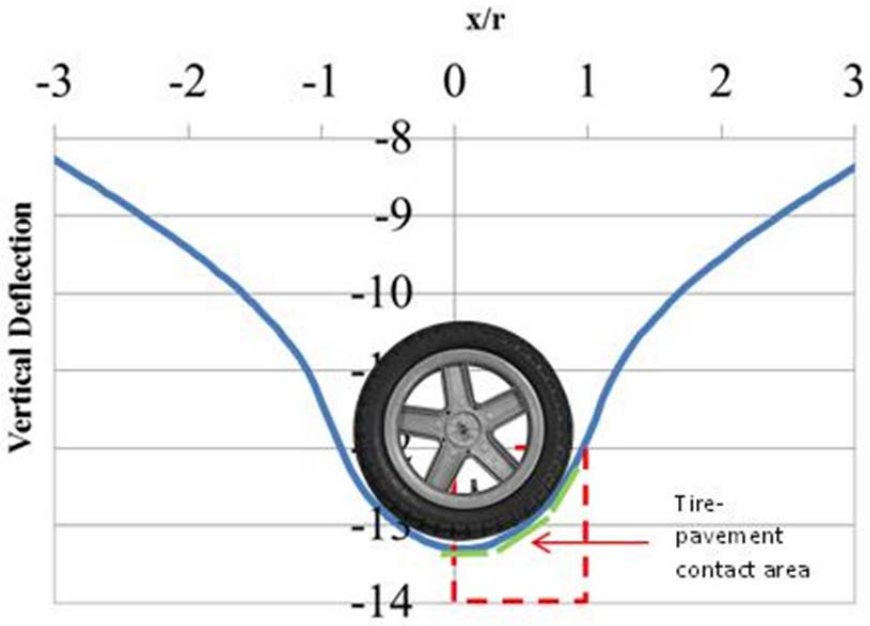

Figure 2.4: Location of the wheel in the deflection basin and tire/pavement contact area where gradient is considered for energy needed to move up the side of basin in the MSU approach.

Massachusetts Institute of Technology

In the MIT approach, excess fuel consumption (EFC) due to deflection-induced PVI is calculated from the energy dissipation that a moving load generates within the pavement structure *(21, 22)*. The model relates pavement material and structural properties to the rolling resistance due to pavement deflection. The pavement

is modeled as a viscoelastic beam on an elastic foundation subjected to a moving load at constant speed. To maintain this speed, extra power is provided by the vehicle to compensate for the dissipated energy, δE, due to viscoelastic deformation of the beam, leading to excess fuel consumption. The deflection-induced PVI model calculates the excess energy consumption as a function of vehicle speed *c*, axle load *P*, and temperature and material dependent relaxation time $\tau(T)$ using the following equation *(21, 22)*:

$$\delta E = \frac{c_{cr}}{c} \times \frac{P^2}{bk\ell_s^2} \times F\left(\frac{c}{c_{cr}}; \frac{\tau(T)c_{cr}}{\ell_s}\right)$$

where δE is the dissipated energy due to the pavement deflection as a function of two dimensionless numbers, one related to the vehicle speed, c/c_{cr} (where c_{cr} is the critical speed), and the other to the relaxation time of the pavement material capturing the viscoelastic nature of the top layer, $(\tau(T)\, c_{cr})/\ell_s$, with $\ell_s = (\frac{Eh^3}{12}/k)^{1/4}$, the Winkler length of the beam of width b, top layer modulus E, top layer thickness h, and elastic subgrade modulus k. The dissipated energy relates to the square of vehicle load, $E \propto P^2$, and the inverse of vehicle speed $\delta E \propto \sim 1/c$. An increase in temperature results in a change in the complex modulus of the viscoelastic pavement, leading to an increase in the dissipated energy. The variation in pavement material properties due to temperature is modeled and calculated separately for asphalt and concrete pavements.

The time-temperature superposition principle is used to establish this temperature dependence and find the material relaxation time at any given temperature T from the relaxation time, measured at a reference temperature T_{ref} using the WLF equation for asphalt pavements *(31)*.

For practical use and fast computation, a fit of the log of dimensionless expression of energy dissipation to a two-dimensional surface, is used adapted from Louhghalam et al. *(22)*:

$$\log_{10}\frac{\delta E\ell_s^2 bkc}{P^2 c_{cr}} = \log_{10} F\left(\Pi_1 = \frac{c}{c_{cr}}; \Pi_2 = \zeta = \frac{\tau c_{cr}}{\ell_s}\right) = \sum_{i=0}^{i=5}\sum_{j=0}^{j=3} p_{ij}{\Pi_1}^i \times \log_{10}(\Pi_2)^j$$

Coefficients p_{ij} (coefficient of determination of $R^2 = 0.972$) are tabulated in Table 2.2, for $0.03 < c/c_{cr} < 0.5$ and $0.0001 \leq \zeta \leq 12{,}000$. Having the material and structural properties of a pavement in hand, the equation shown above is used to evaluate the dissipated energy and fuel consumption.

Table 2.2: Coefficients p_{ij} (with 95% Confidence Bounds)

j\i	0	1	2	3	4	5
0	-1.918 (-1.922, -1.915)	4.487 (4.379, 4.596)	-19.54 (-20.64, -18.44)	59.58 (54.61, 64.55)	-92.51 (-102.6, -82.39)	56.23 (48.63, 63.83)
1	-0.4123 (-0.4135, -0.4111)	-1.802 (-1.824, -1.78)	4.014 (3.864, 4.163)	-4.628 (-5.04, -4.217)	1.375 (0.9895, 1.761)	-
2	-0.06942 (-0.06969, -0.06915)	0.2153 (0.2111, 0.2194)	-0.8618 (-0.8794, -0.8441)	0.7344 (0.7124,0.7563)	-	-
3	-0.009575 (-0.009656,-0.009495)	0.0203 (0.0196, 0.021)	0.04669 (0.04542,0.04797)	-	-	-

Fuel Use Models

For their initial comparisons the modelers converted the energy consumed by the pavement (following the OSU approach) or the additional energy required by the vehicle to move up the side of the deflection bowl (the MSU and MIT approaches) into excess fuel consumption due to structural response, as described in the companion modeling report *(23)*. For the simulations presented in this report, the modelers' EFC calculations were not used directly. Instead, as described later in this report, the modelers' energy calculations were first used in the simulations of dissipated energy across the year and were then converted to EFC.

2.3.3 Dissipated Energy due to Structural Response Modeling Results

A preliminary investigation was performed to develop a further understanding of the many assumptions that needed to be common across each modeling group to enable comparison of the models. The preliminary investigation consisted of comparison of the calculated results from each modeling group for a theoretical elastic structure and a theoretical viscoelastic structure. Once it was determined that all modeling groups were using exactly the same assumptions, modeling of the field test sections was begun.

The effects of vehicle suspension dynamics on the wheel load were not simulated by any of the structural response modelers. Perfect bonding is assumed between different pavement layers by all modelers. All of the modelers assumed the combined asphalt layers to be viscoelastic and the other pavement layers and the subgrade to exhibit isotropic linear elastic behavior. Only asphalt-surfaced sections were included in the simulations because the approach for the concrete sections had not yet been finalized.

All of the modelers used the vehicles shown in Table 2.3 to calculate the energy consumed in the pavement or by the vehicle due to structural response. All wheels were considered to be single tire wheels (one wheel on each end of the axle) for all vehicles, including what would normally be dual wheels on the heavy truck. This assumption was made based on sensitivity analyses performed in preliminary modeling using the OSU approach which indicated little sensitivity of energy dissipation between a dual wheel and a single wheel with the same load. The heavy truck was assumed to have a steering single axle and two tandem axles. The steering single axle was ignored and the total load and tare weight were divided across the eight wheels on the tandem axles. Contact areas were found by dividing the wheel loads by their respective tire pressures. Uniform vertical contact stresses with no lateral stresses were assumed for all wheels.

Table 2.3: Vehicles Used for Structural Response Modeling

Vehicle Class	Number of Wheels	Tare Mass (metric tons)	Load Mass (metric tons)	Tire Pressure (KPa)	Load (kN)	Load per Tire (kN)	Contact Area (m^2)
Medium car	4	1.46	0	242	14.308	3.577	0.0148
SUV	4	2.50	0	269	24.500	6.125	0.0230
Heavy truck	8	13.6	21.3	759	302.82	37.853	0.0500

Two speeds were used for the structural response modeling: 50 km/hr (31.3 mph) and 100 km/hr (61.5 mph). The vehicle speeds were used to determine the viscoelastic properties of the combined asphalt layers. Two temperatures were used for the modeling: 30°C and 45°C (86°F and 113°F). These temperatures were based on analysis of typical values at one-third depths in the asphalt layer for asphalt thicknesses typical of those in the field test sections found using previous calculations with the *EICM* software documented in a report by Ongel et al. *(33)*. Results of preliminary analyses using the OSU model showed that the dissipated energy calculated by uniformly applying the one-third depth temperature is almost equal to the dissipated energy calculated by simulating the calculated temperature gradients from Ongel et al.

2.4 Annual Impact Simulation Approach and Experiment Design

2.4.1 Simulation Approach

The steps in the overall process of using the modeling results to calculate annual *excess fuel consumption* (EFC), meaning the fuel consumption relative to fuel consumption on an "ideal" pavement, are shown in Figure 2.5 and discussed in the remainder of this chapter. The objective of the simulations was to estimate EFC from structural response ($EFC_{Structural\ response}$ or EFC_S) across a year using the modeling results from the three modeling groups along with realistic joint hourly distributions of traffic flows, axle load spectra, pavement temperatures, and vehicle speeds, and to then compare EFC_S with EFC from roughness and macrotexture ($EFC_{IRI,\ MPD}$).

The ideal pavement was defined as:

- Structural response: no energy and fuel consumed by structural response
- Roughness: IRI of 38 inches/mile (0.6 m/km), which is approximately the smoothest pavement measured on the California state network
- Macrotexture: MPD of 0.5 mm, which is typical of new dense-graded asphalt mixes

Simulations were run for two sets of conditions:

- Simulations for each section using the traffic and climate for that section
- Simulations for each section for a factorial of traffic and climate variables representative of conditions across the state

The first step in the simulation of EFC_S was to establish the simulation factorial, framework, assumptions, and calculation methods, and review them with the modeling teams. Once concurrence was achieved, the approach was documented. Cumulative annual temperature distributions at one-third depth in the asphalt layers were simulated for each test section for the nine California pavement design regions using the approach developed by Lea et al. *(34).* Axle load spectra data were taken from the *CalME* pavement design database. Data from the Caltrans PeMS database (*dot.ca.gov/hq/traffops/mpr/source.html)* were used to develop two vehicle speed regimes, one for a typical urban location and the other for a typical rural location.

The next step was the simulation of annual EFC from structural response, roughness, and macrotexture for the two sets of conditions noted above. EFC_{IRI} and EFC_{MPD} were calculated for the measured IRI and MPD on each section assuming that IRI and MPD remained constant across the year and were calculated using the equations calibrated in NCHRP Report 720 by Chatti and Zaabar *(11)* for each vehicle type and speed.

Figure 2.5 shows a more detailed flow chart of the EFC_S simulation process used in this step. First, the results of the modeling factorial (three axle loads, two speeds, two temperatures) for energy consumed by structural response (whether by the pavement or by the vehicle without consideration of inefficiency, depending on the approach in each model) were used to develop continuous functions of energy consumed by structural response for each model approach (OSU, MSU, MIT). The continuous function was used for interpolation between the few values in the modeling factorial to all conditions of temperature and traffic across the year for each section. Extrapolation was needed for a few extremely heavy truck axle loads. The simulation of EFC_S used the continuous energy function for each section to calculate the hourly energy consumed across all weekdays and weekends with the joint distribution of traffic flow and composition (cars, SUVs, trucks), axle load spectra for

the trucks, traffic speed for cars and trucks, and asphalt temperature across the year. Traffic flow, axle load distributions, and traffic speeds for weekdays and weekends were assumed to be constant across the year.

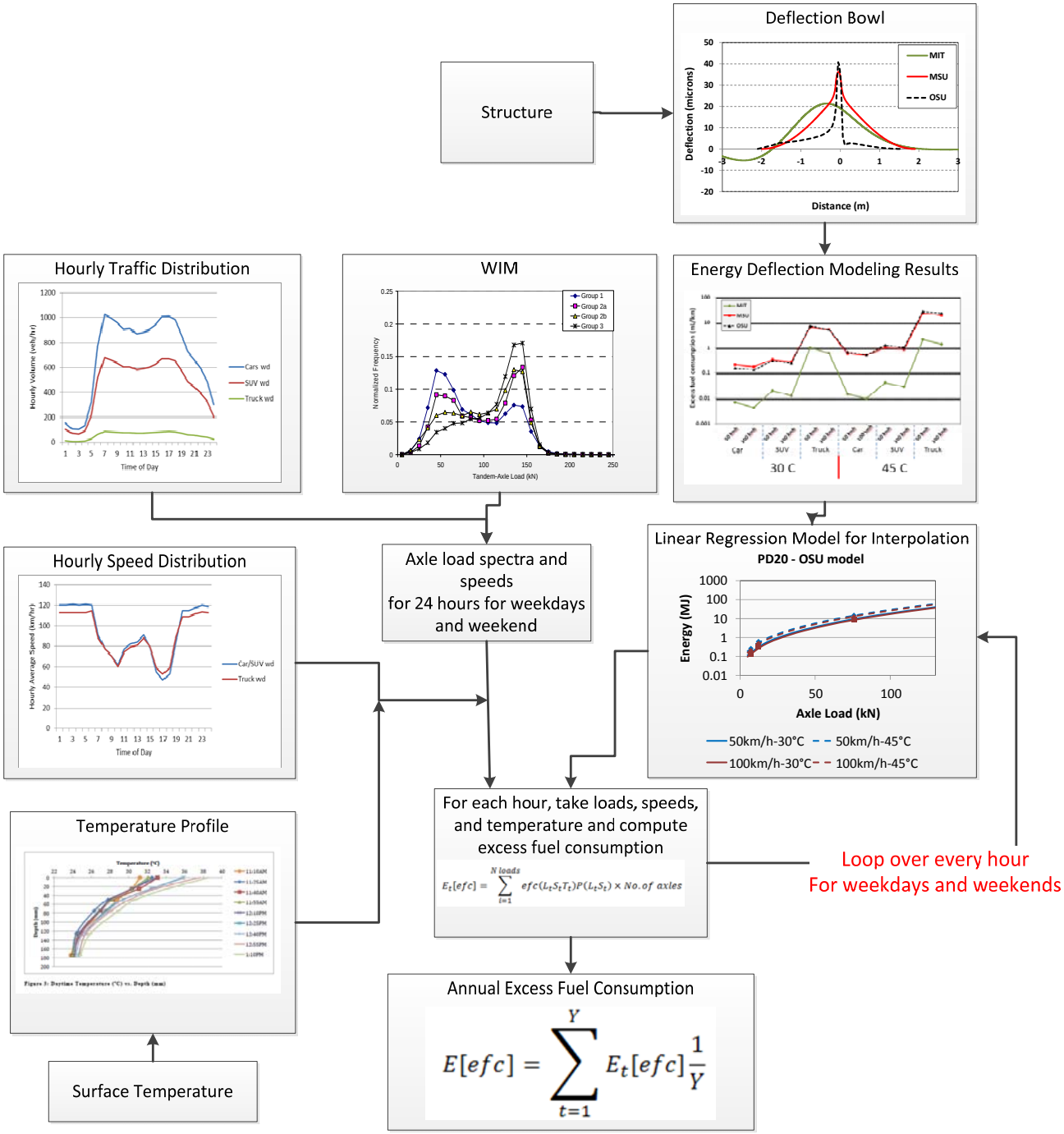

Figure 2.5: Flowchart of approach for simulation of annual excess fuel consumption due to structural response.

The final step in the simulations was to sum the EFC for each mechanism (structural response, IRI, MPD) across the year. The results were then reviewed by all of the modeling teams and their comments were incorporated into this report, which has been prepared for submission to Caltrans and then industry.

2.4.2 Simulation Experiment Design Factorial

Calculations were made for a full factorial experiment design for EFC_S. The factorial for the simulation experiment considered the following variables and factor levels:

- Pavement structures: asphalt-surfaced test sections, PD 7 through PD 23, with exception of PD 17 for which deflection time history data were not available (concrete-surfaced sections PD 1 through PD 6 will be simulated later), totaling fifteen sections, with three sections (PD 13, PD 18, and PD 22) having two structural subsections, resulting in a grand total of eighteen pavement structures
- Hourly pavement temperature: for each of the nine California pavement design climate regions (Figure 2.6) for each day of the year
- Truck axle load distribution: for each of the four main axle load spectra considered for pavement design in *CalME*, and considering cars and SUVs, and with separate hourly distributions for weekdays and weekends
- Truck percentage and Car-to-SUV ratio: 5, 10, and 15 percent trucks out of total vehicles, with a ratio of 60 percent cars and 40 percent SUVs assumed constant for the vehicles that are not trucks
- Traffic flow: hourly distribution of total traffic for weekends and weekdays
- Traffic speed: hourly distributions of average truck and car/SUV speeds for weekdays and weekends

The factorial for calculation of EFC_{IRI} and EFC_{MPD} using the NCHRP Report 720 equation considered the following:

- Pavement section: all sections and subsections
- Truck percentage and Car-to-SUV ratio: all trucks were assumed to be heavy articulated trucks, medium cars or SUVs, with the same 5, 10, and 15 percent levels for trucks, and the 60 to 40 percent split between cars and SUVs for the vehicles that are not trucks.
- Traffic speed: Hourly distributions of average truck and car/SUV speeds for weekdays and weekends

The assumption that all trucks are heavy articulated trucks will increase the fuel consumption due to roughness, since NCHRP Report 720 *(11)* found heavy trucks to be approximately twice as sensitive to IRI as light trucks and very slightly more sensitive to MPD than light trucks. This assumption was made due to difficulty in separating Caltrans truck classification data into heavy and light trucks within the time available for the

simulations. An evaluation of the overall effect on the sensitivity of the results to this assumption has not yet been performed, but it is primarily applicable to the few rough sections included in the factorial.

Hourly Pavement Temperature Assumptions

Hourly pavement temperatures were calculated for each pavement section using the same method used to develop the temperature distributions used in the *CalME* pavement design database, which are documented in Reference *(35)*. *CalME* uses a database of pavement temperatures calculated using the stand-alone *EICM* version 3 *(33)*. The weather data includes thirty years (1961 to 1990) of daily maximum and minimum temperatures, daily average percent sunshine, daily average rainfall, and daily average wind speed for representative cities in six climate regions. The database was recently increased to consider three additional mountain climate regions in the state, now totaling nine, which is aligned with the Caltrans Performance Grade (PG) asphalt specifications.

The *EICM* program was used to evaluate twenty-eight different flexible pavements and four different composite pavements with combinations of layer thicknesses covering the expected range in the state for each climate region and for several albedos. Using the database of pavement temperatures referenced above, the *CalME* approach computes temperatures below the surface using a fast one-dimensional finite element method routine. This process uses an internal database of thermal diffusivity constants for each material, where diffusivity is a function of the heat capacity and the thermal conductivity *(34)*. This approach was used for the asphalt thicknesses in each of the eighteeen subsections for each of the nine climate regions, with an assumed surface albedo of 0.1 used for all cases. Figure 2.7 shows an example of the cumulative temperature distributions across the year calculated for PD 7 and the nine climate regions.

One year was used for the simulations to simplify the calculations and reduce computation time. That year, 1961, was compared with several other years in the temperature database as well as with 2014, one of the hotter years in recent California history for overall air temperature. The comparison, shown in Figure 2.8, indicates that 1961 was somewhat hotter than 1980 or 1999, and had a hotter spring and a cooler winter than 2014. Therefore, it was not atypical of recent temperatures and was suitable for the simulations.

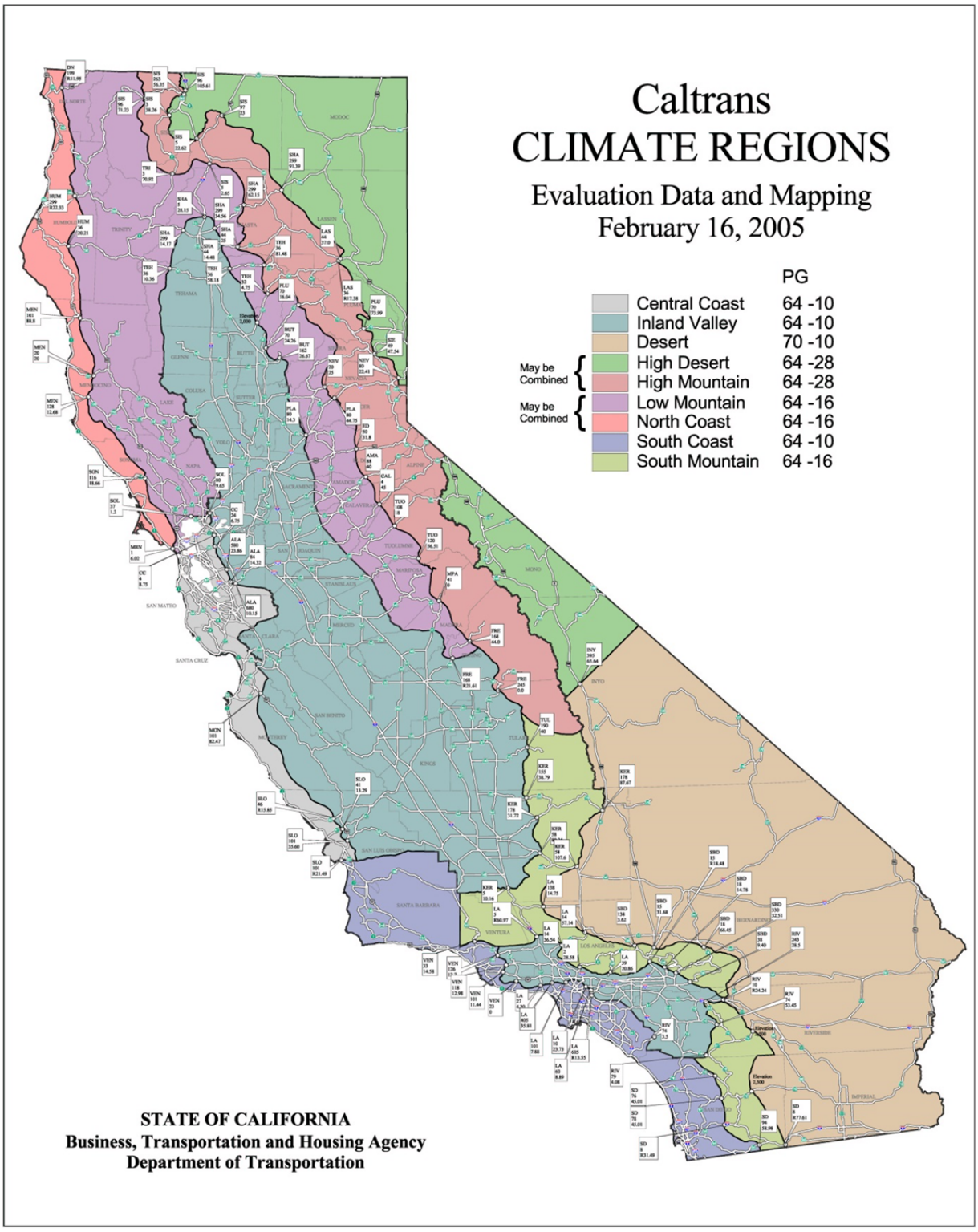

Figure 2.6: Nine California pavement design climate regions.

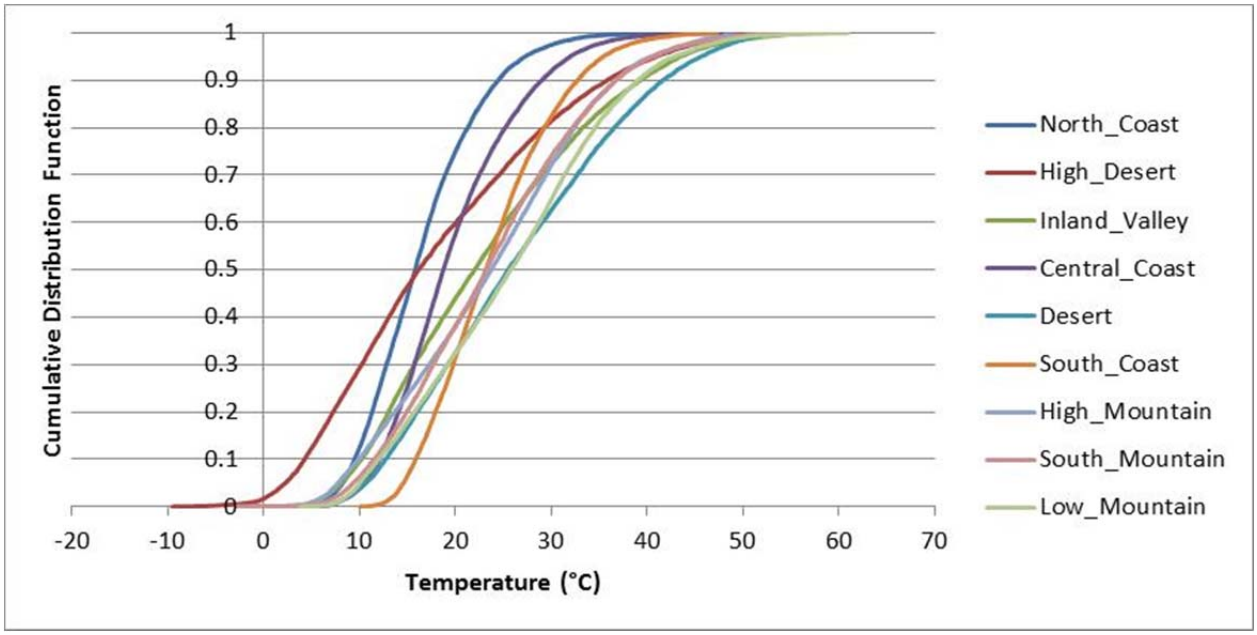

Figure 2.7: Example cumulative distributions of pavement temperature at one-third of asphalt depth from *CalME* 1-d approximation and interpolation based on database of EICM runs for nine California climate regions (PD 7 example shown).
(Note: 0°C = 32°F, 20°C = 67°F, 40°C = 104°F, 60°C = 140°F.)

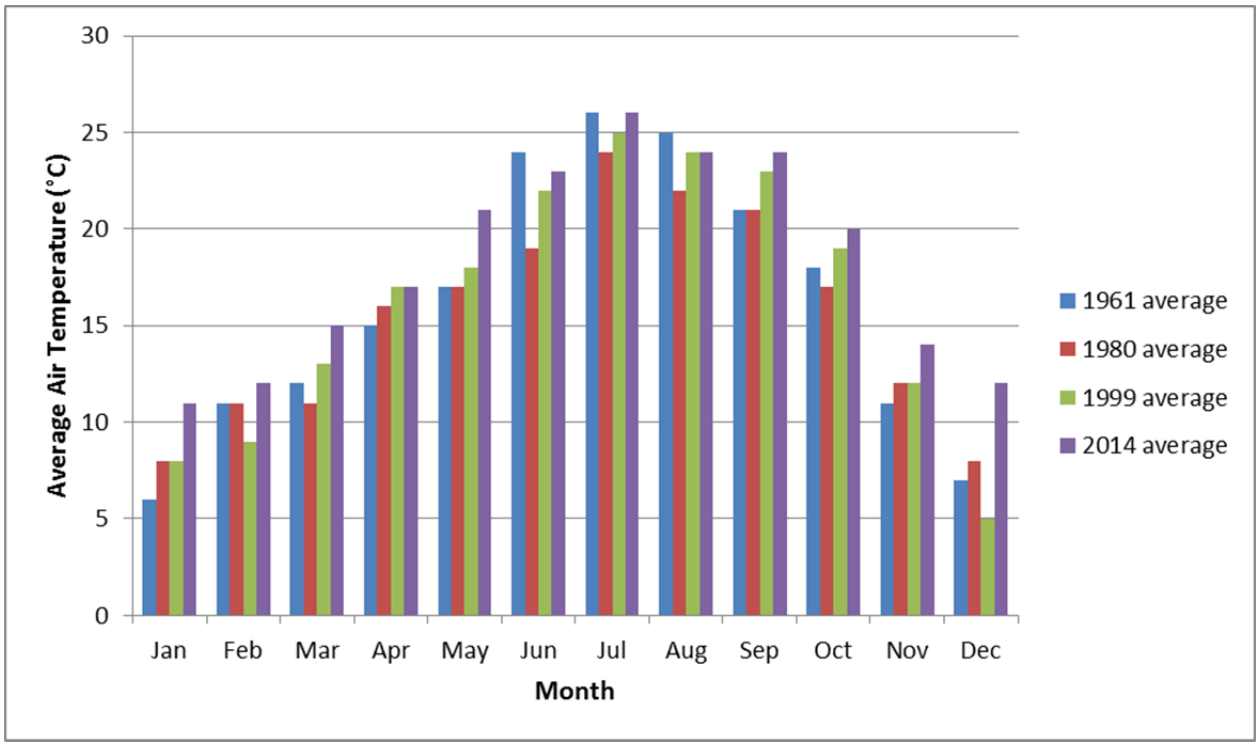

Figure 2.8: Comparison of average monthly air temperatures for 1961, used for simulations, and other years.

Axle Load Spectra Assumptions

In 1987 Caltrans began installing weigh-in-motion (WIM) stations on California's state highways to collect truck traffic data, and since then it has maintained a detailed historical database of truck traffic information from measurements taken at more than eighty sites across the state. The WIM truck traffic database includes data for the period 1991 to 2003 that was obtained from the Caltrans Office of Truck Services; this is the collected data for all 108 WIM stations installed before 2003. Caltrans typically selects one week's worth of data for each month from each station and checks the data to see whether the WIM system is operating properly, to calibrate drift, and to properly code vehicle records that contain questionable data elements. An overview of the California WIM system can be found in the literature *(35)*.

In 2006 *(36)* California WIM data were grouped by cluster analysis into fifteen axle load spectra groups, and a decision tree was developed to determine the group category assignment for any highway section in the database (Figure 2.9). Based on axle load spectra, the WIM sites were grouped into groups and subgroups: Level 1 includes Groups 1a and 1 b; Level 2 includes Groups 2aa, 2ab, 2ba, and 2bb; and Level 3 includes Groups 3a and 3b (Table 2.4). The inputs for the decision tree are the geographic location of the highway section (district, county, highway number, and Post Mile) and the traffic volume and composition. These inputs have been obtained from the Caltrans annual report of annual average daily truck traffic (AADTT). The flowchart can be seen in Figure 2.9.

The four most common axle load distribution groups *(36)* for tandem axles appears in Figure 2.10 (the groups shown here had similar distributions to those found for steering singles, singles, and tridems, which are not shown. It can be seen in the figure that Group 1 tended to have more unloaded axles than loaded axles, while Groups 2a, 2b, and 3 tended progressively to more loaded axles and fewer unloaded axles. Group 3 is the prevalent group on long-haul interstate sections, particularly on Interstate 5, which runs north and south from Mexico to Oregon. For the simulations of the individual sections, the most appropriate WIM for the test sections was selected using Figure 2.9.

All truck axles were treated as single axles, meaning that tandem axles were treated as two singles and tridems as three singles. This was done to simplify calculations and because this assumption has not been extensively evaluated in previous finite element simulations using the OSU model. All cars were assumed to have two axle loads of 1,620 lb (7.2 kN) and all SUVs were assumed to have two axle loads of 2,745 lb (12.2 kN).

Table 2.4: WIM Site Groupings Based on All Axle Load Spectra

Level 1 Groups	Level 2 Groups	Level 3 Groups	WIM Site
1	1	1a	011, 020, 040, 097, 057/058, 077/078, 079/080, 006, 022, 023, 026, 035, 036, 044, 045, 046, 065, 067, 068, 074, 081, 094, 003/004, 008/009, 012/013, 015/016, 017/018, 037/038, 041/042, 047/048, 051/052, 055/056, 059/060, 061/062, 082/083, 084/085, 095/096, 102, 103/104, 106, 848, 854, 856
		1b	014, 024, 031/032, 033/034, 039, 049, 063, 064, 076, 087/088, 089/090, 091/092, 093, 098, 099, 100/101, 107, 111/112
2	2a	2aa	001, 007, 027, 029, 050, 073, 105
		2ab	010, 043, 072, 075,113, 804, 828
	2b	2ba	108, 812, 846
		2bb	005, 021, 066, 069/070, 110, 814
3	3	3a	002, 028, 030
		3b	025, 071

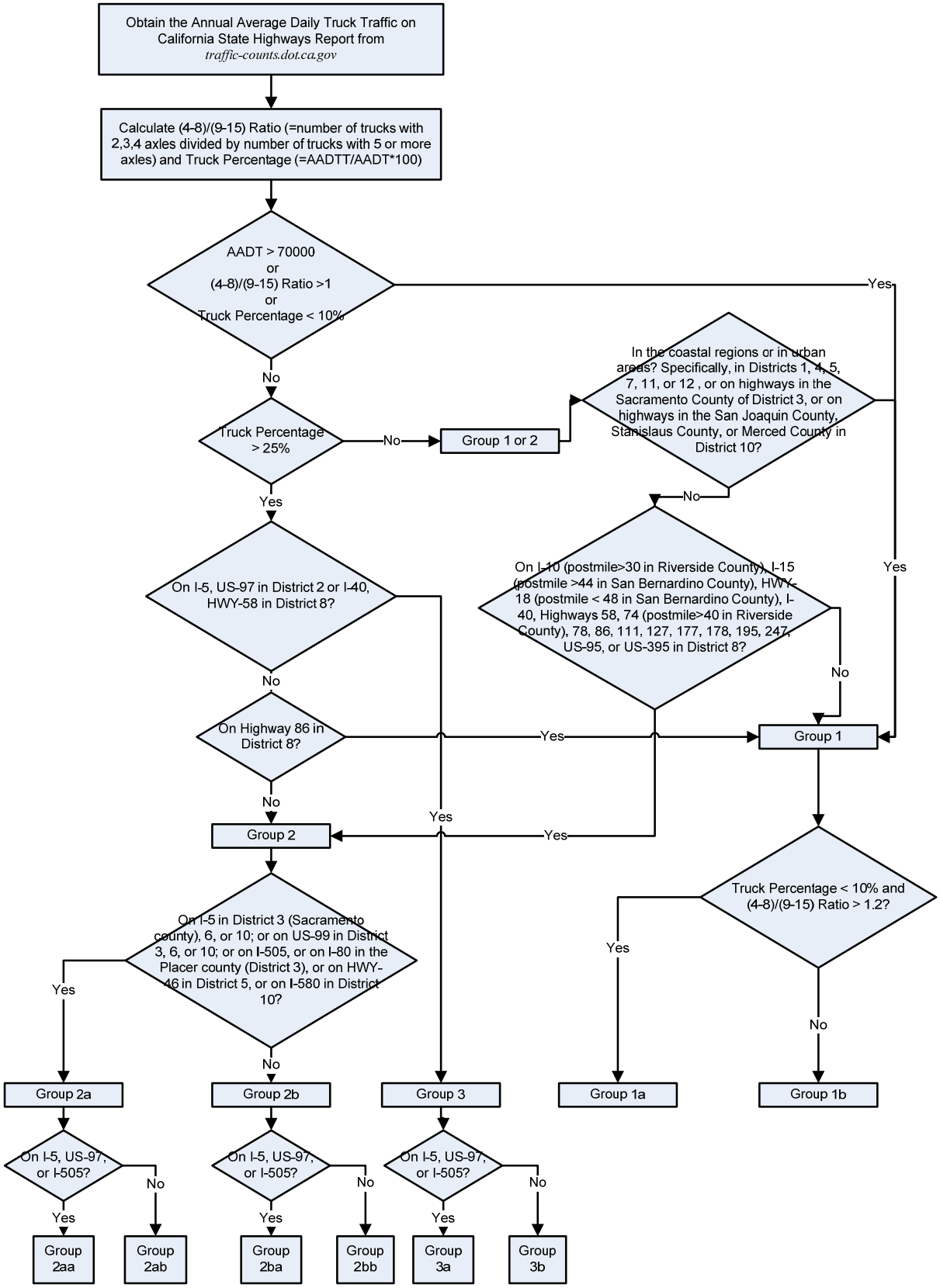

Figure 2.9: Flowchart for grouping highways based on axle load spectra.

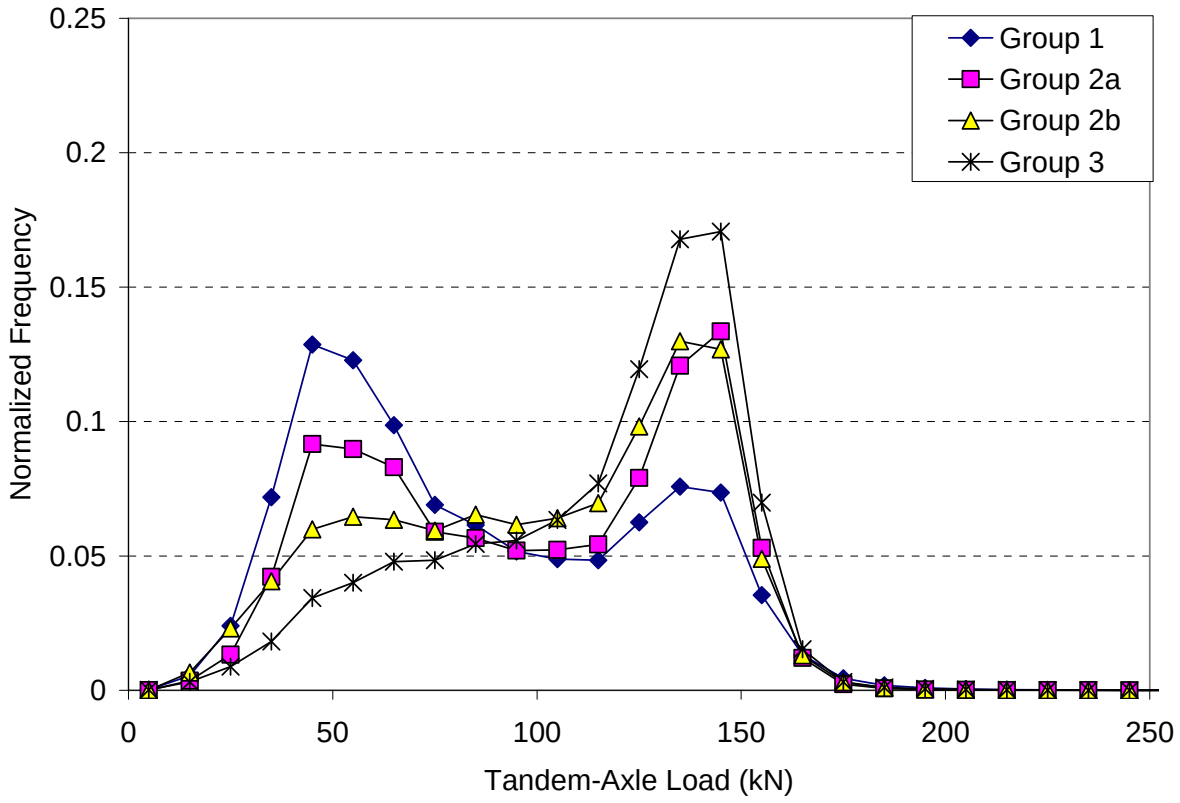

Figure 2.10: Four most common axle load spectra groups on California state highways. (10 kN = 2,250 lb)

Hourly Axle Load Spectra Assumptions

The statewide axle load spectra data were converted into hourly single axle spectra data for weekdays and weekends, for typical urban and rural sections (defined later), and for each test section. The hourly frequencies of occurrence of the axle loads for cars and SUVs were found by using the hourly vehicle counts for typical urban and rural sections and each Pavement Deflection (PD) section included in the statewide spectra data. The hourly occurrence frequencies of the truck axle loads for each WIM group were taken directly from the *CalME* database. Figure 2.11 shows examples of hourly frequencies of occurrence for the axle loads, in this case on a rural section for Group 2a with 10 percent overall trucks for four periods (nighttime, morning peak, daytime, and afternoon peak) during weekdays and weekends.

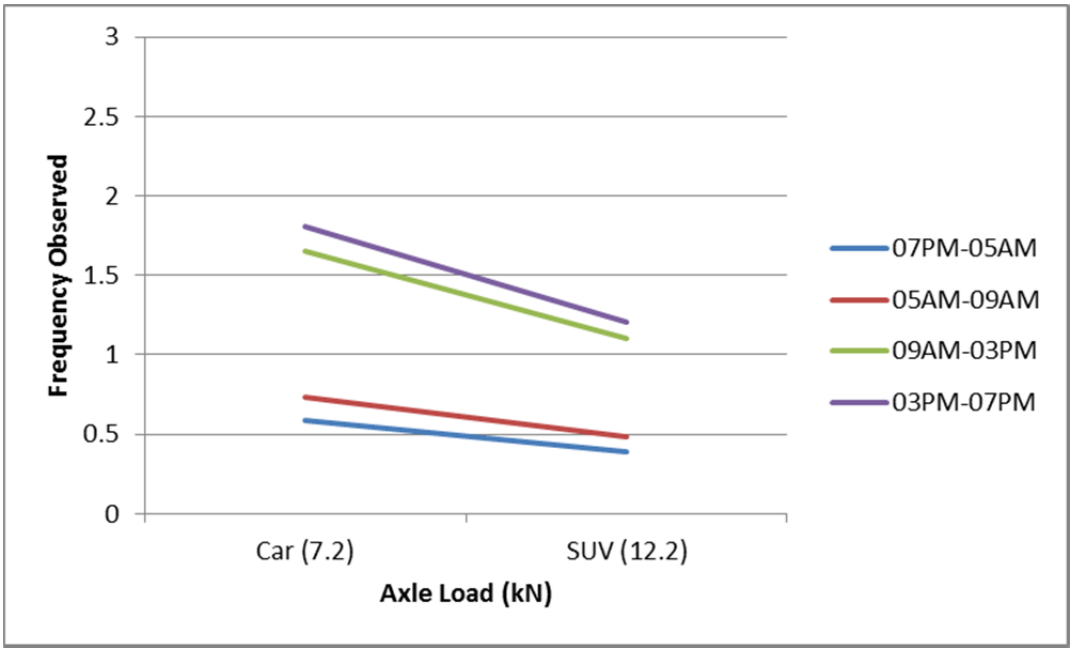

a. Car and SUV axle load frequencies per car and SUVs per weekend day

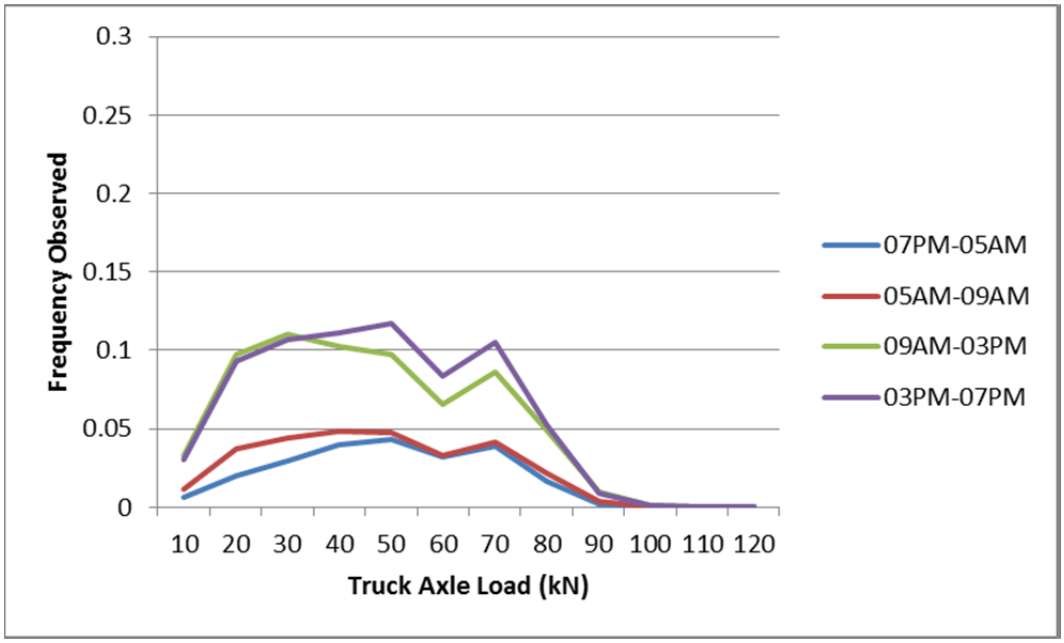

b. Truck axle load frequencies per truck per weekend day

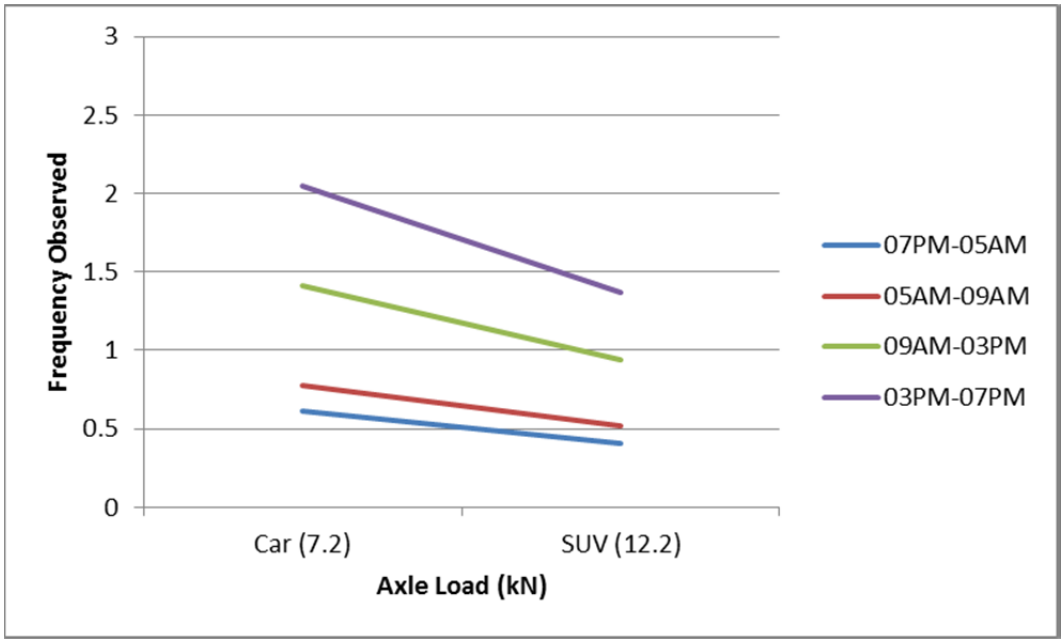

c. Car and SUV axle load frequencies per car and SUVs per weekday

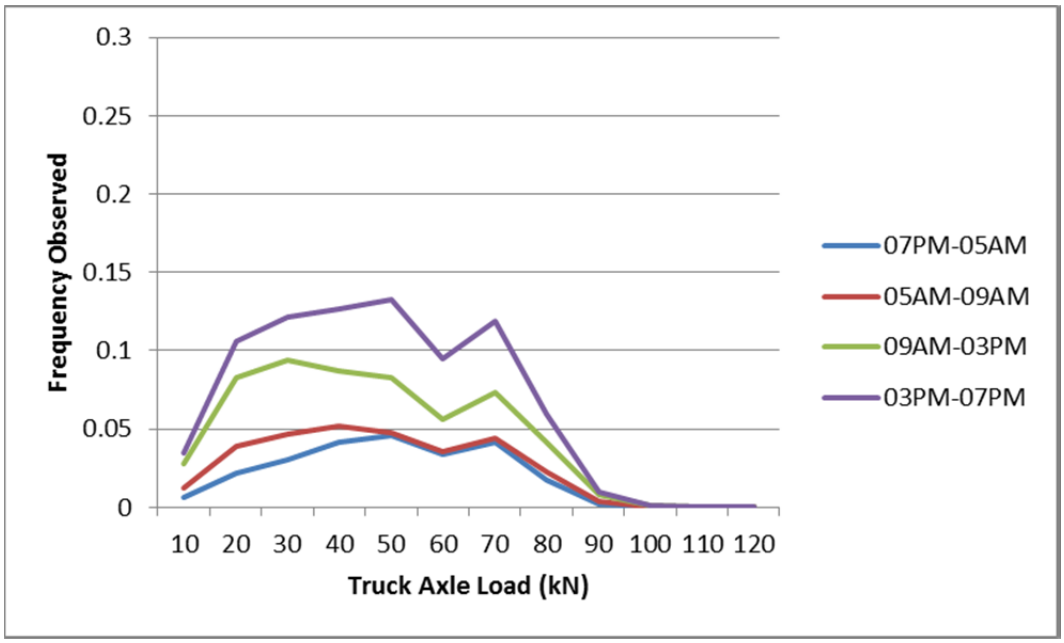

d. Truck axle load frequencies per truck per weekday

Figure 2.11: Example axle load frequencies for different weekday periods for rural section with Group 2a axle load spectrum and 10 percent trucks.

Traffic Volume and Speed Distribution Assumptions

The vehicle definitions used in the traffic data are the following:

1. Cars: compact, mid-size, full-size automobiles, and equivalent vehicles
2. SUVs: Sport utility vehicles, minivans, pickup trucks, utility trucks, commercial delivery vans and trucks, and equivalent vehicles (gross vehicle weight up to 8,500 lbs [37.8 kN])
3. Trucks: Commercial trucks, tractor-trailers, and equivalent vehicles (gross vehicle weight over 8,500 lbs)

Using data extracted from the California vehicle miles-traveled (VMT) database *(37)*, the generic proportional traffic split for nontruck vehicles of 0.6 for cars and 0.4 for SUVs was applied to all sections.

Hourly average traffic volumes and speed data for each section for both weekdays and weekends during the period January 1, 2014 to December 31, 2014 were collected from the California Freeway Performance Measurement System *(PeMS, 38)*, a Caltrans real-time traffic information web-application. The data on percentage of trucks for each section were acquired from the report *Annual Average Daily Truck Traffic on the California State Highway (37)*.

The hourly average speeds for cars and SUVs were extrapolated from PeMS data *(38)*. The hourly average speeds for cars and SUVs were extrapolated from the average speeds on the innermost lane (Lane 1) and those for trucks were extrapolated from the average speeds on the outermost lane (truck lane).

Urban and Rural Road Assumptions

Every ten years the United States Census Bureau identifies urban areas based on new census population data *(39)*. Caltrans used the 2010 adjusted Census Bureau data for transportation planning purposes within its district offices and local agencies.

For this project, one section was selected from the state network to represent all typical urban sections and another to represent all typical rural sections. The selected urban section is located on southbound Interstate 5 in Los Angeles County (Post Mile 17.93) and the selected rural section is located on State Route 152 in Merced County (Post Mile R32.106). These two sections were selected as “representative” for the sensitivity analysis of traffic volume and speed distribution. As expected, there is a wide range of volume and speed patterns on California state highways. The simulations for the individual sections with their section-specific data used the information found in the databases that best fit that specific section.

For the simulations, data on the sections were then sampled to collect traffic volume and speed for both weekdays and weekends. For peak periods during weekdays, the hourly traffic volumes on the selected urban section reach 1,800 vehicles per hour per lane (vphpl) but only 650 vphpl on the selected rural section.

The traffic volume on the typical urban section is shown in Figure 2.12 and the speed distribution is shown in Figure 2.13. It can be seen that traffic volume peaks in the morning and afternoon during weekdays—from 7 a.m. to 9 a.m. and 3 p.m. to 7 p.m., respectively—with associated speed reductions, and has one peak period from 1 p.m. to 5 p.m., with a speed reduction, during weekends.

The traffic volume on the typical rural highway is shown in Figure 2.14 and the speed distribution is shown in Figure 2.15. The typical traffic pattern on the rural highway shows that even though there are peak traffic volumes in the inbound direction on both weekdays and weekends, there are no associated speed reductions during those peak periods. No speed reduction occurs because during these peak periods the traffic volumes on the rural section do not exceed the highway's service capacity.

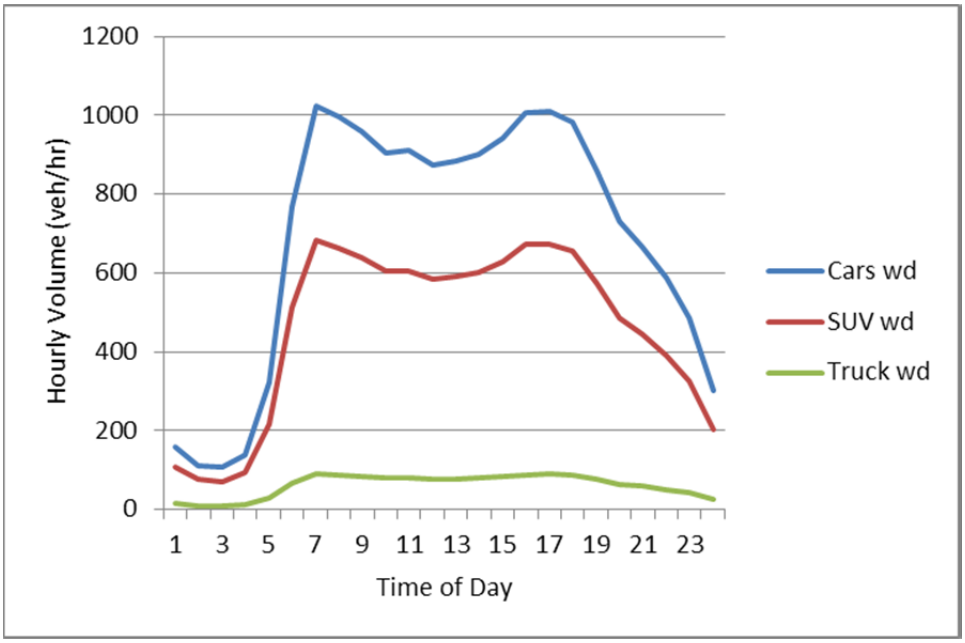

a. Weekday distributions

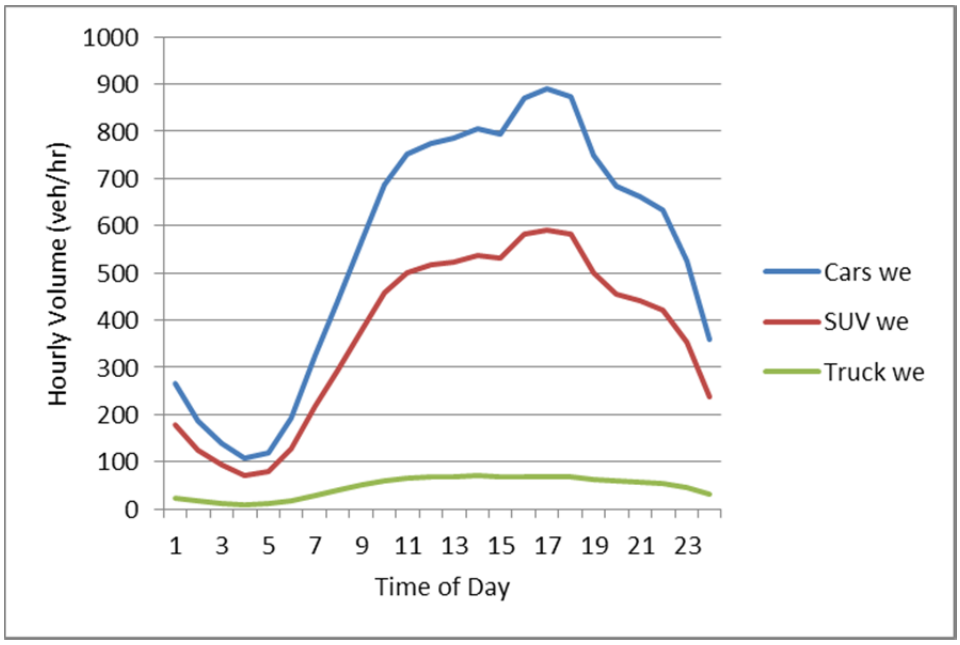

b. Weekend distributions

Figure 2.12: Urban volume distributions.

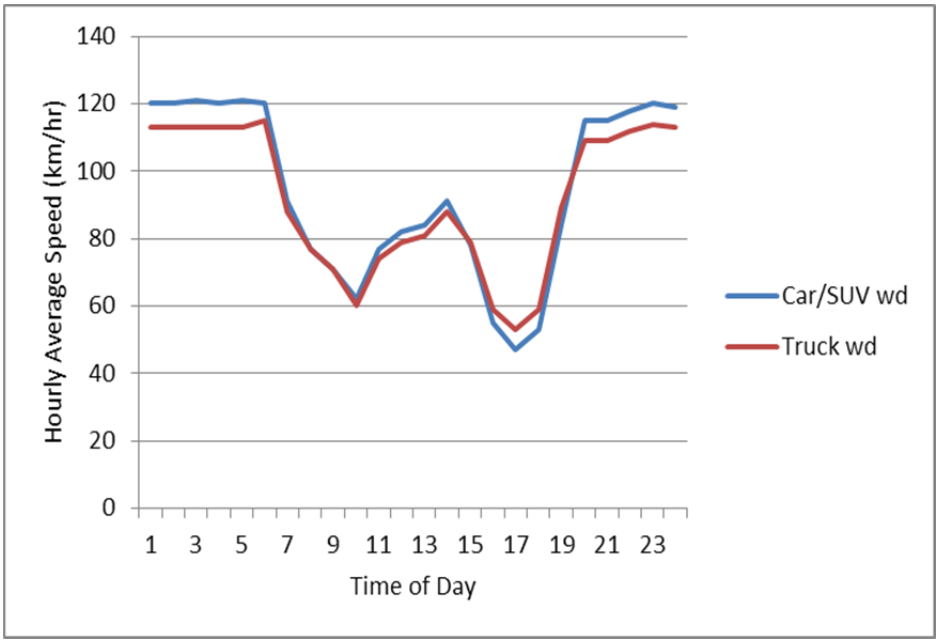

a. Weekday distributions

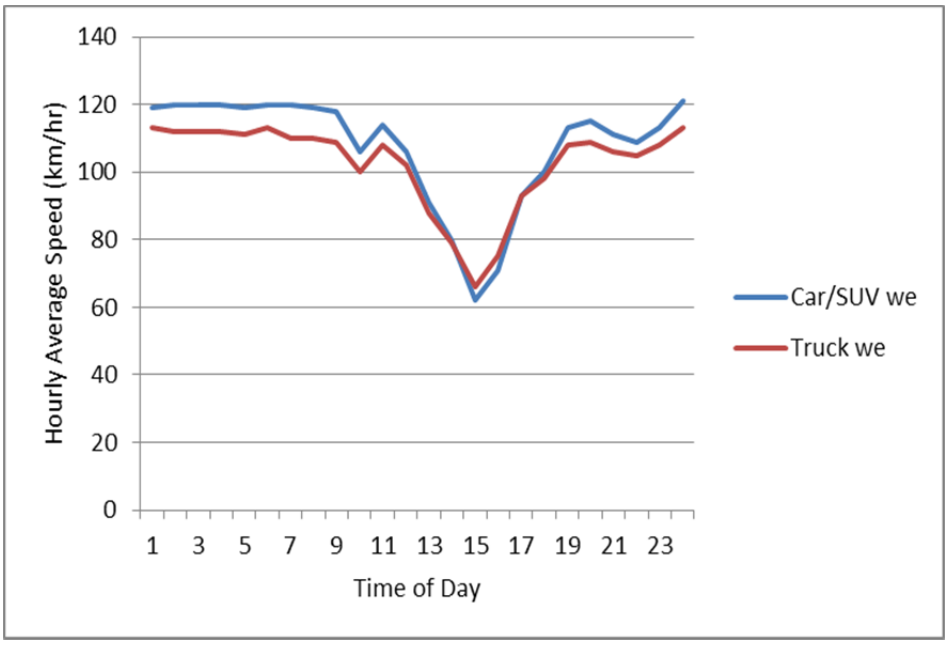

b. Weekend distributions

Figure 2.13: Urban speed distributions.
(120 km/hr = 75 miles/hr)

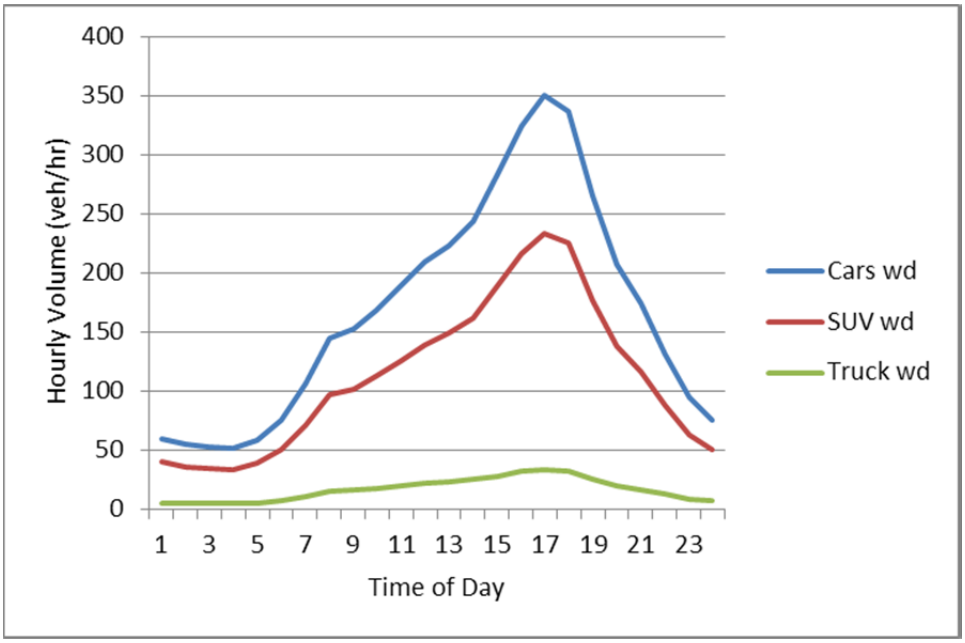

a. Weekday distributions

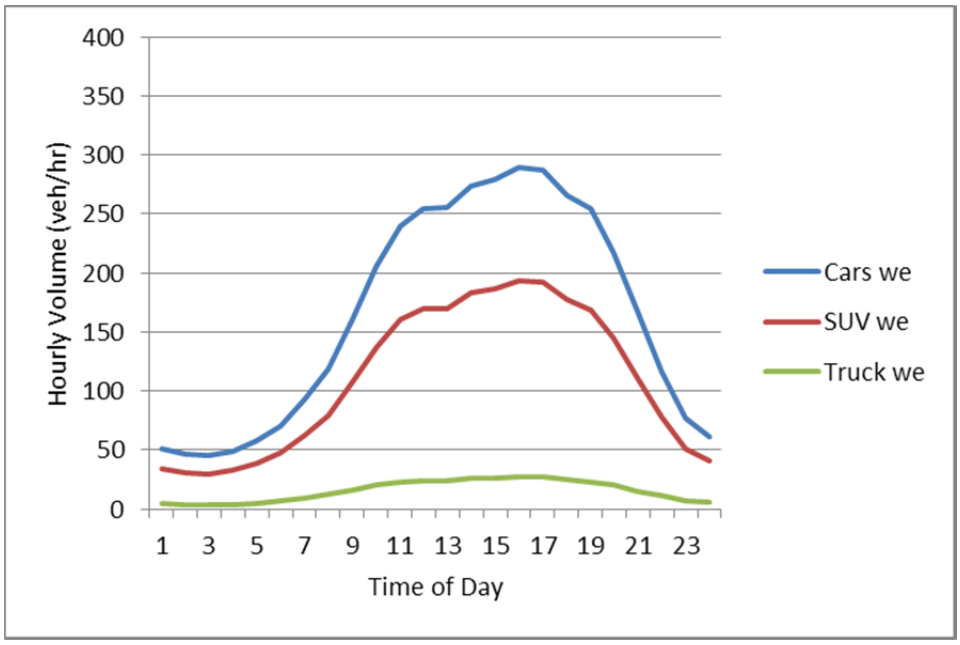

b. Weekend distributions

Figure 2.14: Rural volume distributions.

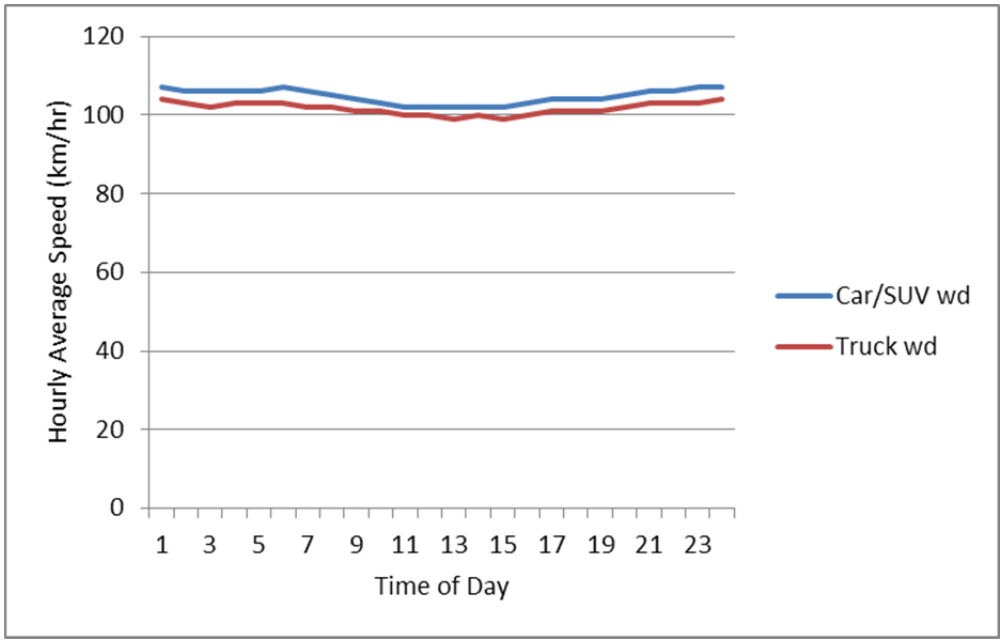

a. Weekday distributions

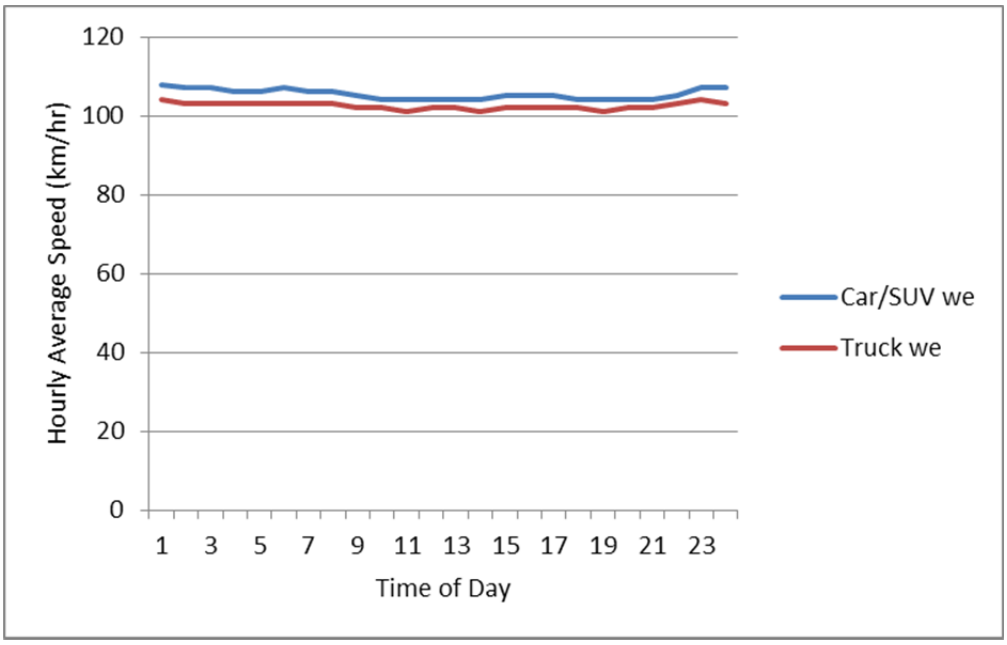

b. Weekend distributions

Figure 2.15: Rural speed distributions.
(100 km/hr = 62 miles/hr)

2.5 Interpolation and Extrapolation of Structural Response Modeling Results

For the simulations, the modeling results for energy for the modeling factorial of three axles loads, two temperatures, and two speeds were used to develop continuous relationships for dissipated energy from pavement structural response versus those three variables using linear regression with transformed variables. Relationships were developed for each modeling group and for each test section. The following relationship was used for the OSU and MSU results, with different coefficients for each set of results:

$$\text{Dissipated energy (MJ)} = exp\left(a_1 + a_2\sqrt[3]{L} + a_3T + a_4v + a_5T\sqrt[3]{L} + a_6v\sqrt[3]{L}\right)$$

For the MIT results the following relationship was used, although the MIT energy dissipation equation shown previously is intended for fast computations such as those performed in this simulation:

$$\text{Dissipated energy (MJ)} = exp(a_1 + a_2\log(L) + a_3\log(T) + a_4\log(v))$$

where L is the axle load (kN),

T is the pavement temperature at one-third depth (ºC) and

v is the speed (km/hr).

All models had $R^2 > 0.997$. Figure 2.16 shows as examples the relationships for the three modeling groups for PD 20. Excess fuel consumption was calculated from the dissipated energy from pavement structural response using the following relationship:

$$\text{Excess fuel consumption } \left(\frac{\text{mL}}{\text{km}}\right) = \frac{\text{W}}{\text{Fuel calorific } \left(\frac{\text{MJ}}{\text{L}}\right)} * 1000$$

where W is the dissipated energy (MJ).

The fuel calorific was assumed to be 34.8 MJ/liter for gasoline *(40, 41)* consumed by cars and SUVs and 40 MJ/liter for diesel used by trucks *(41)*. All trucks were assumed to use diesel and all cars and SUVs were assumed to use gasoline.

In the simulations, vehicles using gasoline were assumed to have 30 percent efficiency in converting the energy in the fuel into useful energy resulting in an effective energy content of 10.5 MJ/liter and vehicles using diesel were assumed to be 40 percent efficient resulting in an effective energy content of 16 MJ/liter.

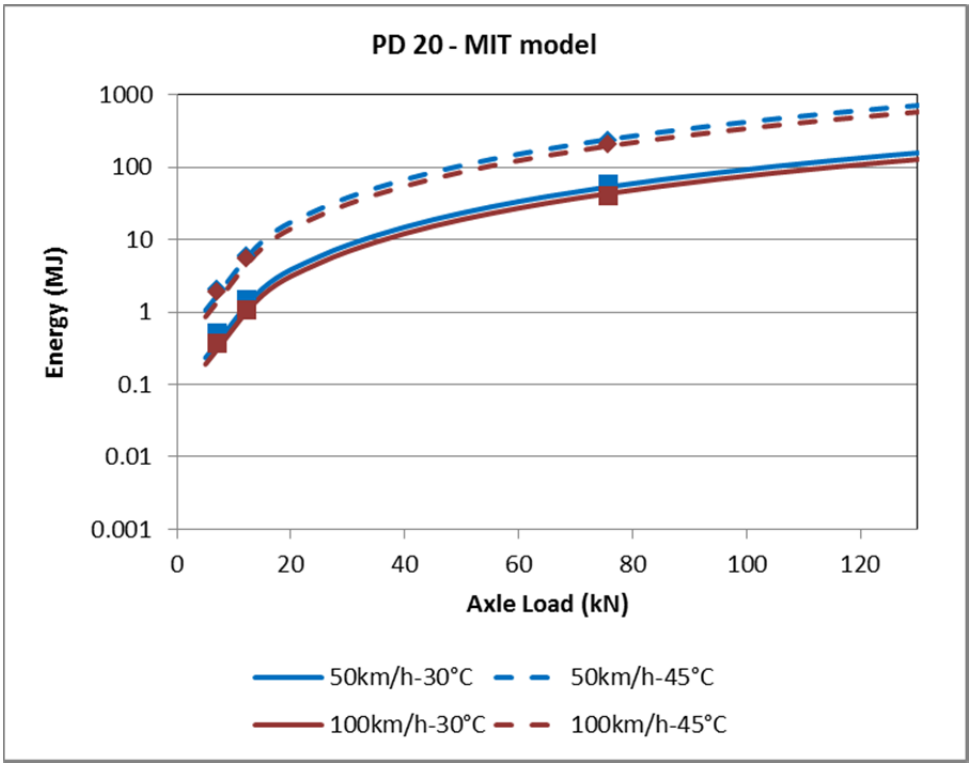

a. Results from the MIT model

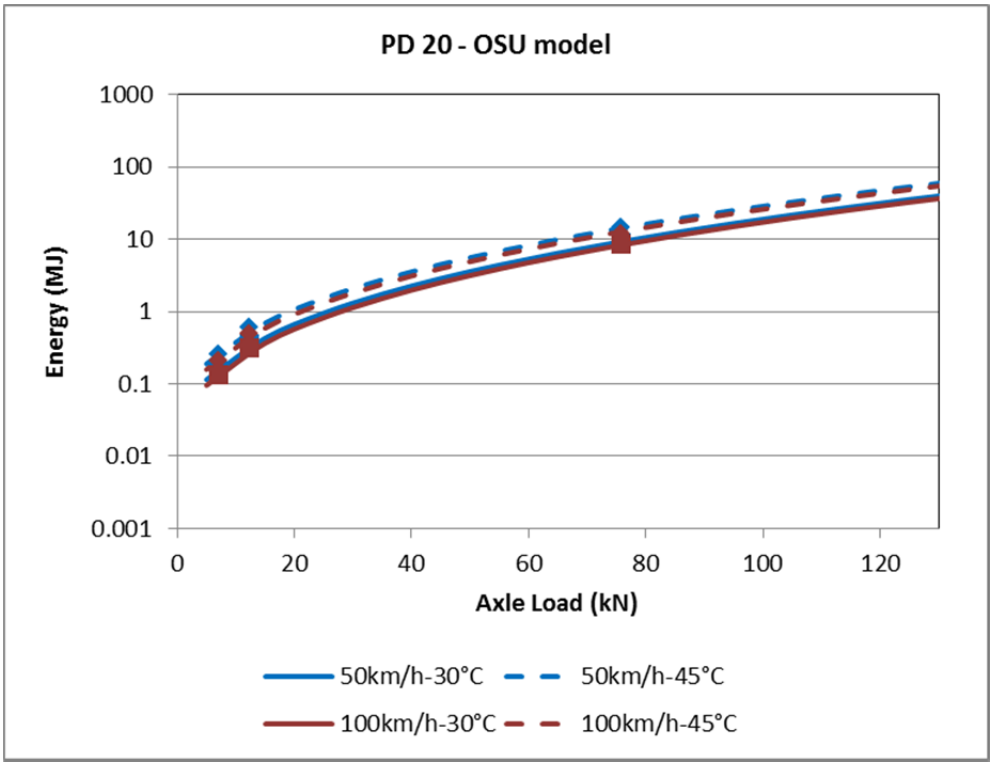

b. Results from the OSU model

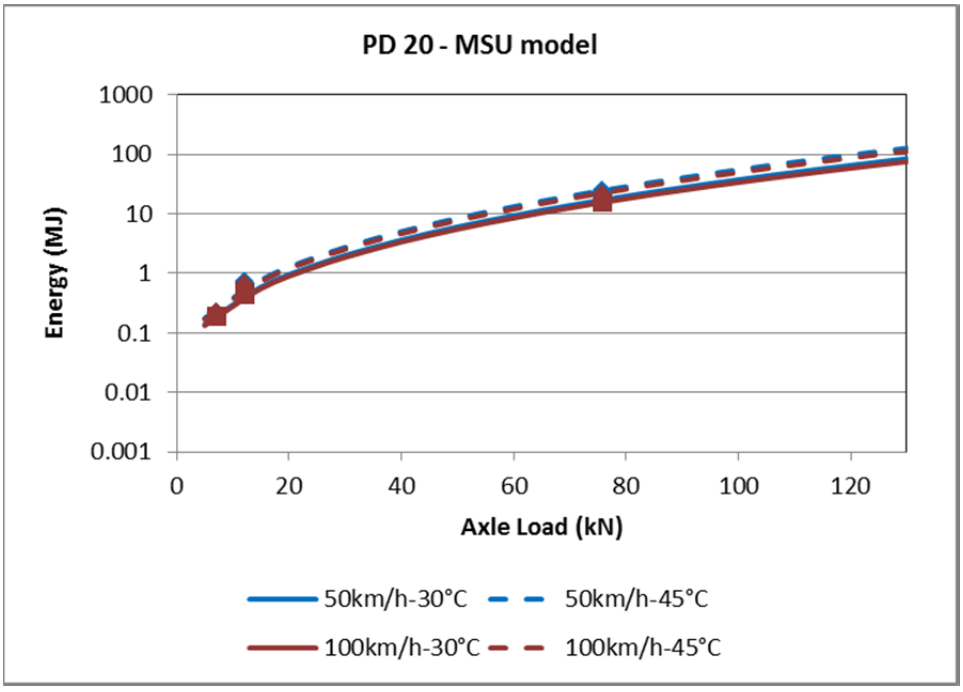

c. Results from the MSU model

Figure 2.16: Best fit continuous relationships for energy consumption versus axle load, temperature, and speed for PD 20.

3. ANNUAL FUEL USE SIMULATION RESULTS FOR TEST SECTIONS

The MATLAB® code used for the simulations calculated excess fuel consumption for the individual test sections with their actual traffic and climate, and across the simulation factorial, and produced the following results for EFC in the unit milliliters of fuel per kilometer traveled per vehicle (mL/km/veh). For the simulations across the factorial, the code produced results for each test section, for each climate region, for rural and urban traffic, for each axle spectrum group, and for truck percentages of 5, 10 and 15 percent. The code calculated EFC for structural response (EFC_S), roughness (EFC_{IRI}), and macrotexture (EFC_{MPD}).

The EFC_S for each asphalt-surfaced test section for which modeling had been performed (including subsections identified from deflection analysis) are shown for the section-specific actual traffic and climate on the sections in Table 3.1 and Figure 3.1, and for the factorial of climate regions and traffic variables in Table 3.2 and Figure 3.2. The results are shown in terms of excess fuel consumption relative to the ideal pavement defined in Chapter 2 and in the notes below Table 3.1 and Table 3.2. The detailed results are included in Appendix D. The sections in Table 3.1, Table 3.2, Figure 3.1, and Figure 3.2 are grouped by pavement type, with concrete pavements (not shown), composite pavements (asphalt on concrete), flexible pavements, and semi-rigid pavements (asphalt on cemented base).

From the results it can be seen that on average across all the test sections analyzed, the MIT model produced the lowest estimates for EFC_S, the MSU model produced the highest estimates, and the results from the OSU model fell between the other two. The results from all of the models are of similar order of magnitude. Sections for which one model presented much different results from the other models are PD 7, PD 14, and PD 16, where the MSU model showed much higher EFC_S, and PD 20, where the MIT model showed much higher EFC_S. The results for these sections were reviewed by the respective modelers, but no apparent errors were found in the calculations. These results indicate that calibration is needed.

The average EFC_{IRI} and EFC_{MPD} for each asphalt-surfaced test section and the section-specific climate and traffic are shown in Figure 3.3. The detailed results by vehicle type for the section-specific simulations are included in Appendix D. The sections are grouped in the figure by pavement type. The results for roughness and macrotexture are similar for nearly all of the sections because most of the sections were selected for moderately low roughness and macrotexture in order to focus on the effects of structural response. The exceptions are the two sections selected for higher roughness: PD 4, which has a concrete surface (results not shown) and PD 14, which has an asphalt surface, as well as PD 18, which has a newly paved and very smooth asphalt surface.

Table 3.1: Summary of Excess Fuel Consumption due to Structural Response, Roughness, and Macrotexture for Each Test Section Simulated with Section-Specific Traffic and Climate

Row Labels	Percent Trucks	Pavement Type[1]	EFC_S [2] (mL/km/veh)			(mL/km/veh)		
			MIT	MSU	OSU	[3]EFC_{IRI}	[4]EFC_{MPD}	EFC IRI+MPD
PD 01		Concrete (JPCP)	Results underway, to be reported in separate technical memorandum					
PD 02		Concrete (JPCP)						
PD 03		Concrete (JPCP)						
PD 04		Concrete (JPCP)						
PD 05		Concrete (CRCP)						
PD 06		Composite, DGAC surface						
PD 07	6.2	Composite, thick DGAC surface	0.07	0.92	0.48	0.21	0.16	0.37
PD 08	3.0	Composite, DGAC surface	0.03	0.09	0.11	0.81	0.12	0.94
PD 10	9.8	Composite, RHMA-G surface	0.02	0.34	0.32	0.39	0.16	0.55
PD 11	4.4	Flexible, old thick DGAC surface	0.02	0.31	0.21	0.71	0.18	0.89
PD 12	3.8	Flexible, new DGAC surface						
PD 13s1	7.2	Flexible, new DGAC surface	0.30	0.52	0.43	0.92	0.05	0.98
PD 13s2	7.2	Flexible, new DGAC surface	0.17	0.23	0.19	0.92	0.05	0.98
PD 14	7.2	Flexible, old thick DGAC surface	0.10	0.56	0.14	3.11	0.09	3.20
PD 15	15.6	Flexible, RHMA-O surface on thick DGAC	0.11	0.07	0.05	0.41	0.30	0.71
PD 16	12.1	Flexible, old thick DGAC surface	0.07	0.54	0.26	0.40	0.09	0.49
PD 17	4.4	Flexible new DGAC surface						
PD 18s1	7.2	Flexible, RHMA-G surface on old DGAC	0.06	0.04	0.03	0.03	0.12	0.14
PD 18s2	7.2	Flexible, RHMA-G surface on old DGAC	0.06	0.04	0.03	0.03	0.12	0.14
PD 19	4.4	Flexible, RHMA-G surface on new DGAC	0.02	0.31	0.18	0.52	0.10	0.62
PD 20	7.2	Semi-rigid, RHMA-O surface	0.61	0.14	0.08	0.89	0.24	1.14
PD 21	13.3	Semi-rigid, RHMA-O surface	0.08	0.10	0.05	1.01	0.31	1.33
PD 22s1	8.7	Semi-rigid, RHMA-G surface	0.09	0.07	0.14	0.62	0.07	0.70
PD 22s2	8.7	Semi-rigid, RHMA-G surface	0.12	0.18	0.14	0.62	0.07	0.70
PD 23	5.4	Semi-rigid, DGAC surface	0.08	0.22	0.28	0.40	0.11	0.51
Average Sections with EFC_S	**7.5**		**0.12**	**0.28**	**0.18**	**0.71**	**0.14**	**0.96**

[1] JPCP is jointed plain concrete pavement, CRCP is continuously reinforced concrete pavement, DGAC is dense-graded asphalt concrete; RHMA-G is gap-graded rubberized hot mix asphalt; RHMA-O is open-graded rubberized hot mix asphalt.
[2] Compared with ideal pavement with no structural response.
[3] Compared with ideal pavement with IRI = 0.6 m/km (38 inches/mile).
[4] Compared with ideal pavement with MPD = 0.5 mm.

Table 3.2: Summary of Excess Fuel Consumption due to Structural Response, Roughness, and Macrotexture for Each Test Section Simulated Across Factorial

Row Labels	Pavement Type[1]	EFC_S [2] (mL/km/veh)		
		MIT	MSU	OSU
PD 01	Concrete (JPCP)	Results underway, to be reported in separate technical memorandum		
PD 02	Concrete (JPCP)			
PD 03	Concrete (JPCP)			
PD 04	Concrete (JPCP)			
PD 05	Concrete (CRCP)			
PD 06	Composite, DGAC surface			
PD 07	Composite, thick DGAC surface	0.14	1.41	0.79
PD 08	Composite, DGAC surface	0.08	0.18	0.26
PD 10	Composite, RHMA-G surface	0.03	0.39	0.36
PD 11	Flexible, old thick DGAC surface	0.04	0.77	0.67
PD 12	Flexible, new DGAC surface			
PD 13s1	Flexible, new DGAC surface	0.43	0.70	0.58
PD 13s2	Flexible, new DGAC surface	0.25	0.31	0.26
PD 14	Flexible, old thick DGAC surface	0.19	0.92	0.22
PD 15	Flexible, RHMA-O surface on thick DGAC	0.12	0.08	0.05
PD 16	Flexible, old thick DGAC surface	0.10	0.66	0.32
PD 17	Flexible new DGAC surface			
PD 18s1	Flexible, RHMA-G surface on old DGAC	0.08	0.06	0.04
PD 18s2	Flexible, RHMA-G surface on old DGAC	0.09	0.07	0.04
PD 19	Flexible, RHMA-G surface on new DGAC	0.06	0.61	0.40
PD 20	Semi-rigid, RHMA-O surface	0.70	0.20	0.11
PD 21	Semi-rigid, RHMA-O surface	0.11	0.11	0.06
PD 22s1	Semi-rigid, RHMA-G surface	0.17	0.12	0.23
PD 22s2	Semi-rigid, RHMA-G surface	0.23	0.34	0.34
PD 23	Semi-rigid, DGAC surface	0.19	0.37	0.42
Average Sections with EFC_S		**0.18**	**0.43**	**0.30**

[1] JPCP is jointed plain concrete pavement, CRCP is continuously reinforced concrete pavement, DGAC is dense-graded asphalt concrete; RHMA-G is gap-graded rubberized hot mix asphalt; RHMA-O is open-graded rubberized hot mix asphalt.

[2] Compared with ideal pavement with no structural response.

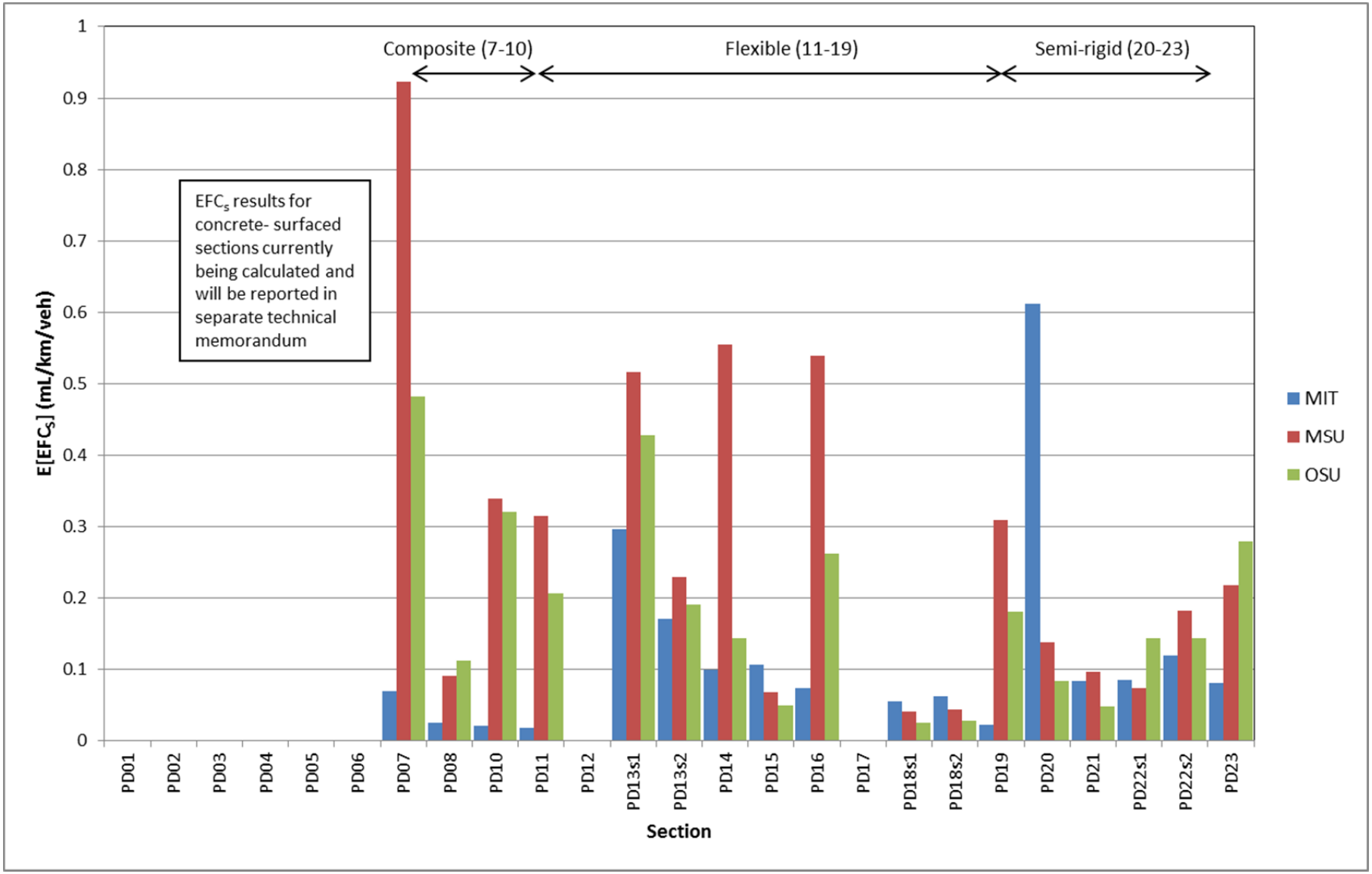

Figure 3.1: Average structural response simulation results in terms of Excess Fuel Consumption due to structural response (EFC_S) by asphalt section relative to no structural response effect (avg mL/km/veh EFC) simulated with section-specific traffic and climate.

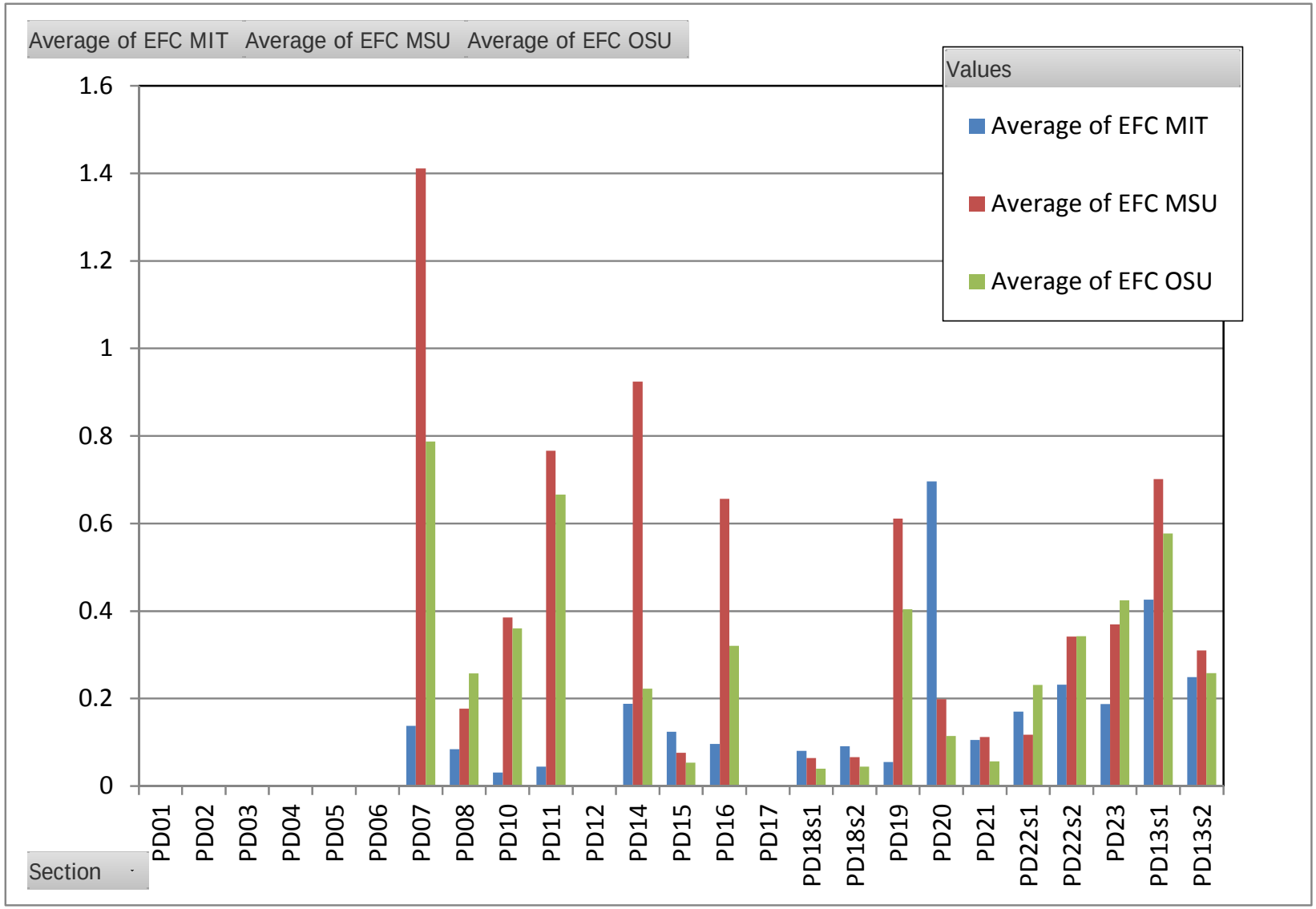

Figure 3.2: Average structural response simulation results in terms of Excess Fuel Consumption due to structural response (EFC_S) by asphalt section relative to no structural response effect (avg mL/km/veh EFC) across traffic and climate factorial.

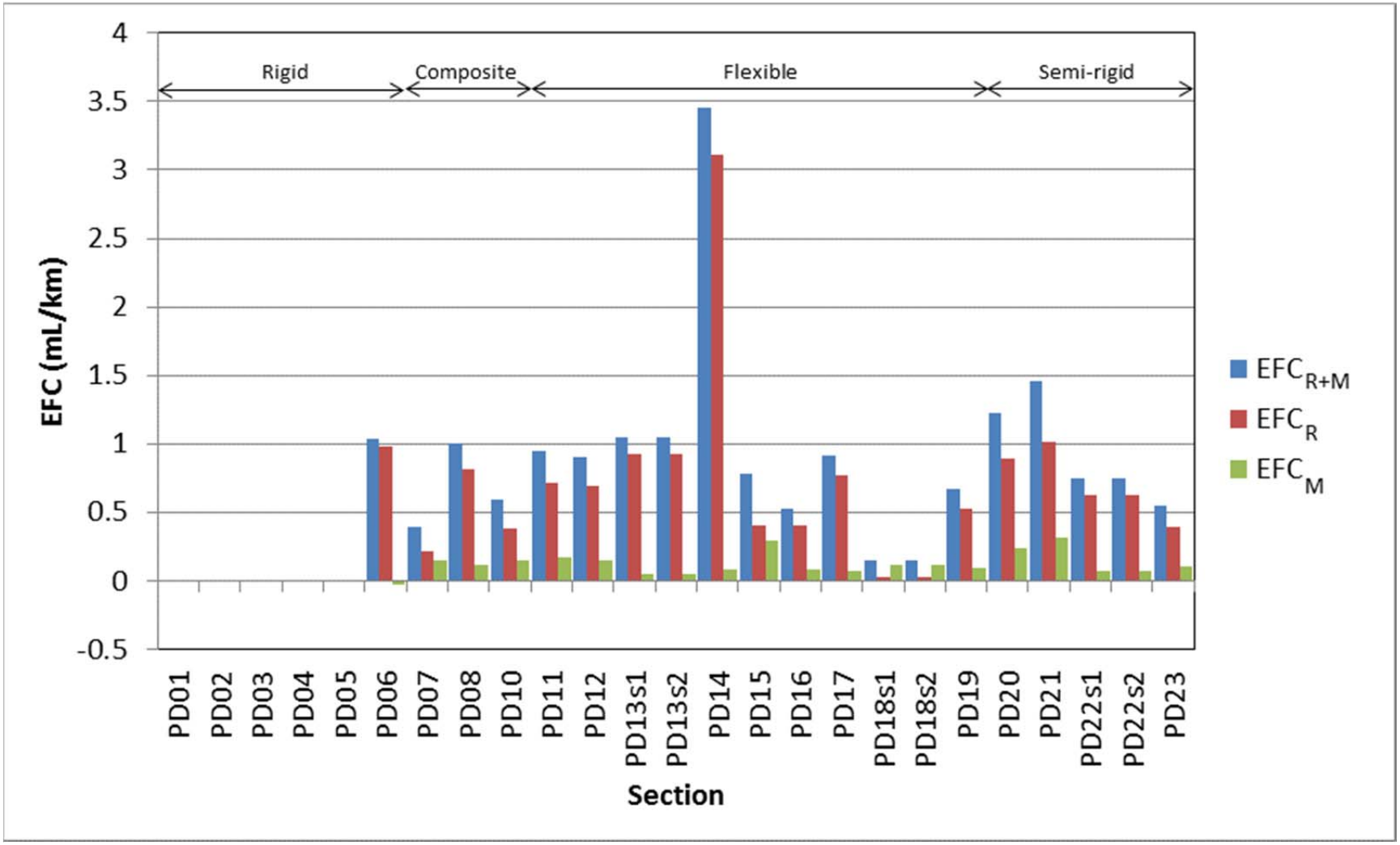

Figure 3.3: Average roughness, macrotexture, and combined roughness and macrotexture simulation results in terms of Excess Fuel Consumption due to roughness and macrotexture (EFC_{IRI}, EFC_{MPD}) and combined roughness and macrotexture ($EFC_{IRI+MPD}$) relative to 38 inches/mile IRI and 0.5 mm MPD by section (avg mL/km/veh EFC) simulated with section-specific traffic and climate.

4. ANALYSIS AND INTERPRETATION

4.1 Analysis of Results for Different Vehicle Types

The average results across the sections for each vehicle type and model approach are shown in Table 4.1; these results based on section-specific data. Based on these results it can be calculated that the ratio of average EFC_S between trucks and cars plus SUVs (weighted assuming 60 percent cars and 40 percent SUVs) is 15:1 for the MIT model, 6.1:1 for the MSU model, and 6.6:1 for the OSU model. These values indicate how much more important truck traffic is for overall EFC_S compared with cars and SUVs according to the results from all of the models, and also illustrate that there are important differences between the MIT model and the other two models with respect to sensitivity to axle loads, with the MIT model being more sensitive.

Table 4.1: Average EFC_S for Each Vehicle Type and Model Approach across the Simulation Factorial and All Sections (mL/km/veh)

MIT Car	MIT SUV	MIT Truck	MSU Car	MSU SUV	MSU Truck	OSU Car	OSU SUV	OSU Truck
0.01	0.03	0.27	0.06	0.11	0.48	0.04	0.07	0.33

4.2 Analysis of Results for Different Structures and Surfaces for Structural Response

4.2.1 Pavement Structure Type

The average EFC_S for each of the asphalt-surfaced pavement types and model approaches are shown in Table 4.2 for the results of simulation using the traffic and climate factorial. From the results it can be seen that the MSU and OSU models tended to rank the pavement types similarly, with the composite sections having the highest EFC_S, followed by the flexible sections and the semi-rigid sections. The OSU model shows the flexible and semi-rigid sections having approximately the same EFC_S on average, while the MSU model shows a greater difference. The MIT model indicated that the composite pavements had the smallest EFC_S and the flexible and semi-rigid pavements had approximately the same value. This may be due to the MIT model's use of a beam rather than a finite element solution combined with the high stiffness of the concrete layer below the asphalt, which affects the model results for the gradient under the wheel (the parameter used for the initial calibration of the current simplified MIT model).

Table 4.2: Average EFC Due to Structural Response by Asphalt-Surfaced Pavement Type and Model from Factorial Simulation

Pavement Type	Average EFC_S (mL/km/veh)		
	MIT	MSU	OSU
Composite	0.08	0.66	0.47
Flexible	0.15	0.41	0.30
Semi-rigid	0.17	0.24	0.26

4.2.2 Pavement Surface Type (Conventional or Rubberized)

Table 4.3 shows the average EFC_S results of the simulation using the traffic and climate factorial for the asphalt-surfaced pavement types—that is, for those with dense-graded hot mix (DGAC) and rubberized surfaces (RHMA)—and for each model approach. From the results it can be seen that the MSU and OSU models tended to rank the asphalt pavement surface mix types differently than the MIT model: results from the MSU and OSU models show the conventional DGAC-surfaced sections with higher EFC_S than the sections with rubberized surface materials, while the MIT model shows similar results for both surface mix types. The maximum thickness of the rubberized surface is 60 mm (2.4 inches, 0.2 ft) and the rubberized layer is on top of thicker layers of existing asphalt in all of the sections. The rubberized layer would be expected to have a small effect on the model results because all of the asphalt layers were treated as a single layer in the backcalculation of stiffness and viscoelastic properties and forward modeling. Although rubberized asphalt often has lower stiffness than conventional asphalt at low and intermediate temperatures and similar or higher stiffness at high temperatures, any localized effects in the rubberized layer at the surface of the pavement would not have been isolated in any of the modeling approaches. Use of the shear frequency sweep results from cores of individual asphalt layers, and use of separate properties for the RHMA and any underlying asphalt layers can be considered in potential future modeling.

Table 4.3: Average EFC Due to Structural Response by Rubberized and Conventional Asphalt-Surfaced Type and Model from Factorial Simulation

Pavement Surface Mix Type	Average EFC_S (mL/km/veh)		
	MIT	MSU	OSU
DGAC	0.18	0.63	0.47
RHMA	0.18	0.22	0.18

4.3 Analysis of Results for Traffic and Climate for Structural Response

4.3.1 Rural and Urban Traffic Regimes

Average results across the simulation factorial are shown for the rural and urban hourly speed and flow regimes and for different percentages of trucks in the traffic flow in Table 4.4 and Figure 4.1. It can be seen that the EFC_S increases as the percentage of trucks increases, which reflects the results shown in Table 4.4. This is expected because dissipated energy should increase approximately as a function of the stiffness of the layer times the strain squared, resulting in a much larger amount of energy being dissipated per vehicle by heavier trucks which cause much larger strains than cars and SUVs. Linear relations fit to the simulation results shown in Figure 4.2 indicate an increase in EFC_S of between 1.5 and 2.5 percent per change in percent trucks for the range of values simulated with the three models.

It can also be seen in the data and Figure 4.1 that the EFC_S is approximately the same for the rural and urban hourly traffic flow and speed regimes, which was surprising. However, this result can be explained with an examination of Figure 2.12 through Figure 2.15 (hourly distribution figures), which show the interaction of hourly traffic speeds and pavement temperatures for the two regimes, and the fact that high temperatures and slow traffic increase energy dissipation in the pavement while cooler temperatures and faster traffic have the opposite effects. Urban weekday peak volumes and the resulting maximum speed reductions occur in the early morning, when pavement temperatures are cool, and in the early evening afternoon, when the pavement is still hot but has cooled from its highest temperature, which occurs during the early afternoon.

On the other hand, the rural weekday peak traffic volume peaks in the late afternoon, the hottest part of the day. Therefore, the slow speeds at cool and warm temperatures of the urban traffic regime peaks have approximately the same effect as the high temperatures of the rural traffic regime high-traffic flows, resulting in approximately the same net result for the rural and urban flow regimes. Weekend traffic volume distributions are similar for the urban and rural regimes. Weekend urban traffic slows during the hot time of the day. Urban speeds are higher outside the peak weekend flows at the hot time of the day, but rural speeds are slower than urban speeds across the rest of the day. It appears that these interactions effectively cancel each other out, although the MSU and OSU models indicate that the urban traffic regime does result in a slightly higher EFC_S than the rural regime.

Table 4.4: Average EFC_S (mL/km/veh) for Rural and Urban Speed and Flow Regimes and Different Percentages of Trucks from Factorial Simulation

Speed	Trucks	Average EFC_S MIT	Average EFC_S MSU	Average EFC_S OSU
Rural	5%	0.11	0.31	0.21
	10%	0.18	0.43	0.31
	15%	0.25	0.56	0.40
Urban	5%	0.11	0.31	0.22
	10%	0.18	0.44	0.32
	15%	0.25	0.57	0.42

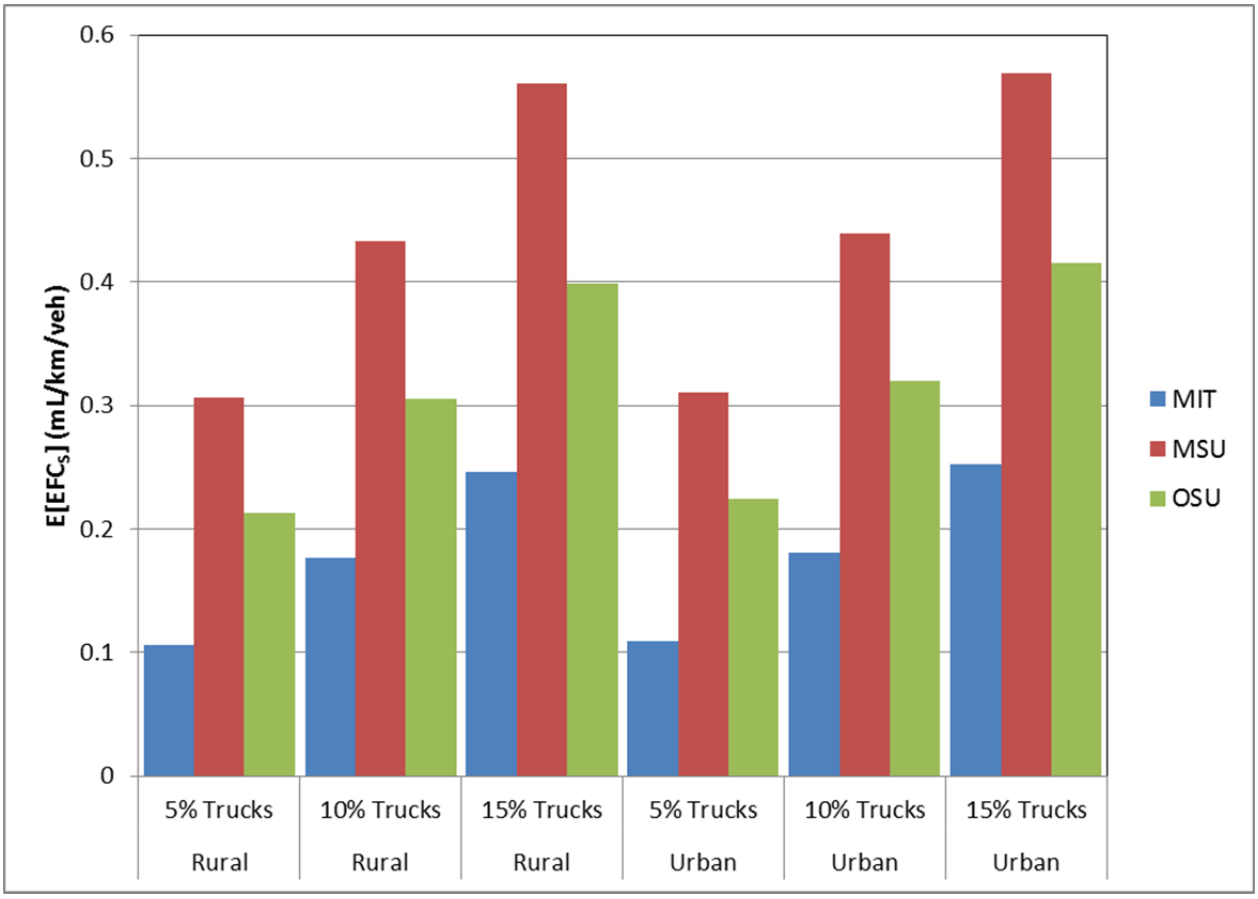

Figure 4.1: Structural response simulation results: factorial by percent of trucks and vehicle speed regime (urban/rural) from factorial simulation.

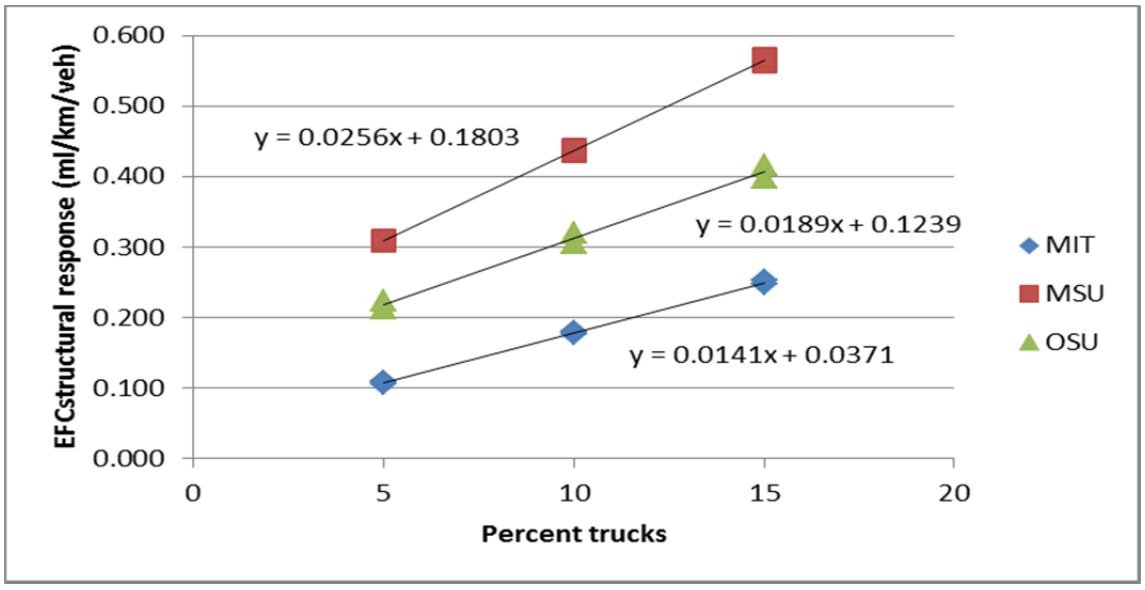

Figure 4.2: Average structural response simulation results across factorial with change in percent trucks.

4.3.2 Climate Region

Average results across the simulation factorial are shown for the nine pavement design climate regions in Table 4.5 and Figure 4.3. From the results shown in the table and the figure it can be seen that the climate region with the highest EFC_S was the hot Desert region, the region with the lowest EFC_S was the cool North Coast Region, and the results for the other regions were consistent with the cumulative distributions of pavement temperatures seen previously in Figure 2.7. The High Desert, with its extremes of cold winters and hot summers, resulted in EFC_S similar to the Central Coast region, which has consistently moderate temperatures centered just below 20°C (67°F). All of the models were consistent between each other in their rankings of EFC_S across the climate regions.

Table 4.5: Average EFC_S (mL/km/veh) for Nine Pavement Design Climate Regions from Factorial Simulation

Row Labels	Average of EFC_S MIT	Average of EFC_S MSU	Average of EFC_S OSU
Central Coast	0.13	0.36	0.23
Desert	0.24	0.53	0.42
High Desert	0.15	0.38	0.26
High Mountain	0.19	0.45	0.32
Inland Valley	0.20	0.46	0.34
Low Mountain	0.22	0.49	0.37
North Coast	0.11	0.31	0.18
South Coast	0.17	0.43	0.29
South Mountain	0.19	0.45	0.32

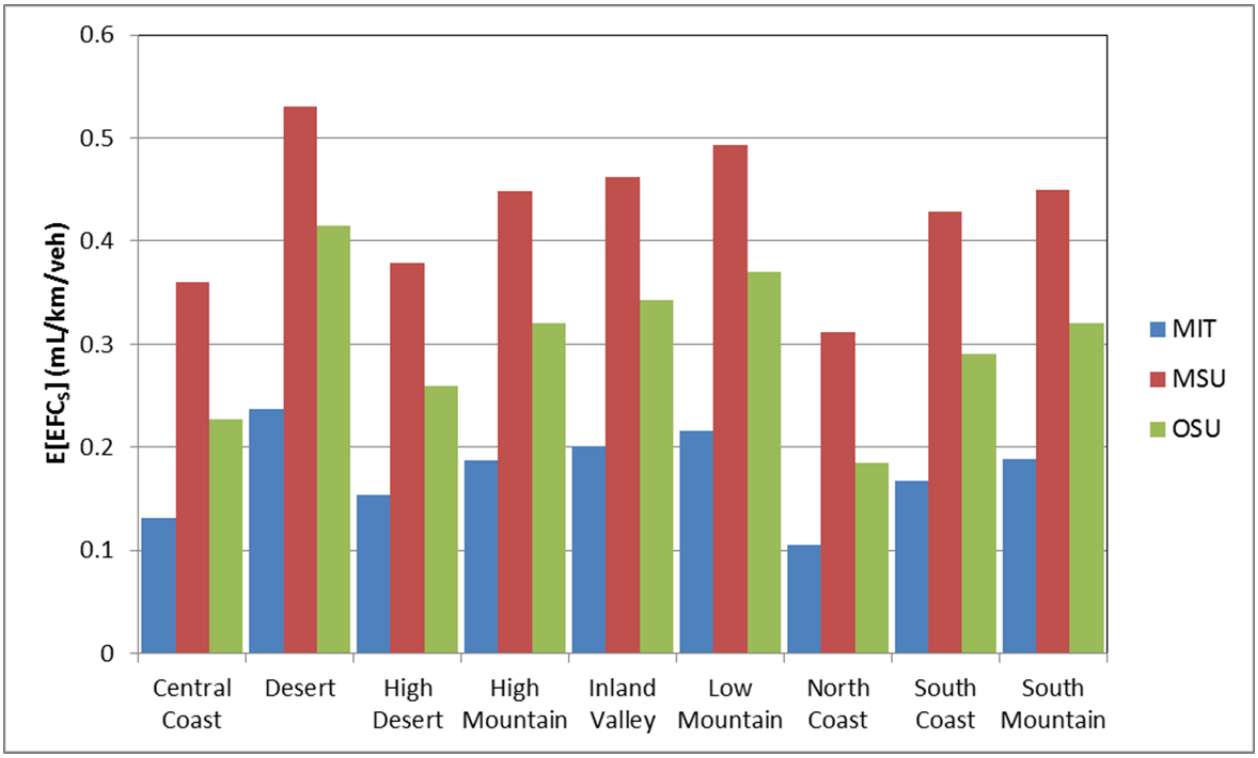

Figure 4.3: Average structural response simulation results by climate region across factorial.

4.3.3 Axle Load Spectra

Average results across the simulation factorial are shown for the four axle load spectra in Table 4.6 and Figure 4.4. From the results in Table 4.6 and Figure 4.4 and the spectra shown in Figure 2.10 it can be seen that the heavier Group 3 spectrum produced the highest simulated EFC_S while the lighter Group 1 spectrum produced the lowest EFC_S. Groups 2a and 2b have similar distributions of heavy axle loads, but differ somewhat for medium and light loads. However, all of the models consistently showed that the net effect of the Group 2a and 2b distributions produced nearly identical values of EFS_S. The results show that axle load spectrum is an important consideration in analyzing EFS_S because of the large influence of truck axle loads.

Table 4.6: Average EFC_S (mL/km/veh) for Four Axle Load Spectra from Factorial Simulation

Row Labels	Average of EFC_S MIT	Average of EFC_S MSU	Average of EFC_S OSU
Group 1	0.13	0.35	0.25
Group 2a	0.18	0.43	0.31
Group 2b	0.18	0.44	0.31
Group 3	0.21	0.49	0.35

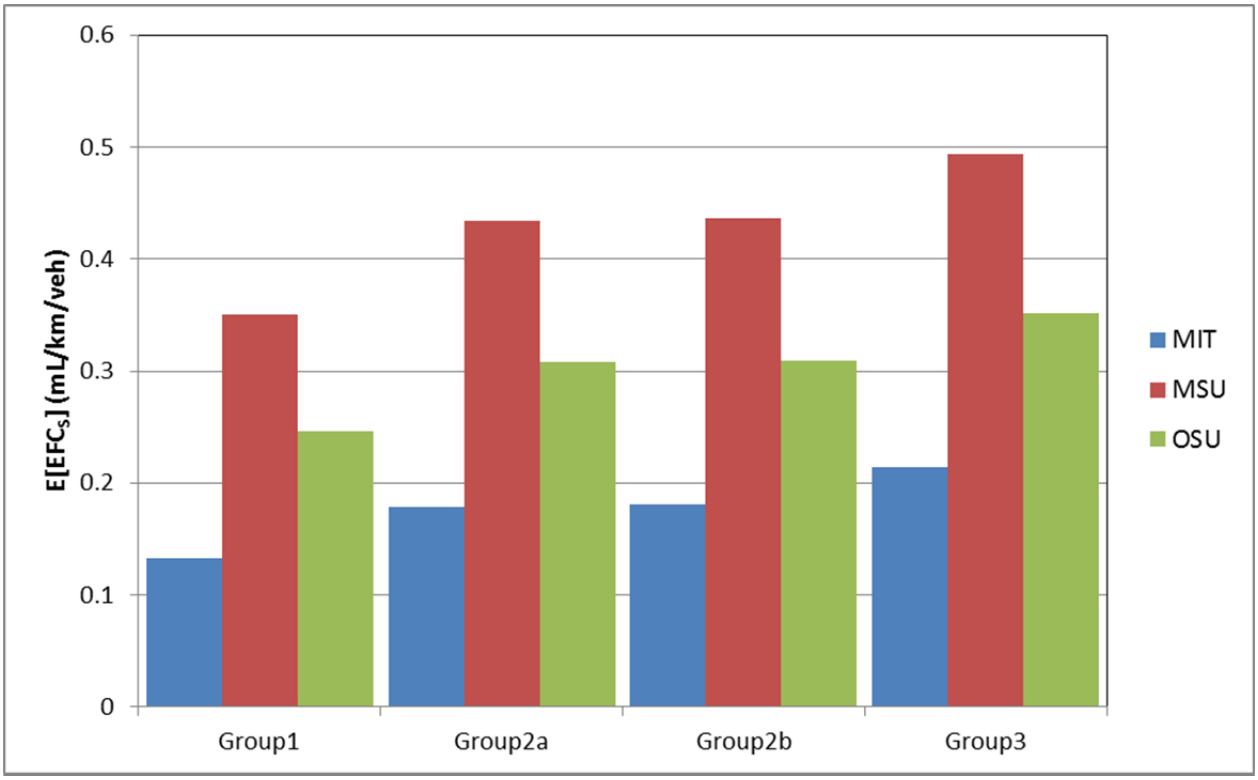

Figure 4.4: Average structural response simulation results by axle load spectrum group across factorial.

4.4 Analysis of Results for Different Surfaces for Roughness and Macrotexture

Figure 4.5 shows the sensitivity of EFC_{IRI} and EFC_{MPD} from the NCHRP 720 models to IRI and MPD above the values set for the ideal pavement of 38 inches/mile (0.6 m/km) for IRI and 0.5 mm for MPD across all sections and the full factorial. From the results it can be seen that for the general ranges on the state highway network—for IRI of 38 to 253 inches/mile (0.6 to 4 m/km) and for MPD of 0.5 to 2 mm—EFC is much more sensitive to IRI than to MPD. As noted previously, the field sections were selected to have IRI values less than 100 inches/mile (1.6 m/km) except for a few sections to provide a check of the independence of the effect of structural response and roughness during field validation of the EFC_S models.

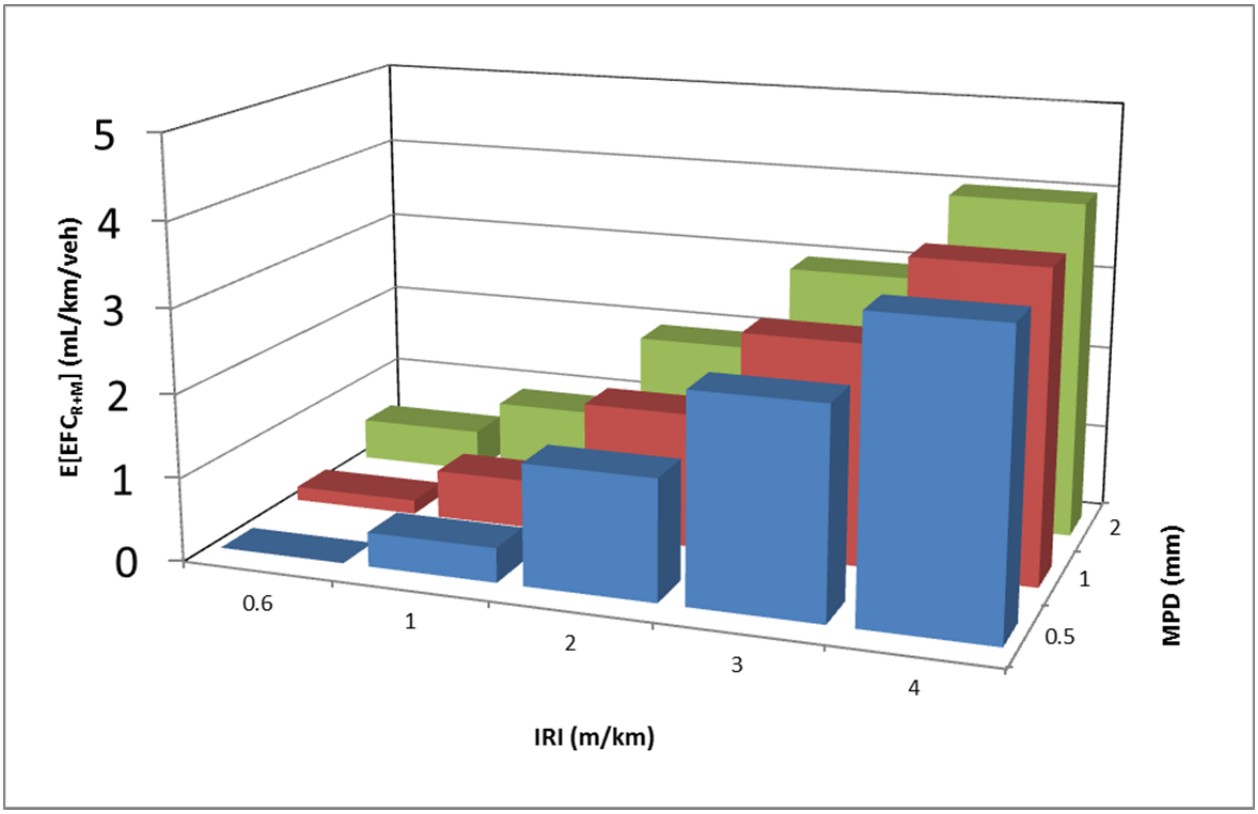

Figure 4.5: Average combined EFC for roughness and macrotexture across factorial.
(Notes: [a.] IRI of 1 m/km = 63.4 inches/mile, IRI of 3 m/km = 190 inches/mile; [b.] EFC relative to IRI above 38 inches/mile [0.6 m/km] and MPD above 0.5 mm)

4.5 Summary of Results and Interpretation

The results shown in Table 4.7 are a summary of the distributions of EFC results for structural response, roughness, and macrotexture from the modeling and simulations performed as part of this study to date. These results were used to make a recommendation regarding the need for experimental work posed by the following objective of this project:

> Use the model results to simulate the annual vehicle excess fuel consumption caused by pavement structural response on each of the asphalt-surfaced test sections for typical traffic and climate in California and to compare those results with the excess fuel consumption caused by roughness and surface macrotexture, and then prepare a report summarizing the results. Based on those results regarding the importance of fuel consumption attributed to structural response, include in the report a recommendation regarding the need for Phase II experimental work.

Looking at the results in the table it can be seen that the effects on excess fuel consumption due to structural response are between 15 and 21 percent of the combined effects of roughness and macrotexture based on the OSU model, between about 14 and 19 percent based on the MIT model, and between about 29 and 33 percent based on the MSU model. It should be remembered when interpreting these results that the values for EFC from structural response are relative to no structural response, while the values for EFC from roughness and

macrotexture are relative to approximate minimum values of IRI and MPD found on the state network, and that nearly all of the sections considered had relatively low roughness values (IRI less than 100 inches/mile [1.6 m/km]). The result of the choices made to compare EFC from structural response and EFC from surface characteristics is to increase the importance of EFC from structural response compared to EFC from roughness. This choice was made for this study with the understanding that the intent of the state pavement management system and funding for maintenance and rehabilitation is to reduce roughness across the network over the coming years.

With those caveats in mind, it is apparent from these results that while structural response is not as important as roughness in terms of potential for reducing EFC on the state highway network, the potential for reducing EFC through consideration of structural response is not so small that it should be ignored.

Table 4.7: Descriptive Statistics for EFC Results for Site-Specific Traffic and Climate of Asphalt-Surfaced Test Sections
(Note: sections were selected for mostly low IRI and macrotexture)

	Structural Response EFC_S[1] (mL/km/veh, [% of EFC_{IRI}+EFC_{MPD}])			EFC_{IRI} and EFC_{MPD}[2] (mL/km/veh)
Statistic	**MIT**	**MSU**	**OSU/Lyon**	
Minimum	0.02 (14%)	0.04 (29%)	0.03 (21%)	0.14
Average	0.12 (14%)	0.28 (33%)	0.18 (21%)	0.85
Maximum	0.61 (19%)	0.92 (29%)	0.48 (15%)	3.20
Notes: [1]: Relative to no structural response [2]: Relative to IRI = 38 in/mi (0.6 m/km) and MPD = 0.5 mm				

A first-order estimate of the percent change in fuel (for either gasoline or diesel) used for operation of vehicles on the network if EFC_S were to be reduced to zero is shown in Table 4.8, based on the average results from simulation of the asphalt-surfaced sections using an average change from the section-specific simulations. Table 4.9 shows an estimate of the percent change in fuel use if EFC_S were to be reduced to zero for the Inland Valley and Desert regions portion of the factorial simulations that have hot climates compared with the cool and populous South Coast and Central Coast regions, based on the results of the factorial simulation. Table 4.10, shows an estimate of the percent change in fuel use if EFC_{IRI} were to be reduced to zero, based on the average results of the section-specific simulations. For the comparisons, the estimates of changes in total fuel consumption (EFC) in the tables are applied equally to all vehicle and fuel types, which is not correct but sufficiently accurate for the purposes of this first-order analysis. The baseline fuel economy estimates are based on the approximate average fuel use for each vehicle type from recent results *(40)*:

- Cars: 24 mpg (100 mL/km)
- SUVs: 16 mpg (150 mL/km)
- Trucks: 6 mpg (278 mL/km)
- Combined average used for estimates from section-specific simulations assumes 7.5 percent trucks, 55 percent cars, 37.5 percent SUVs: 19 mpg (139 mL/km)
- Combined average used for estimates from factorial simulations assumes 10 percent trucks, 54 percent cars, 36 percent SUVs: 19 mpg (146 mL/km)

The results in Table 4.8 indicate that on average across all sections and the section-specific simulations the percent change in fuel use due to structural response ranges from 0.09 percent for the MIT model to 0.20 percent for the MSU model, with the OSU model falling in between.

The results in Table 4.9 from the factorial simulations and across the different models show that the range of increased fuel use is 0.14 to 0.36 percent for the hotter regions in the state, depending on the model and region—Desert and Valley—compared with 0.09 to 0.29 percent for the cooler Central and South Coast regions. These results indicate that the extra fuel consumption due to structural response is greater by a factor of about 1.4 for hotter inland regions compared with cooler coastal regions.

The results in Table 4.10 show that on average across all sections analyzed for structural response using section-specific data the percent change in fuel use if roughness is reduced to 38 inches/mile (0.6 m/km) is 0.51 percent, which is approximately three times the reduction obtained from reducing structural response to zero for the OSU model. However, it must be kept in mind that all but one of the sections analyzed for structural response were relatively smooth (IRI over 100 inches/mile [1.6 m/km]). Also shown in the table is the percent change in fuel use if the rough section (PD 14) has its IRI reduced from 227 to 38 inches/mile (3.57 to 1.6 m/km), which was 2.23 percent.

These estimates do not consider weighting of the results for the amount of traffic occurring in different climate regions or on different types of structures across the state highway network, or any other variables. They are intended only as a first-order estimate, and they are comparisons with an idealized pavement with zero structural response effect on vehicle fuel economy. It is also clear from the results presented elsewhere in this report that pavements with a high percentage of heavy truck traffic operating in hot climates, and particularly under slow speeds, will have a much greater impact than those shown by these averages; it is also clear that those pavements operating in cool climates with a high percentage of fast-moving vehicles will have much less impact than is estimated in the tables. Calibrated models for EFC_S will allow those more detailed project-level analyses.

Table 4.8: Approximate Percent Change in Fuel Economy across Asphalt-Surfaced Sections and Site-Specific Simulations if EFC_S Reduced to Zero

Vehicle Type	Assumed Current Fuel Consumption			Change if Reduce EFC_S to Zero (mL/km/veh)			Percent Change if Reduce EFC_S to Zero		
	mL/km	L/100 km	mpg	MIT	MSU	OSU	MIT	MSU	OSU
Cars	100	10	24						
SUVs	150	15	16						
Trucks	378	38	6						
Weighted total	139			0.12	0.28	0.18	0.09%	0.20%	0.13%
Note: assumes 7.5 percent trucks, 55.5 percent cars, and 37 percent SUVs									

Table 4.9: Approximate Percent Change in Fuel Economy across Asphalt-Surfaced Factorial and All Sections if EFC_S Reduced to Zero for Hot Inland Valley Climate and Desert Regions and Cool Coastal Regions

	Assumed Current Fuel Consumption	Change if Reduce EFC_S to Zero (mL/km/veh)			Percent Change if Reduce EFC_S to Zero		
Vehicle Type	mL/km	MIT	MSU	OSU	MIT	MSU	OSU
Weighted total Inland Valley	146	0.20	0.46	0.34	0.14%	0.32%	0.24%
Weighted total Desert	146	0.24	0.53	0.42	0.16%	0.36%	0.28%
Weighted total Central Coast	146	0.13	0.36	0.23	0.09%	0.25%	0.16%
Weighted total South Coast	146	0.17	0.43	0.29	0.11%	0.29%	0.20%
Note: assumes 10 percent trucks, 54 percent cars, and 36 percent SUVs							

Table 4.10: Approximate Percent Change in Fuel Economy across All Asphalt-Surfaced Sections Analyzed and for a High Roughness Section Only (PD 14) if IRI Reduced to 0.6 m/km (38 inches/mile) Using Section-Specific Simulations

	Assumed Current Fuel Consumption	Change if Reduce IRI to 38 inches/mile (0.6 m/km) (mL/km/veh)		Percent Change if Reduce IRI to 38 inches/mile (0.6 m/km)	
Vehicle Type	mL/km	Across All Sections	Rough Section (PD 14)	Across Sections (Average IRI = 82 inches/mile [1.29 m/km])	PD 14 (IRI = 226 inches/mile [3.57 m/km])
Weighted total	139	0.71	3.11	0.51%	2.23%
Note: assumes 7.5 percent trucks, 55.5 percent cars, and 37 percent SUVs					

5. CONCLUSIONS AND RECOMMENDATIONS

5.1 Conclusions

The following conclusions have been drawn from the results of this study:

- General modeling conclusions:
  - The three modeling approaches produced different results, although with similar orders of magnitude. Overall, the MIT approach produced the smallest estimates of excess fuel consumption due to structural response (EFC_S), as expected from the modeling approach, while the MSU approach produced the largest, and the OSU approach generally produced EFC_S results in between the others. However, there were a number of exceptions to these average results for individual sections.
  - Without field validation to determine how well each approach models the broad range of pavement structures in the field experiment factorial, the best modeling approach is not apparent.
  - Field validation, and if necessary field calibration, is needed to produce models that can be used in practice because of there are limitations in any modeling approach.
- Results for seventeen asphalt-surfaced sections analyzed for excess fuel consumption due to structural response and averages across the factorial of climate and traffic conditions show the following:
  - Compared to an ideal pavement with no structural response, EFC_S ranged from 0.02 to 0.61 mL/km/veh for the MIT model, 0.03 to 0.48 mL/km/veh for the OSU model, and 0.04 to 0.92 mL/km/veh for the MSU model, using section-specific traffic and climate data. The sections had an average of 7.5 percent trucks. Across all sections, the MIT, MSU, and OSU models predicted average EFC_S of 0.12, 0.18, and 0.28 mL/km/veh, which translates to average fuel economy percentage changes of 0.09, 0.13, and 0.20 percent in fuel economy per vehicle across all vehicles.
  - Compared to an ideal pavement with no structural response, EFC_S ranged from 0.03 to 0.70 mL/km/veh for the MIT model, 0.04 to 0.79 mL/km/veh for the OSU model, and 0.06 to 1.41 mL/km/veh for the MSU model, across the test sections from simulation of the factorial of traffic and climate data. The factorial had an average of 10 percent trucks. Across all sections, the MIT, MSU, and OSU models predicted average EFC_S of 0.18, 0.30, and 0.43 mL/km/veh, which translates to average fuel economy changes of 0.12, 0.21, and 0.29 percent per vehicle across all vehicles.
  - These results show that the EFC_S increases as the percentage of trucks increases, with trucks having between 6 and 15 times greater increase per vehicle than cars and SUVs, depending on the model.

- EFC_S is approximately 1.4 times greater in the Desert and Inland Valley climate regions compared with the average of the cooler Central and South Coast climate regions, based on results of the factorial simulation.
- EFC_S increases at a rate of approximately 0.014 to 0.025 mL/km/veh (depending on the model) with each one percent increase in the percentage of trucks.
- From the section-specific simulations, excess fuel consumption due to roughness (IRI) and macrotexture (MPD) ranged from 0.14 to 3.20 mL/km/veh compared with an ideal pavement, with an IRI of 38 inches/mile (0.6 m/km) and macrotexture of 0.5 mm, with the effects of roughness approximately ten times greater than those of macrotexture.
- The combined effects of roughness and macrotexture on EFC far exceeded the EFC values calculated based on the effect of structural response using the MIT, OSU, and MSU models. The combined effect of roughness and macrotexture was roughly seven times greater than the structural response result from the MIT model, five times greater than the OSU model's result, and three times greater than the result from the MSU model. It should be noted that these are average values across section-specific simulations with an average truck percentage of 7.5 percent, and that the sections analyzed for structural response were nearly all fairly smooth (IRI less than 100 inches/mile [1.6 m/km]). Compared with the one rough section (PD 14, IRI of 226 inches/mile [3.57 m/km]), these ratios become 27, 18, and 11 times greater for roughness plus macrotexture effects versus structural response effects for the MIT, OSU, and MSU models respectively.
- It should be noted that none of the models includes predictions of damage caused by traffic and the environment which would change stiffness; damage must be predicted separately using mechanistic-empirical or other models. Similarly, change in IRI over time must be predicted separately from the models used in this study.

- Within the factorial of climate regions and traffic across the seventeen asphalt-surfaced sections analyzed for structural response:
  - Results are generally more sensitive to pavement temperature (climate region) compared with urban versus rural traffic speed and volume patterns typical for California.
  - Axle loads are very important, as was reflected in the high sensitivity of EFC_S to axle load spectra and the percentage of trucks.
  - The MIT model ranked the pavement types (composite, flexible, semi-rigid) differently from the OSU and MSU models for EFCS. MIT ranked them 1, 2, and 3 in terms of best to worst, while OSU and MSU ranked them 3, 2, and 1, for the small sample of each type in the factorial analyzed.

- General conclusions
  - Although it appears to be generally less important than the effects of roughness for the sections analyzed, the results for EFC_S appear to be sufficiently large, and the differences between the models large enough, to warrant field validation and calibration of the models. Field testing is necessary to enable consideration of structural response in project-level and network-level analysis to support decision-making.
  - Calibration should focus on the most sensitive variables:
    - Pavement structure in terms of asphalt thickness and stiffness/phase angle master curve (analysis of the concrete sections in the field section factorial needs to be completed as well)
    - Wheel load
    - Pavement temperature, which is important for asphalt pavements
    - Speed, which is important for asphalt pavements and may be important for concrete pavements
  - Validation and calibration should consider any possible interaction of roughness and structural response and include a check on the EFC model for roughness used in this study by including several rough sections in the field section factorial.

5.2 Recommendations

- Complete and improve modeling
  - Model the concrete pavements using different approaches.
  - Consider multiple layers in the asphalt, particularly near the surface to better evaluate the effects of rubberized asphalt surface materials.
  - Check the effects of full dynamic pavement modeling (inertial effects in the pavement) on more than the one section analyzed which showed an approximate 6 percent increase in EFCS compared with the results for the OSU model (results presented in companion modeling report [23]), if it is decided that the cost of addition modeling is warranted by the potential additional accuracy.
- Begin field validation and calibration of the models and rerun the simulations with the improved and calibrated models for all pavement surface types.

REFERENCES

1. Van Dam, T., J. Harvey, S. Muench, K. Smith, M. Snyder, I. Al-Qadi, H. Ozer, J. Meijer, P. Ram, J. Roesler, A. Kendall. 2015. *Towards Sustainable Pavement Systems: A Reference Document.* FHWA-HIF-15-002. Federal Highway Administration, U.S. Department of Transportation. *www.fhwa.dot.gov/pavement/sustainability/ref_doc.cfm* (Accessed March 12, 2015)
2. Sandberg, U. (ed.). 2011. *Rolling Resistance—Basic Information and State of the Art on Measurement Methods.* VTI Report MIRIAM_SP_01. Prepared under the Models for Rolling Resistance in Road Infrastructure Asset Management Systems (MIRIAM) project. VTI (Swedish National Road and Transport Research Institute), Linköping, Sweden. *www.miriam-co2.net/Publications/MIRIAM_SoA_Report_Final_110601.pdf* (Accessed July 30, 2015).
3. Jackson, R., J. R. Willis, M. Arnold, and C. Palmer. 2011. *Synthesis of the Effects of Pavement Properties on Tire Rolling Resistance.* Report No. 11-05. National Center for Asphalt Technology, Auburn, AL.
4. Panagouli, O.K., and Kokkalis, A.G. 1998. "Skid Resistance and Fractal Structure of Pavement Surface. Chaos, Solutions & Fractals," 9(3), 493-505.
5. Flintsch, G., E. de León, K. McGhee, and I. Al-Qadi. 2002. "Pavement Surface Macrotexture Measurement and Applications." *Transportation Research Record: Journal of the Transportation Research Board,* Vol. 1860. Transportation Research Board of the National Academies, Washington, DC.
6. Chupin, O., J. M. Piau, and A. Chabot. 2013. "Evaluation of the Structure-Induced Rolling Resistance (SRR) for Pavements Including Viscoelastic Material Layers." Materials and Structures. Vol. 46, No. 4. Springer Netherlands.
7. Flugge, W. 1975. Viscoelasticity. Springer Verlag, Berlin, New York, NY.
8. Bell, C., A. Wieder, and M. Fellin. 1994. *Laboratory Aging of Asphalt Mixtures: Field Validation. SHRP-A-390.* Strategic Highway Research Program, Transportation Research Board, National Academy of Science. *onlinepubs.trb.org/onlinepubs/shrp/SHRP-A-390.pdf* (Accessed April 28, 2015)
9. California Air Resources Board (CARB). *California Greenhouse Gas Emission Inventory: 2000-2012, 2014 Edition.* California Environmental Protection Agency. May 2014. *www.arb.ca.gov/cc/inventory/pubs/reports/ghg_inventory_00-12_report.pdf.* (Accessed July 30, 2015)
10. Bennett, C. R., and Greenwood, I. D. 2003. Volume 5: HDM-4 Calibration Reference Manual, International Study of Highway Development and Management Tools (ISOHDM), World Road Association (PIARC).
11. Chatti, K. and I. Zaabar. 2012. *Estimating the Effects of Pavement Condition on Vehicle Operating Costs.* NCHRP Report 720. Transportation Research Board, Washington, DC. *onlinepubs.trb.org/onlinepubs/nchrp/nchrp_rpt_720.pdf* (Accessed July 30, 2015)

12. Wang, T., J. Harvey, and A. Kendall. 2014. “Greenhouse Gas Emission of Maintenance Treatments on California Pavement Network: A Life Cycle Assessment Approach.” Environmental Research Letters. Vol. 9, No. 3, 034007. IOP Publishing, Ltd., Bristol, UK.
13. Pouget, S., C. Sauzéat, H. Benedetto, and F. Olard. 2012. “Viscous Energy Dissipation in Asphalt Pavement Structures and Implication for Vehicle Fuel Consumption.” Journal of Materials in Civil Engineering. Vol. 24, No. 5. American Society of Civil Engineers, Reston, VA.
14. Thom, N., T. Lu, and T. Parry. 2010. “Fuel Consumption Due to Pavement Deflection Under Load.” Proceedings of the 2nd International Conference on Sustainable Construction Materials and Technologies. Ancona, Italy.
15. Kelly, J. M. 1962. Moving Load Problems in the Theory of Viscoelasticity. PhD. Dissertation. Stanford University, Stanford, CA.
16. Perloff, W. H., and F. Moavenzadeh. 1967. “Deflection of Viscoelastic Medium Due to a Moving Load.” 2nd International Conference on Asphalt Pavements. Ann Arbor, MI.
17. Hopman, P. C. 1993. VEROAD: a Linear Viscoelastic Multilayer Program for the Calculation of Stresses, Strains and Displacements in Asphaltic Road Constructions: A Viscoelastic Halfspace. Delft University of Technology, Netherlands.
18. Huang, Y. H. 1967. “Stresses and Displacements in Viscoelastic Layered Systems under Circular Loaded Areas.” 2nd International Conference on Asphalt Pavements. Ann Arbor, MI.
19. Hajj, E. Y., P. E. Sebaaly, and R. V. Siddharthan. 2006. “Response of Asphalt Pavement Mixture under a Slow Moving Truck.” Asphalt Concrete: Simulation, Modeling, and Experimental Characterization. *Geotechnical Special Publication No. 146.* American Society of Civil Engineers, Reston, VA.
20. Akbarian, M., S. Moeini-Ardakanil, F. J. Ulm, and M. Nazzal. 2012. “Mechanistic Approach to Pavement–Vehicle Interaction and its Impact on Life-Cycle Assessment.” *Transportation Research Record: Journal of the Transportation Research Board,* Vol. 2306, pp. 173-179. Transportation Research Board of the National Academies, Washington, DC.
21. Loughalam, A., M. Akbarian, and F. J. Ulm. 2013. “Flugge’s Conjecture: Dissipation vs. Deflection Induced Pavement-vehicle-Interactions (PVI).” Journal of Engineering Mechanics. American Society of Civil Engineers, Reston, VA.
22. Louhghalam, A., M. Akbarian and F.J. Ulm. 2014. Scaling Relations of Dissipation-Induced Pavement—Vehicle Interactions, *Transportation Research Record: Journal of the Transportation Research Board,* Vol. 2457, pp. 95-104. Transportation Research Board of the National Academies, Washington, DC.
23. Coleri, E., J. Harvey, I. Zaabar, A. Louhghalam, and K. Chatti. 2016. Model Development, Field Section Characterization, and Model Comparison for Excess Vehicle Fuel Use Due to Pavement Structural Response. UCPRC-RR-2015-04 (not yet published).

24. Hultqvist, B. A. 2013. *Measurement of Fuel Consumption on Asphalt and Concrete Pavements North Of Uppsala. Measurements with Light and Heavy Goods Vehicle.* SE-581 95. VTI (Swedish National Road and Transport Research Institute), Linköping, Sweden.
25. Hammarström, U., J. Eriksson, R. Karlsson, and M. R. Yahya. 2012. *Rolling Resistance Model, Fuel Consumption Model and The Traffic Energy Saving Potential of Changed Road Surface Conditions.* VTI rapport 748A. VTI (Swedish National Road and Transport Research Institute), Linköping, Sweden. *http://62.119.60.72/en/publications/rolling-resistance-model-fuel-consumption-model-and-the-traffic-energy-saving-potential-of-changed-road-surface-conditions* (Accessed July 30, 2015).
26. Zaabar, I., Chatti, K., Lee, H.S., and Lajnef, N. 2014. Backcalculation of Asphalt Concrete Modulus Master Curve from Field Measured Falling Weight Deflectometer Data Using a New Time Domain Viscoelastic Dynamic Solution and Genetic Algorithm. Transportation Research Record: Journal of the Transportation Research Board, Vol. 2457, pp 80-92.
27. Zaabar, I., Chatti, K., and Lajnef, N., "Time-domain Viscoelastic backcalculation of Pavement Structure Properties from Falling Weight Deflectometer Using Hybrid Approach", accepted for presentation at the 3rd International Conference on Transportation Infrastructures - ICTI 2014, Pisa, Italy, April 22-25, 2014.
28. K. Chatti, I. Zaabar, (2013) DYNABACK-VE. A Windows form application written in C++ for parallel computing with multithreading to backcalculate the layer properties including the master curve of HMA layer(s) and the depth-to-stiff layer if it exists. It is user friendly software with a Matlab-based user interface.
29. Lee, H. S., 2013. *ViscoWave—A New Solution for Viscoelastic Wave Propagation of Layered Structures Subjected to an Impact Load.* International Journal of Pavement Engineering, Vol. 15, Issue 6, pp 542-557.
30. K. Chatti, I. Zaabar, (2013) ViscoWave-II. A Windows form application written in C++ for parallel computing with multithreading to estimate the time-domain dynamic viscoelastic pavement response under FWD load pulse. It is user friendly software with a C++ based user interface.
31. Ferry, J. 1980. Viscoelastic Properties of Polymers. 3rd Edition. John Wiley & Sons.
32. Yoo, P.J., I. Al-Qadi, M.A. Elseifi, and I. Janajreh. 2006."Flexible Pavement Responses to Different Loading Amplitudes Considering Layer Interface Condition and Lateral Shear Forces." International Journal of Pavement Engineering: 7(1):73-86.
33. Ongel, A., J. Harvey. 2004. *Analysis of 30 Years of Pavement Temperatures using the Enhanced Integrated Climate Model (EICM).* Report for the California Department of Transportation. University of California Pavement Research Center Report UCPRC-RR-2004-05. *www.ucprc.ucdavis.edu/PDF/Climate%2030%20Years.pdf*.
34. Lea, J., and J. Harvey. "The Simplified Thermal Modeling Approach Used in CalME." Transportation Research Board Annual Meeting, Paper 10-32912-29388. January 22-26, 2012.

35. Lu, Q., J. Harvey, J. Lea, R. Quinley, D. Redo, and J. Avis. 2002. *Truck Traffic Analysis Using Weigh-in-Motion (WIM) Data in California.* University of California Pavement Research Center, UCPRC-TM-2008-08. [in process.]
36. Lu, Q., Harvey, J. 2006. Characterization of Truck Traffic in California for Mechanistic Empirical Design. *Transportation Research Record: Journal of the Transportation Research Board,* Vol. 1945, pp. 61-72. Transportation Research Board of the National Academies, Washington, D.C.
37. California Department of Transportation. Traffic Census Data. Division of Traffic Operations, Sacramento, CA. *http://traffic-counts.dot.ca.gov* (Accessed July 27, 2015)
38. California Department of Transportation. Performance Measurement System Data. *pems.dot.ca.gov/.* (Accessed July 27, 2015)
39. U.S. Bureau of the Census. 2010. Census Urban and Rural Classification and Urban Area Criteria. (Accessed July 31, 2015, website no longer active)
40. Oak Ridge National Laboratory. Appendix B, Transportation Energy Data Book from the Center for Transportation Analysis of the Oak Ridge National Laboratory. U.S. Department of Energy. *www.afdc.energy.gov/fuels/fuel_comparison_chart.pdf* (Accessed October 14, 2015).
41. U.S. Environmental Protection Agency. Light-Duty Automotive Technology, Carbon Dioxide Emissions, and Fuel Economy Trends: 1975 Through 2014, Executive Summary. EPA-420-S-14-001, October 2014. *www3.epa.gov/fueleconomy/fetrends/1975-2014/420s14001.pdf* (Accessed November 15, 2015).

APPENDIX A: TEMPERATURE DISTRIBUTION DATA

PD 07 - Pavement Temperature (1/3 Depth)

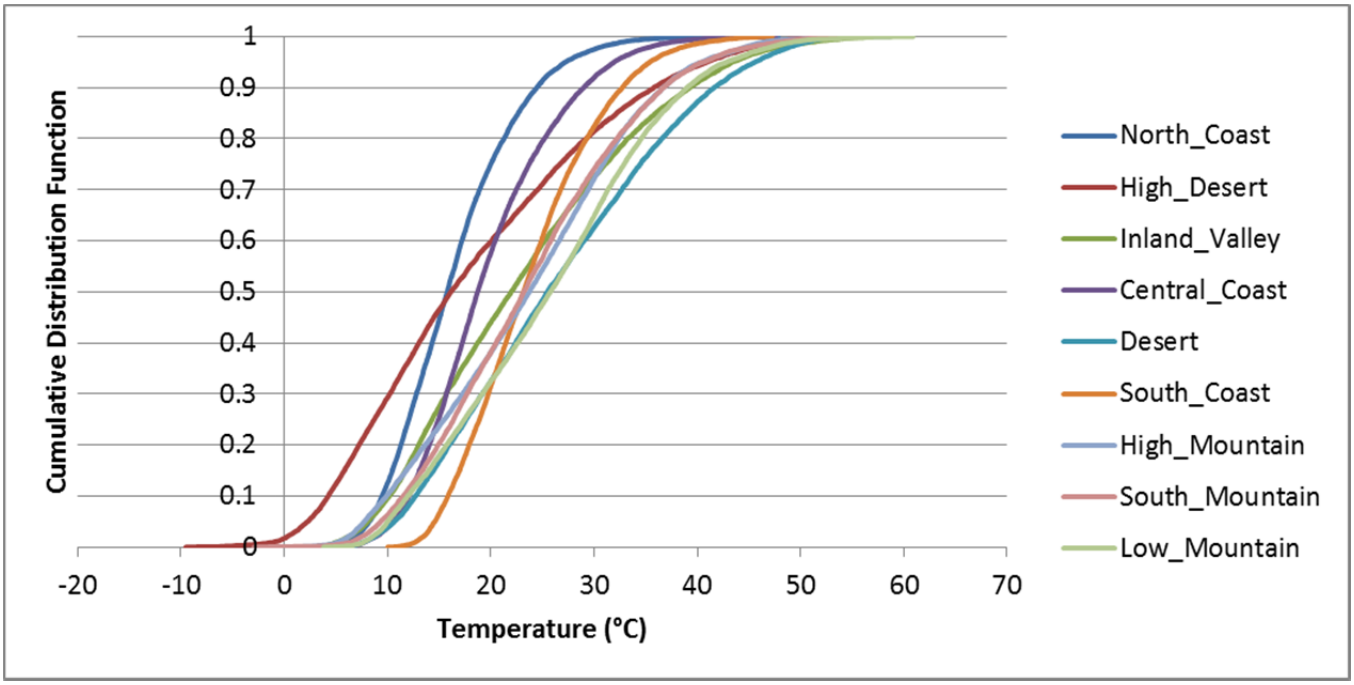

PD 08 - Pavement Temperature (1/3 Depth)

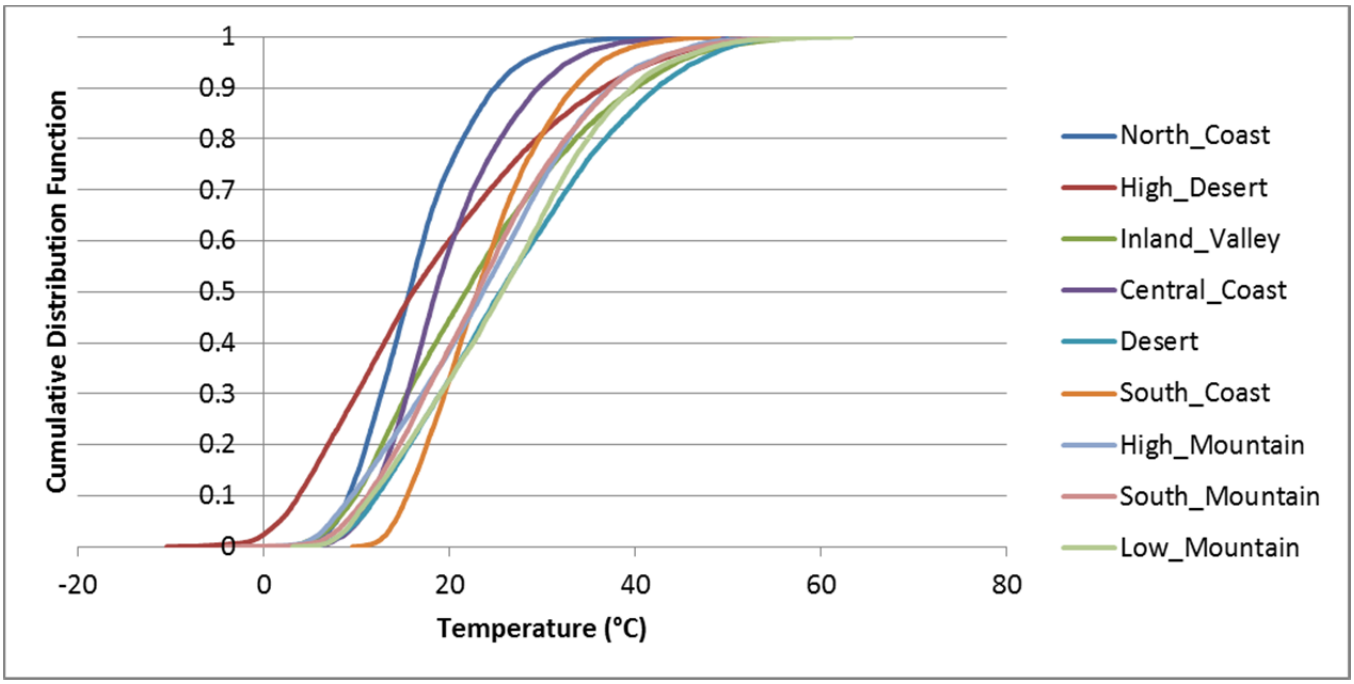

PD 10 - Pavement Temperature (1/3 Depth)

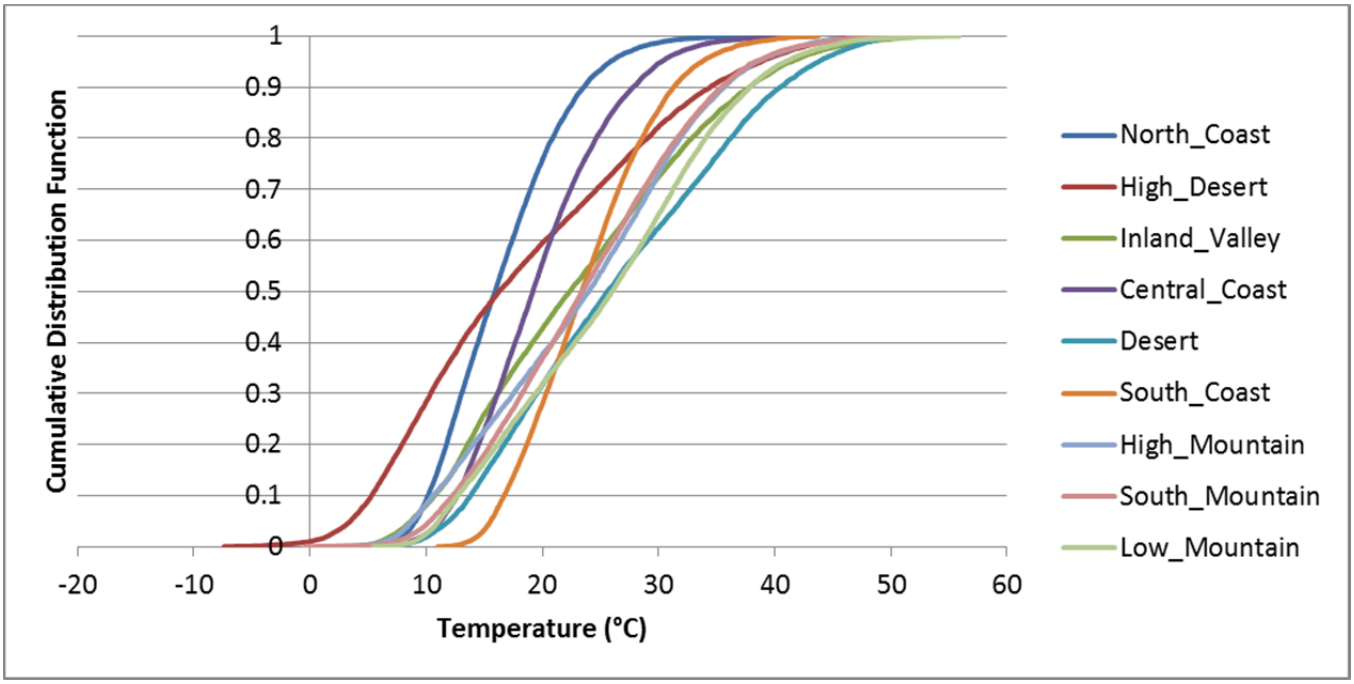

PD 11 - Pavement Temperature (1/3 Depth)

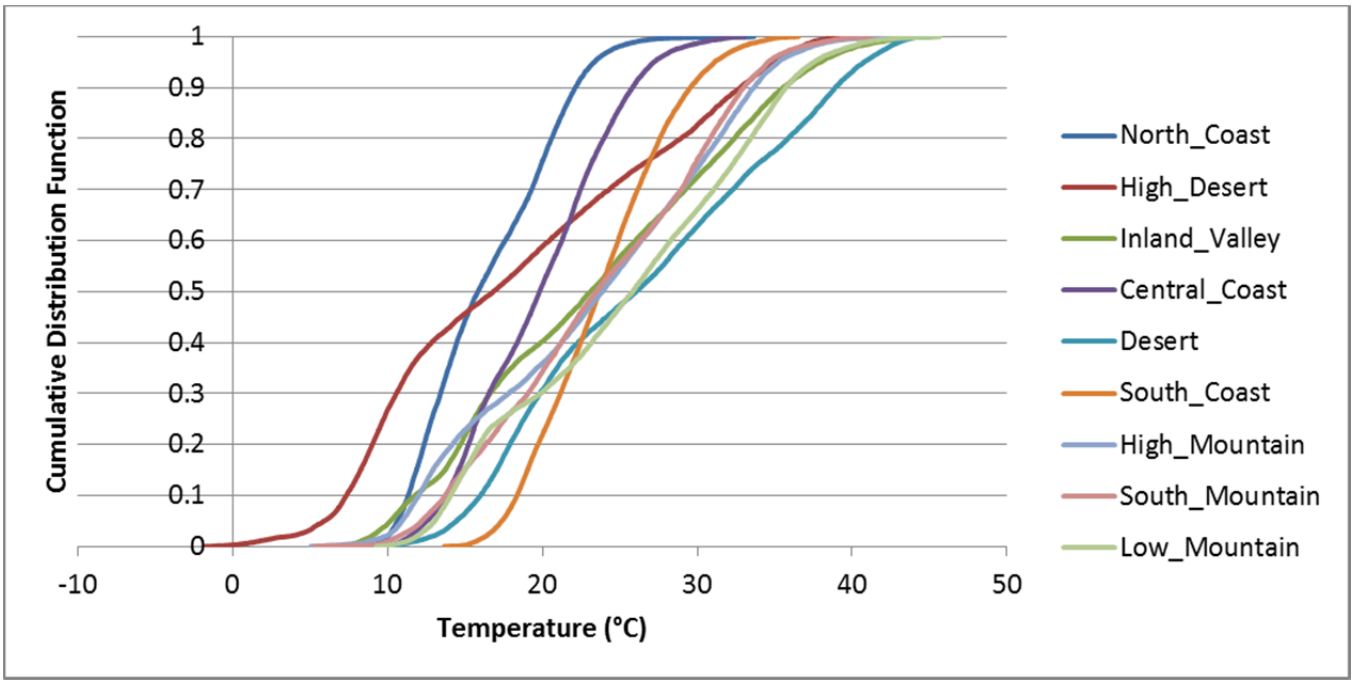

PD 13s1 - Pavement Temperature (1/3 Depth)

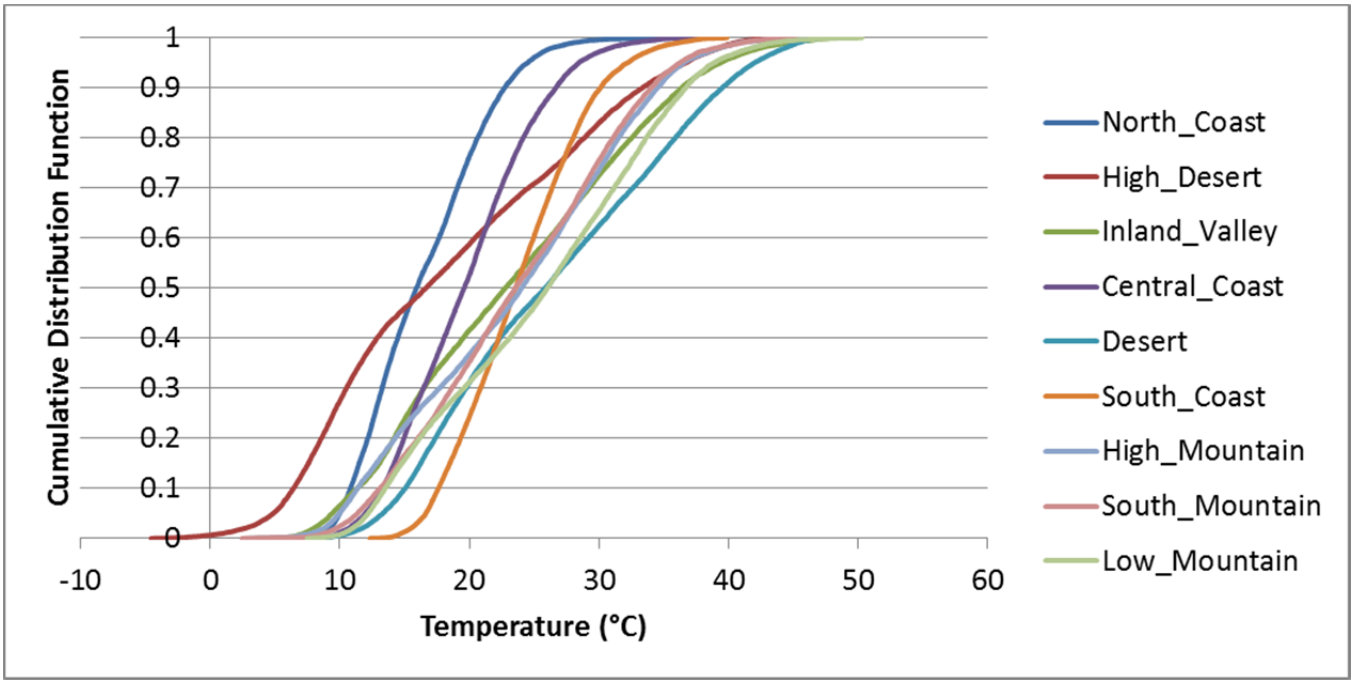

PD 13s2 - Pavement Temperature (1/3 Depth)

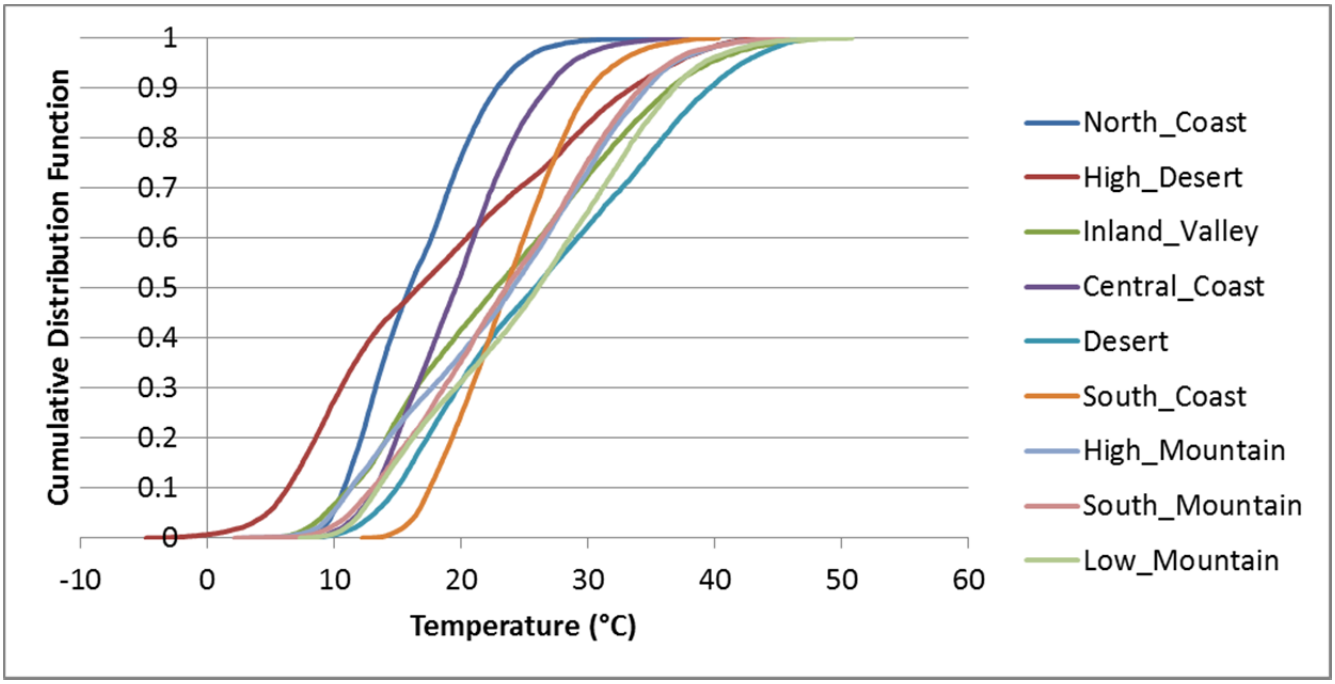

PD 14 - Pavement Temperature (1/3 Depth)

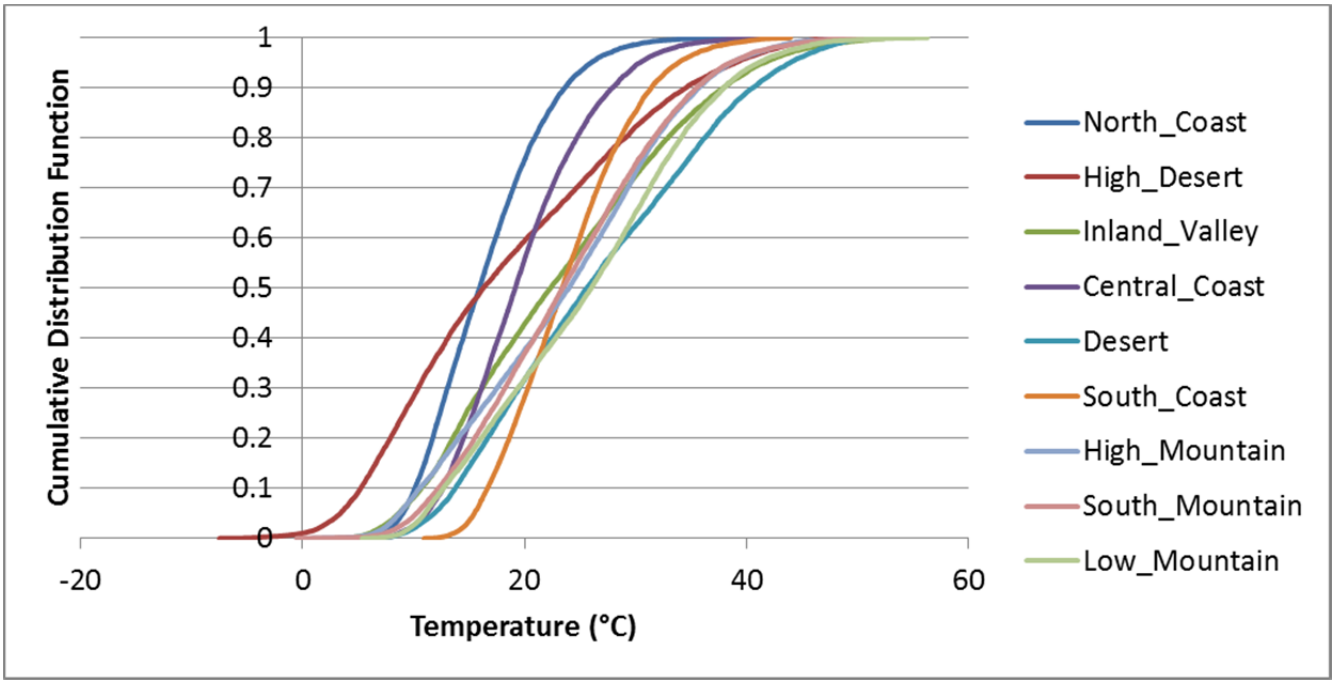

PD 15 - Pavement Temperature (1/3 Depth)

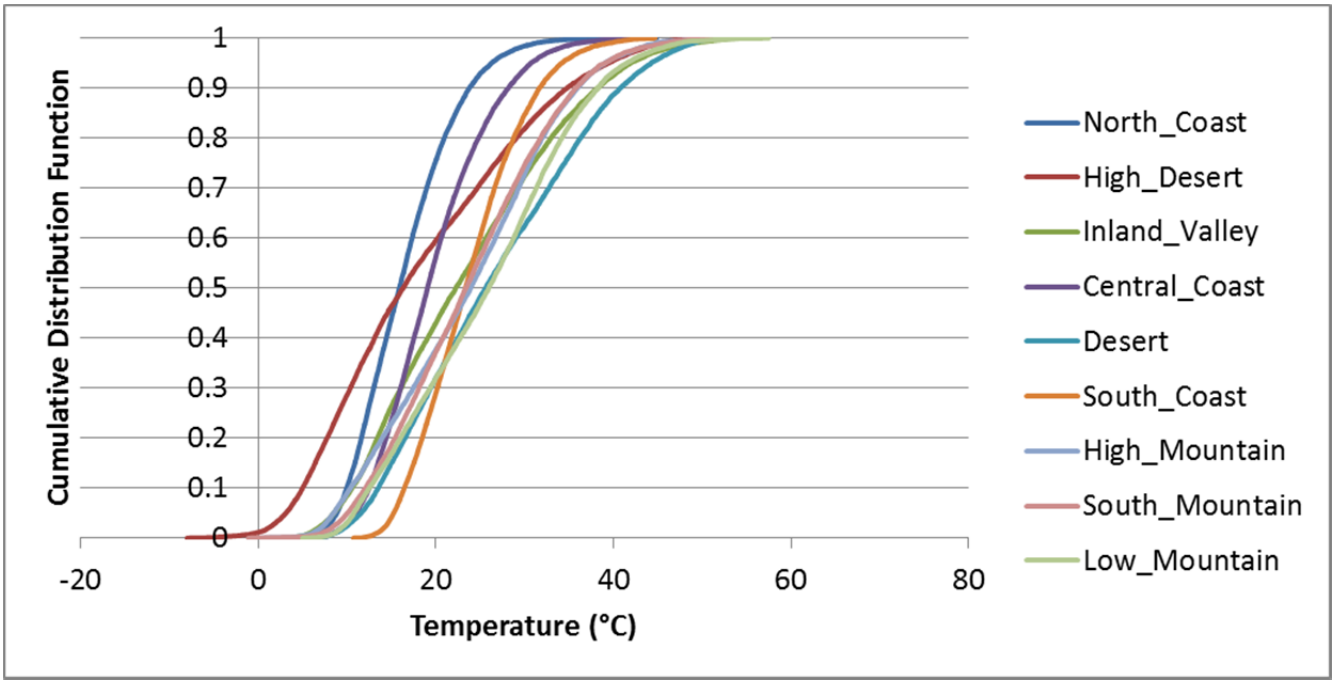

PD 16 - Pavement Temperature (1/3 Depth)

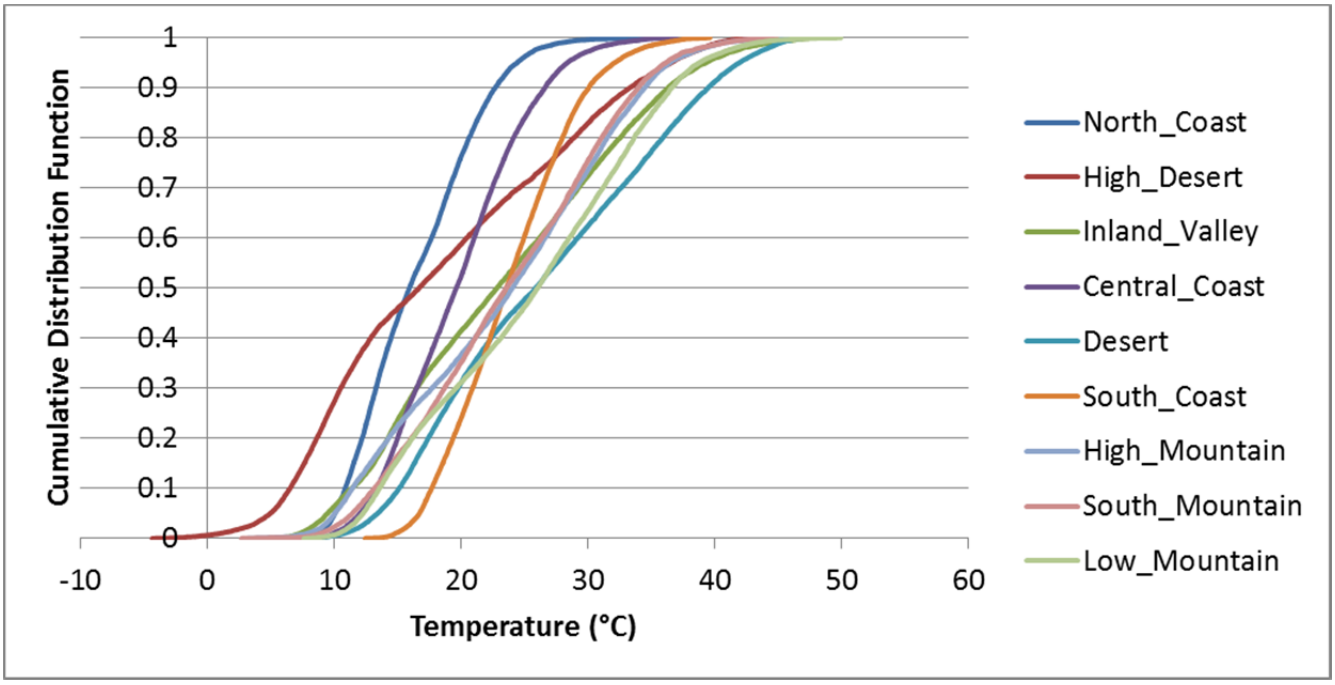

PD 18s1 - Pavement Temperature (1/3 Depth)

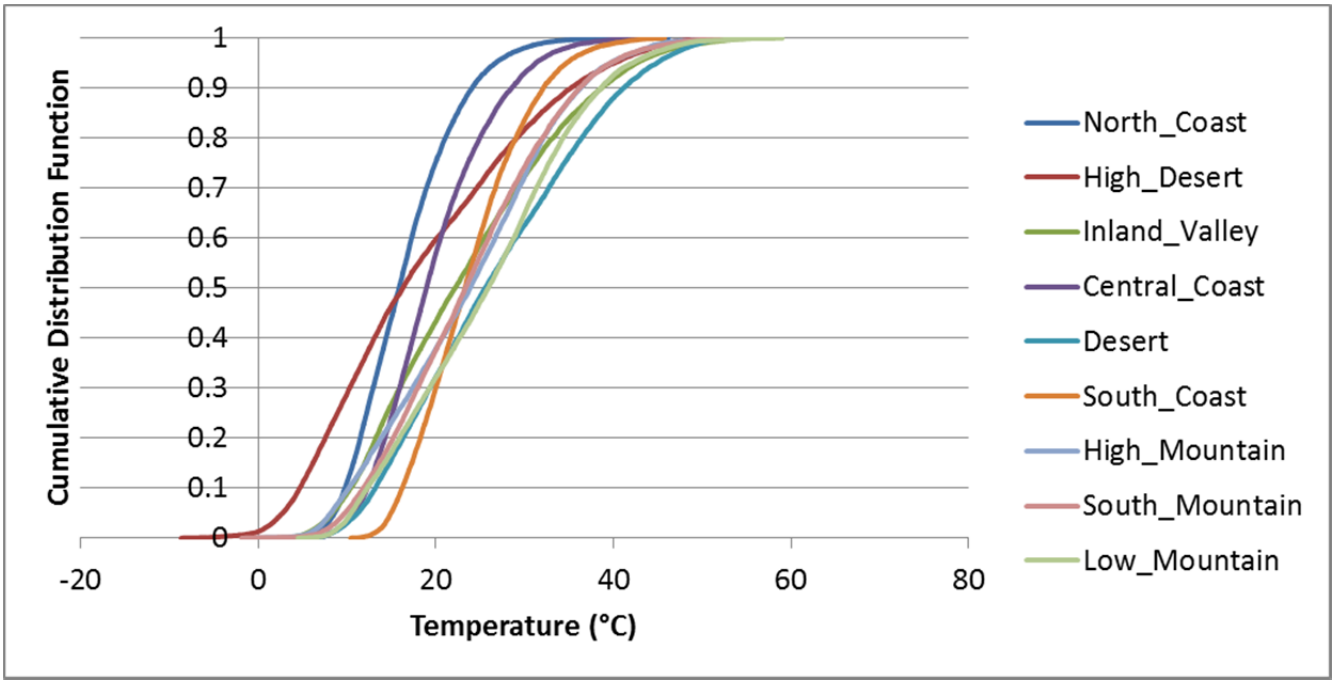

PD 18s2 - Pavement Temperature (1/3 Depth)

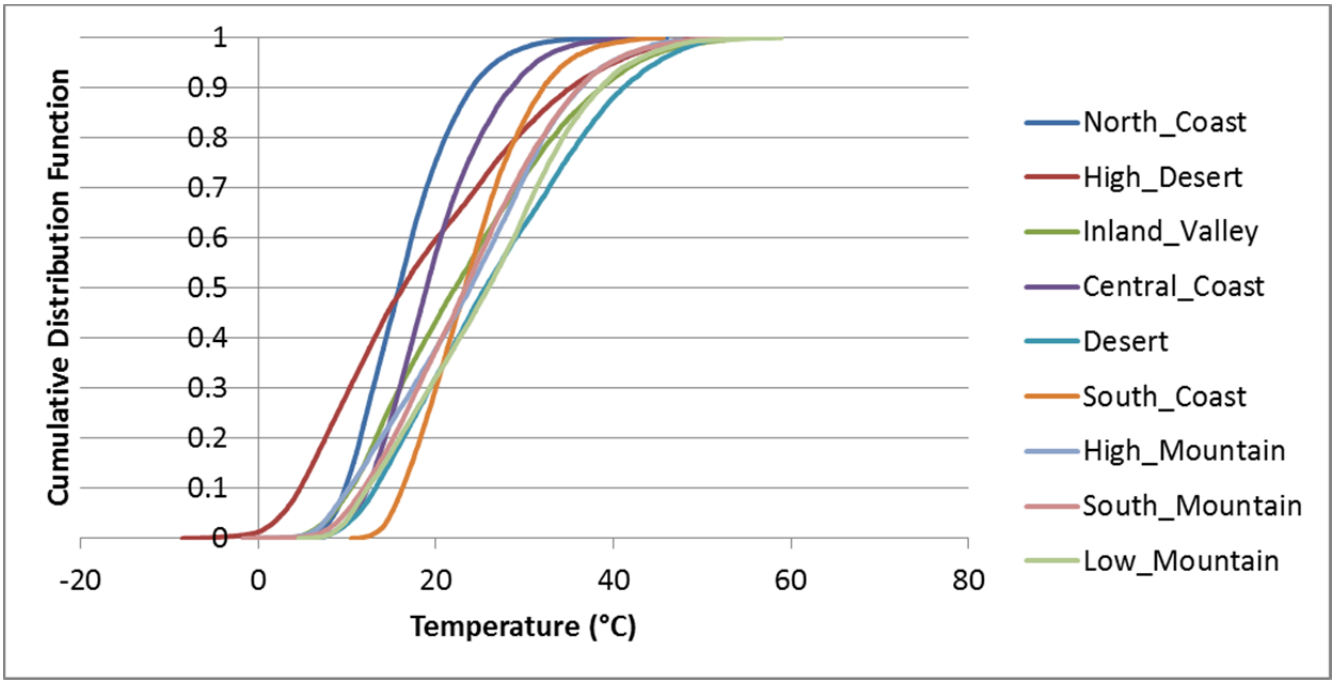

PD 19 - Pavement Temperature (1/3 Depth)

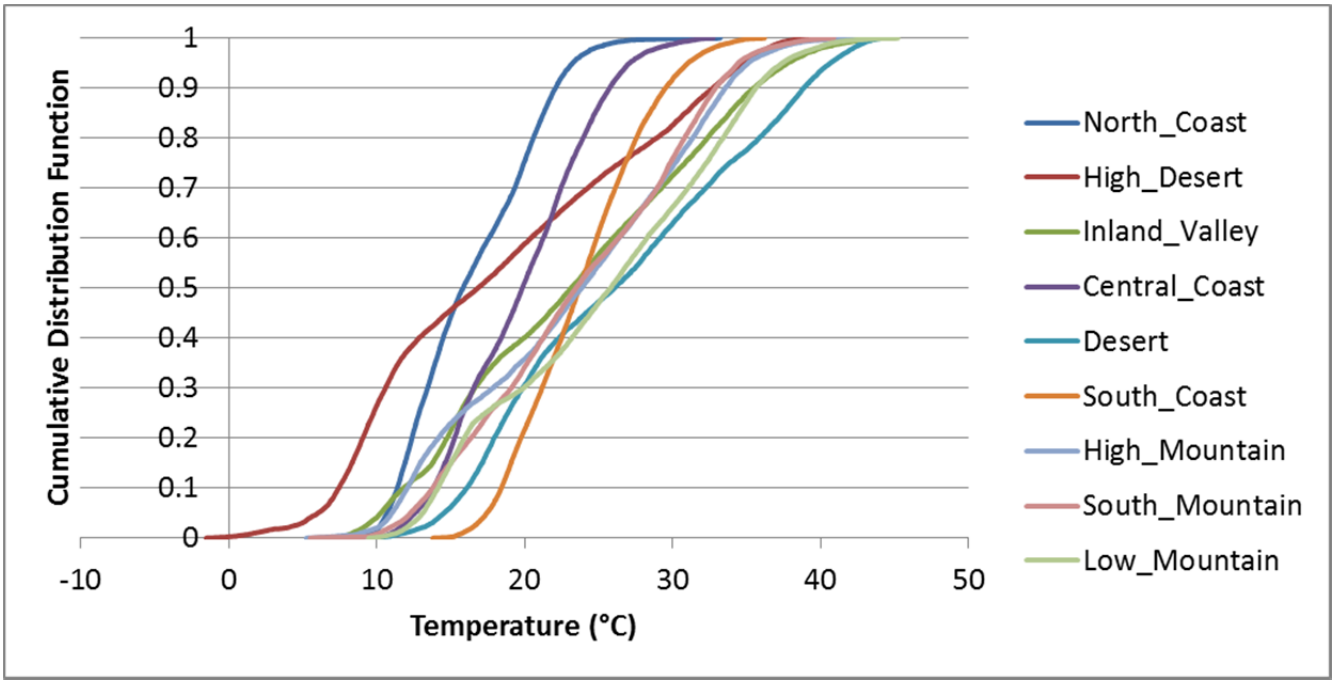

PD 20 - Pavement Temperature (1/3 Depth)

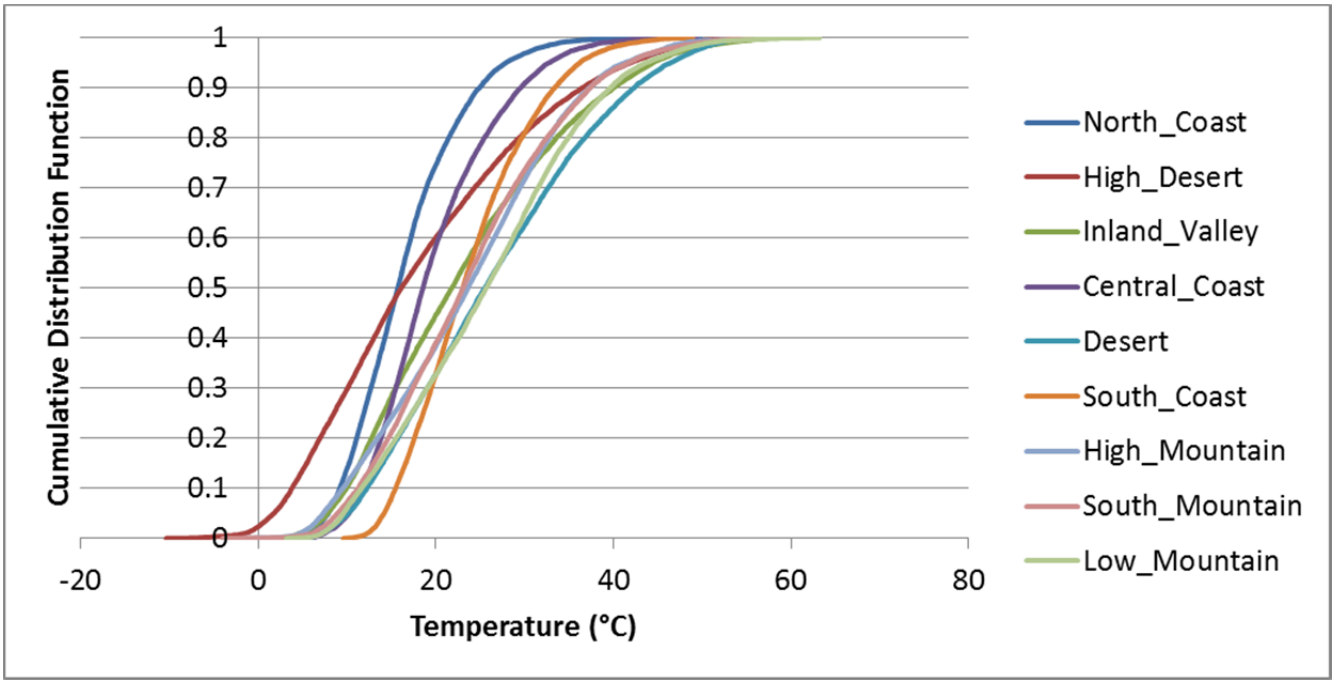

PD 21 - Pavement Temperature (1/3 Depth)

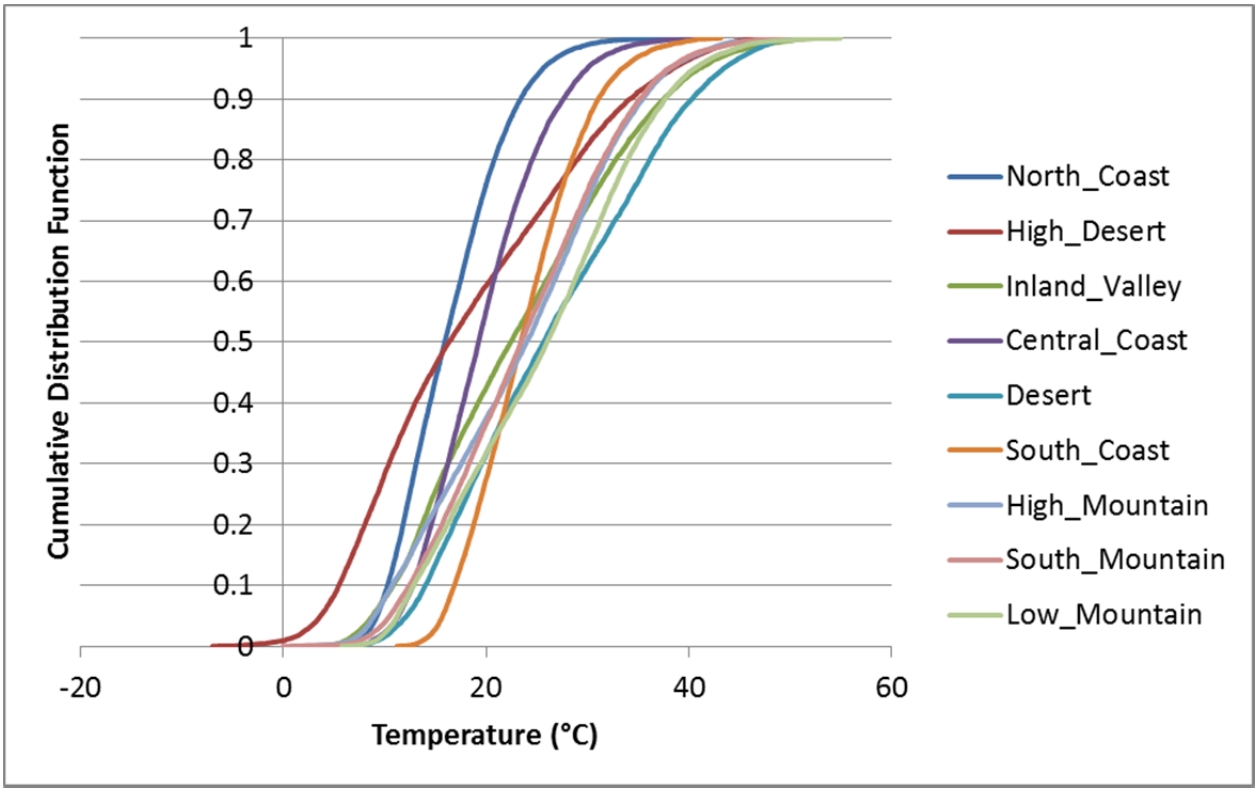

PD 22s1 - Pavement Temperature (1/3 Depth)

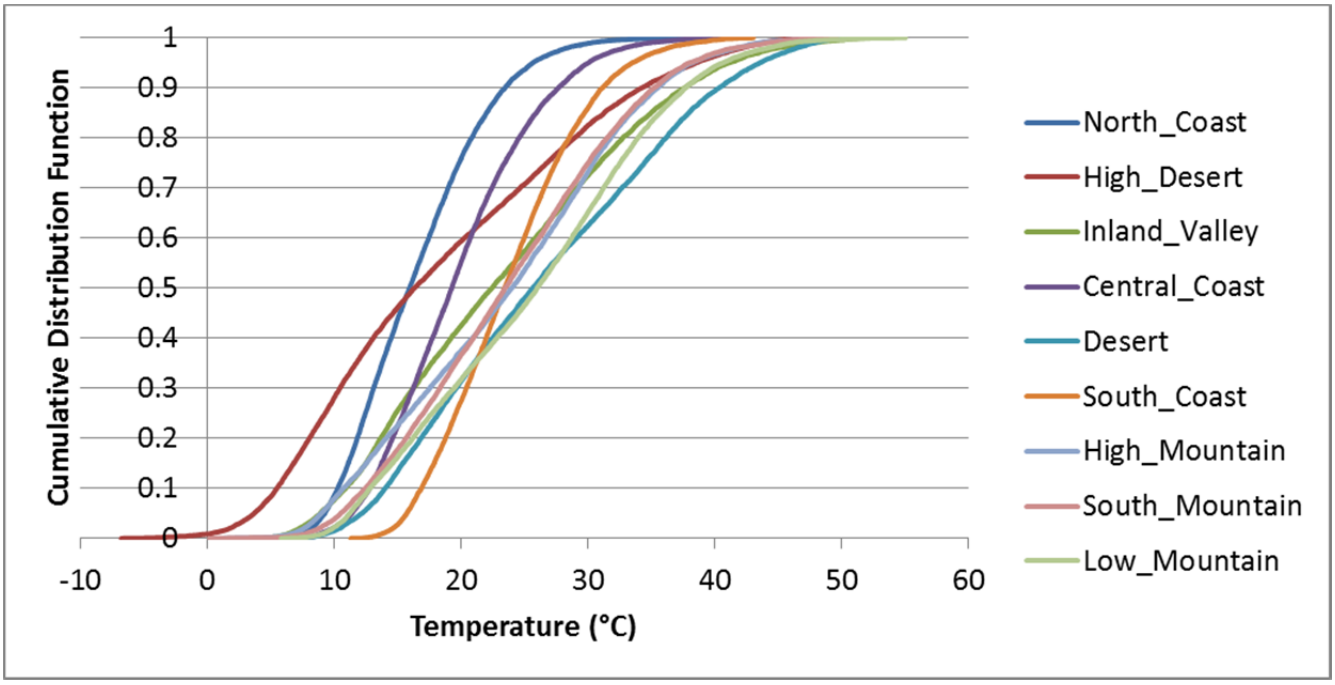

PD 22s2 - Pavement Temperature (1/3 Depth)

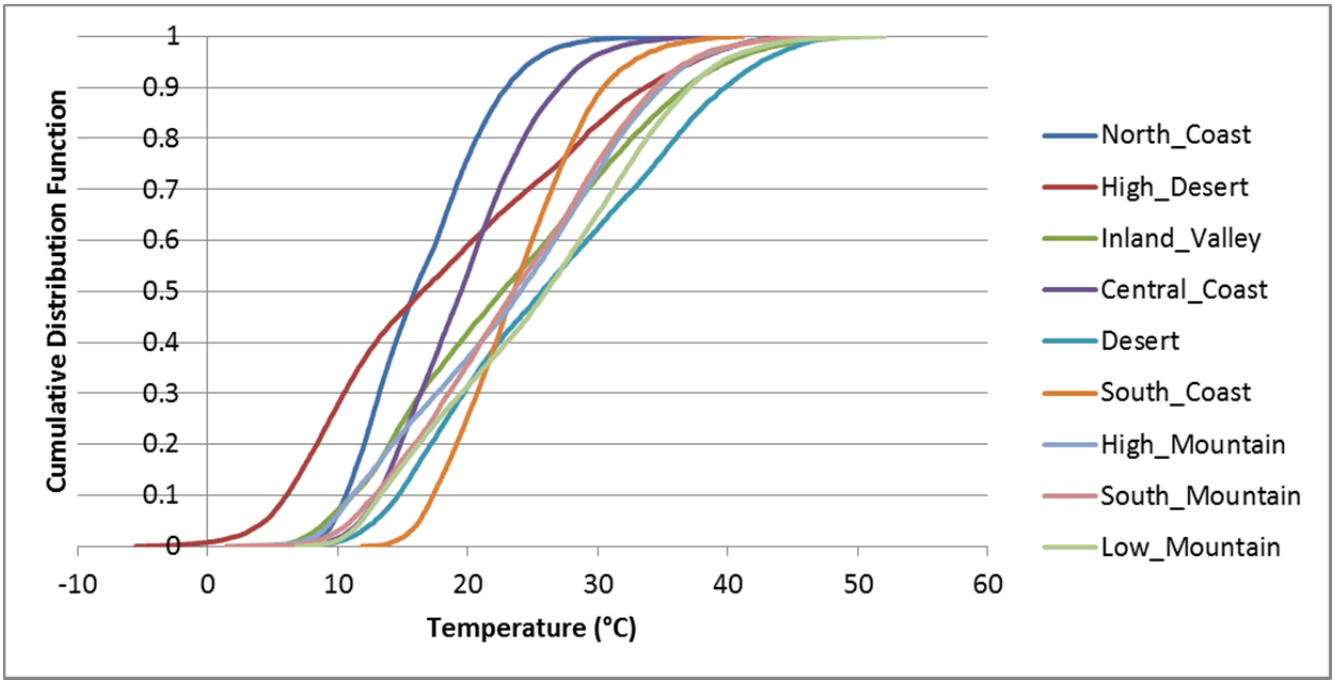

PD 23 - Pavement Temperature (1/3 Depth)

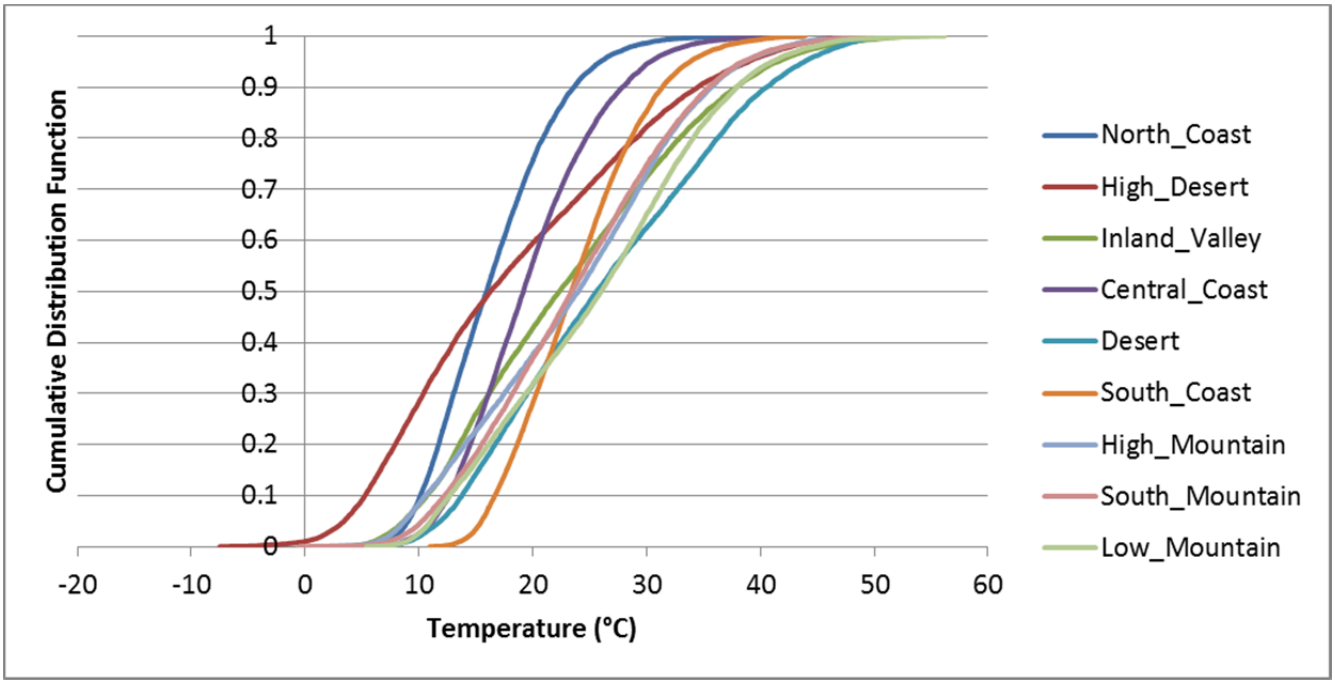

Temperature Comparison (Data Year: 1961)

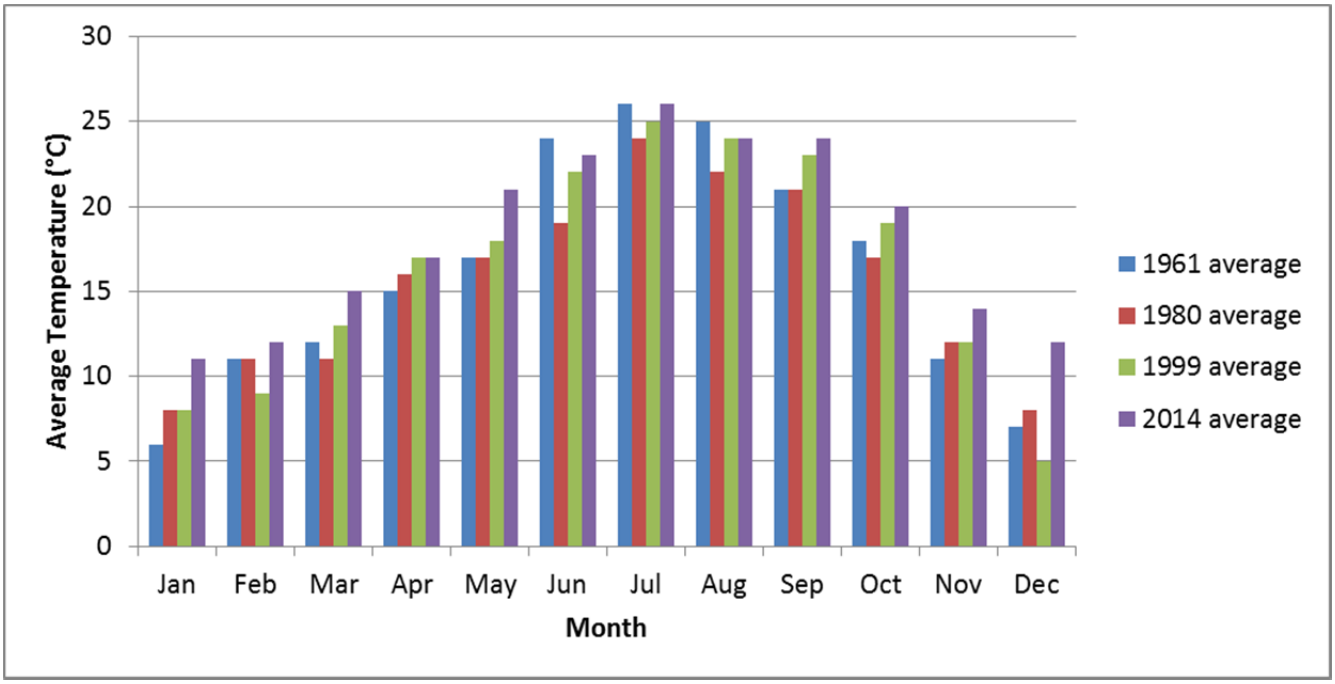

APPENDIX B: AXLE LOAD SPECTRUM DATA

PD 01

Truck, Weekday

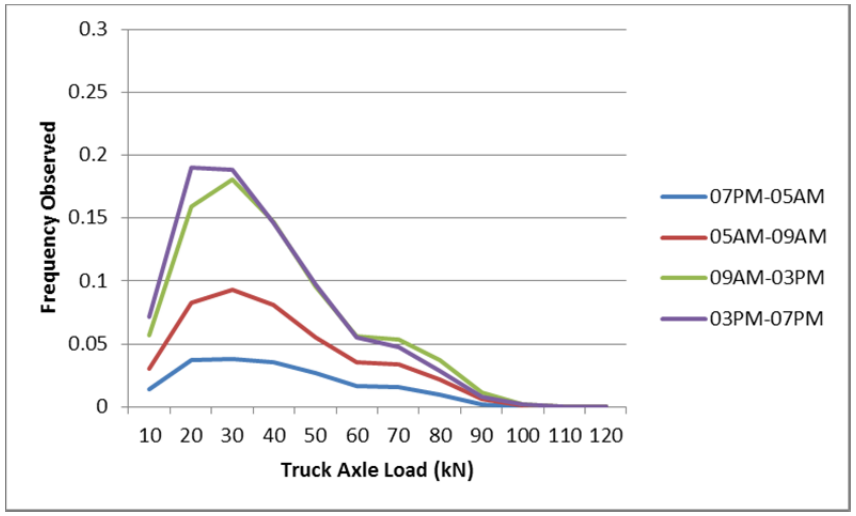

Car/SUV, Weekday

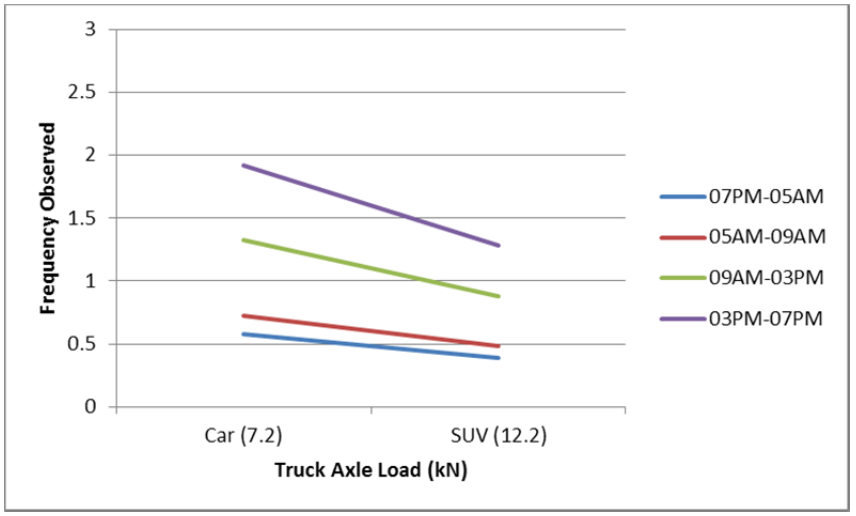

Truck, Weekend

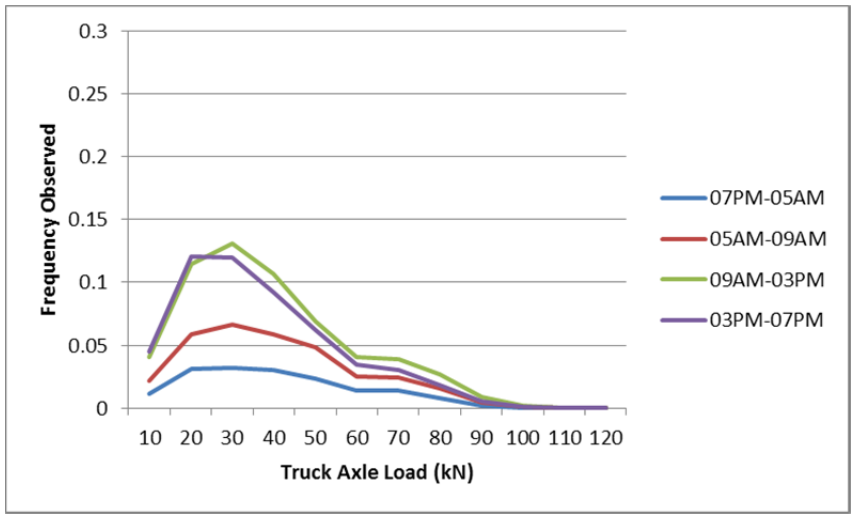

Car/SUV, Weekend

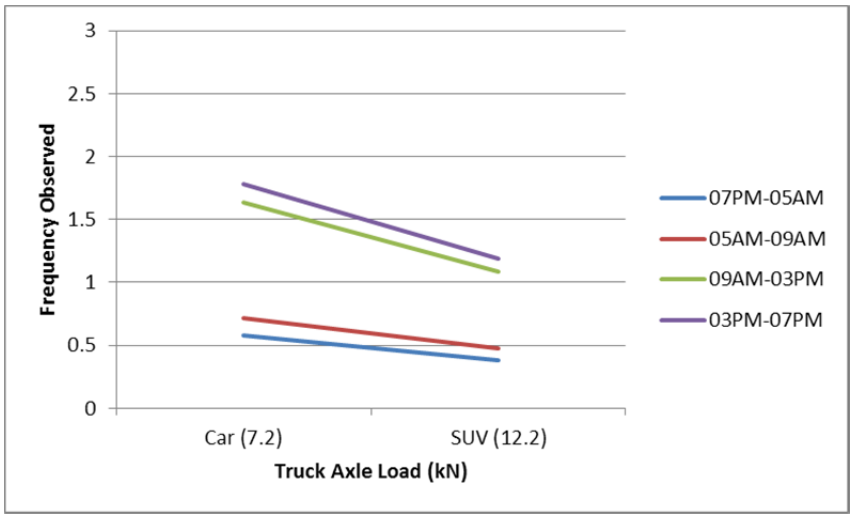

PD 02

Truck, Weekday

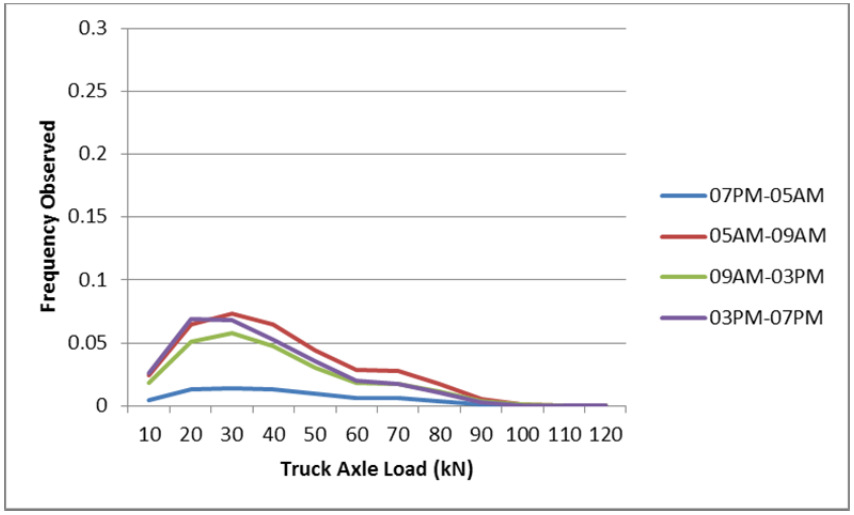

Car/SUV, Weekday

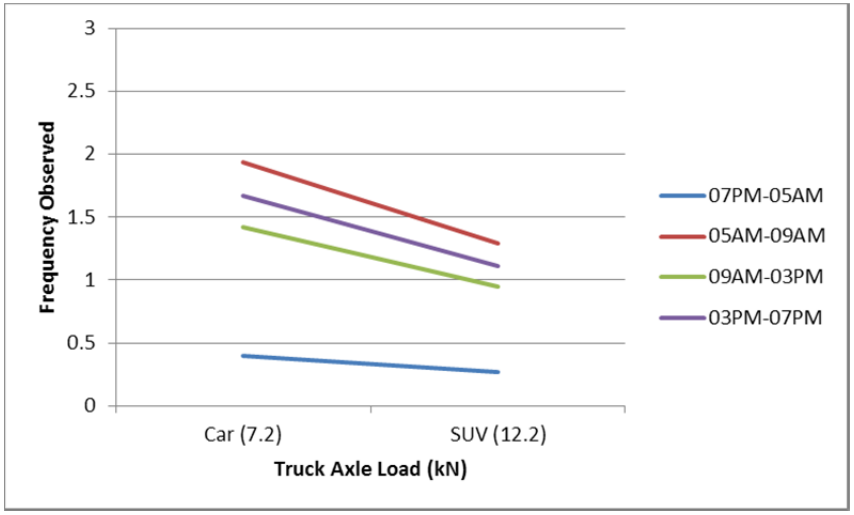

Truck, Weekend

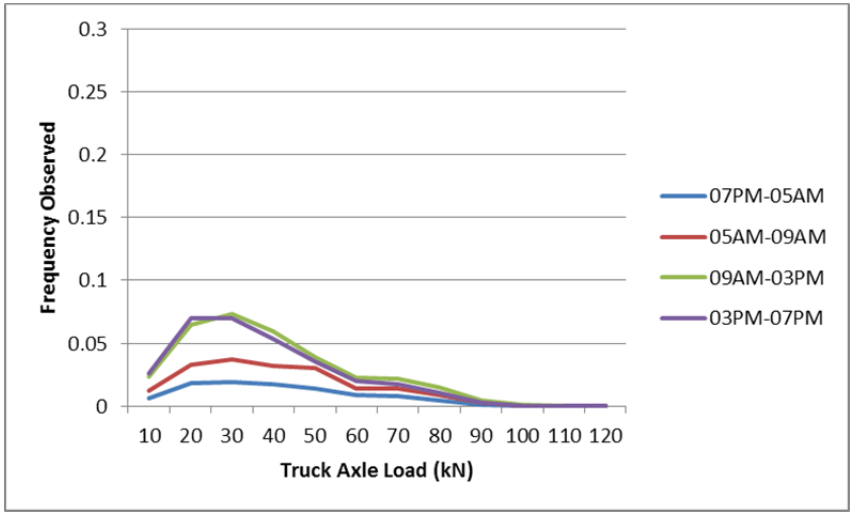

Car/SUV, Weekend

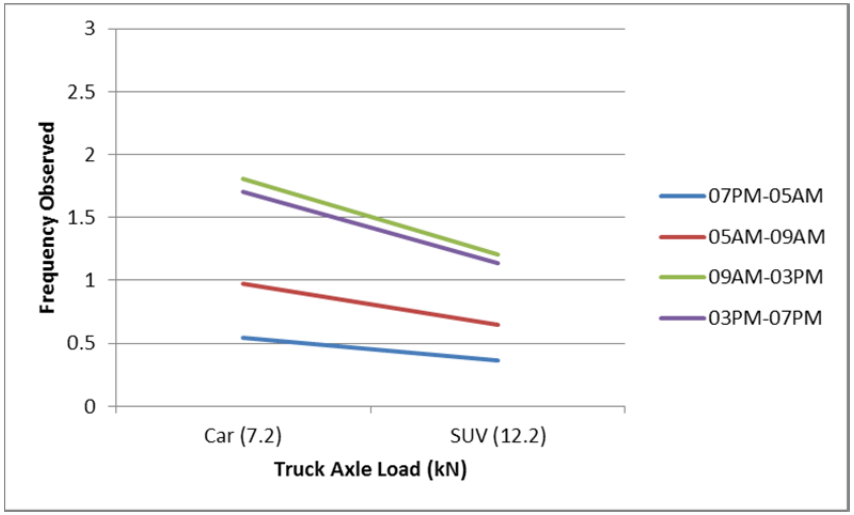

PD 03

Truck, Weekday

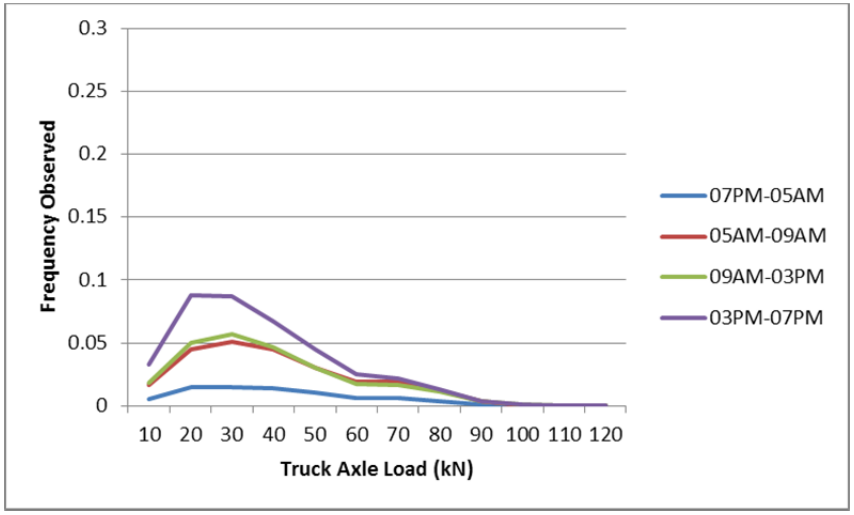

Car/SUV, Weekday

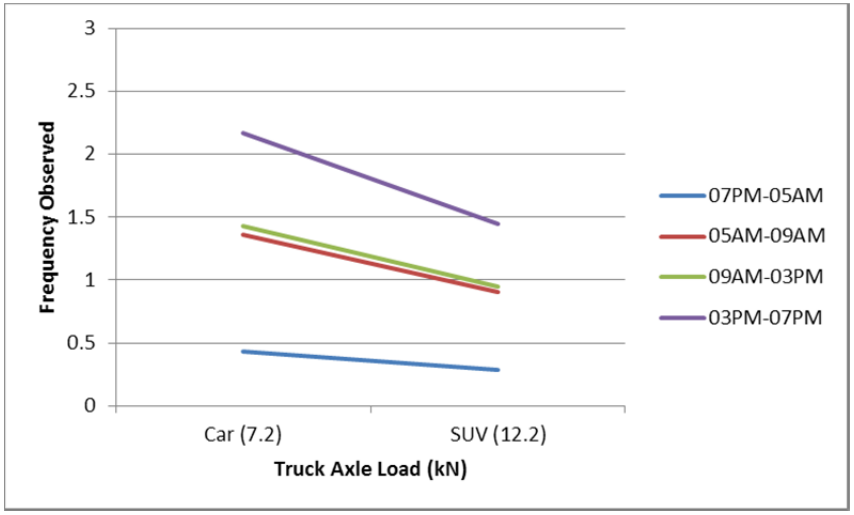

Truck, Weekend

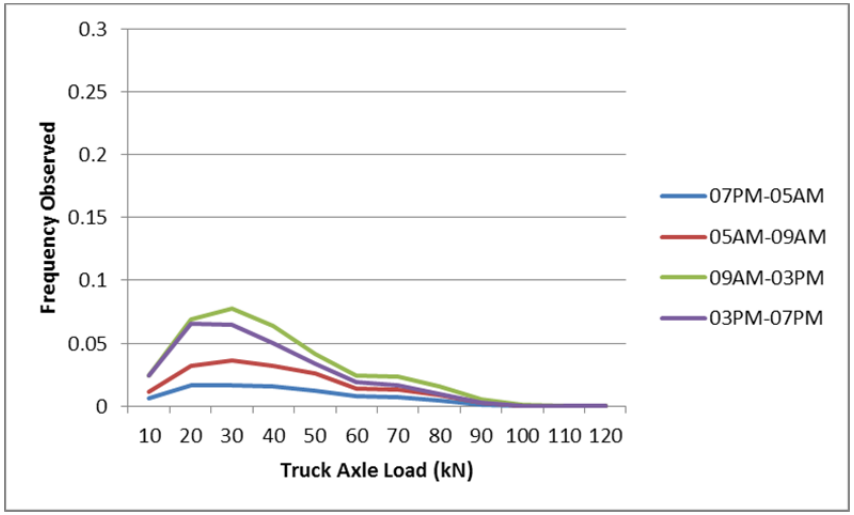

Car/SUV, Weekend

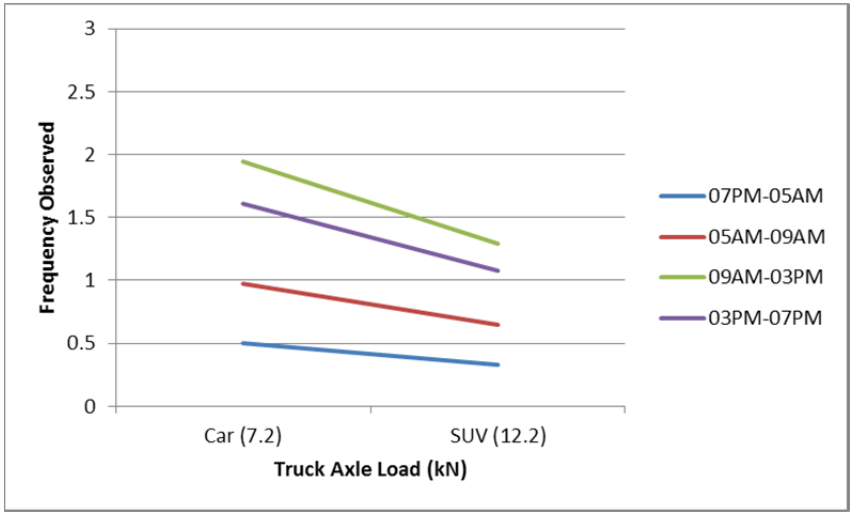

PD 04

Truck, Weekday

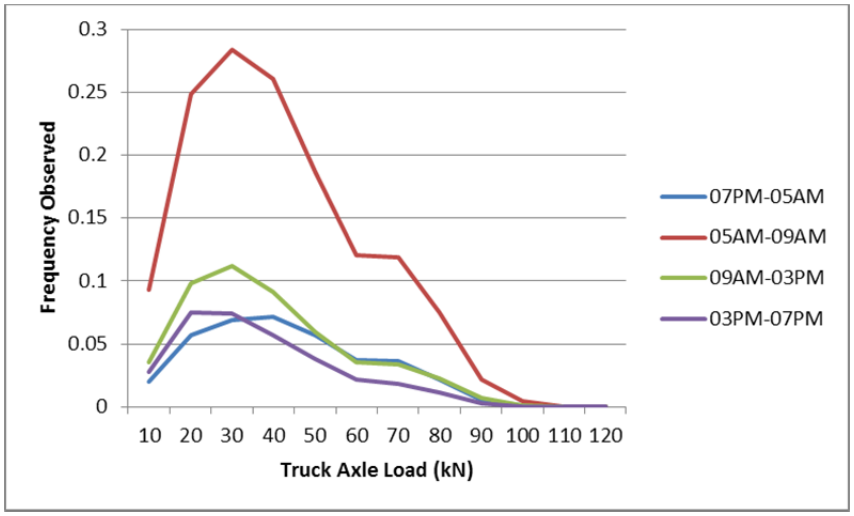

Car/SUV, Weekday

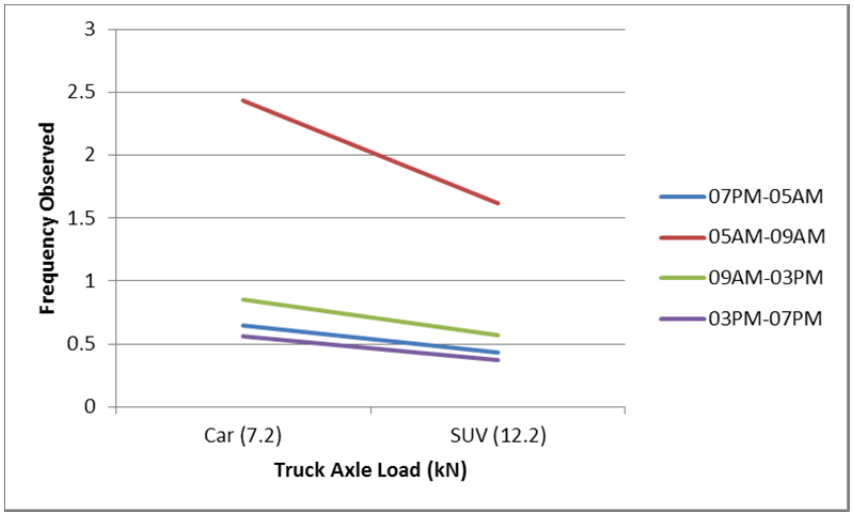

Truck, Weekend

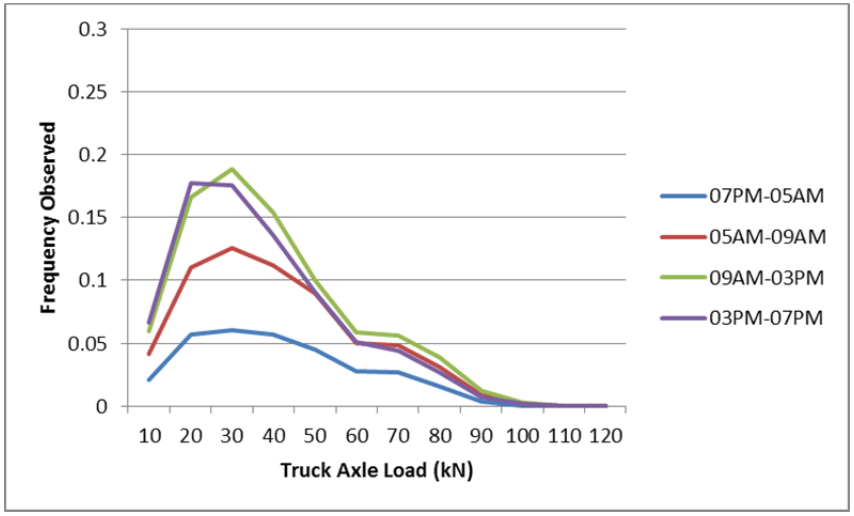

Car/SUV, Weekend

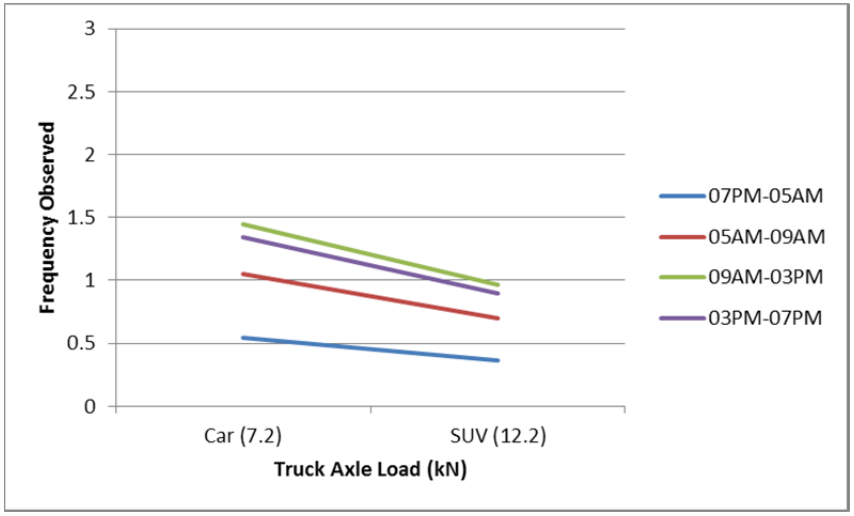

PD 05

Truck, Weekday

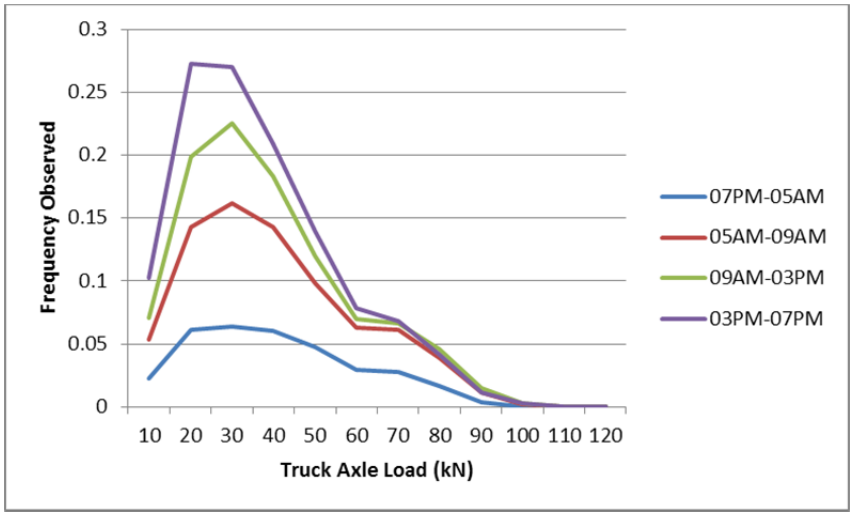

Car/SUV, Weekday

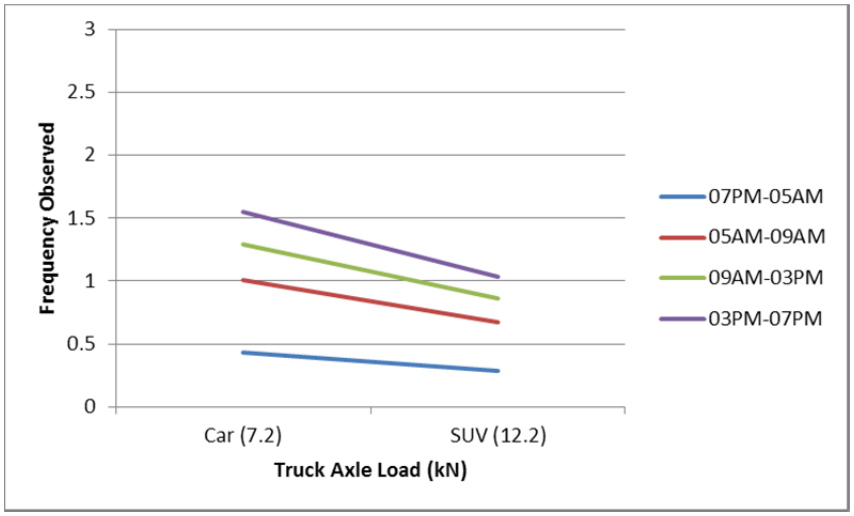

Truck, Weekend

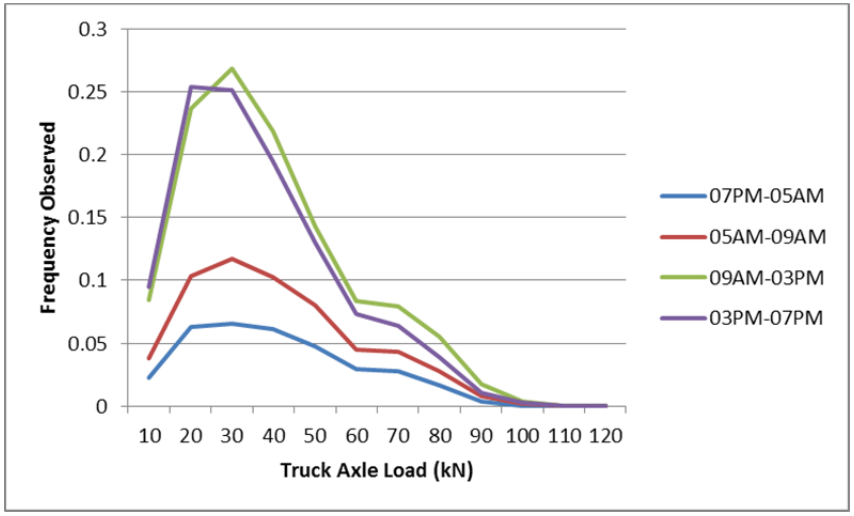

Car/SUV, Weekend

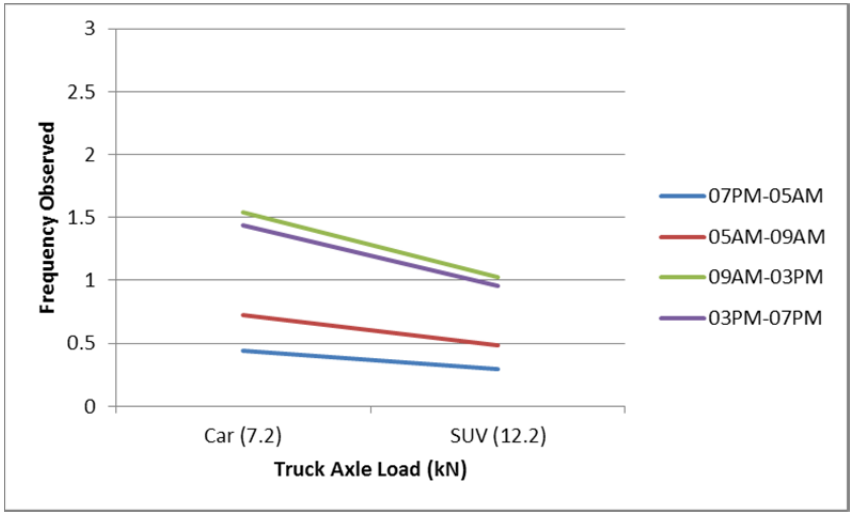

PD 06

Truck, Weekday

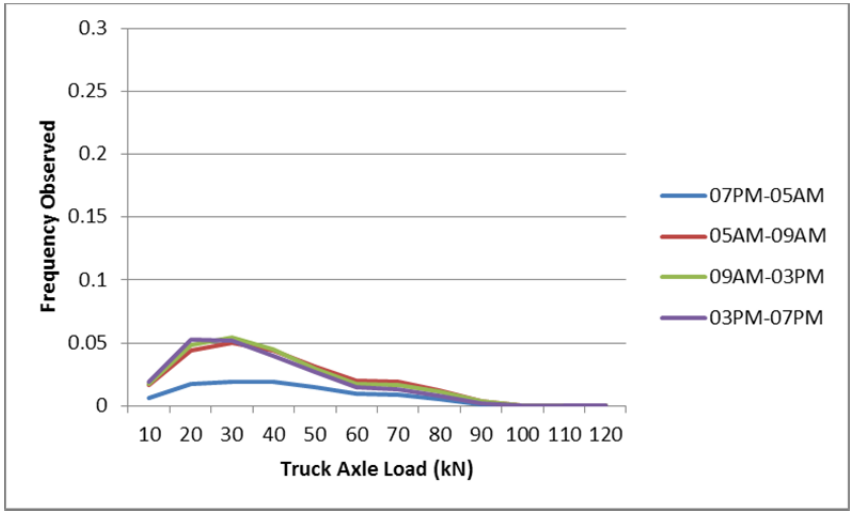

Car/SUV, Weekday

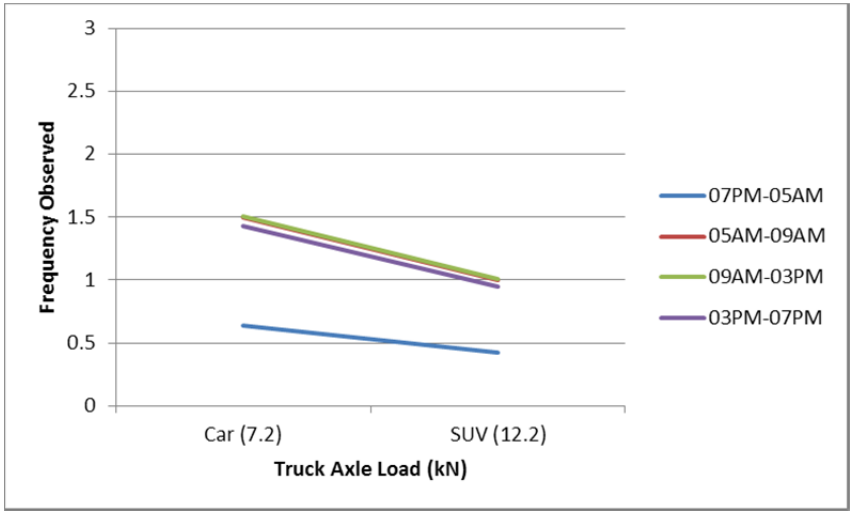

Truck, Weekend

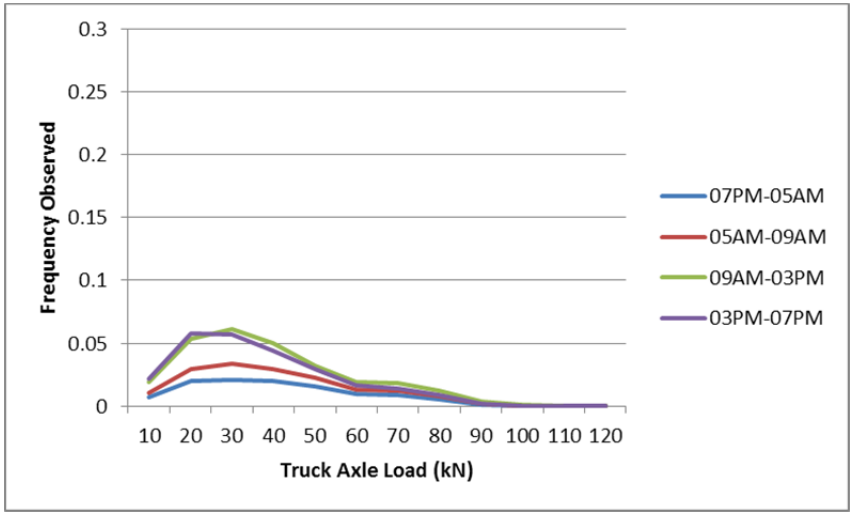

Car/SUV, Weekend

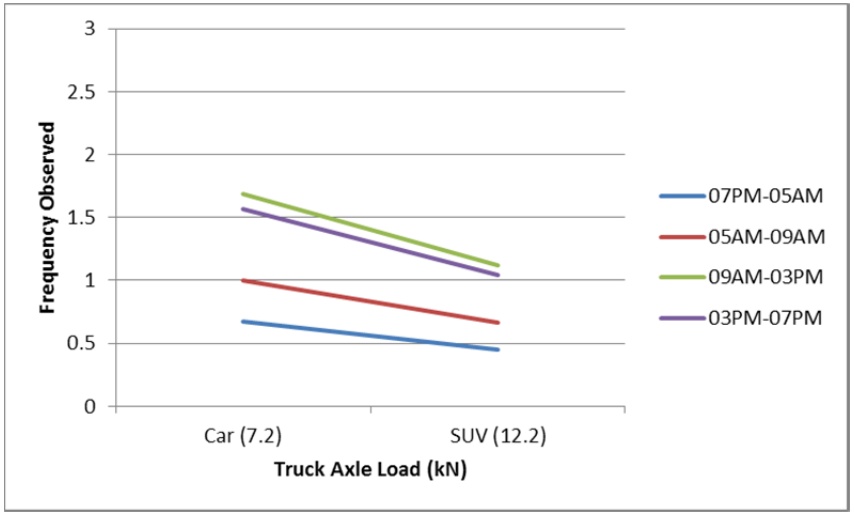

PD 07

Truck, Weekday

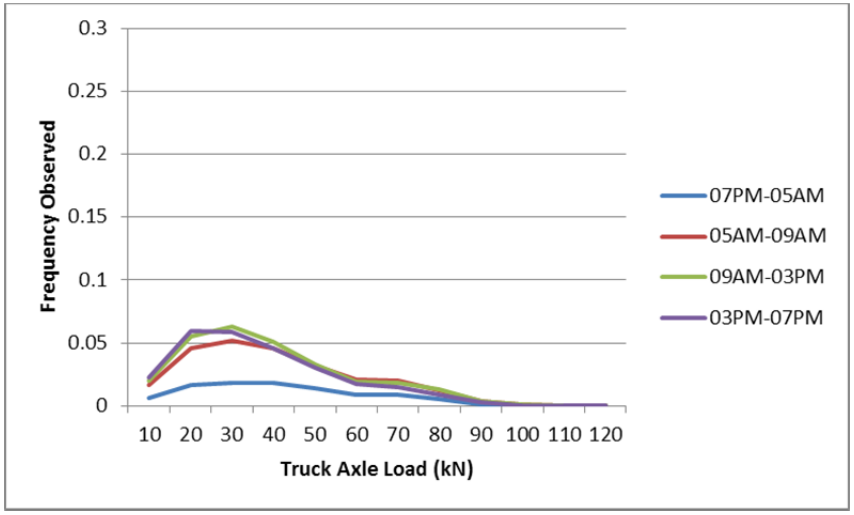

Car/SUV, Weekday

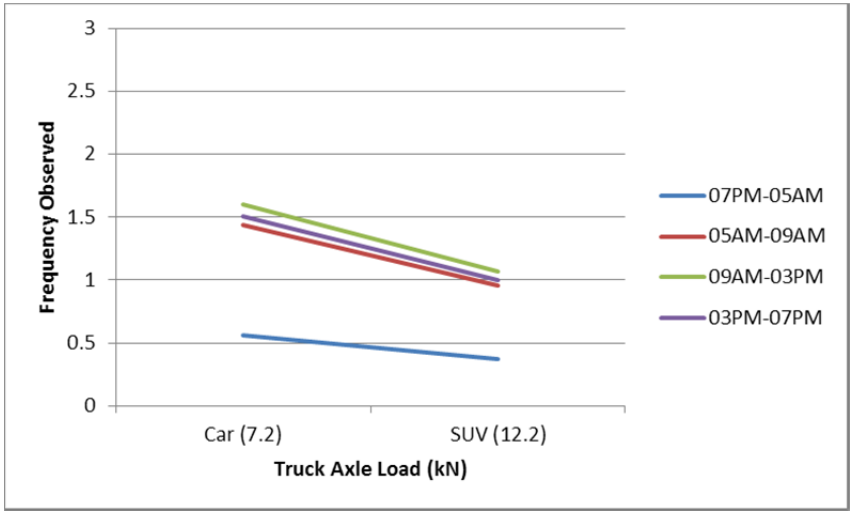

Truck, Weekend

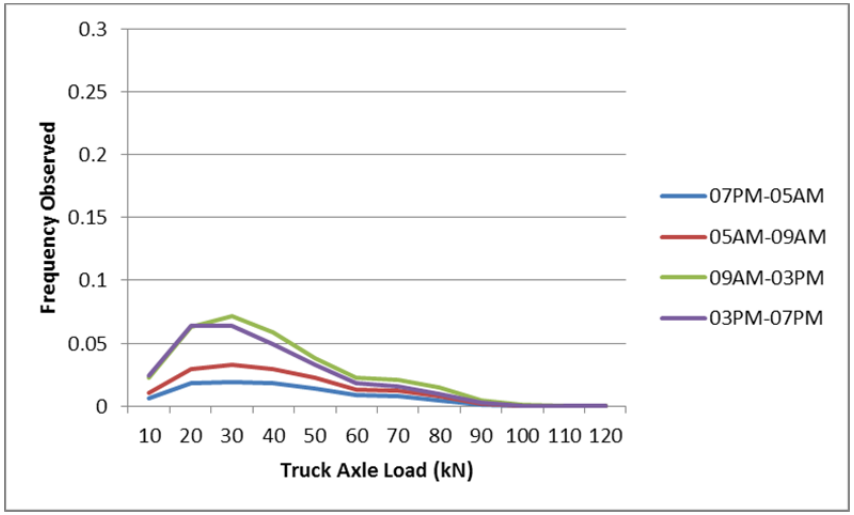

Car/SUV, Weekend

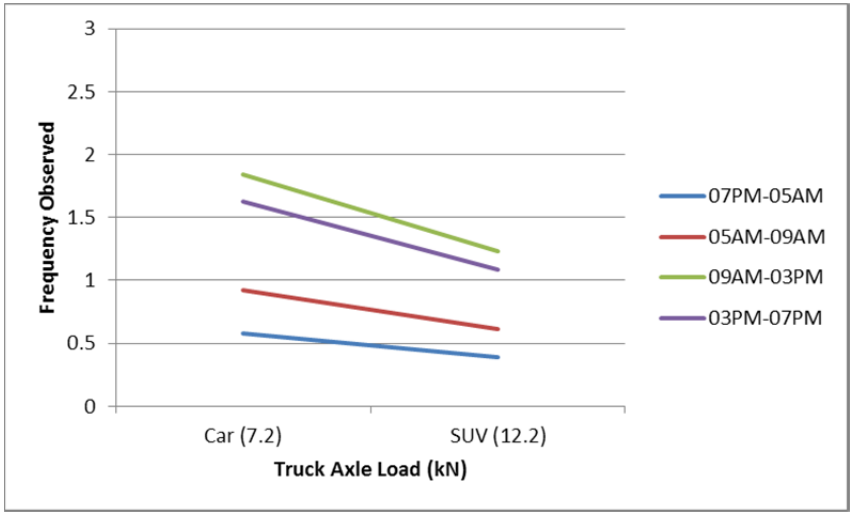

PD 08

Truck, Weekday

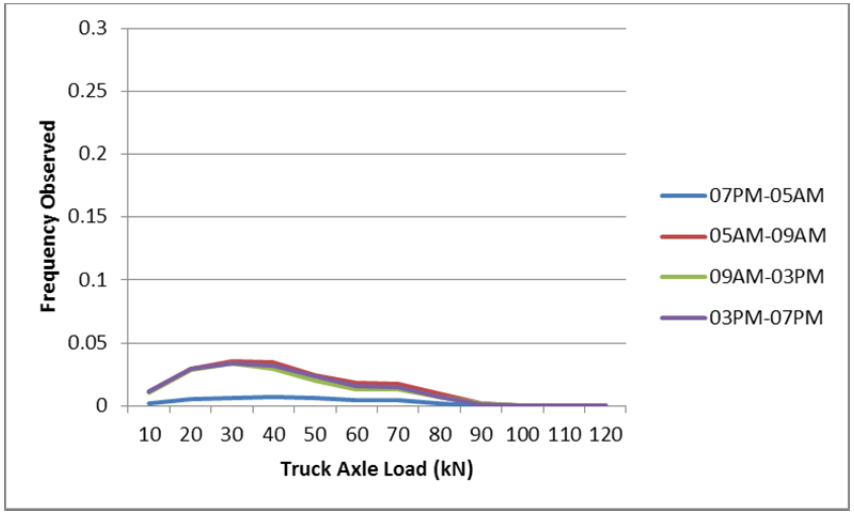

Car/SUV, Weekday

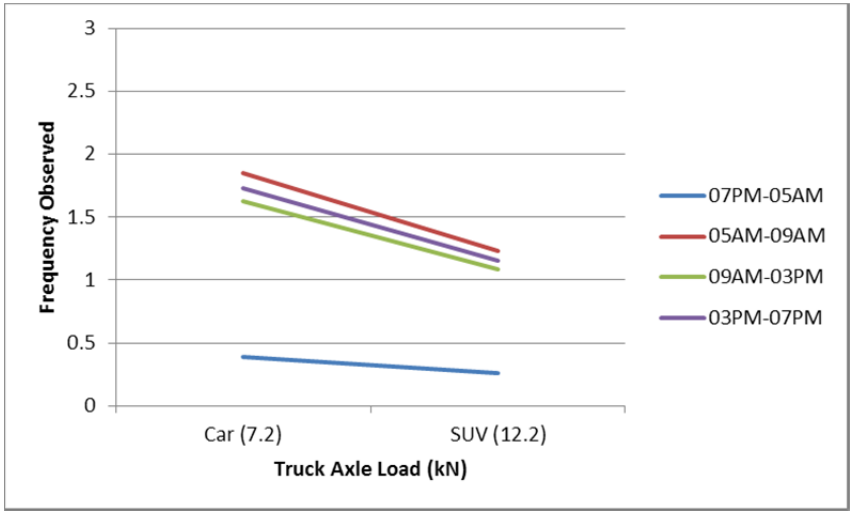

Truck, Weekend

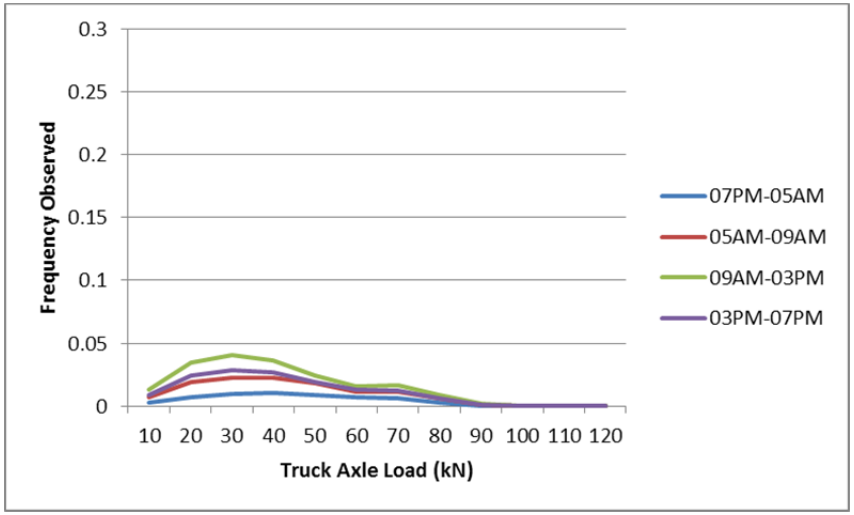

Car/SUV, Weekend

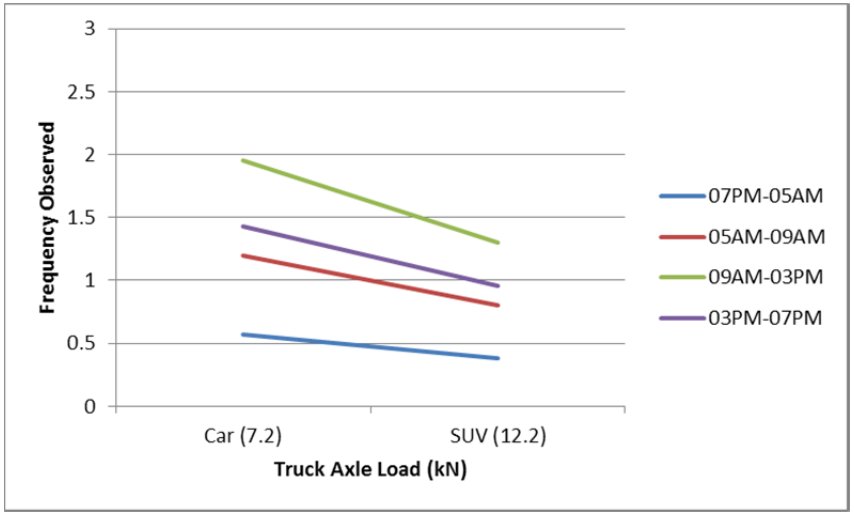

PD 10

Truck, Weekday

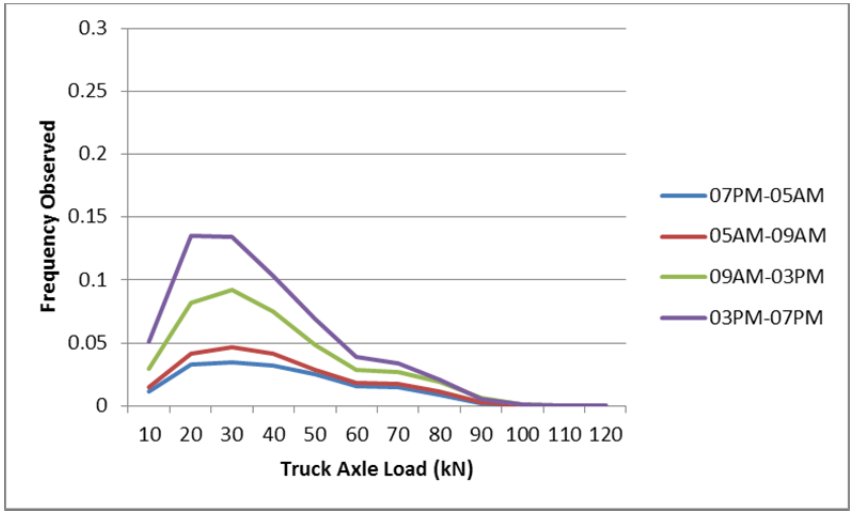

Car/SUV, Weekday

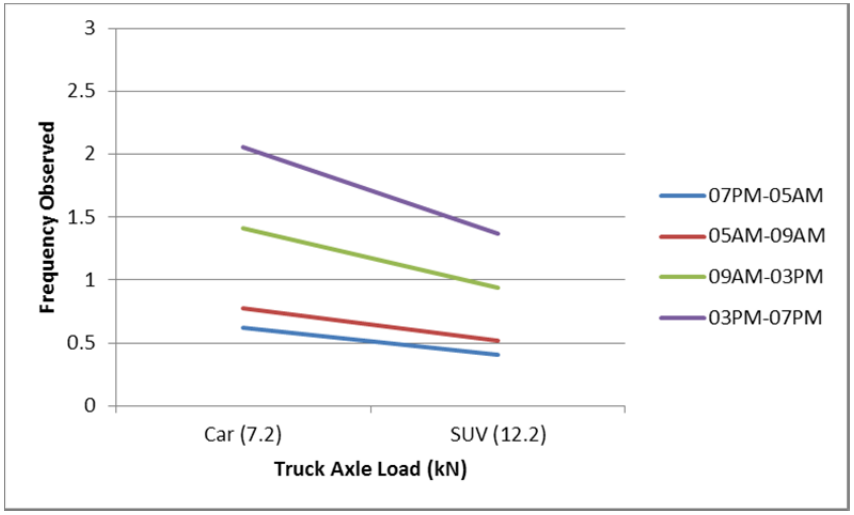

Truck, Weekend

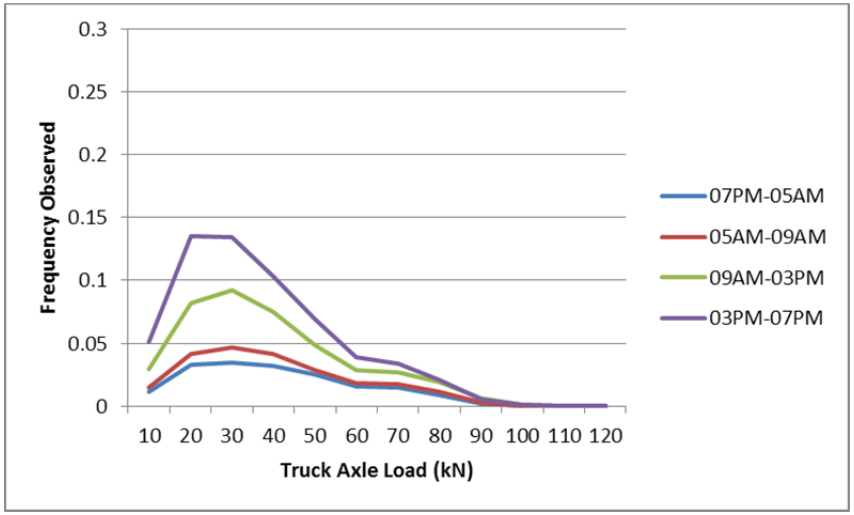

Car/SUV, Weekend

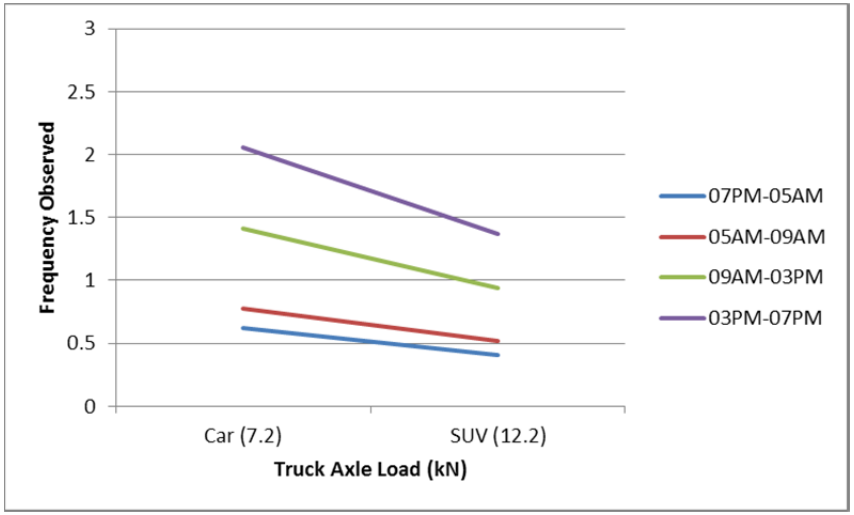

PD 11

Truck, Weekday

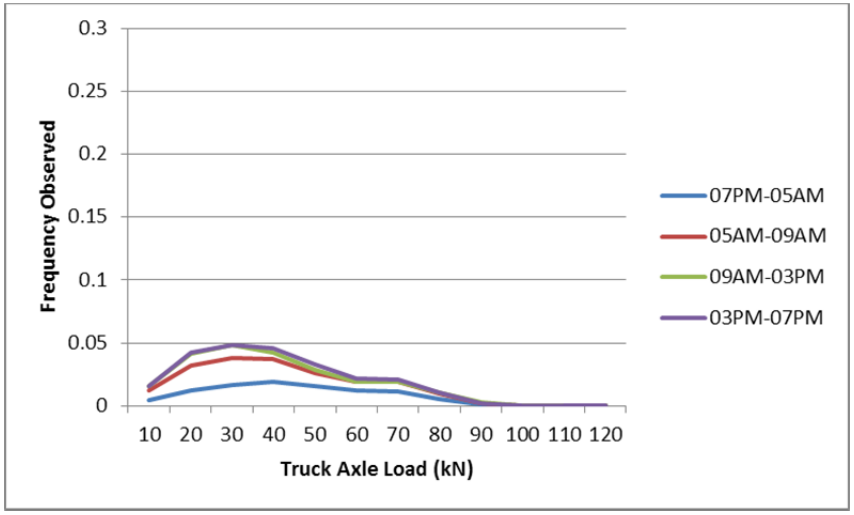

Car/SUV, Weekday

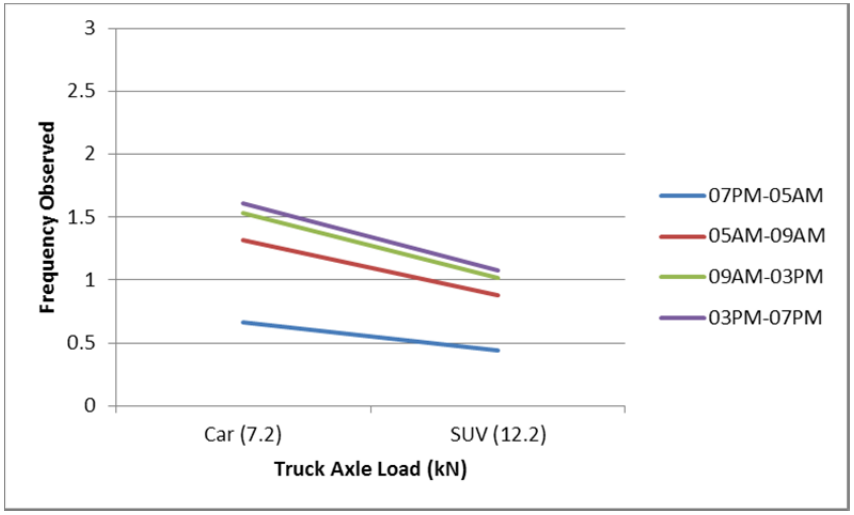

Truck, Weekend

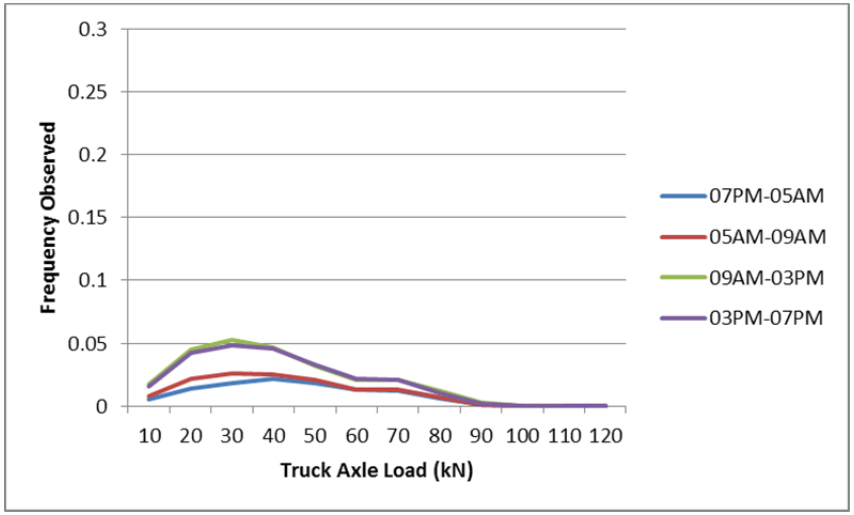

Car/SUV, Weekend

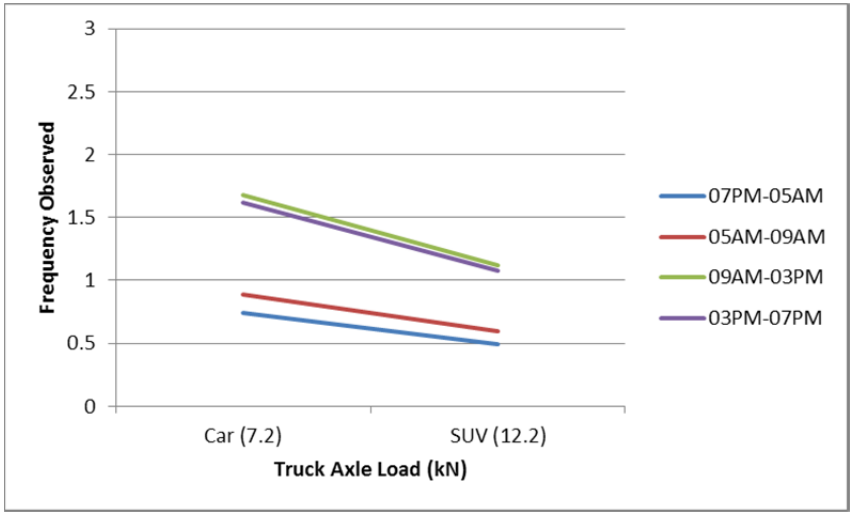

PD 12

Truck, Weekday

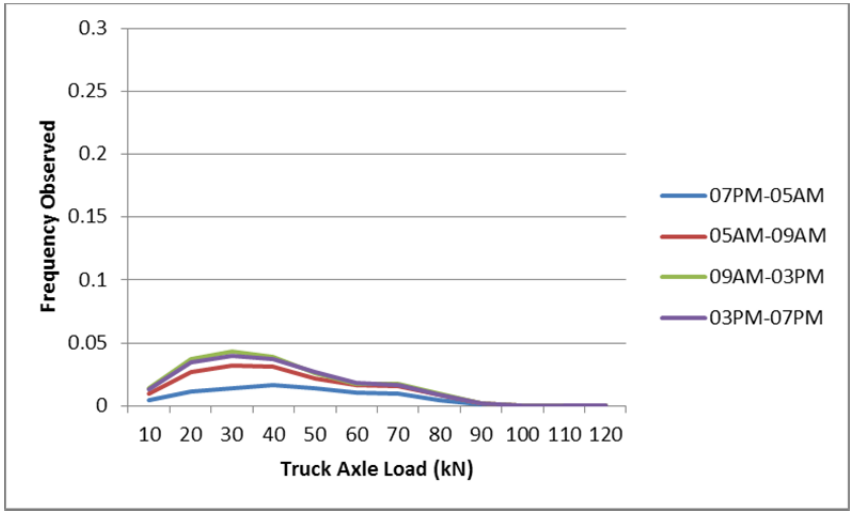

Car/SUV, Weekday

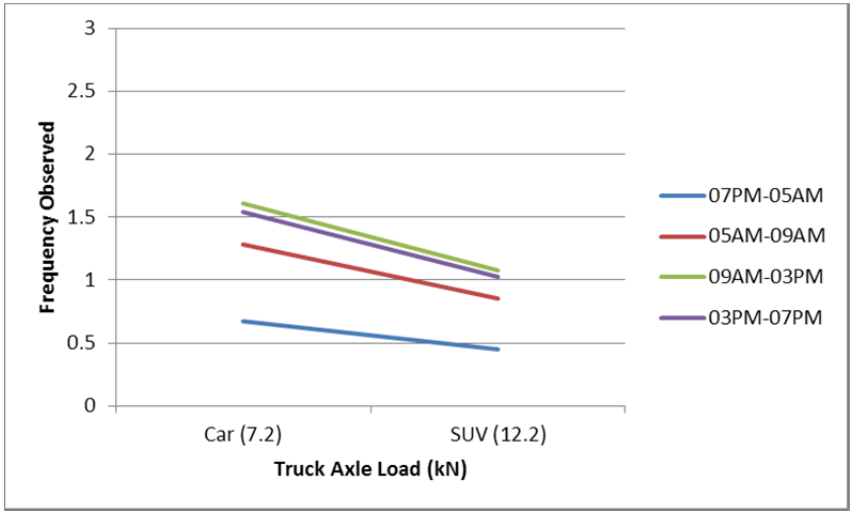

Truck, Weekend

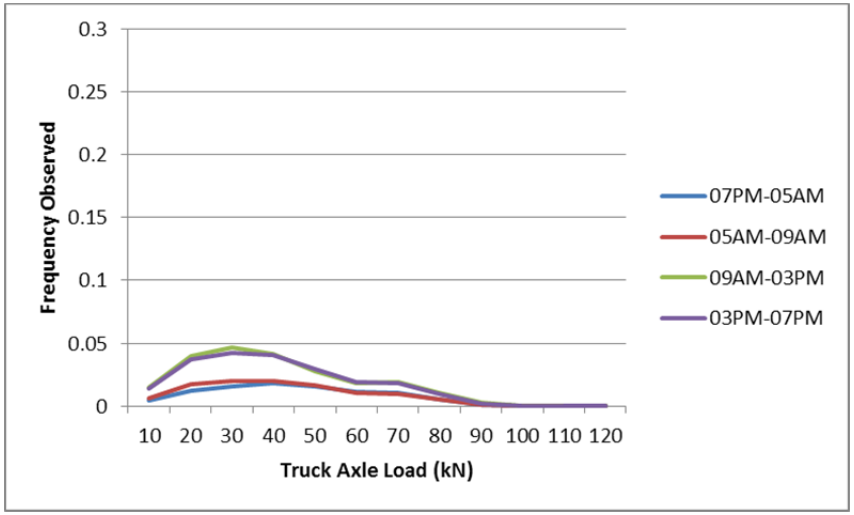

Car/SUV, Weekend

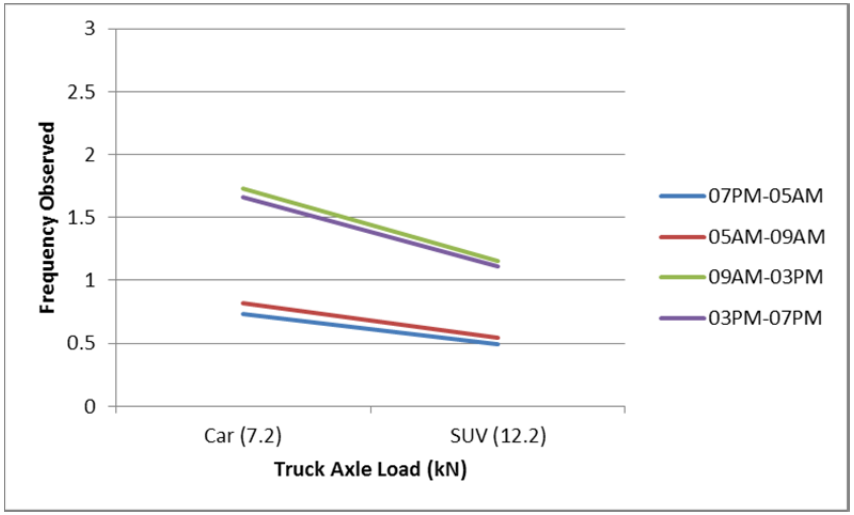

PD 13s1

Truck, Weekday

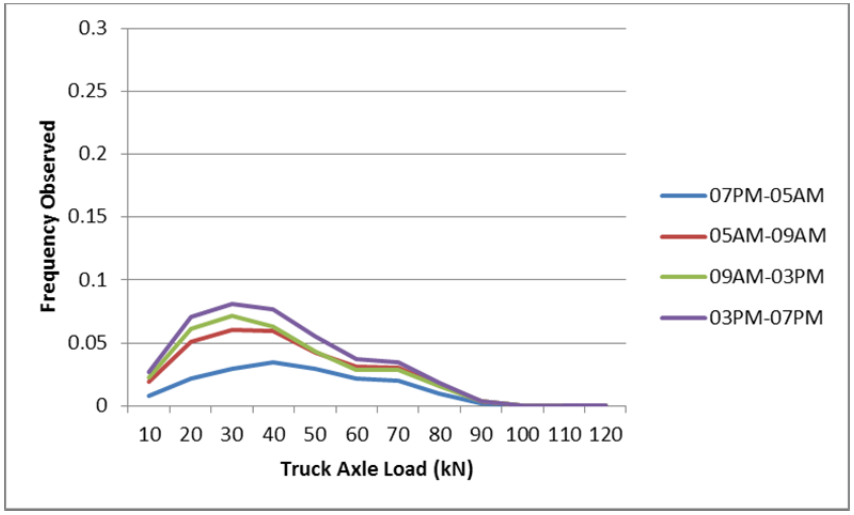

Car/SUV, Weekday

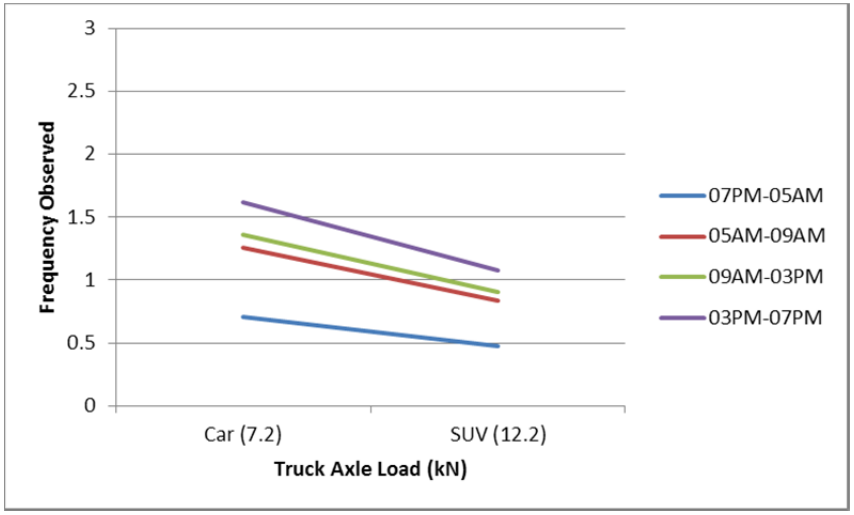

Truck, Weekend

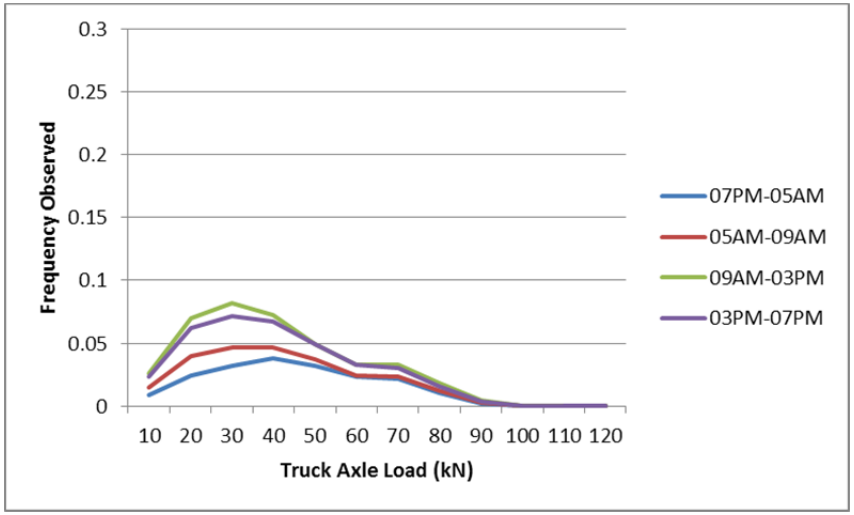

Car/SUV, Weekend

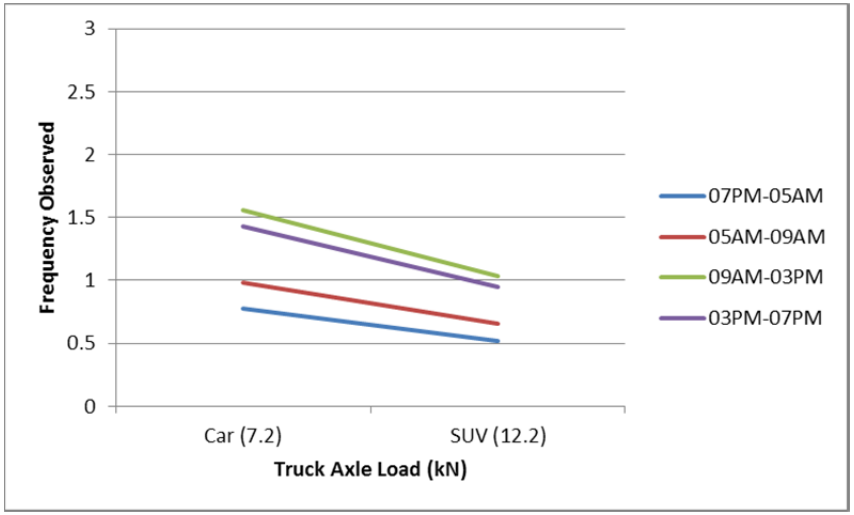

PD 13s2

Truck, Weekday

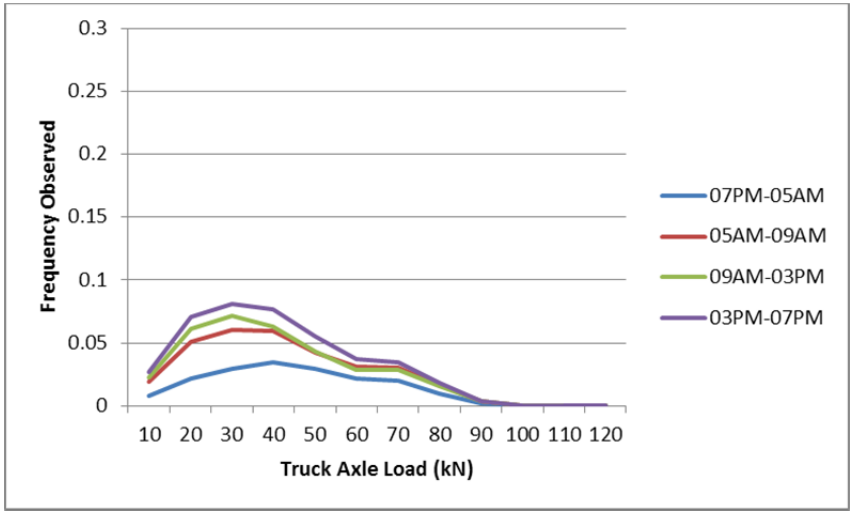

Car/SUV, Weekday

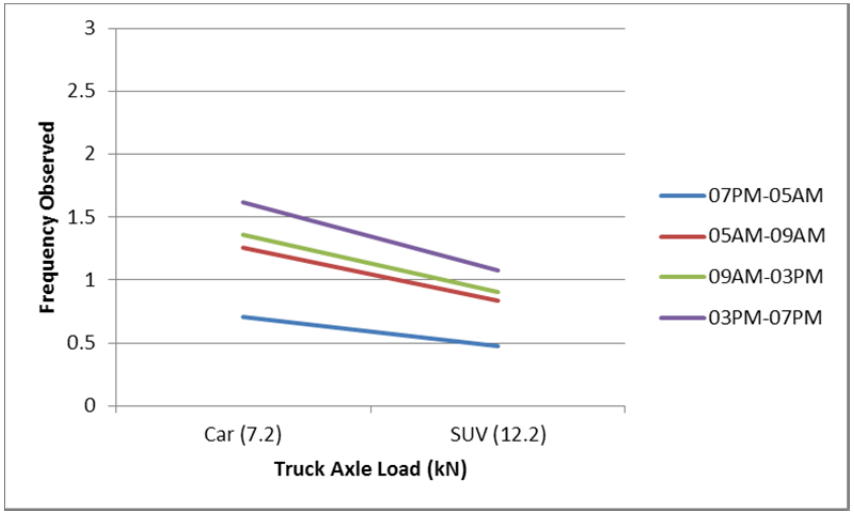

Truck, Weekend

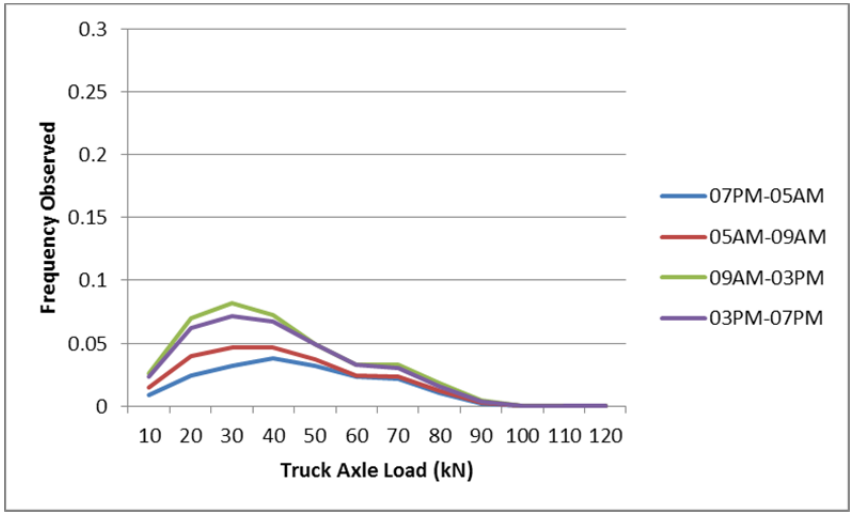

Car/SUV, Weekend

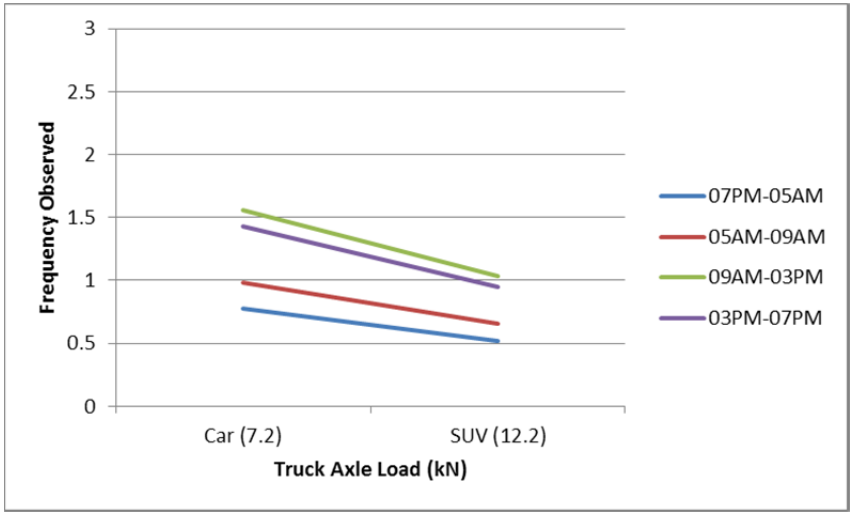

PD 14

Truck, Weekday

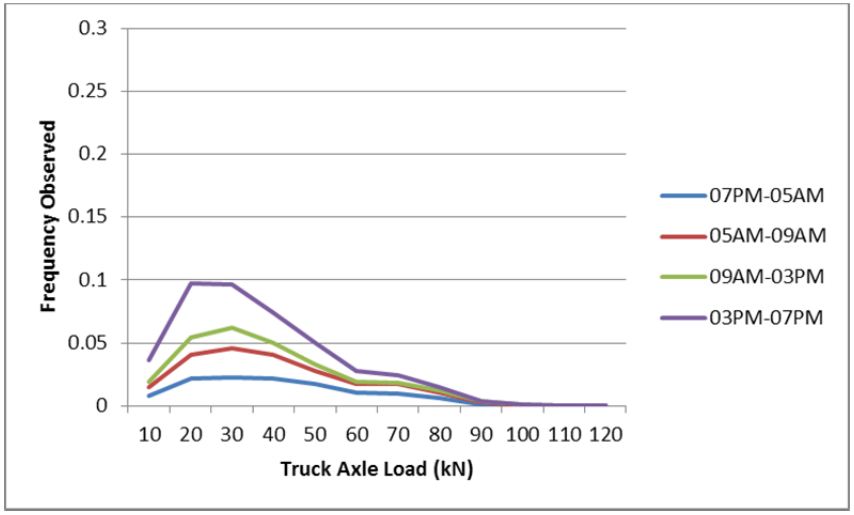

Car/SUV, Weekday

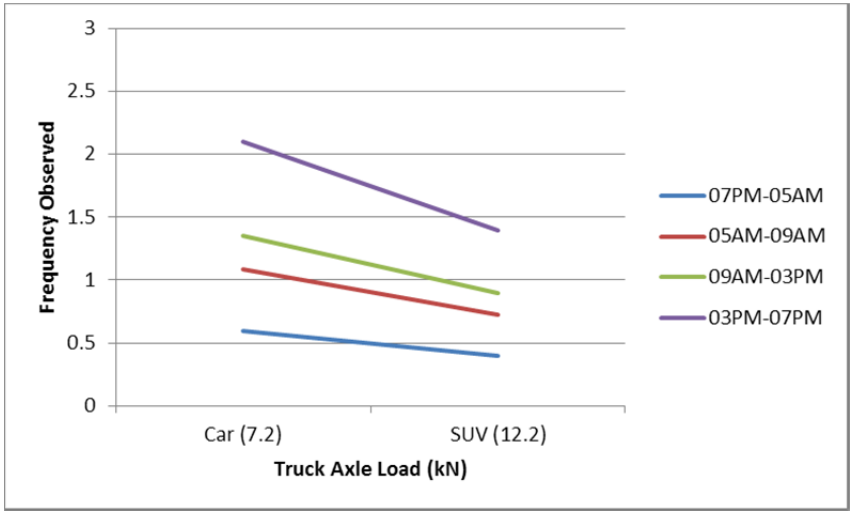

Truck, Weekend

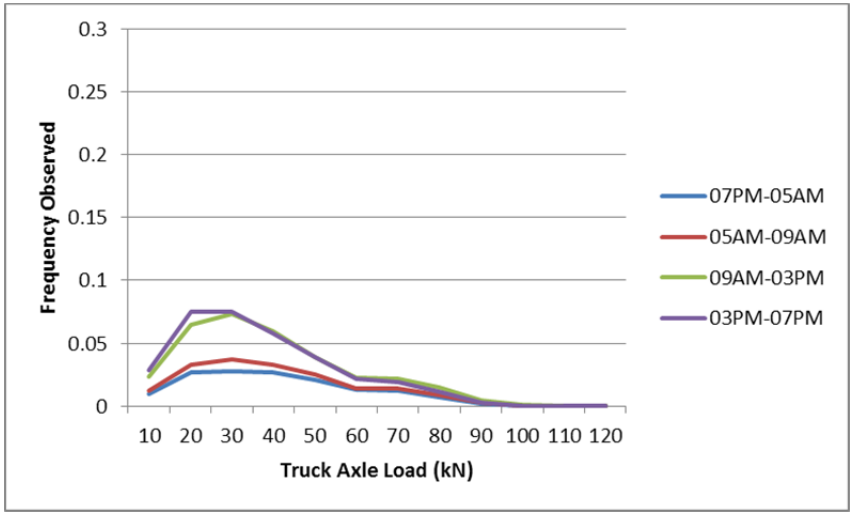

Car/SUV, Weekend

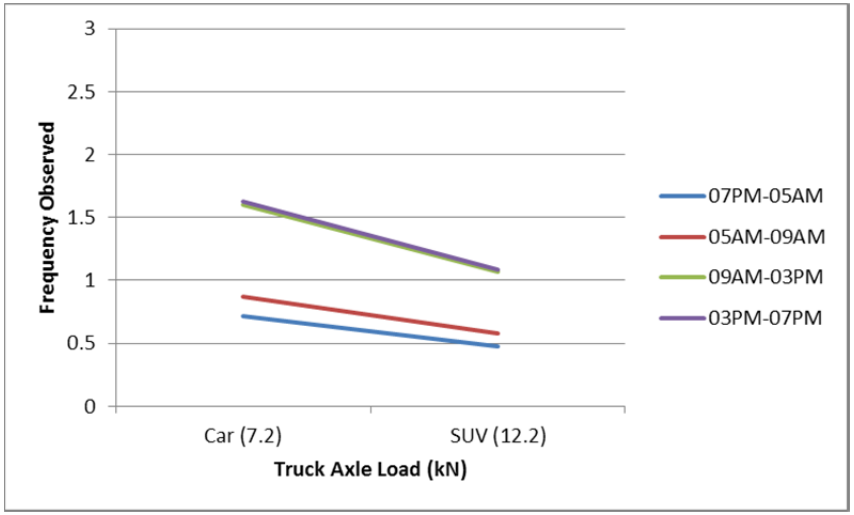

PD 15

Truck, Weekday

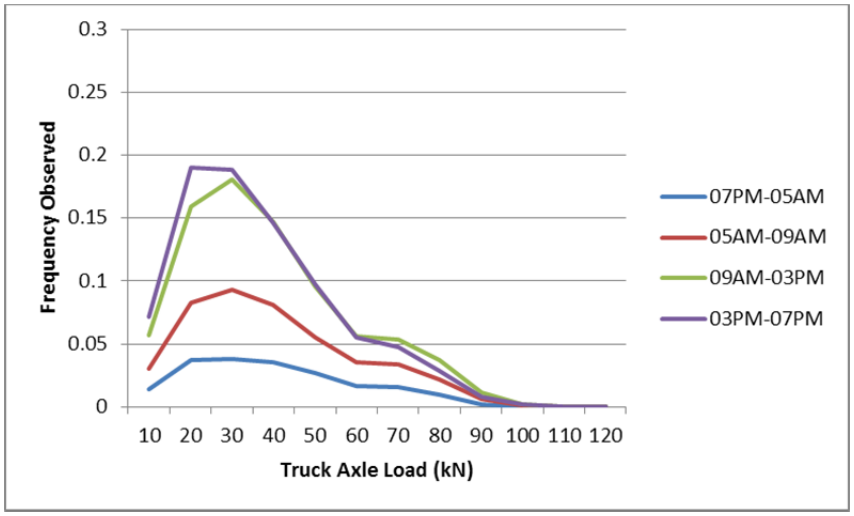

Car/SUV, Weekday

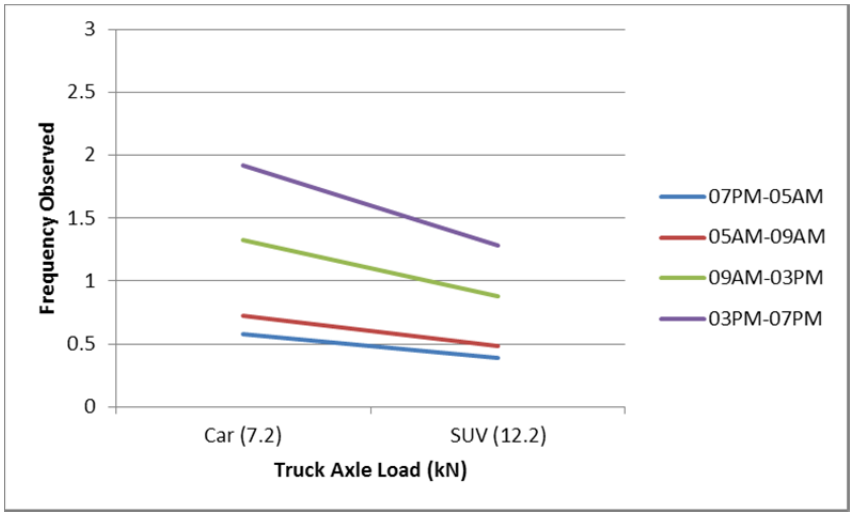

Truck, Weekend

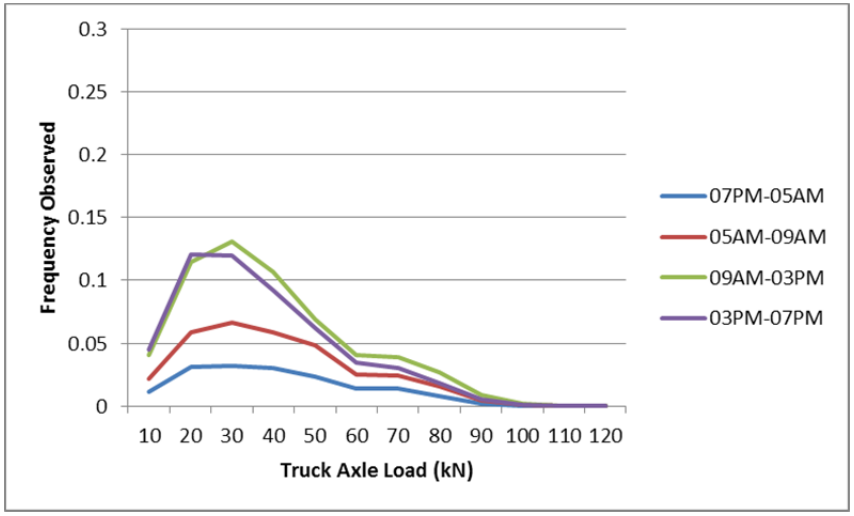

Car/SUV, Weekend

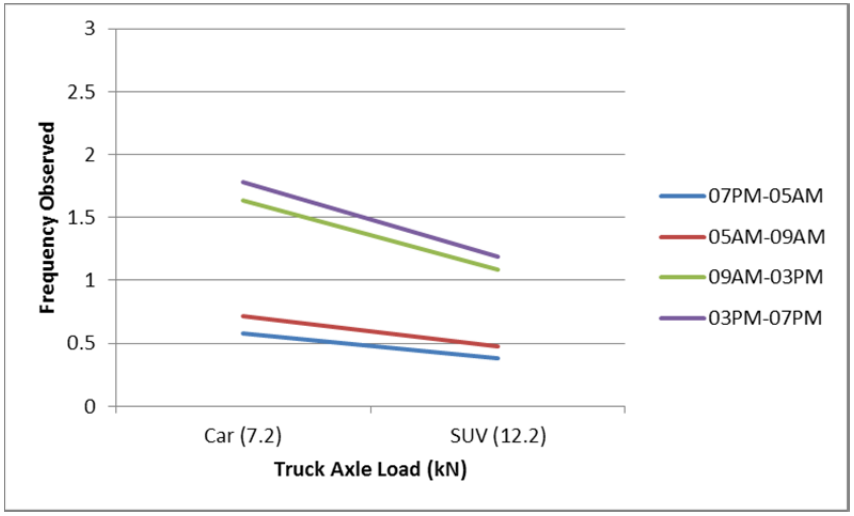

PD 16

Truck, Weekday

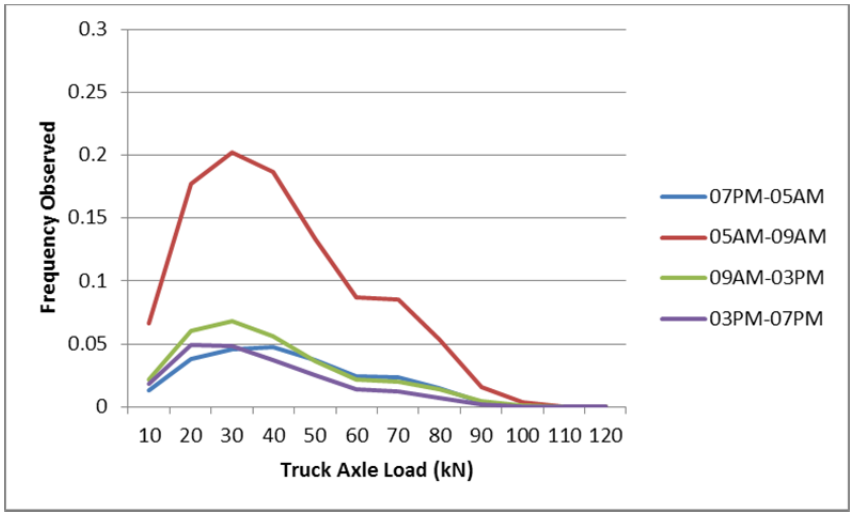

Car/SUV, Weekday

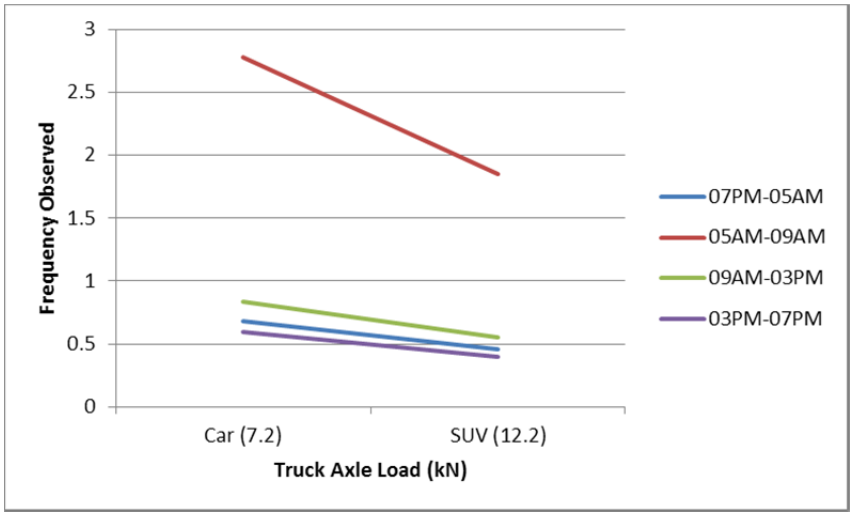

Truck, Weekend

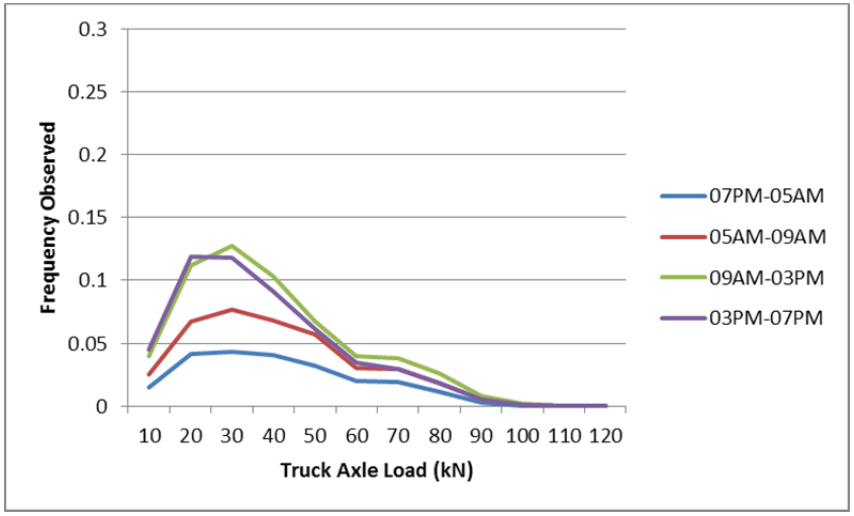

Car/SUV, Weekend

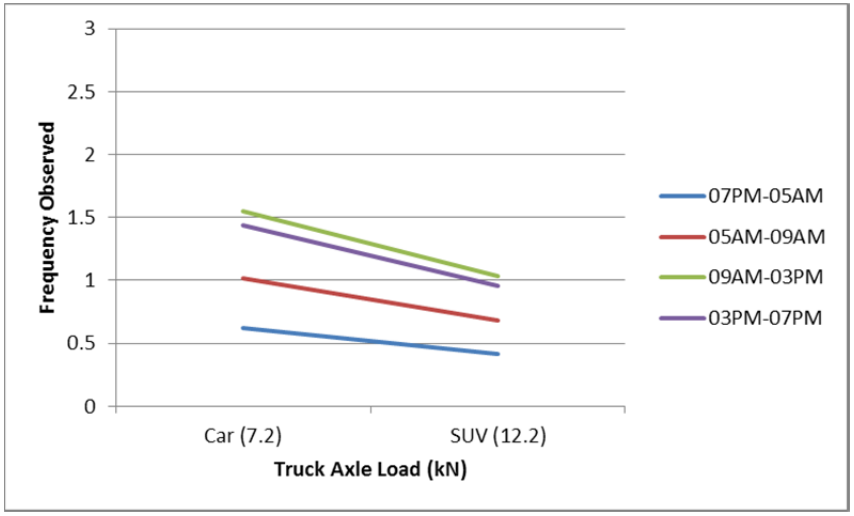

PD 17

Truck, Weekday

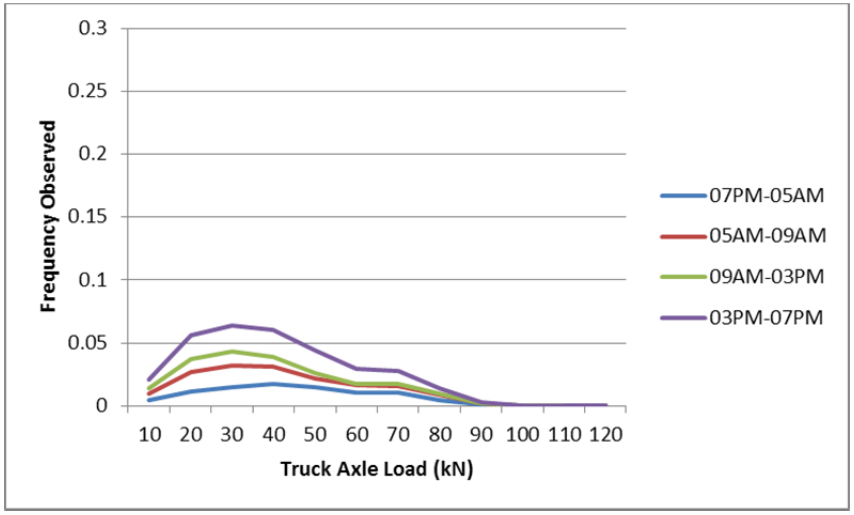

Car/SUV, Weekday

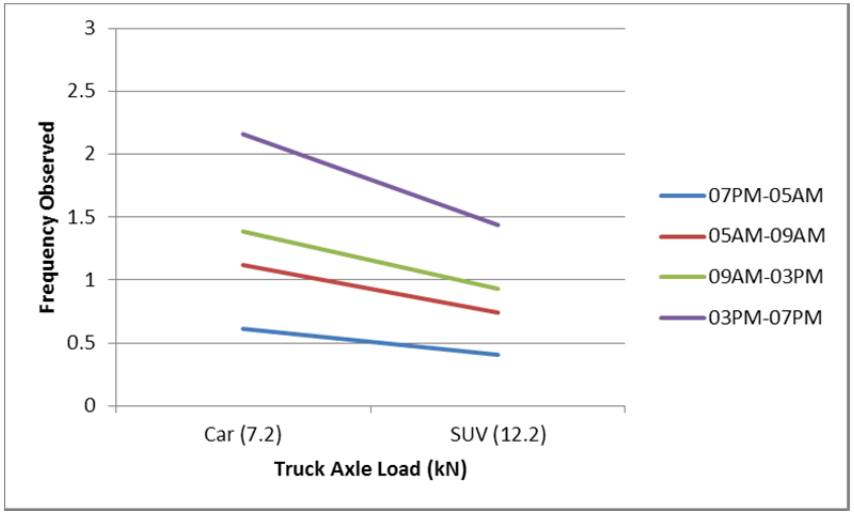

Truck, Weekend

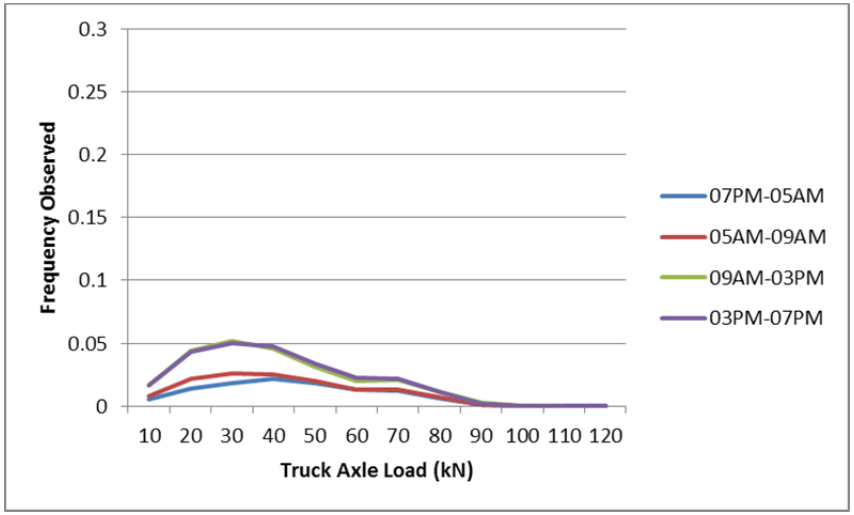

Car/SUV, Weekend

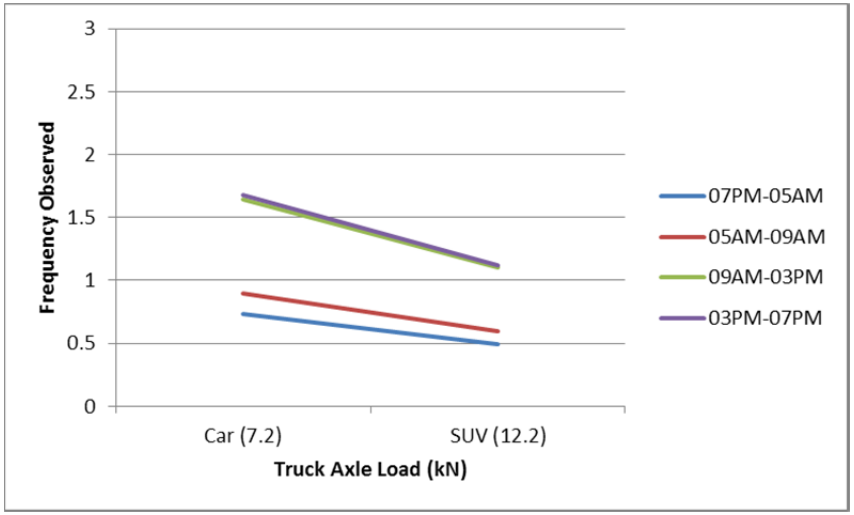

PD 18

Truck, Weekday

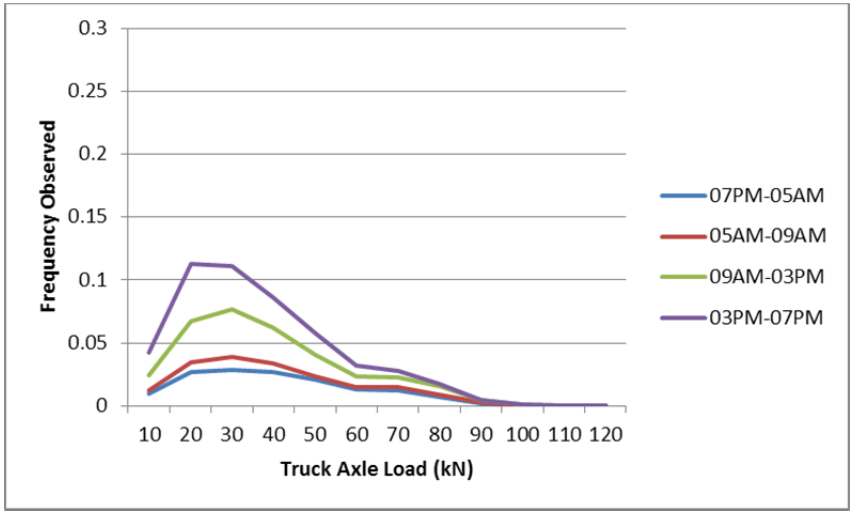

Car/SUV, Weekday

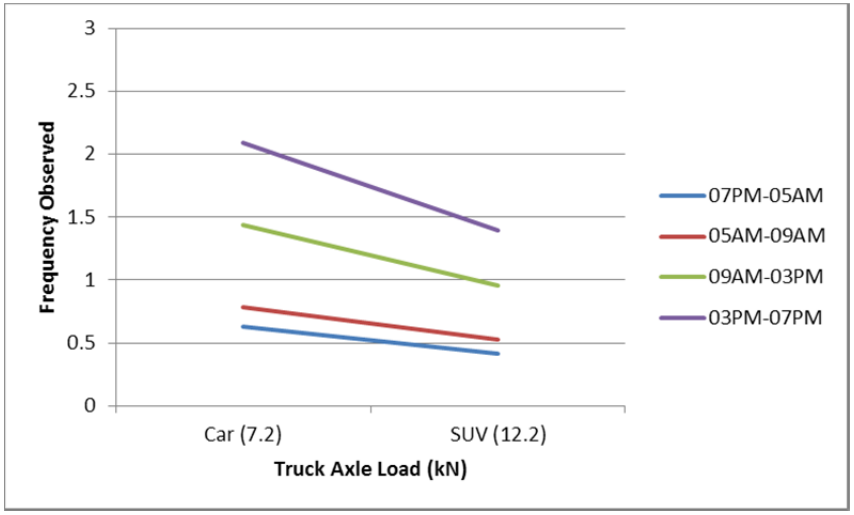

Truck, Weekend

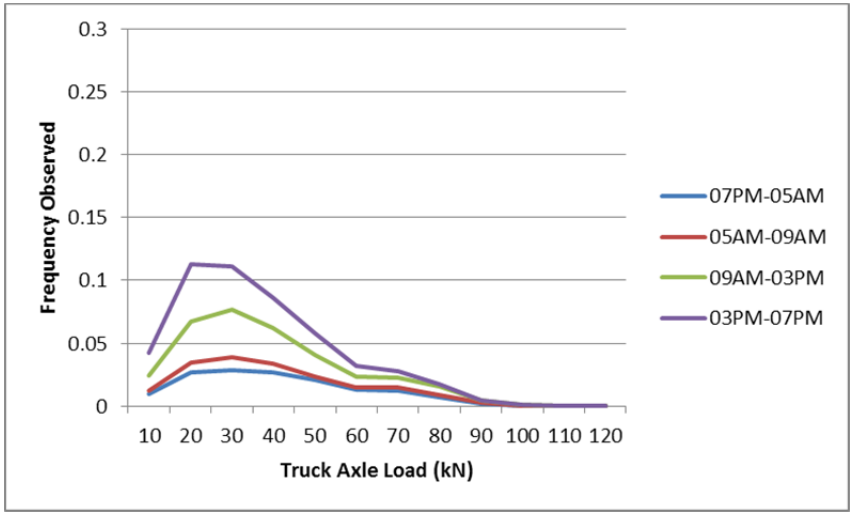

Car/SUV, Weekend

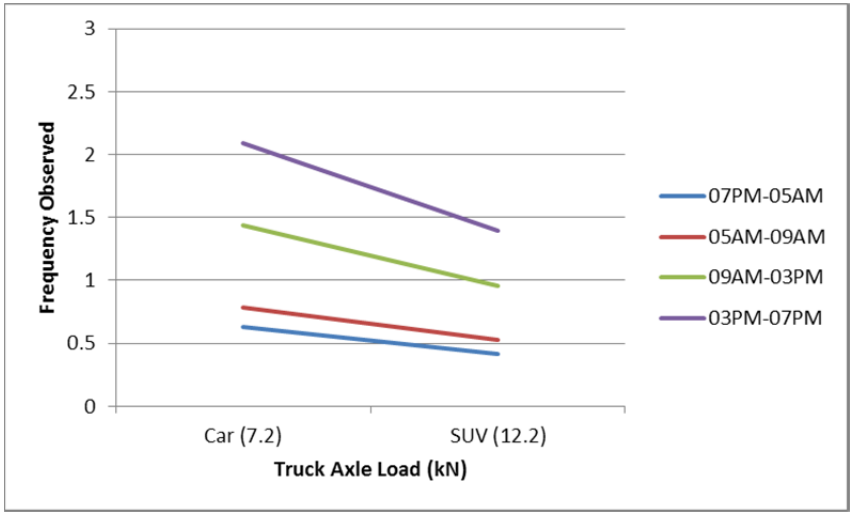

PD 18s2

Truck, Weekday

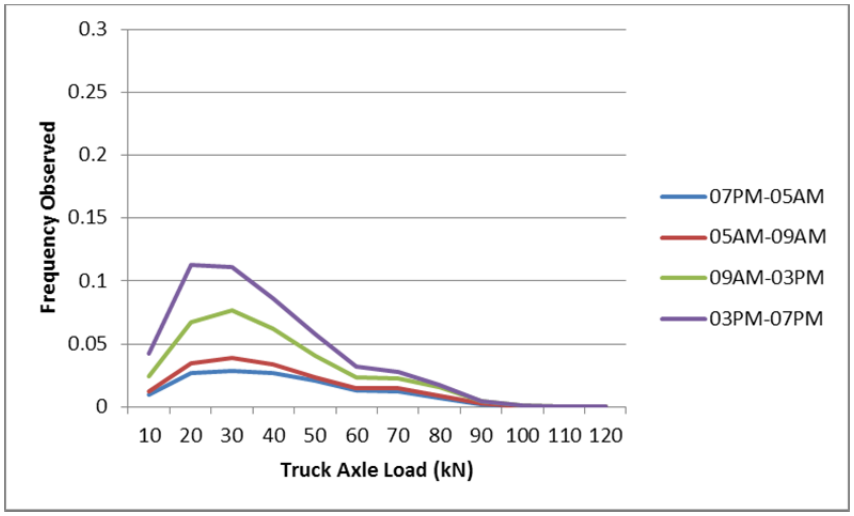

Car/SUV, Weekday

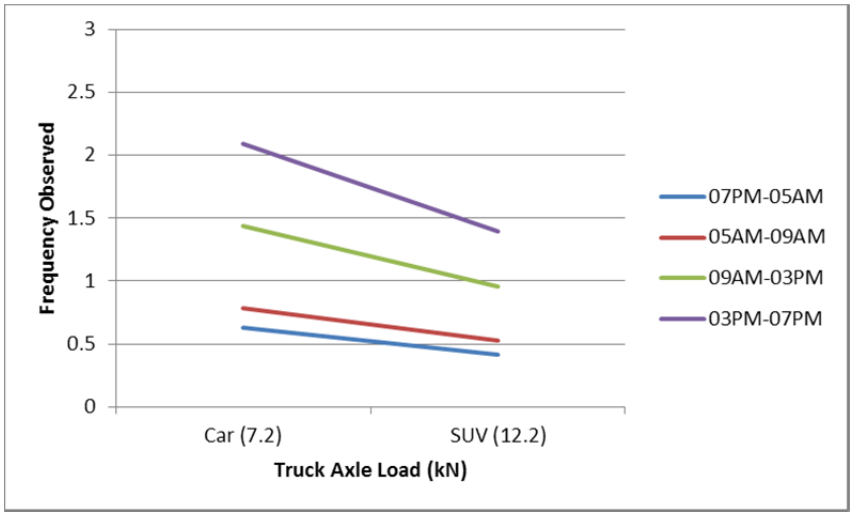

Truck, Weekend

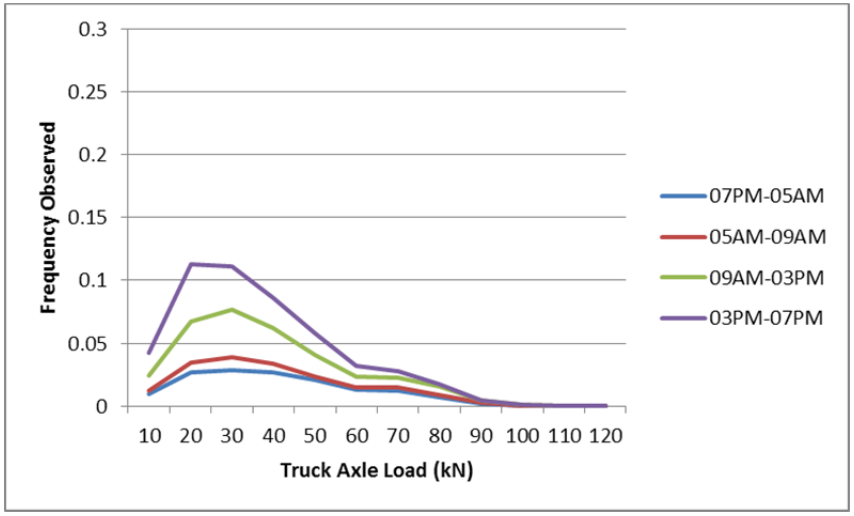

Car/SUV, Weekend

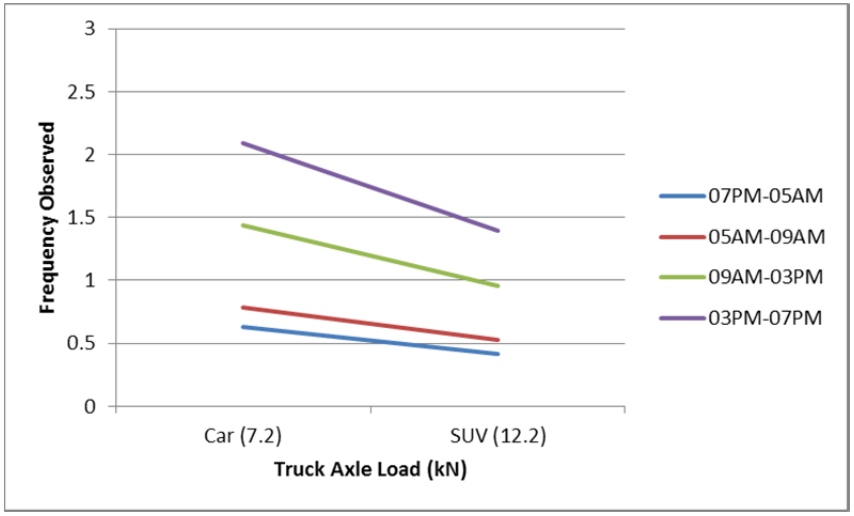

PD 19

Truck, Weekday

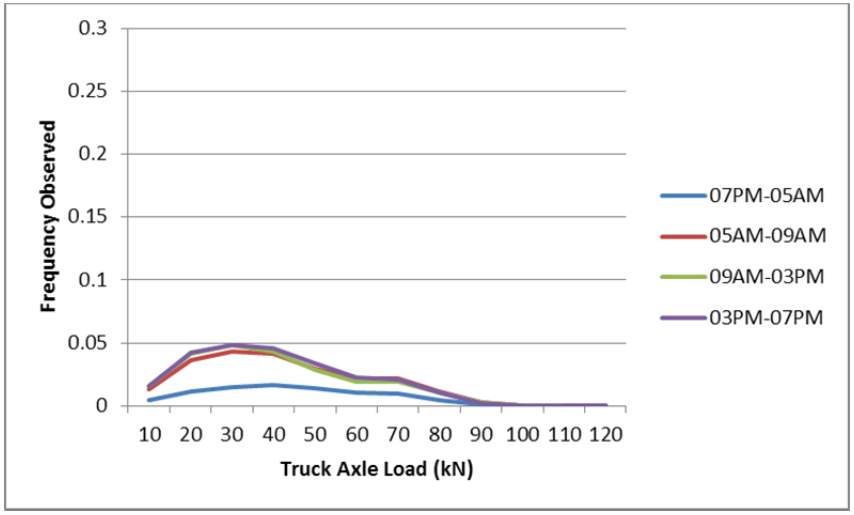

Car/SUV, Weekday

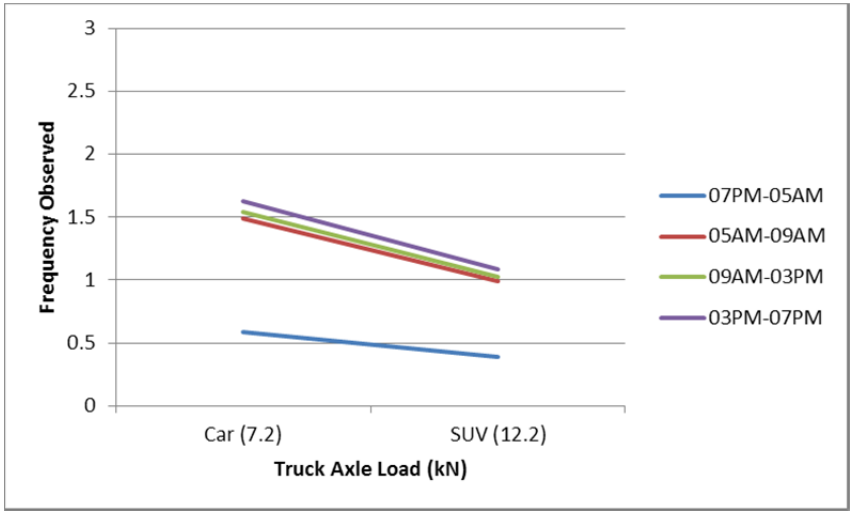

Truck, Weekend

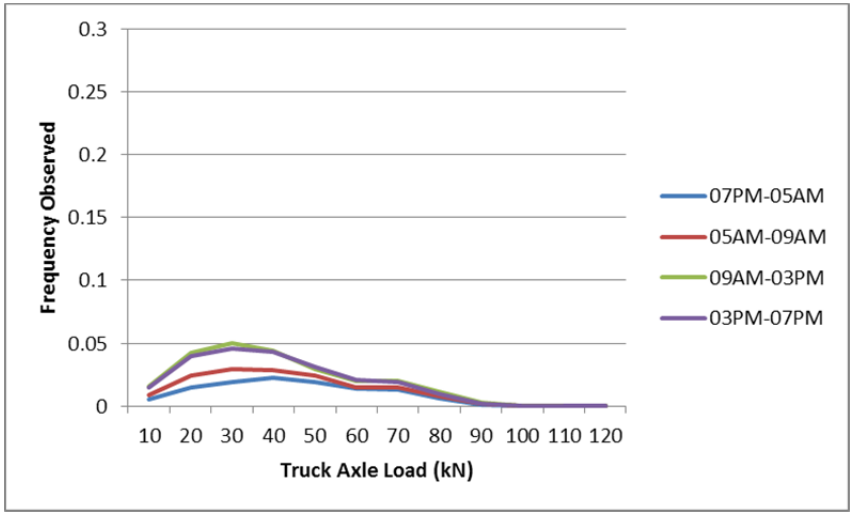

Car/SUV, Weekend

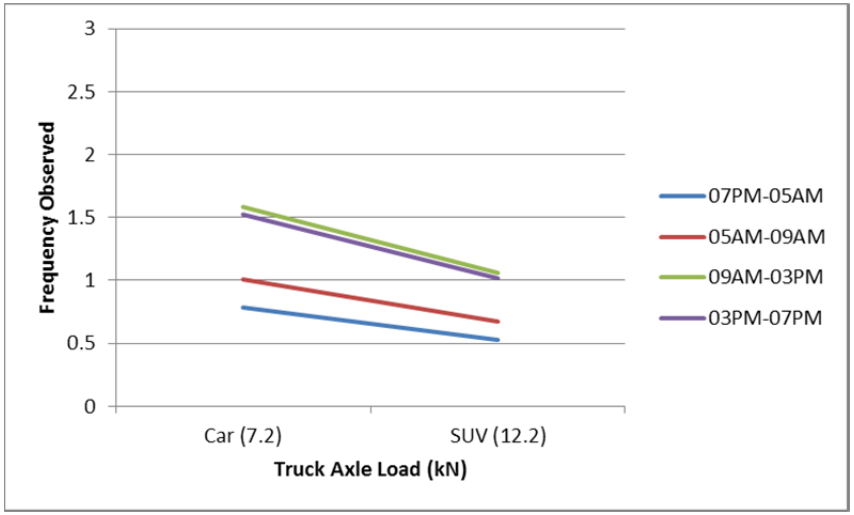

PD 20

Truck, Weekday

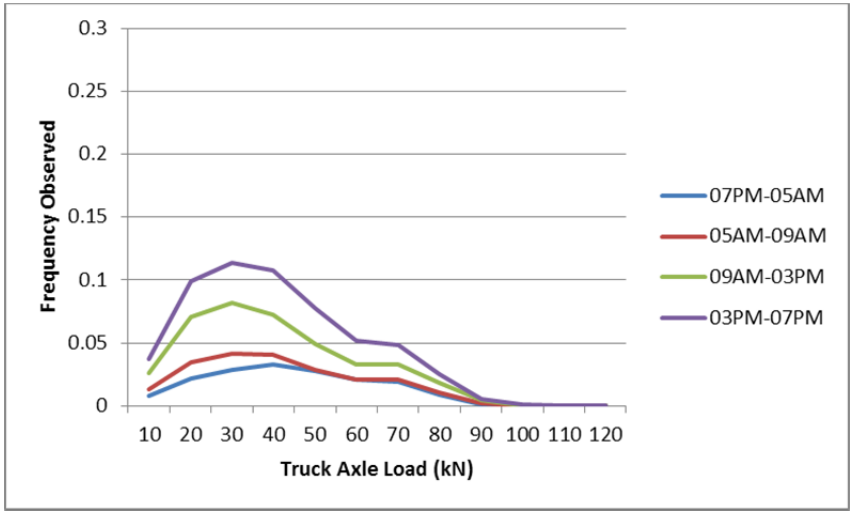

Car/SUV, Weekday

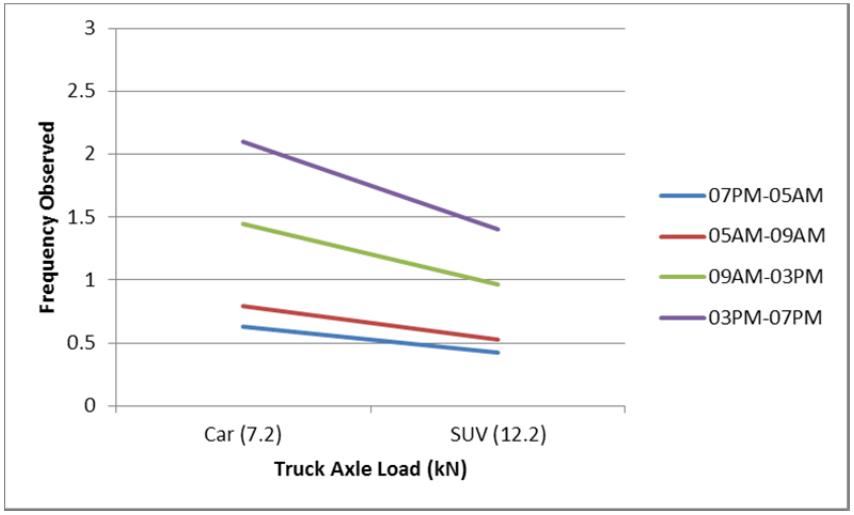

Truck, Weekend

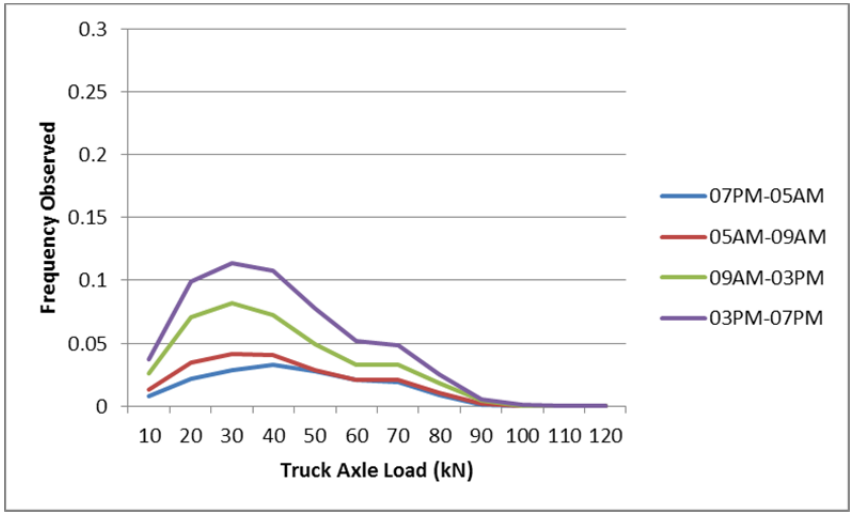

Car/SUV, Weekend

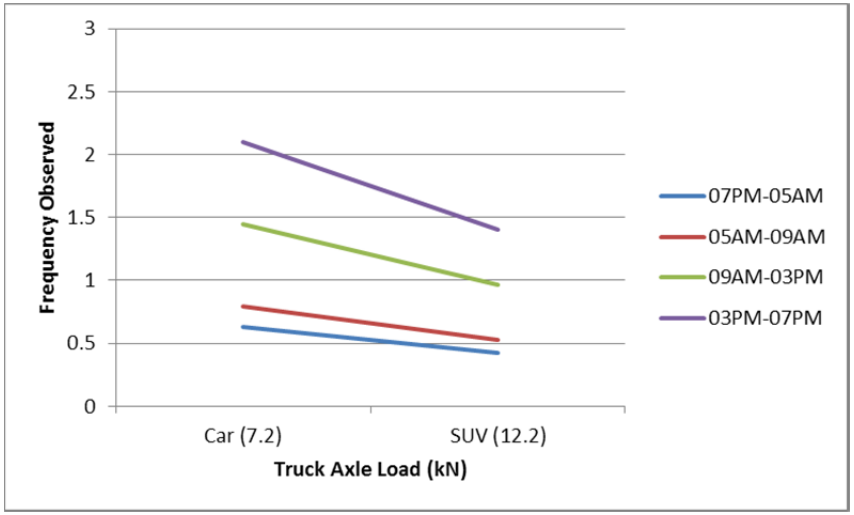

PD 21

Truck, Weekday

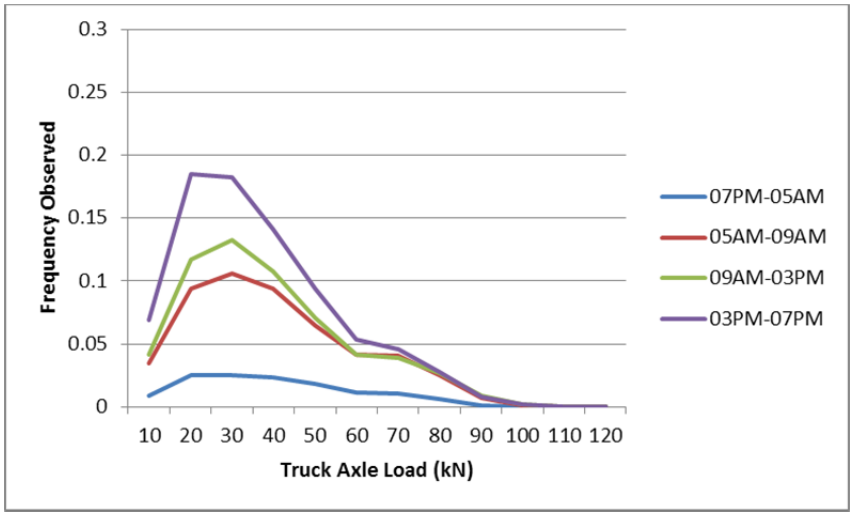

Car/SUV, Weekday

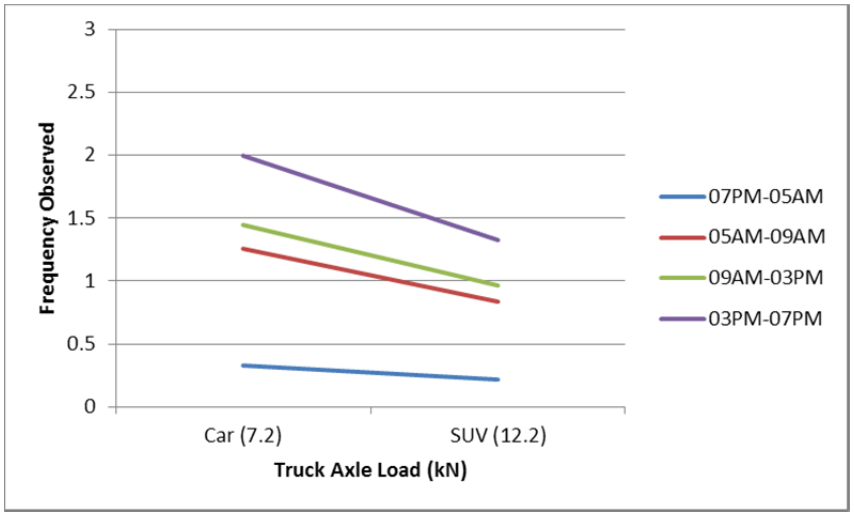

Truck, Weekend

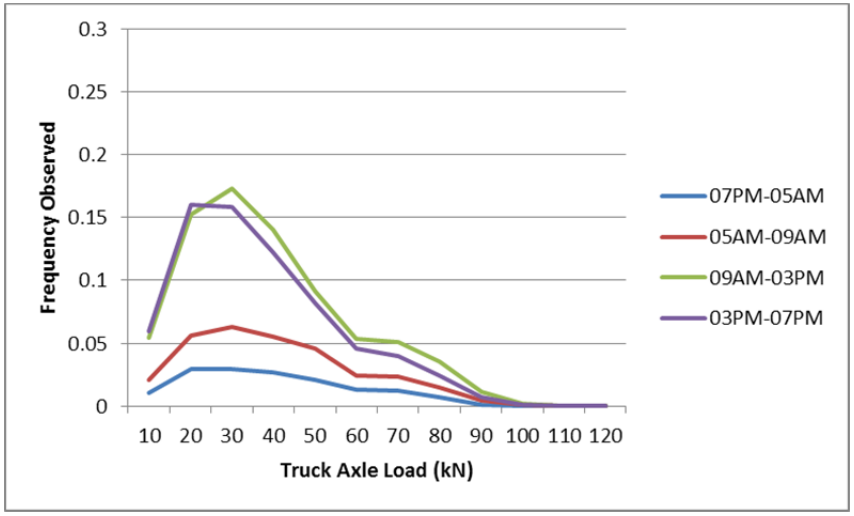

Car/SUV, Weekend

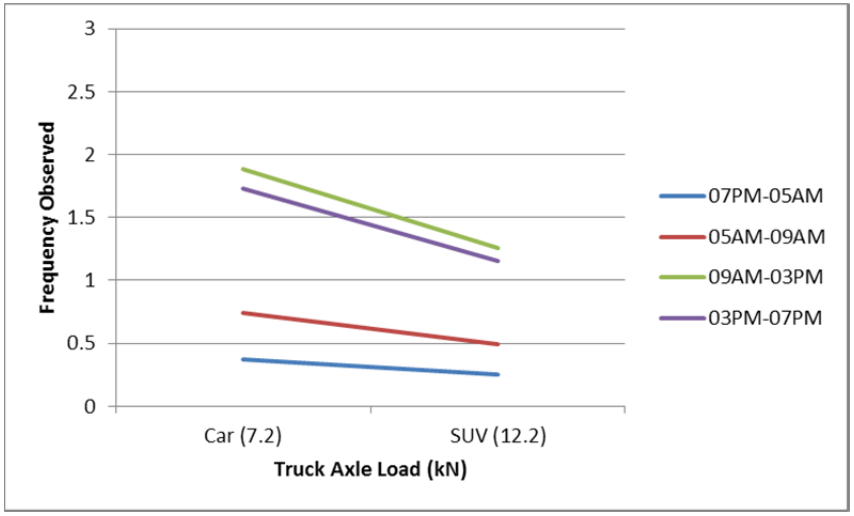

PD 22s1

Truck, Weekday

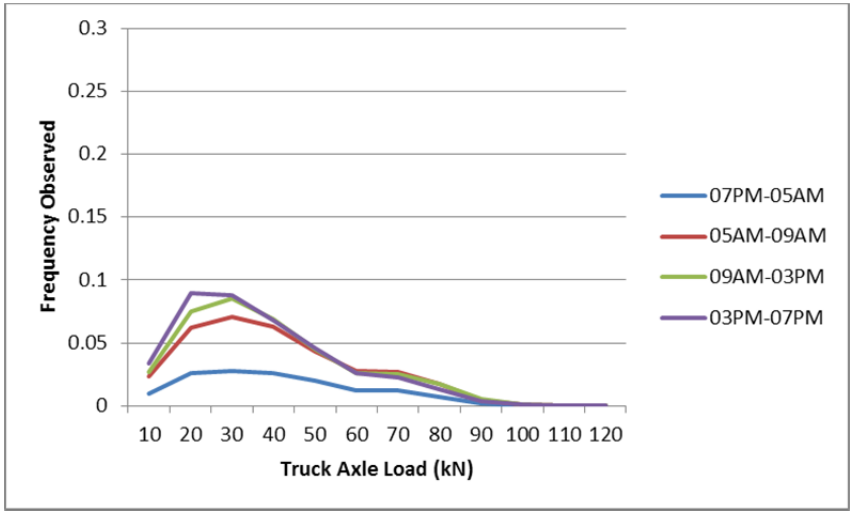

Car/SUV, Weekday

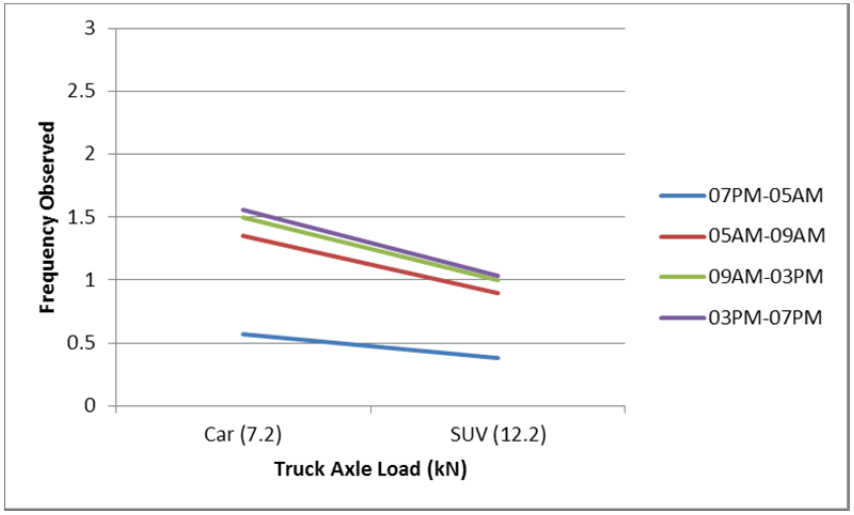

Truck, Weekend

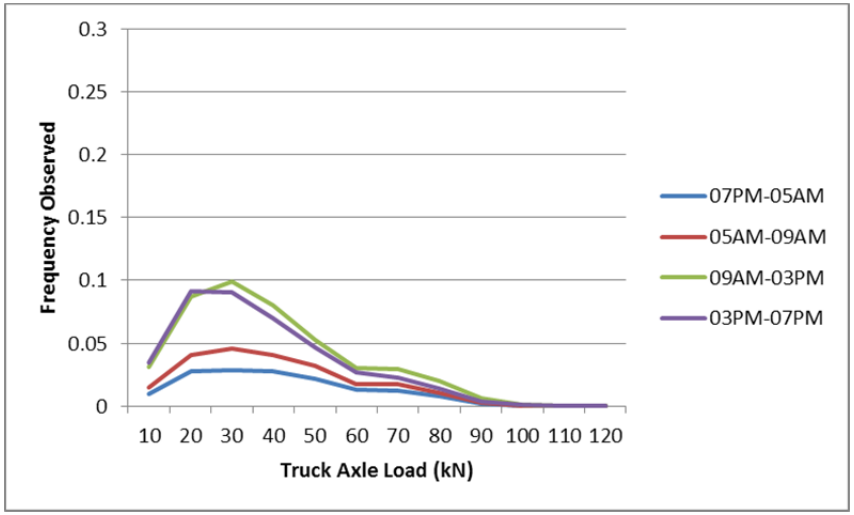

Car/SUV, Weekend

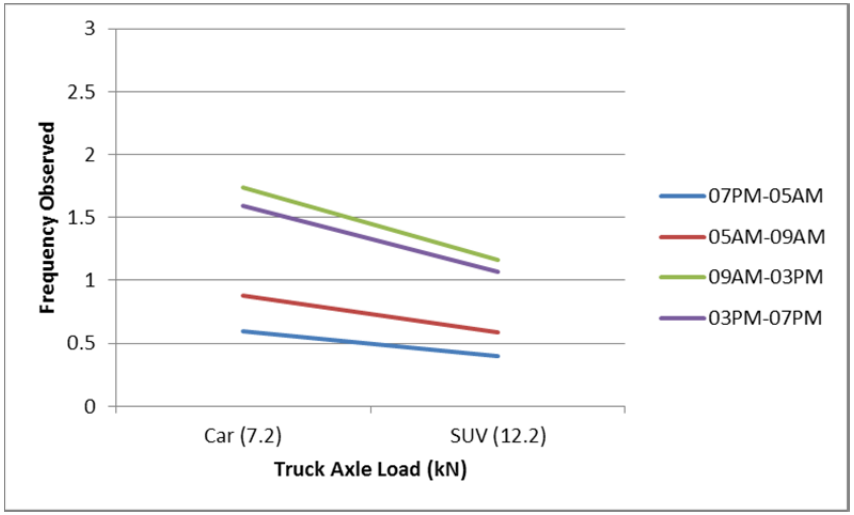

PD 22s2

Truck, Weekday

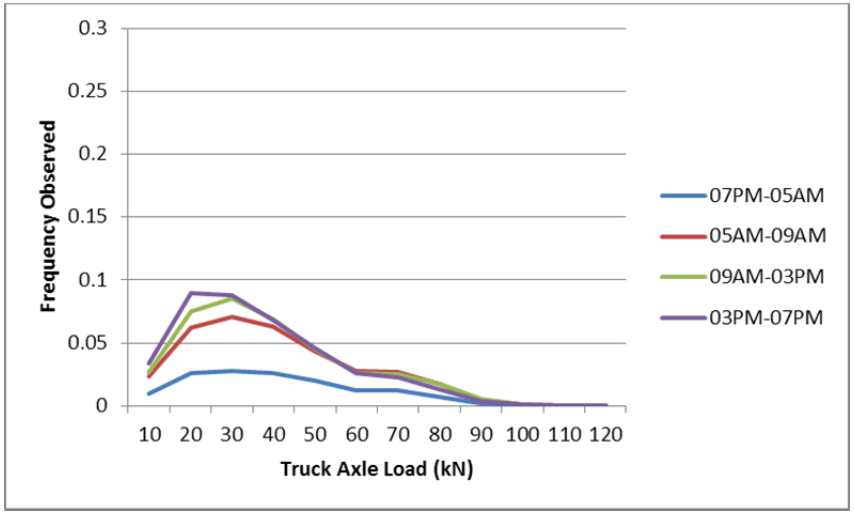

Car/SUV, Weekday

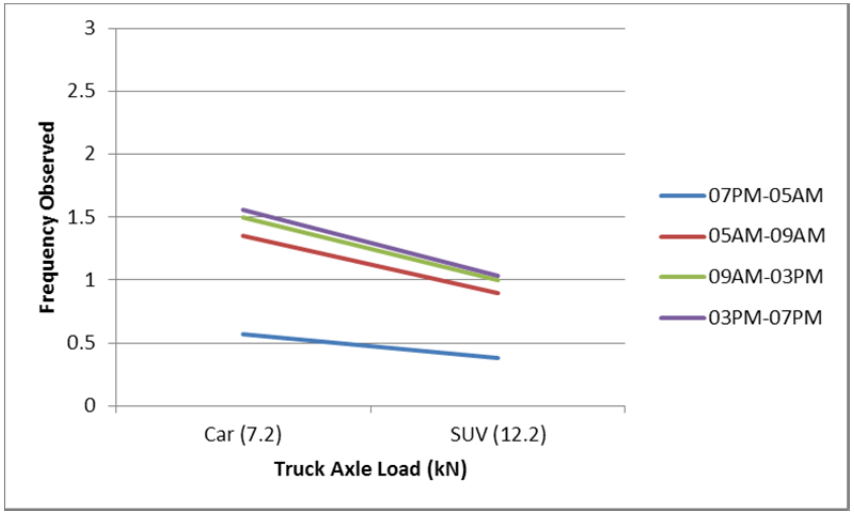

Truck, Weekend

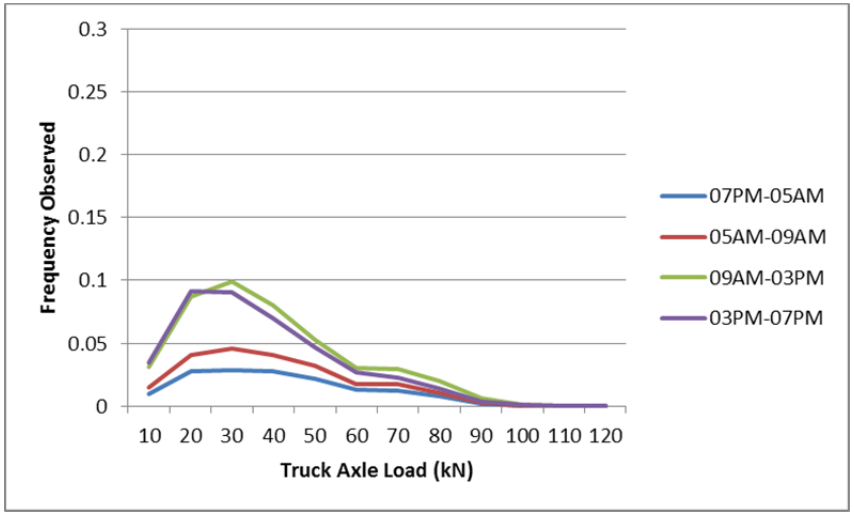

Car/SUV, Weekend

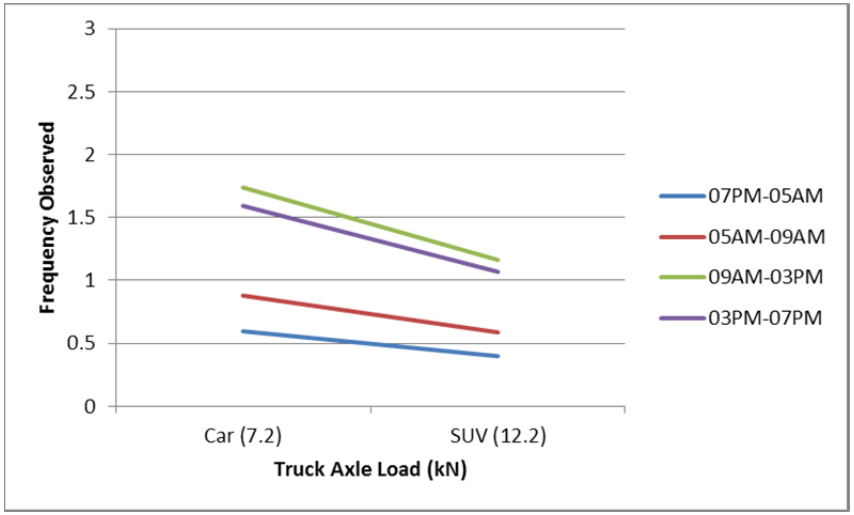

PD 23

Truck, Weekday

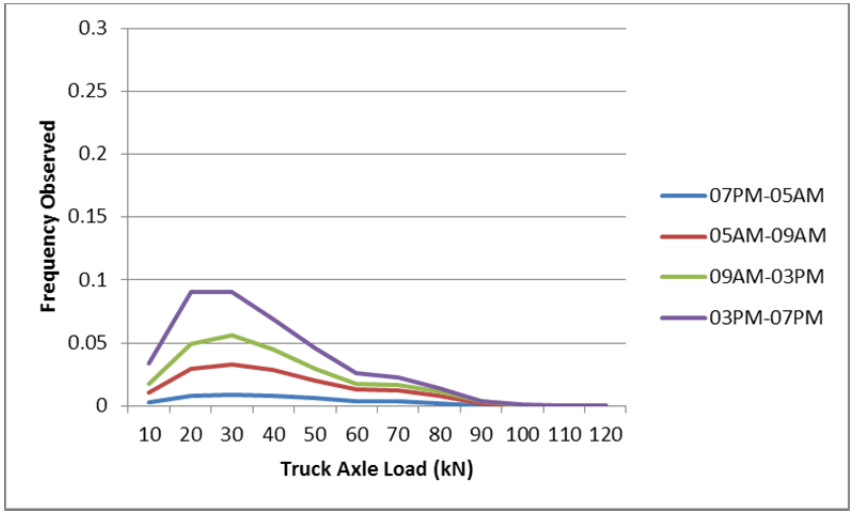

Car/SUV, Weekday

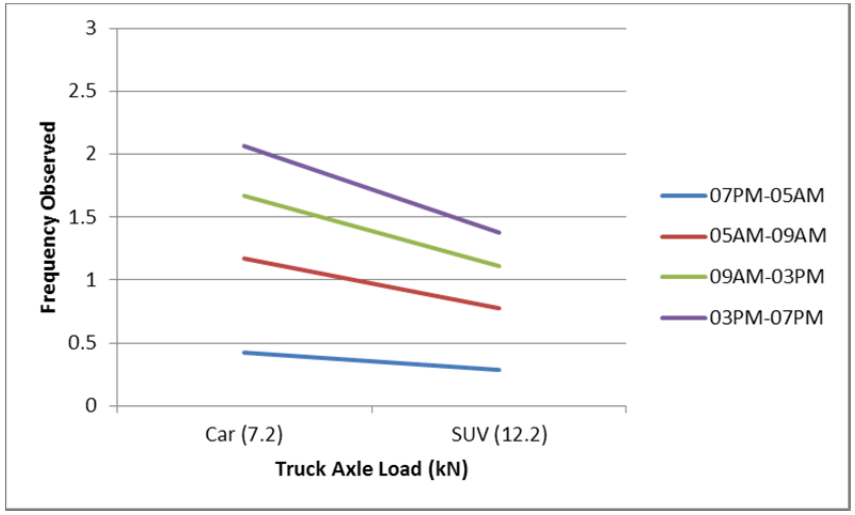

Truck, Weekend

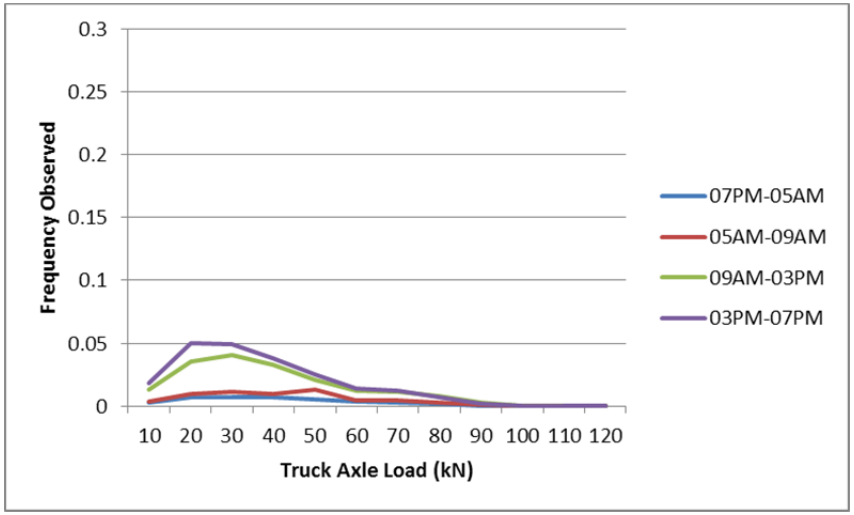

Car/SUV, Weekend

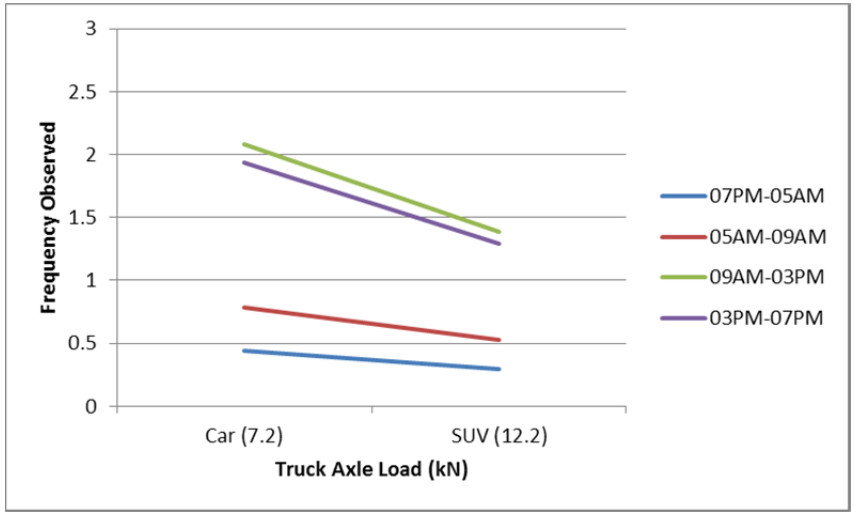

APPENDIX C: TRAFFIC DISTRIBUTION DATA

General Description on Traffic Information for PD Sections

- Traffic information includes hourly volumes for cars, SUVs, and trucks, and hourly average speeds for cars/SUVs and trucks for weekdays and weekends for each PD section.
- The hourly traffic volumes for each PD section were acquired from January 1, 2014 to December 31, 2014 on the California Freeway Performance Measurement System (PeMS), the Caltrans real-time traffic information web-application.
- The heavy vehicle proportion for each PD section was extrapolated from the Annual Average Daily Truck Traffic on California State Highways published by Caltrans Traffic Census.
- The generic proportion for cars to SUVs was extrapolated as 60 percent to 40 percent, based on California vehicle registration.
- The hourly average speeds for cars/SUVs were extrapolated from the average speeds on the innermost lane (Lane 1) and those for trucks were extrapolated from the average speeds on the outermost lane (truck lane) on the PeMS.
- Typical traffic patterns of urban and rural highways were generated for both weekdays and weekends.

Traffic Information (Urban Highway)

Hour	Traffic Volume (veh/hr)						Speed (km/hr)			
	Weekday			Weekend			Weekday		Weekend	
	Car	SUV	Truck	Car	SUV	Truck	Car/SUV	Truck	Car/SUV	Truck
00-01	160	106	14	266	178	23	120	113	119	113
01-02	112	75	10	186	124	16	120	113	120	112
02-03	106	71	9	140	94	12	121	113	120	112
03-04	137	92	12	108	72	10	120	113	120	112
04-05	322	215	28	120	80	11	121	113	119	111
05-06	768	512	67	191	128	17	120	115	120	113
06-07	1,024	682	90	326	217	29	91	88	120	110
07-08	995	664	87	442	294	39	77	77	119	110
08-09	959	640	84	568	379	50	71	71	118	109
09-10	905	603	79	686	458	60	62	60	106	100
10-11	910	606	80	751	501	66	77	74	114	108
11-12	875	584	77	773	516	68	82	79	106	102
12-13	884	590	78	785	523	69	84	81	91	88
13-14	900	600	79	805	537	71	91	88	80	79
14-15	941	627	83	795	530	69	78	79	62	66
15-16	1,006	671	88	871	581	68	55	59	71	75
16-17	1,010	673	89	889	592	67	47	53	93	93
17-18	982	654	86	874	582	67	53	59	100	98
18-19	859	573	75	750	500	63	84	89	113	108
19-20	731	487	64	683	455	60	115	109	115	109
20-21	665	443	58	661	441	58	115	109	111	106
21-22	587	391	51	632	421	55	118	112	109	105
22-23	486	324	43	527	352	46	120	114	113	108
23-24	302	201	27	358	238	31	119	113	121	113
Total Volume, Average Speed	16,626	11,084	1,458	13,187	8,793	1,125	94	91	108	103

Traffic Information (Rural Highway)

Hour	Traffic Volume (veh/hr)						Speed (km/hr)			
	Weekday			Weekend			Weekday		Weekend	
	Car	SUV	Truck	Car	SUV	Truck	Car/SUV	Truck	Car/SUV	Truck
00-01	60	40	5	51	34	5	107	104	108	104
01-02	55	36	5	46	31	4	106	103	107	103
02-03	53	35	5	45	30	4	106	102	107	103
03-04	52	34	5	49	33	4	106	103	106	103
04-05	59	39	5	58	38	5	106	103	106	103
05-06	76	51	7	70	47	7	107	103	107	103
06-07	106	71	11	93	62	9	106	102	106	103
07-08	145	97	15	119	79	12	105	102	106	103
08-09	153	102	16	161	107	16	104	101	105	102
09-10	169	113	18	206	137	20	103	101	104	102
10-11	189	126	20	240	160	23	102	100	104	101
11-12	209	139	22	254	170	24	102	100	104	102
12-13	223	149	23	255	170	24	102	99	104	102
13-14	243	162	25	274	183	26	102	100	104	101
14-15	283	189	28	279	186	26	102	99	105	102
15-16	324	216	32	289	193	27	103	100	105	102
16-17	350	233	34	287	192	27	104	101	105	102
17-18	337	225	32	266	177	25	104	101	104	102
18-19	265	177	26	254	169	23	104	101	104	101
19-20	207	138	20	217	145	20	105	102	104	102
20-21	174	116	17	167	111	15	106	103	104	102
21-22	131	88	13	117	78	11	106	103	105	103
22-23	95	63	9	77	51	7	107	103	107	104
23-24	75	50	7	61	41	6	107	104	107	103
Total Volume, Average Speed	4,033	2,689	400	3,935	2,624	370	105	102	105	102

APPENDIX D: DETAILED SIMULATION RESULTS FOR EACH STRUCTURAL MODELING APPROACH

Table D.1: Excess Fuel Consumption for Structural Response (mL/km/veh) by Vehicle Type for Section-Specific Actual Traffic and Climate

	Total MIT	Total MSU	Total OSU	MIT Car	MIT SUV	MIT Truck	MSU Car	MSU SUV	MSU Truck	OSU Car	OSU SUV	OSU Truck
PD07	0.069686	0.923578	0.482863	0.007536	0.022097	0.196289	0.241076	0.407059	1.531446	0.111499	0.195556	0.885102
PD08	0.02613	0.090937	0.112755	0.003625	0.01063	0.109389	0.02846	0.045687	0.156854	0.031342	0.053522	0.242906
PD10	0.020599	0.339176	0.320801	0.001699	0.004982	0.043395	0.070239	0.118099	0.419985	0.05661	0.099806	0.421582
PD11	0.017969	0.314396	0.207019	0.002076	0.006088	0.063605	0.087044	0.145791	0.597787	0.046976	0.08528	0.496597
PD13s1	0.296414	0.516262	0.429231	0.026378	0.077344	0.745582	0.101732	0.183925	0.960041	0.099595	0.168035	0.693297
PD13s2	0.170192	0.229082	0.191341	0.015083	0.044224	0.427159	0.045898	0.082304	0.418677	0.04367	0.073915	0.312764
PD14	0.099955	0.55569	0.143879	0.010222	0.029971	0.264571	0.113467	0.212319	1.172547	0.031137	0.056184	0.266731
PD15	0.10657	0.068777	0.049455	0.006795	0.019923	0.173023	0.009302	0.017444	0.094803	0.006628	0.012342	0.065481
PD16	0.07412	0.539392	0.261878	0.005745	0.016845	0.154358	0.10418	0.184174	0.815196	0.044586	0.08204	0.444079
PD18s1	0.05553	0.041274	0.02583	0.00507	0.014867	0.13672	0.007528	0.014419	0.087204	0.003931	0.007897	0.058484
PD18s2	0.062461	0.043454	0.028602	0.005711	0.016747	0.152938	0.00818	0.015505	0.089917	0.004311	0.008688	0.06516
PD19	0.022386	0.308304	0.181164	0.002631	0.007715	0.080496	0.081663	0.140694	0.640219	0.044308	0.078318	0.414957
PD20	0.612604	0.138603	0.083225	0.039468	0.115723	1.071071	0.017274	0.035139	0.294454	0.011408	0.022373	0.160884
PD21	0.08455	0.097093	0.048679	0.005443	0.015961	0.15655	0.017234	0.030158	0.132902	0.007085	0.012998	0.070598
PD22s1	0.086019	0.073411	0.143164	0.008075	0.023677	0.215543	0.017197	0.029473	0.116636	0.028157	0.05177	0.270647
PD22s2	0.120053	0.182087	0.143843	0.01149	0.033688	0.304155	0.04129	0.071491	0.296631	0.028067	0.051282	0.260077
PD23	0.08155	0.217218	0.279561	0.010101	0.029616	0.269506	0.052113	0.091013	0.414192	0.057149	0.103127	0.516133